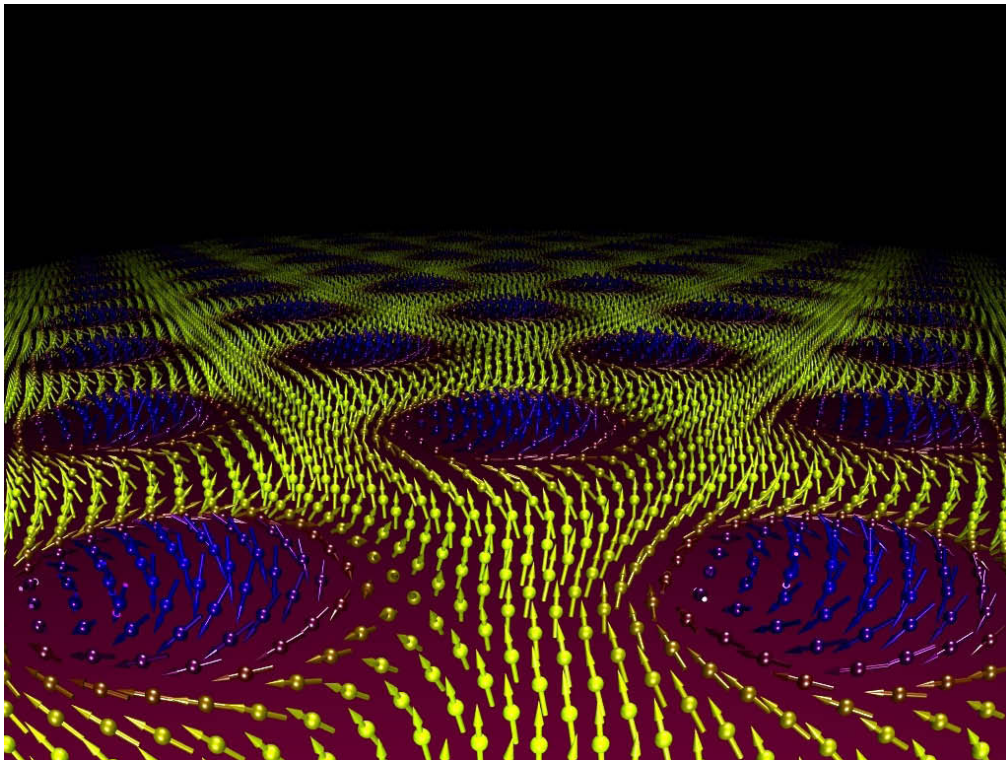


ANNUAL REPORT 2008
Forschungs-Neutronenquelle
Heinz Maier-Leibnitz (FRM II)



Title image: Real space depiction of the magnetic spin structure of the skyrmion line lattice found in manganese silicon, which was shown for the first time with the help of neutrons at the FRM II. See section [5.1](#). [published in *Science* **323** (2009) p915-919.]

Contents

Directors' report	2
The year 2008 in pictures	4
I. Instrumentation	7
1. Central Services and Reactor	8
1.1. The operation of the neutron source FRM II	8
1.2. Development of high density fuels	9
1.3. Detector and electronics lab: Fast high resolution detectors developed	14
1.4. Irradiation facilities: 10 tons of doped silicon	16
1.5. Sample environment: Solutions for the cold and the hot	19
1.6. HELIOS – polarized ^3He gas for neutron instrumentation	21
1.7. Development of higher-m supermirrors	23
2. Diffraction	24
2.1. Improved efficiency at the structure powder diffractometer SPODI	24
2.2. HEiDi and POLI-HEiDi	26
2.3. The new small-angle scattering instrument SANS-1	29
2.4. Biological membranes under study at the reflectometer REFSANS	31
2.5. Polarized and unpolarized neutron reflectometry with <i>N-REX</i> ⁺	33
2.6. Proteins under study at KWS-2	35
3. Inelastic scattering	37
3.1. MIRA – The beam line for very cold neutrons	37
3.2. RESEDA operates with two arms	39
3.3. First year of operation of the backscattering spectrometer SPHERES	40
3.4. Paramagnetic experiments and soft matter physics at J-NSE	43
3.5. Molecular motions in pharmaceutical products – Research at TOFTOF	46
4. Nuclear physics and Applied Science	48
4.1. Element determination in 3D at PGAA	48
4.2. Neutron periscopes used for imaging	52
4.3. Towards a new measurement of the electric dipole moment of the neutron (nEDM)	55
4.4. Particle physics at the cold neutron beam facility MEPHISTO	57
4.5. MEDAPP: A versatile beam not only for medical applications	59
4.6. Radiology and partial tomography of large wooden samples using fission neutrons at NECTAR	63
4.7. Unprecedented intensity of low-energy positrons at NEPOMUC	65
4.8. Microscopy with positrons	67
4.9. High resolution analysis of the Auger-transition in copper	69
II. Scientific highlights	71
5. Condensed Matter	72
5.1. Skyrmion lattice in a chiral magnet	72
5.2. Phonon Anomalies and the Energy Gap in Superconductors	74
5.3. Absolute <i>d</i> -spacing value determination by Larmor diffraction	76
5.4. Inelastic neutron scattering on solid deuterium	78
5.5. Development of residual strains in composite castings	81

5.6. Insight into the symmetry of a mineral	83
5.7. Coincident Doppler broadening measurement on thin tin layers	85
III. Facts and figures	87
6. Events	88
6.1. Industrial activities	88
6.2. Neutron scattering at the FRM II as a part of the "Fortgeschrittenenpraktikum"	89
6.3. NEUWAVE: International workshop on energy selective neutron imaging	90
6.4. JCNS laboratory	91
6.5. German neutron scattering conference	92
6.6. Neutrons for crystallographers	93
6.7. Workshop on biomolecular dynamics and protein-water interactions	94
7. Facts	95
7.1. The FRM II goes public	95
7.2. User office: Organizing the increasing number of scientists	98
7.3. Publications	100
7.4. Committees	112
7.5. Partner institutions	118
7.6. Staff	120
Imprint	125

Directors' report

In its 4th year of operation FRM II delivered 241 full power days, for the first time with a reactor cycle length of 60 days. Congratulations to our reactor staff on so reliably delivering neutrons for science and industry.

Yet, our reactor staff achieved another record. Almost 10 tons of high purity silicon have been transformed to silicon perfectly doped by phosphorus. Doped silicon is the starting material for the production of semiconductors required in high current applications.

Production of molybdenum-99

In early 2008 a feasibility study on the production of the radioisotope molybdenum-99 was started by FRM II in collaboration with the company IRE. Technetium-99m, which is a daughter isotope of molybdenum-99, covers about 80 % of the demand for radioisotopes in nuclear medicine applications. In summer 2008 it became public what has been known to experts for a while that there is a real possibility of Tc-99m shortages. Due to the unforeseen shutdown of the Petten high flux reactor it happened that within Europe the supply chain for Tc-99m broke down for several months. The short life time of 2.6 days of Mo-99 made it impracticable to bridge the lack of isotopes by imports from overseas. The root cause of the problem is the ongoing closure of research reactors worldwide. In May 2009 the feasibility study will be finalized. FRM II is able to approximately cover the European need for Mo-99, provided one of our irradiation positions and the transport chain for the Mo-99 within FRM II are upgraded. Investments would be in the order of 5 Million Euros, with an anticipated implementation time of 5 years. In December 2008, both, the Federal Government of Germany and the Free State of Bavaria declared their principle willingness to finance this upgrade. Specific details depend on the results of the feasibility study and further negotiations with the Federal Government. FRM II is optimistic to start the project in the course of 2009.

At the end of 2007 the positron source lost its intensity, and this was the beginning for a world record. An electrical short-circuit in the extraction device, at the front end of the beam tube, was identified as the cause of the problem soon after. As a consequence the complete insert of the beam tube had to be replaced. Only one reactor cycle was needed to build that new insert. Of course the scientists responsible for NEPOMUC did more than a simple replacement. Subtle improvements of the extraction device resulted in an almost doubling of

the positron intensity. Today a mono-energetic positron fluence of 9×10^8 p/cm²s is available, unprecedented in the world.

21 instruments in routine operation

The year 2008 also set a new record for the usage of FRM II: 21 instruments are now in routine operation, 4 of which are operated by JCNS. These instruments showed an availability of 85%, when compared to the actual reactor operation days. An additional 9 instruments are under construction. With some optimism they will all be operating by 2012 at the latest. About 500 proposals were submitted in 2008, creating an overload factor of two and allowing 700 scientists to visit FRM II. These figures demonstrate how successfully the instrumentation of FRM II has been developed in a short period of time. This is certainly a credit to all the universities, Max Planck Institutes and Helmholtz groups who have taken part in creating a world class instrumentation at FRM II.

Among others the commissioning of SPHERES was completed: it is now one of the leading backscattering spectrometers, and fully available for user experiments. Sadly, this success was overshadowed by the death of our beloved colleague Michael Prager who had been the scientific advisor of SPHERES and its first regular user.

Instrumentation is no end in itself. Excellent science is the final goal. Among others the scientific highlights of 2008 include:

- Strain measurements with a 10^{-6} relative precision by means of Larmor diffraction [Repper et al: 'Investigations of lattice spacing on IN718 via neutron Larmor diffraction', Proceedings of the ICRS8, August 6-8, 2008, Denver, Colorado, USA; section 5.3]
- In-situ stress determination during casting [Was-muth, thesis TUM 2009; section 5.5]
- Separation of local and long range motion in simple organic molecules [C. Smuda et al. J. Chem. Phys. 129 (2008), 014513; section 3.5],
- Discovery of the interplay of Kohn anomalies and superconductivity [Aynajian et al., Science 319 (2008) 1509; section 5.2].

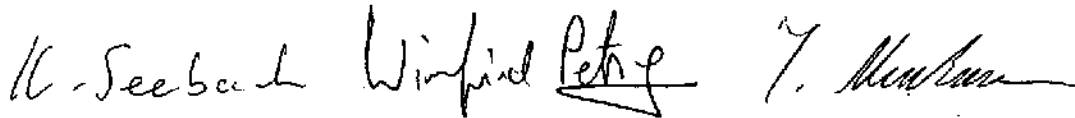
FRM II is a visitor attraction: The Bavarian Minister for Environment, Health and Consumer Protection, Dr. Otmar Bernhard (18 March), Ms Hannelore Gabor, the major of Garching together with the city council of Garching (14 July), MdB Ms Ilse Aigner and the panel for education of the parliamentary group of CDU/CSU (9 September),

the Federal Minister for Environment Sigmar Gabriel (9 September) are the most prominent visitors of 2008.

No less important: a total of 3000 people visited FRM II, among those 563 pupils and 738 students. About 280 scientists came to Garching on the occasion of the Deutsche Neutronenstreutagung taking place from 14 - 17 September 2008. In 2008 FRM II and JCNS merged their user offices; at the moment the deadlines for scientific proposals of the two institutes are shifted by three months, however these will be merged by 2010. The joint proposal round will enhance the already strong cooperation between FRM II and JCNS.

Strengthening our user office and our public relation department by new personnel meanwhile shows fruits: a regular news letter for the scientific users has been launched, highlights are regularly displayed on the home page of FRM II and, last but not least, a broader public is increasingly more aware of FRM II and its versatile scientific possibilities.

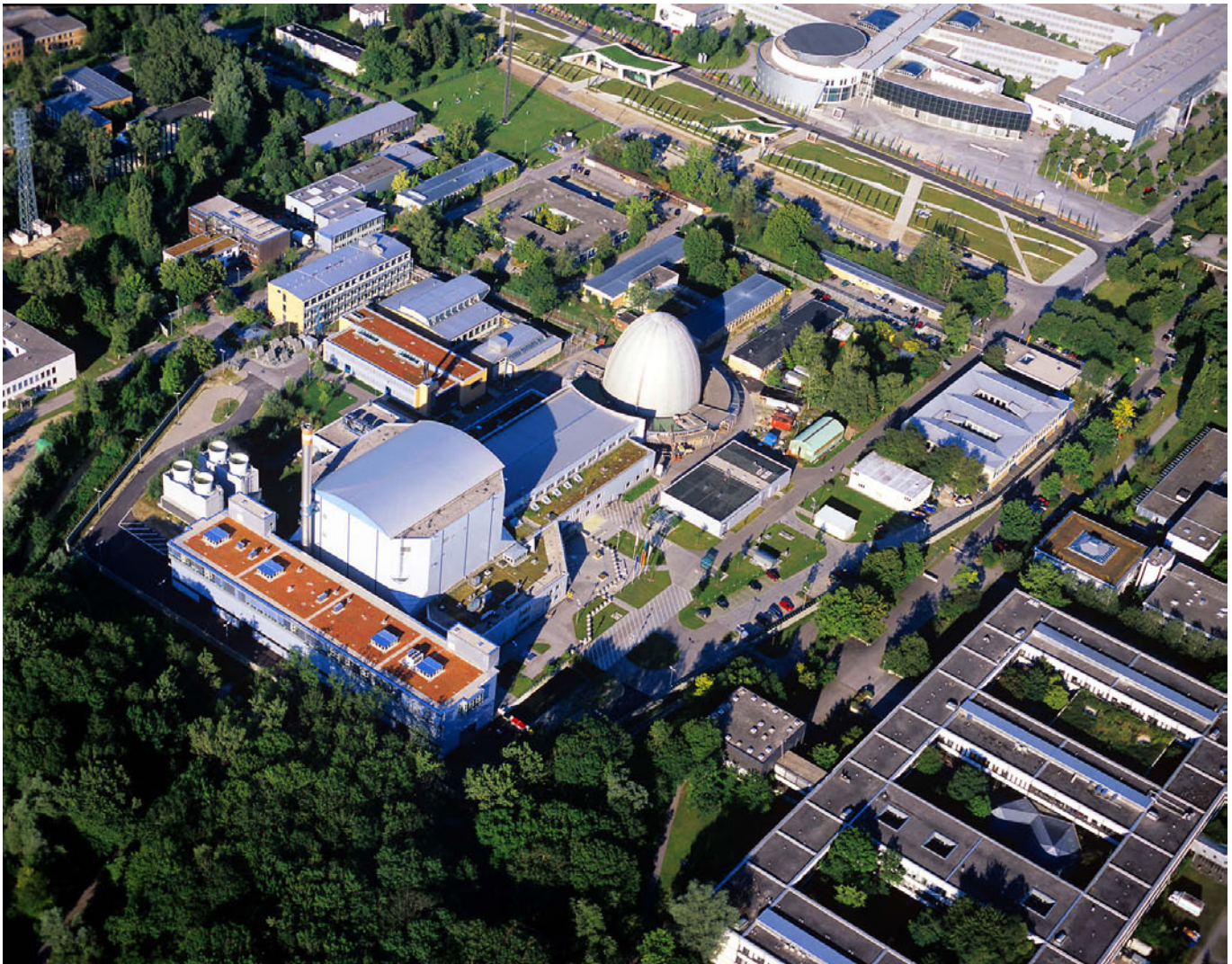
All this is based on the strong commitment of our staff to its daily business. Our reward is the satisfaction of our users and visitors. In recognition of the efforts of all of us Winfried Petry was presented with the Bundesverdienstkreuz am Bande in early 2008.



Klaus Seebach

Winfried Petry

Ingo Neuhaus



The FRM II from the bird's eye view.

The year 2008 in pictures



11 February 2008: The Bavarian Minister for Science, Dr. Thomas Goppel (right), awarded Prof. Dr. Winfried Petry in February with the Bundesverdienstkreuz.



June 2008: Happy about the chance they were offered by the Erasmus Mundus Program “Master of Materials Science Exploiting Large Scale Facilities”: International students who received an EU grant to perform their masterthesis at FRM II.



May 2008: Members of the Junge Physikalische Gesellschaft (JDPG) from the Friedrich-Alexander-Universität Erlangen-Nürnberg visited the FRM II. Their enthusiastic conclusion: “We could ask many questions during the tour, and every single one was answered.” (Photo: JDPG)



8 May 2008: In the presence of the Bavarian Ministerpräsident Günther Beckstein (back, left) and the Prime Minister of Québec, Jean Charest (back, right), the operational manager of itm AG, Oliver Buck (right), signed a contract with the Director of Marketing and Business Development from Draximage, Francois Bergeron.



14 July 2008: Members of the city council of Garching visited FRM II. They enjoyed a guided tour with Dr. Johann Meier, Dr. Jürgen Neuhaus (from the left) and Prof. Winfried Petry (fourth from right) showing the politicians the new experimental hall east.



5 September 2008: Members of the Committee on Education, Research and Technology Assessment in Parliament visited the FRM II: (from left to right) Andreas Lämmel, Carsten Müller, Ilse Aigner (meanwhile the German Minister for Agriculture), Marcus Weinberg, Marion Seib, Anette Hübinger, Helmut Brandt. Prof. Dr. Winfried Petry (fourth from left) welcomed the politicians.



9 September 2008: The German Minister for Environment, Sigmar Gabriel (third from right) with the Vice President of the Bavarian Parliament, Prof. Peter Paul Gantzer (right-most), regard into the reactor pool. The three directors of the FRM II, Dr. Ingo Neuhaus, Dr. Klaus Seebach and Prof. Dr. Winfried Petry (from left), guided the visitors through the neutron source.



15-17 September 2008: The German neutron scattering conference took place at the FRM II.



18 October 2008: The queue of visitors waiting for registration at FRM II at the open day stretched sometimes throughout the whole foyer of the physics department.



October 2008: Representatives of German companies in the USA visited the FRM II. Dagmar Cassan (3rd from left, the director of the United States Office for Economic Development of the State of Bavaria, had organized the guided tour. Dr. Peter Link (rightmost) guided one group through the experimental hall.



15 December 2008: The former scientific director of the FRM II Prof. Dr. Wolfgang Gläser with his wife Helga was honoured with a colloquium on the occasion of his 75th birthday.

Part I.
Instrumentation

1. Central Services and Reactor

1.1. The operation of the neutron source FRM II

I. Neuhaus¹

¹ZWE FRM II, TU München

Reactor cycles

In 2008 the FRM II was operated securely in five cycles (no. 10b, no. 15, no. 16, no. 17 and no. 18a) with totally 252 days of full operational power. In the cycles no. 10b, no. 15, no. 16 and no. 17 the fuel elements were used until the newly permitted fuel irradiation level of 1200 MWd was reached. The fuel element FRM-021 has reached an irradiation level of 703,1 MWd in 2008, as the cycle no. 18 was stopped at the end of the year due to the holidays. With its full availability on 251.4 days, the FRM II has again reached a high standard. Every cycle was performed on time with high precision as announced in autumn 2007.

The experiences with the fuel elements FRM-013, FRM-018, FRM-019, FRM-020 and FRM-021, that were used in the year 2008, were again very positive. The positions of the control rod, when reaching the criticality, and the curves of the control rod as a function of the fuel irradiation level were almost identical in all cycles. In total 1815 recurring checkups, rounds of inspection of referees to 18 different areas of interest, maintenance measures and in total 69 advices of amendment were performed to assure and even enhance the high standard in safety and systems engineering of the FRM II.

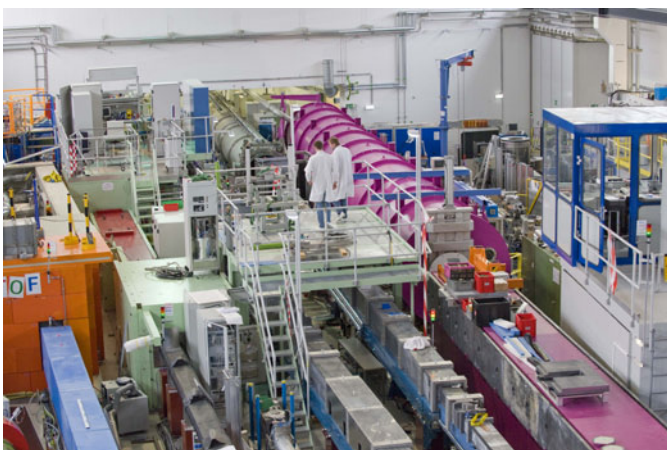


Figure 1.1.: The extension of the neutron guide hall west (back of the picture) has been opened for the experimental usage in 2008.

Usage of the neutron source

Both the cold neutron source as well as the hot neutron source were fully available for the scientific users without restriction during the whole operation in 2008. The extension of the neutron guide hall west could be used for the first time in the year 2008 (see 1.1).

We applied for a conversion of the assembly hall to a new neutron guide hall east. It has to be part of the atomic law permission of the FRM II in order to be used for the scientific experiments.

The planning for the development, building and operation of a source for ultra cold neutrons is in progress, such that a first review with the inspecting and regulatory authority, referees and the FRM II-staff could take place. The authorization procedure will start in 2009.

Reportable incident

In the year 2008, there was one reportable incident, which was reported to the inspecting authority on time. The incident was not influencing the security of the reactor, the safety of the staff or the environment. Radioactivity was not released. One unit of batteries of a emergency cooling pump was out of order. Meanwhile, the other two emergency cooling pumps could have cooled the fuel element, in case of loss of external electricity.

1.2. Development of high density fuels

R. Hengstler¹, H. Breitzkreutz¹, R. Jungwirth¹, W. Petry¹, A. Röhrmoser¹, W. Schmid¹, H. Palancher², E. Welcomme², S. von den Berghe³, A. Leeneers³

¹ZWE FRM II, TU München

²Commissariat à l'Énergie Atomique, Cadarache

³Studiecentrum voor Kernenergie, Centre d'étude de l'énergie nucléaire SCK-CEN

Since 2003 TUM engages for the development of high density Uranium fuel with the aim of decreasing the enrichment from 93% ²³⁵U in the actual FRM II fuel element to an enrichment below 50%. Also since the beginning this project is conducted in close cooperation with the French Commissariat à l'Énergie Atomique (CEA) and the fuel manufacturer AREVA-CERCA. Today this program encompasses four main topics:

- Irradiation of full large fuel test plates made of UMo grains with a density of 8 gU/cm³ dissolved in an Al matrix, so called disperse UMo
- Development of an industrial fabrication technology for large fuel plates made of monolithic UMo with a density up to 16 gU/cm³
- Exploring new material combinations for high density fuels by heavy ion bombardment
- Calculation of the neutronics and hydraulics of a future high density core at FRM II.

Here we report about the progress achieved in 2008.

Post irradiation examinations for IRIS-TUM

In September 2008 the final report for the post irradiation examinations (PIE) done in the hot cells of the Belgian Nuclear Research Centre SCK-CEN at Mol have been received. This report contains optical and scanning electron microscopy (SEM) examinations performed on small samples punched out of the large fuel plates 8002 and 8503, both irradiated to a maximum LEU (Low Enriched Uranium) equivalent burn up of 54%/56% (1.2) in IRIS-device at OSIRIS reactor in Sarclay, France. The essential results are: The UMo grains show a huge variety in shape on account of their production by milling whereupon layers of UO₂ are incorporated. After burnup a huge fraction of interface area shows up, which is comparable to French IRIS-results at high temperatures with fuel made of atomized powder.

The interdiffusion layer (IDL) forms at the interface of UMo grain and Al matrix, independently whether Si or not is contained in the Al matrix. In parts of the samples this IDLs eats up the Al matrix completely. The IDL has a typical thickness of 5 - 6 µm, with a small tendency to be thinner in the sample containing Si in the Al matrix. Compared to irradiations of test plates with atomized powder and no Si content the IDL is thinner. The Si concentration is considerably enhanced in the IDL, when compared to the Al-matrix.

For atomized powder a strong peak in Xe concen-

tration at the interface IDL/Al matrix is observed. This strong peaking is supposed to be the origin of the delaminating (pillowing) observed in former test irradiations on samples made of atomized powder. This peaking of the Xe intensity is much less in the IRIS-TUM samples and Xe is distributed all over the IDL. There is no difference in the capability of the UMo grains to store the gaseous fission products for both samples. No direct delaminating is observed at the two interfaces Al matrix/IDL and IDL/UMo grain. Cracks seen in some of the SEM pictures are assigned to the preparation of the samples, knowing that the irradiated material becomes extremely brittle.

We are now waiting for the transport of the samples from plates 7003 and 8501 to SCK-CEN. These samples have been irradiated to a much higher burn-up of 66,5%/88,3% LEU equivalent. From the in-situ measurements of the swelling it is expected to see clear traces of delaminating in the SEM pictures.

The irradiation campaign IRIS-TUM will be followed by an irradiation of large test plates made out of disperse UMo fuel, but now based on atomized powder with different coatings and additions to the Al matrix. Further the heat flux during irradiation should reach values above 400 W/cm² in order to simulate the conditions of FRM II.

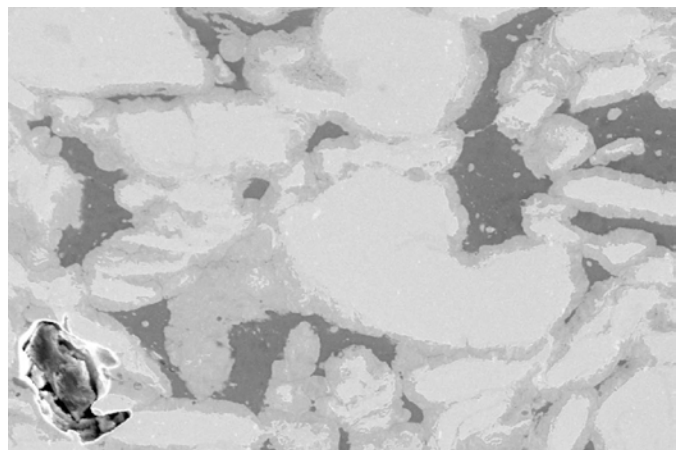


Figure 1.2.: Scanning electron microscopy picture of a sample from the top edge of the irradiated plate 8503 (Si addition in the Al matrix).

Development of an industrial fabrication technology for large monolithic fuel plates

Prior to irradiation tests of large monolithic fuel plates an industrial fabrication process has to be established. Although monolithic fuel plates may be produced on a laboratory scale, irradiation tests of these plates will not be conclusive, because the production process strongly influences the cladding/UMo monolithic interface.

The TUM/CEA/AREVA-CERCA consortium studied the fabrication of UMo monolithic fuel plates during 2005-2007 and tentatively manufactured full size plates for the irradiation program IRIS V. As the program unfolded technical information were obtained and gathered with the international community. UMo foils were produced at laboratory scale and different methods to clad the UMo foils within aluminium were investigated. Based on these first results TUM and AREVA-CERCA decided to pursue a common effort on the development of monolithic fuel plates. Now emphasis will be more dedicated to the foil and cladding package preparation and further studies will be performed in order to investigate various processing techniques to join the fuel foil with the cladding.

The sputtering process offers the advantage, that perfect layers from any material can be grown on any substrate in any size. This means firstly, that monolithic full size foils and blank sheets from any given UMo alloy can successfully be produced. It means secondly, that a given UMo foil or blank sheet can be surrounded with a layer of any desired material, be it as a diffusion barrier or as a cladding. It means thirdly, that bonding between the different layers is not a problem at all, because the layers will have the maximum physically possible adhesion to each other.

As a proof of principle for this two-step process a small DC-magnetron sputtering device has been built and operated at the TUM Institute for Radiochemistry. In a first experiment with this setup we could reach a deposition rate for DU8Mo (depleted U with 8wt% Molybdenum) of 5 $\mu\text{m}/\text{h}$. X-ray diffraction (XRD) of the sample showed that the favoured UMo γ -phase has been produced.

In parallel a large sputtering plant for the production of full size plates was mounted inside a glove box to enable operation under inert atmosphere (1.3). The inert atmosphere guarantees, that the concentration of oxygen during the production of foils, barrier layers or cladding and even during handling of the material is always below 10ppm, which results in a nearly complete suppression of oxidation and oxide layer formation in all process steps. This sputtering plant is currently installed in a radioisotope laboratory and will be ready for operation within the next weeks.

A full R&D program has now been defined between TUM and AREVA-CERCA.

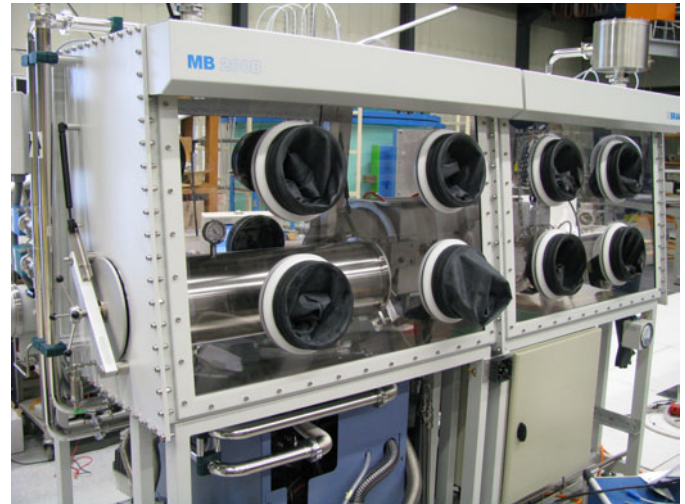


Figure 1.3.: DC-magnetron sputtering plant for foil production and barrier / cladding deposition in full size.

Exploring new materials combinations for high density fuels by heavy ion bombardment

In 2006 our consortium has shown, that it is possible to grow the IDL out-of-pile using ^{127}I at 80MeV within some hours without activating the samples (1.4). Since then big progress has been made to improve the reliability of this method. We have build up a complete new irradiation setup at the tandem accelerator Maier-Leibnitz Laboratorium in Garching (MLL) which allows monitoring and controlling the irradiation conditions like flux, fluency, as well as vacuum and sample temperature automatically. The new setup allows the irradiation of up to 8 samples without opening the vacuum chamber.

In principal there are three possibilities to overcome the formation of the undesired IDL at the UMo-Al interface:

- Addition of a diffusion limiting element to the Al-matrix containing the UMo particles (e.g. Si, Ti, Bi)
- Creation of a ternary UMo alloy by adding another element (e.g. Nb or Pt)
- Insertion of a diffusion barrier between the interface UMo-Al (e.g. a thin layer of Zr or a UO_2 layer)

AREVA-CERCA has provided in total 21 different dispersed UMo-Al samples for testing all of those approaches. The first batch of samples consists of 7wt%Mo particles dispersed in an Aluminum matrix which contains different concentrations of a second element (e.g. 2wt%Si, 5wt%Si, 2wt%Bi, 5wt%Bi). Each of those samples has been produced with and without an UO_2 layer at the interface UMo-Al as a diffusion barrier. The second batch of samples consists of 4 different ternary UMo alloys dispersed in a pure Aluminum

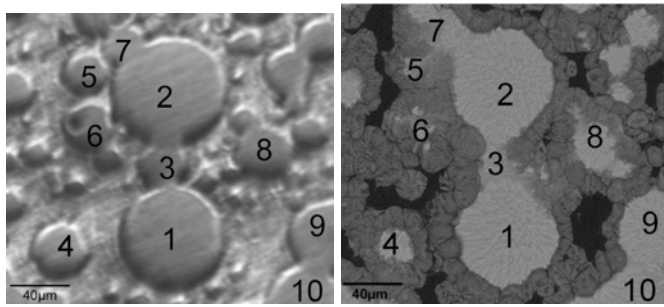


Figure 1.4.: OM (left) and SEM (right) picture of samples before and after irradiation by 80 MeV ^{127}I . The formation of the interdiffusion layer is clearly visible.

matrix. Meanwhile all samples have been irradiated at the MLL with 80 MeV ^{127}I and are currently examined at TUM by X-ray diffraction, optical and scanning electron microscopy. The aim is to find the most promising material combination for a future in-pile test.

In 2008, it has been found that the IDL of in-pile irradiated U7wt%Mo/Al samples consists of an amorphous U-Al compound. In contrast, in 2007 it has been found that the IDL of in-pile irradiated UMo/Al samples consists mainly of UAl_3 . Up to now, the IDL formed during heavy-ion bombardment was found to consist of UAl_3 . Therefore an experimental campaign has been started to determine the irradiation conditions which lead to the formation of an amorphous and a crystalline IDL, respectively. For this reason we have irradiated 10 U7wt%Mo/Al samples provided by AREVA-CERCA at different conditions (temperature, angle of the incoming ion beam, fluency). Post irradiations examinations to specify the composition of the IDL created during heavy-ion bombardment are underway at CEA-Cadarache and at the beamline ID22 at ESRF which provides intensive X-ray radiation at a 100 nanometer scale.

A further prerequisite for using UMo as a future fuel in research reactors is precise knowledge of its thermal conductivity and in particular its change in the course of burn-up. The specific heat capacity of cast U8Mo was determined by differential scanning calorimetry, its thermal diffusivity was measured by the laser flash method and its mass density by Archimedes' principle. From these results, the thermal conductivity of U8Mo in the temperature range from 40 °C to 250 °C was calculated (1.5). It shows good accordance with the literature data for UMo with 8 and 9 wt.-% Mo, is higher than for 10 wt.-% Mo and lower than for 5wt.-% Mo in the measured temperature range. The electric conductivity of rolled and cast U8Mo was measured by a four-wire method and the electron based part of the thermal conductivity calculated by the Wiedemann-Frantz law. Rolled and cast U8Mo was irradiated at about 130 °C with 80 MeV ^{127}I ions to receive the same iodine ion density in the damage peak region as the fission product density in the FRM II fuel after the targeted nuclear burn-up. XRD anal-

ysis of rolled samples reveals the tetragonal lattice structure. XRD of the irradiated U8Mo showed a change of the lattice parameters as well as the creation of UO_2 in the superficial sample regions, but no phase change by irradiation was observed. Yet, the determination of the electron based part of the thermal conductivity of the irradiated samples failed due to high measurements errors which are caused by the low thickness of the damage region in the ion irradiated samples.

Combined calculation of the neutronics and thermohydraulics of a high density core at FRM II

TUM reported on new coupled neutronics/ burnup/ thermohydraulics calculations for evaluating the temperature evolution in the fuel during the operation of a FRM II fuel element. With respect to irradiation resistance this is an aspect of highest interest. The results show clearly a decrease in maximum temperatures in the fuel with the fuel element burnup. Those calculations are based in a vast variety of classical modules and use a cylindersymmetrical model of the FRM II core. Those calculations are a main reference for any further developments.

With new computer capabilities there is in general an increasing demand for 3-dimensional results with high spatial resolution. This is particularly true for nuclear reactor physics, both for neutronics as well as for thermohydraulic problems. To address this for the calculations of a new fuel element for FRM II, a new coupled calculation system is currently under development. It combines MCNPX, a well known Monte Carlo Code for the neutronics and CFX, a commercial 3d-CFD (Computational Fluid Dynamics) code for the thermohydraulics. Both codes are state-of-the-art codes in their fields.

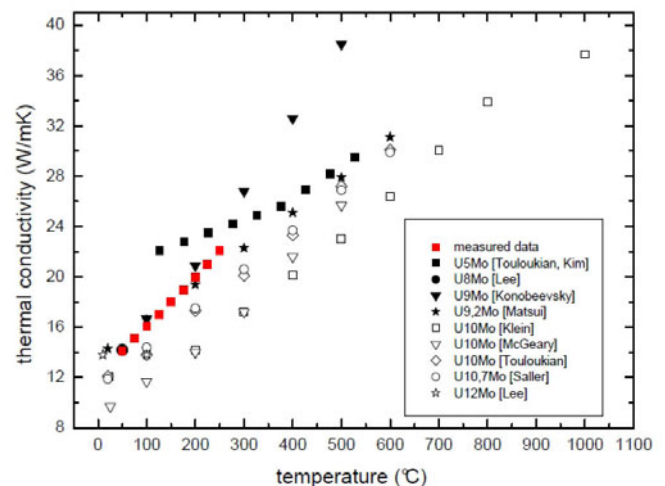


Figure 1.5.: Thermal conductivity of UMo: literature and measured (red) values.

In the Monte Carlo (MC) simulation, all necessary particles including delayed gammas were included to get the distribution of the energy deposition as accurate as possible. A cylindrical mesh with 13.200 cells was superimposed on the geometry of the core to define a grid for this. Several million particles were simulated to reduce the statistical error in the local energy deposition to less than 1% for all of these cells.

Due to computational limitations of the thermohydraulic CFX calculation, a separate model had to be set up for the neutronic side, the MC simulation. The CFX model takes advantage from the cylindrical symmetry of the FRM II core and therefore includes only a small extract from the MC model. Especially the CFD model was constructed to include every single detail of the real geometry in order to resemble the flow as close as possible. Consequently, a mesh consisting of more than half a million nodes was used for the subsequent calculations with conjugate heat transfer in CFX. As only one fuel plate was regarded, the influence of the installations in the D₂O tank was averaged in the MC calculations in order to maintain the cylindrical symmetry.

The resulting heat distribution in the fuel plate was averaged in 64 cells for each fuel and cladding and then reimported into MCNPX to account for different material temperatures and the effect on the neutronics calculation. This was achieved by stochastic interpolation with a square root-weighting between material libraries for different temperatures that were precompiled using NJOY. Both codes, MCNPX and CFX, are linked via a set of Perl-scripts and a proprietary FORTRAN interface.

In a first step, calculations were made for the current fuel element. Final convergence was achieved after only two full calculational cycles. All values like maximum temperature, temperature distribution, heat flux, pressure drop and others are in good agreement with those calculated formerly at evaluating the FRM II with the more classical approaches. The system presented here provides a much larger variety of flow property details (1.6). By solving the Navier-Stokes equations, CFX resolves yet unknown details of the flow in the cooling channels of the compact core. The agreement mentioned beforehand can be seen as a first validation of the code system. Next steps will include the evaluation of possible future fuel elements with UMo fuel.

[1] **van den Berghe S., et al.**

Transmission electron microscopy investigation of irradiated U7 wt%Mo dispersion fuel.

J. Nucl. Mater., **375**, (2008), 340-346.

[2] **Breitkreutz H., Röhrmoser A., Petry W.**

3-dimensional coupled neutronic and thermohydraulic calculations for a compact core combining MCNPX and CFX.

ANIMMA 2009, Marseille.

[3] **Böning K., Petry W.**

Test irradiations of full sized U₃Si₂ – Al fuel plates up to very high fission densities.

Journal of Nuclear Materials, **383**, (2009), 254–263.

[4] **Hengstler R.**

Thermal and Electrical Conductivity of a Monolithic Uranium – Molybdenum Alloy for Research Reactor Fuels.

Master's thesis, Technische Universität München (2008).

[5] **Hengstler R., Bogenberger C., Breitkreutz H., Jungwirth R., Petry W., Schmid W., Gradel G., Wieschalla N., Schmahl W., Schneider J., Beck L., Carli W., Jarousse C.**

Physical properties of monolithic U8Mo.

RRFM 2009, Vienna.

[6] **Jarousse C., Halle L., Petry W., Jungwirth R., Röhrmoser A., Schmid W.**

FRM II and AREVA-CERCA common effort on monolithic UMo plate production.

RRFM 2009, Vienna.

[7] **Leenaers A., van den Berghe S., Anselmet M., Noiret J., Lemoine P., Röhrmoser A., Petry W.**

Irradiation behavior of atomized and ground U(Mo) dispersion fuel.

Transactions of RERTR 2008 - 30th International Meeting on Reduced Enrichment for Research and Test Reactors, 5 - 9 October, 2008, -, (2008), -.

[8] **Palancher H., Welcomme E., Martin P., Valot C., Bleuët P., Tucoulou R., Lemoine P.**

Advances in the characterization of annealed atomized UMo/Al particles using synchrotron radiation.

RERTR 2008, Washington.

[9] **Palancher H., Wieschalla N., Martin P., Tucoulou R., Sabathier C., Petry W., Berar J.-F., Valot C., Dubois S.**

Uranium-molybdenum nuclear fuel plates behaviour under heavy ion irradiation: An x-ray diffraction analysis.

Journal of Nuclear Materials, **385**, (2009), 449–455.

[10] **Petry W., Röhrmoser A., Boulcourt P., Chabre A., Dubois S., Lemoine P., Jarousse C., Falgoux J. L., van den Berghe S., Leenaers A.**

UMo full size plate irradiation experiment IRIS-TUM a progress report.

Transactions of the RRFM 2008, Hamburg, Germany, March 2008.

[11] **Ripert M., Dubois S., Noiret J., Lemoine P., van den Berghe S., Leenaers A., Röhrmoser A., Petry W., Jarousse C.**

Overview on high density UMo fuel in-pile experiments in OSIRIS.

Transactions of the RRFM 2008, Hamburg, Germany, March 2008.

- [12] **Röhrmoser A., Petry W.**
Fuel plate temperatures during operation of FRM II.
 Transaction of RRFM 2009, March, 23 - 25, Vienna, Austria, -, (2009), 7.
- [13] **Schmid W., Jungwirth R., Petry W., Böni P., Beck L.**
Manufacturing of thick monolithic layers by DC-magnetron sputtering.
 Transactions of the RRFM 2008, Hamburg, Germany, March 2008, -, (2008), 4.
- [14] **Schmid W., Jungwirth R., Petry W., Böni P., Beck L.**
- [15] **Welcomme E., Palancher H., Sabathier C., Martin P., Allenou J., Valot C., Charollais F., Anselmet M., Jungwirth R., Petry W., Beck L., Jarousse C., Tucoulou R., Lemoine P.**
Heavy ion irradiation of UMo7/Al fuel: methodological approach.
 Transactions of RRFM 09, Vienna/Austria, March 22 - 25, 2009, accepted, -, (2009), -.
- Manufacturing of thick monolithic layers by DC-magnetron sputtering.*
 Transactions of the RRFM 2008, Hamburg, Germany, March 2008, -, (2008), 4.

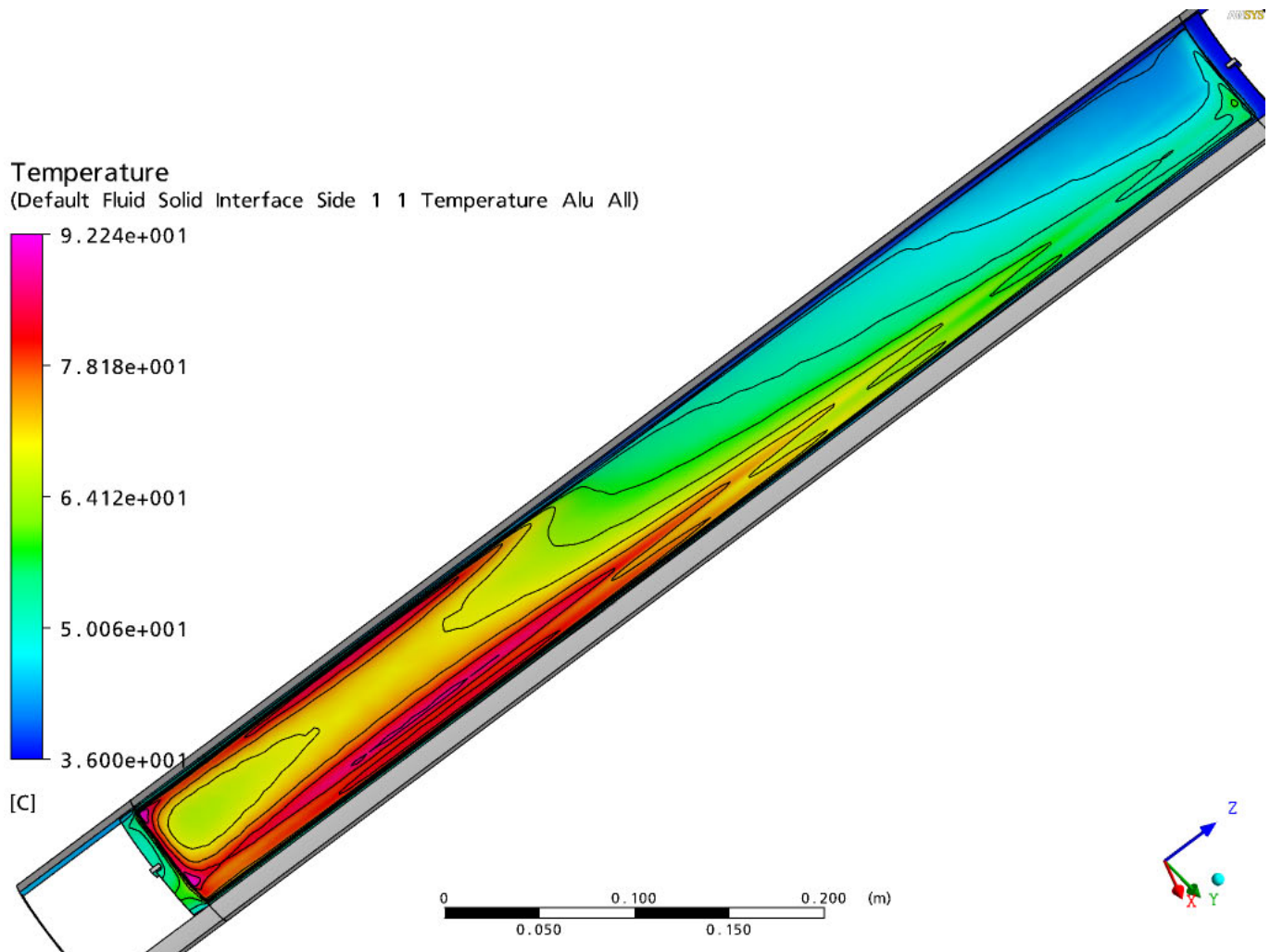


Figure 1.6.: Distribution of temperature on the surface of a fuel plate.

1.3. Detector and electronics lab: Fast high resolution detectors developed

I. Defendi¹, C. Hesse¹, M. Panradl¹, M. Petertill¹, T. Schöffel¹, K. Zeitelhack¹

¹ZWE FRM II, TU München

Laboratory infrastructure

Two important laboratory infrastructure projects could be completed in 2008. In the gas detector lab a new semi-automatic pumping and pure gas filling station for ³He-based neutron detectors was brought into operation. It is part of the program to investigate the performance of all ³He-based 2D-detectors (so called multi-wire proportional chambers: MWPCs) operated at FRM II neutron scattering instruments. The program aims to optimize their performance eventually requiring a refill of gas. This way the detection efficiency of the 2D-detector operated at *STRESS-SPEC* e.g. could be increased by more than 25%. In 2009 we aim to add a gas recovery and cleaning system to the filling station to recycle the expensive ³He filling of the detectors. This will allow a frequent performance scan of the detectors in use and their permanent optimization at reasonable costs.

Beginning of 2008 we completed the new detector test beam station installed at the instrument *TREFF* on beam line NL5 in the neutron guide hall. Equipped with a Graphite double monochromator and a cooled Be-filter *TREFF* provides a well collimated high quality $\lambda = 4.74\text{\AA}$ neutron beam in a wide dynamic intensity range. The new detector test beam station allows the precise efficiency calibration of detectors and monitors and the investigation of their rate capability. In addition, it has been specifically designed for the detailed study of the performance of 2D-position sensitive detectors. The test

bench consists of an air pad based movable arm which is coupled to the *TREFF* sample table instead of the *TR-EFF* second arm. It carries a set of adjustable apertures for proper beam collimation and intensity setting and a computer controlled x-y table driven by precision linear stages. In this way, 2D-detectors can be automatically scanned with a well collimated beam in horizontal ($\Delta x = 1000\text{ mm}$) and vertical ($\Delta y = 300\text{ mm}$) direction with $20\ \mu\text{m}$ precision. The test bench integrates a flexible detector electronics and data acquisition system and allows a compact and versatile test environment. Figure 1.7 shows a photograph of the new test beam station during a rate capability test with the *SANS1* prototype detector consisting of an array of eight 1 m long position sensitive detectors (PSDs).

New projects and upgrades

Apart from our standard service and maintenance activities three outstanding projects dominated the activities of the detector group. During summer we completed the design of the new $1 \times 1\text{ m}^2$ active area 2D-detector of the new small angle scattering instrument *SANS1* being installed in the neutron guide hall. As reported in detail in [1] it consists of a linear array of 1 m long position sensitive ³He detectors with 8 mm diameter each mounted on a rail system inside the 22 m long evacuated flight tube. The individual detectors will be read out by an advanced version of the *mesytec PSD8+* system providing address, position, pulse height and time stamp in list mode data. Figure 1.8 shows a schematic drawing of detector with the linear array of 128 PSDs and the electronics compartment mounted on the rear side of the detector. At present the complete system is under assembly in the detector laboratory. After passing first performance tests it shall be mounted into the *SANS1* flight tube in March 2009.

The detector system of the time-of-flight instrument *TOFTOF* presently consists of 605 detectors (*Dextray* squashed series) filled with 10 bar ³He and 40 cm active length each. They are mounted in 4 rows in an array of 8 racks which is capable to finally carry 1005 detectors. Within the forthcoming upgrade of *TOFTOF* 410 additional detectors have been purchased to fill up the array and cover the complete detectable solid angle. All detectors have been investigated with respect to the performance of gain, detection efficiency and background count rate prior to their foreseen implementation into *TOFTOF*.



Figure 1.7.: *SANS1* prototype detector consisting of 8 PSDs mounted on the x-y scanning table of the new detector test beam station at *TREFF*.

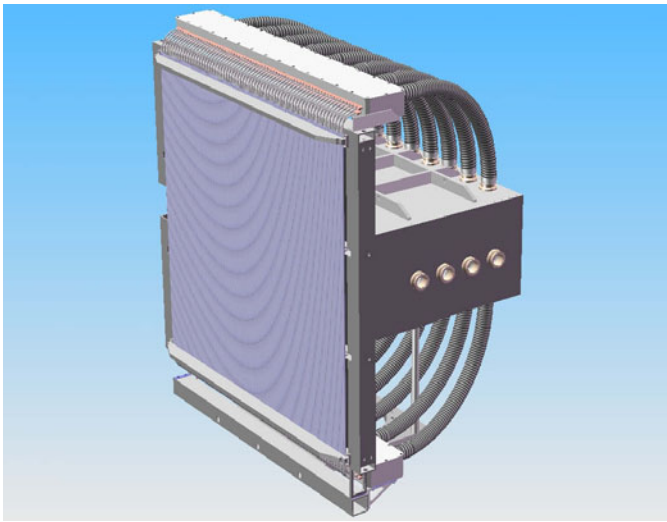


Figure 1.8.: Schematic drawing of the $1 \times 1 \text{ m}^2$ active area 2D-detector of the new SANS1 instrument. It consists of a linear array of 128 1 m long ^3He -PSDs mounted on a rail system inside the 22 m long flight tube.

The detector group was strongly involved in the joint European programme Integrated Infrastructure Initiative for Neutron Scattering and Muon Spectroscopy Joint Research Activities-2 (NMI3-JRA2) Millimetre Resolution Large Area Neutron Detector (MILAND) project dedicated to the development of a fast, high resolution ($\Delta x \approx 1 \text{ mm}$) 2D neutron detector based on a MWPC with 320×320 individual channel readout. In 2008 we finished the development of a 320×320 channel signal processing electronics based on the layout and the results already presented in [2]. Taking advantage of the Time-over-Threshold (ToT) information of each individual

readout channel the systems provides 2D-position and time stamp information for each detected neutron. Together with the final MILAND detector shown in Figure 1.9 the system was tested for the first time in April with a collimated $\lambda = 2.5 \text{ \AA}$ neutron beam at ILL test beam station CT2. A position resolution with high linearity and a width of $\Delta x = \Delta y \approx 1.3 \text{ mm}$ (FWHM) and a global rate capability of 800 kHz at 15% dead time coming closing to the MILAND specifications could be achieved. The MILAND detector revealed excellent efficiency homogeneity of 3% (anode readout) and 5% (cathode readout) without any calibration.

[1] Defendi, I., et al. *FRM-II annual report 2007*, 10–11.

[2] Defendi, I., et al. *FRM-II annual report 2006*, 8–9.

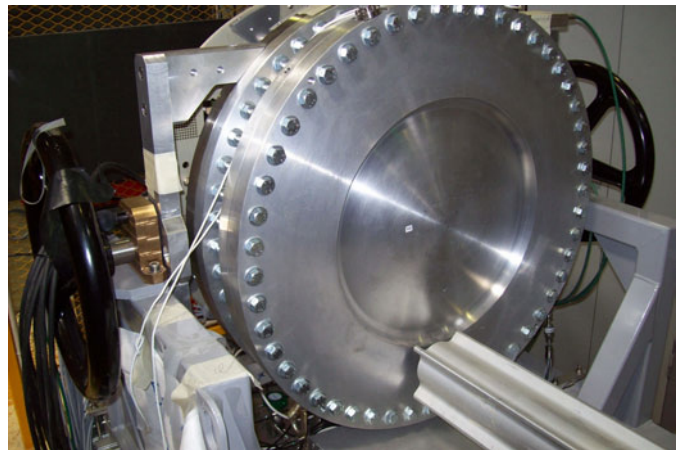


Figure 1.9.: The MILAND detector equipped with the 320×320 channel signal processing electronics developed at FRM II during the performance test at the ILL beam station CT2.

1.4. Irradiation facilities: 10 tons of doped silicon

X. Li¹, H. Gerstenberg¹, J. Favoli¹, V. Loder¹, J. Molch¹, A. Richter¹, H. Schulz¹, T. Schait¹

¹ZWE FRM II, TU München

General

The irradiation service of the FRM II continued its routine operation successfully during the five reactor operation cycles in 2008. Almost 800 irradiations were carried out for different commercial purposes and research projects on our facilities. Table 1 shows the irradiation batches on each irradiation system. After the successful start in 2007, the production of the neutron transmutation doped silicon (NTD-Si) has doubled in 2008. With a total amount of 9800 kg of doped silicon, the goal of 10 tons per year is almost reached. Beside this big business, irradiation of samples for nuclear medicine and geological dating was arranged at the second place with more than 100 batches. With our contribution, the shortage of isotopes for the nuclear medicine could be reduced. A feasibility study of the production of Molybdenum-99 has already begun. The radioisotope is used both in therapy and diagnosis of cancer.

We started a project to design a new irradiation facility between and within the spent reactor fuel elements of the FRM II in 2008. The very strong gamma-radiation can be used for many irradiation applications, for example the study of microstructures in halite. Some measurements were performed to attain information about the gamma-intensity within and between the spent fuel elements. Furthermore, we continued in 2008 our neutron activation analysis for applications in industry, scientific research and education.

Production of isotopes for the nuclear medicine

An interesting project for the nuclear medicine is the optimization of an effective production of the radioactive isotope ¹⁷⁷Lu, which may help create the first successful radiopharmaceutical for solid tumors. ¹⁷⁷Lu emits a low beta energy, which reduces radiation side effects and produces a tissue-penetration range appropriate for

smaller tumors. 14 samples were irradiated on our capsule irradiation system (KBA). The irradiation time averaged 14 days. The samples could be delivered to the hospital within 3 days after a successful radiochemical separation of Yb/Lu in ITM (Isotopen Technologien München AG). In order to improve the through-put, a software update on the control system of the KBA was tested and approved by the regulating authority. With this update, multi-sample-irradiation in the irradiation tubes can be operated on the KBA.

The goal of the project BetaMo supported by the Bavarian science foundation and in cooperation with the Physics Department of the Ludwig-Maximilians-Universität München as well as some clinics is the development of radioactive implants for a possible application in medicine, above all for the wound healing process after inflammations and operative procedures. Suitable radioactive radiation can have positive influence on the healing process. The irradiation conditions for such samples producing the pure beta-ray source ³²P were optimized. A routine irradiation for the nuclear medicine is already scheduled.

Irradiations for the fission track dating

About 100 apatite samples from different geological institutes were irradiated in our irradiation channels in 2008 for the fission track dating of geological substances. This method is a radiometric dating technique based on analysis of damage trails, or tracks, left by fission fragments in certain uranium bearing minerals and glasses. The number of tracks correlates directly with the age of the sample and the uranium content. To determine the uranium content, the sample is annealed by heating and exposed to a barrage of thermal neutrons [1]. Due to the high uranium content in the geological samples, the samples were irradiated usually in the position SDA-1 with a relatively low neutron flux between 1×10^{15} and 1×10^{16} cm⁻², which was achieved within few minutes.

New gamma-irradiation facility within and between the spent fuel elements

In order to use the very strong gamma radiation between and within the spent fuel elements, located in the storage pool, as supplementary irradiation source at FRM II, a new facility was designed in 2008. For a special joint research project together with the geology institute of the University of Aachen (RWTH Aachen), halite samples will be irradiated in this system. The samples will be heated up to 150 °C during the entire irradiation, which lasts for

Table 1.1.: Irradiation batches at the FRM II in 2008.

position	irradiation No.
RPA	88
KBA	56
SDA	529
AS/SDA1	105
total	778
total time	8002 h

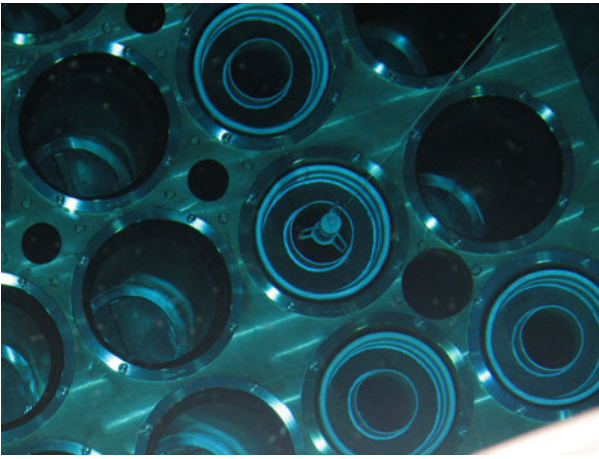


Figure 1.10.: Gamma irradiation positions within and between the spent fuel elements in the storage pool.

weeks. Gamma-radiation can decorate the microstructures in halite. The technique is based on the inhomogeneous distribution of colouring induced by irradiation of the samples with high doses of gamma-rays at approximately 100 °C. Coloured thin sections show a surprisingly rich detail of microstructure (grain, subgrain boundaries, zonation) which can be used to obtain information on the deformation, recrystallization and fluid transport processes in the samples [2]. In this context, gamma intensity and its axial distribution in the centre of some spent fuel elements of the FRM II with different cooling times were measured. Fig 1.11 shows the change of the dose rate dependent on the cooling time and Fig 1.12 shows the axial distribution of gamma intensity within two spent fuel elements. In order to get information of neutron intensity in the irradiation place, gold foils were activated through long time irradiation. The maximal flux of about $3500 \text{ cm}^{-2}\text{s}^{-1}$ was measured in an element with cooling time of 90 days. The value decreases to $250 \text{ cm}^{-2}\text{s}^{-1}$ after 450 days of cooling. The design of this facility will be verified by the TÜV in the beginning of 2009.

Neutron activation analysis (NAA) at FRM II

Some interesting samples from the industry and research institutes were analysed by using the neutron activation analysis (NAA) in our group. This method is a very precise analysis method for the determination of trace elements. Railway brakes made by different manufacturers were analysed, in order to get the information about the characteristic element compositions of the material. To determine the so-called boron equivalent value of graphite, very pure graphite samples were analysed. 40 different elements could be measured by using the NAA. Complementally, some light elements were analysed by using the prompt gamma neutron activation analysis GP-NAA at FRM II [3]. For example, we started a study to

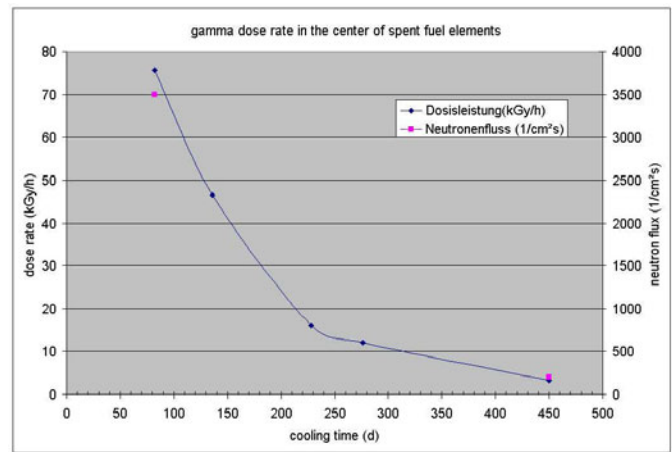


Figure 1.11.: Gamma dose rate and neutron flux within spent fuel elements of the FRM II.

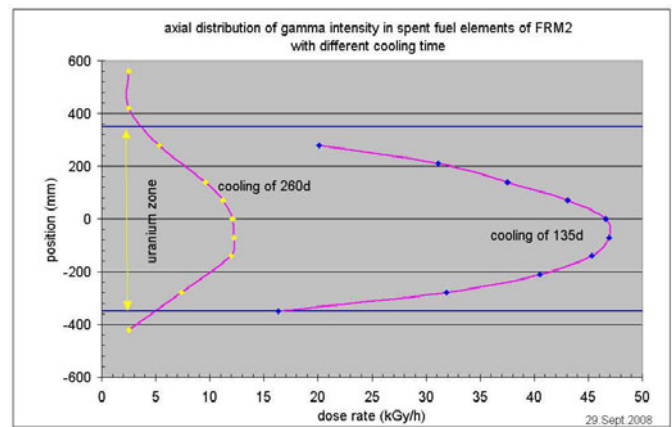


Figure 1.12.: Axial distribution of gamma intensity within two spent fuel elements with different cooling time.

determine two rare isotopes of Ce (namely Ce-136 and Ce-138) in urine samples of human beings, in order to quantify their metabolic pathways. The analysis method will be optimised by changing the irradiation conditions in the next steps. Furthermore, a new gamma-counting place will be set up close to the reactor hall in the spring of 2009.

Silicon doping facility (SDA)

The silicon doping for commercial production has increased rapidly in the last years. The doping work had already begun by using a prototype facility (SDA-opt) at the end of 2005. In 2006 almost 3 tons silicon ingots were irradiated. After the successful commissioning of the new semi-automatic facility, about 4 tons silicon ingots were doped in 2007. With two-shift operation in 2008, the goal of 10 tons per year was almost attained. We entered into a business relationship with seven companies from Europe and Asia. With the quick development in the semi-conductor industry, more and more big

size ingots were irradiated. The current most ingot sizes are 6 and 8-inches. The typical target resistivities are between $22 \Omega \text{ cm}$ and $1050 \Omega \text{ cm}$. One batch with an extremely low target resistivity of $12 \Omega \text{ cm}$ was irradiated in 2008. The doping result was also very satisfying.

In order to control the neutron flux at the irradiation position, 4 SPN-Detectors are mounted in the irradiation tube. The position of the special nickel-absorber liner is changed to compensate the burn-up effect of the fuel element and the movement of the control rod during reactor cycle. Figure 1.14 shows the change of the local neutron flux dependent on the position of the reactor control rod. The smooth run of the curves shows, that our adjustment of the Ni-liner is very effective [4].

[1] Glasmacher, U. A., Wagner, G. A., Puchkov, V. N. *Technophysics*, 354, (2002), 25–48.

[2] Urai, J. L., *et al. Nature*, 324, (1986), 554p.

[3] Li, X., *et al. In: Proceedings of saagas22 (2009)*.

[4] Li, X., *et al. Appl. Radiat. Isotopes*, (2009). In press.



Figure 1.13.: A silicon crystal after the doping.

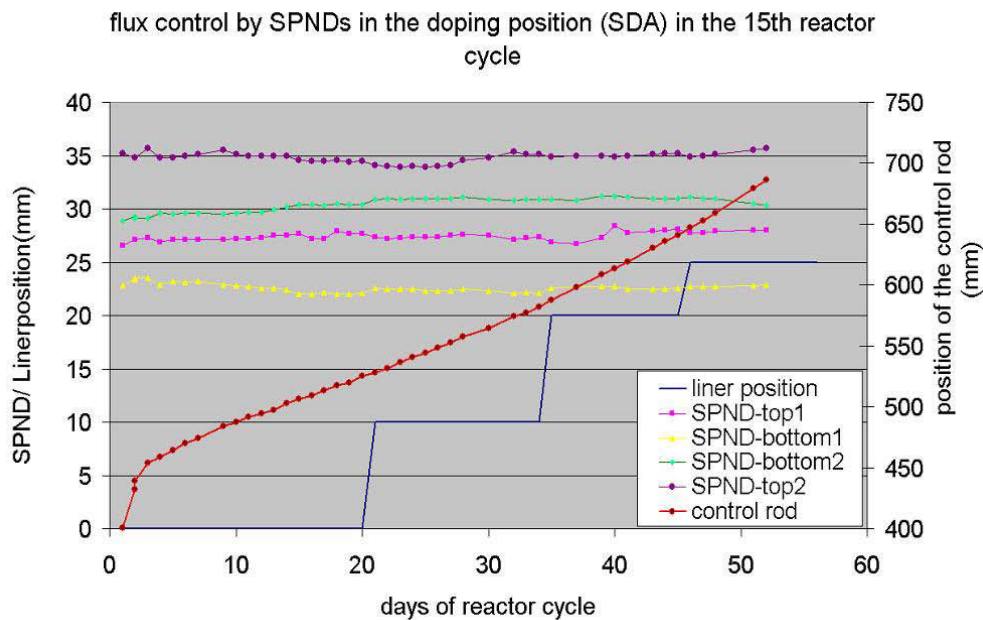


Figure 1.14.: Neutron flux control by SPN-Detectors at the doping position.

1.5. Sample environment: Solutions for the cold and the hot

P. Biber¹, H. Kolb¹, J. Peters¹, A. Pscheidt¹, A. Schmidt¹, J. Wenzlaff¹, M. Wiesheu¹

¹ZWE FRM II, TU München

Shape memory alloy heat switch

For many experiments, e.g. phonon dispersion measurements or soft matter experiments, a wide sample temperature range is requested. It is desirable to cover it in one run without interchanging low and high temperature sample environment devices. Using a high temperature sample holder the FRM II cryogenfree top loading cryostat CCR allows for sample temperatures from 3 K to 800 K.

Alternatively a self-acting heat switch based on shape memory alloy elements was developed for closed cycle cryostat applications. The standard temperature range of a coldhead spreads from 2 K to 300 K. Exceeding room temperature malfunction or severe damage of seals or displacer may occur. The self-acting heat switch breaks the piston type thermal connection of the sample holder to the second stage of the coldhead. It is based on a NiTi shape memory alloy spring which generates a force of 99,39 N at 2 °C. The restoring force necessary to remove the piston at $T > RT$ is minimum 50 N and realized by a steel spring generating a force of 91,4 N. Figure 1.15 shows a section of the switch. Figure 1.16 shows a typical switching characteristic. Even at sample temperatures about 700 K, the coldhead temperature is far off any critical value.

Sample temperature is controlled via a cartridge heater and temperature sensor placed in the sample plate. The robust design provides a fail-save operation as well as stable and easy handling. However the weak thermal coupling of the sample and coldhead results in a longer cool down time (figure 1.17) compared to a pure low temperature application.

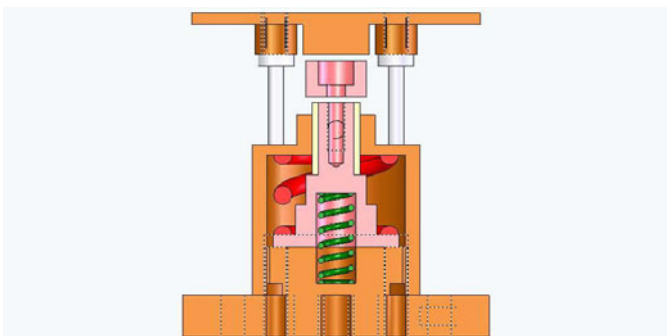


Figure 1.15.: Cross-sectional view of SMA-switch.

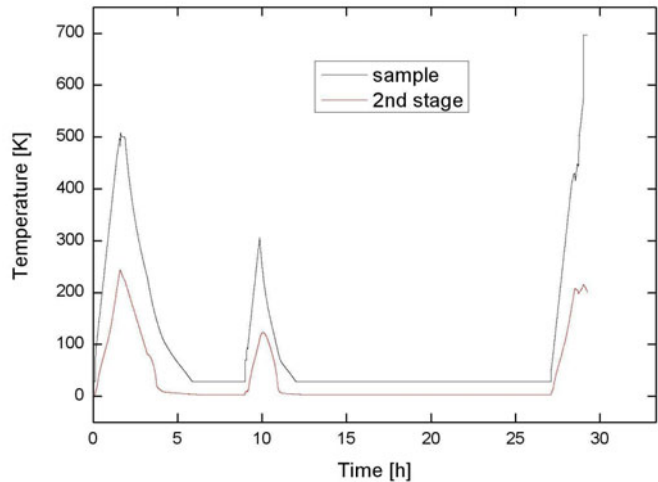


Figure 1.16.: Switching characteristics: coldhead temperature is well below room temperature.

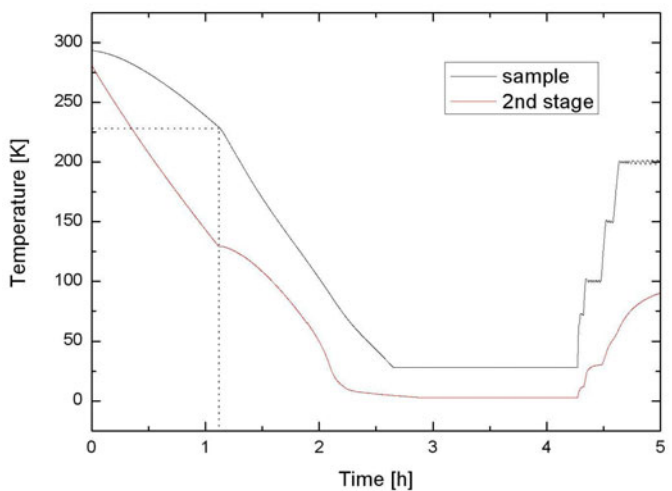


Figure 1.17.: Cool down with SMA switch. The 30 K cutoff of the sample sensor is due to the PT sensor calibration.

High temperature furnace for the 7,5 T magnet

Initiated by a experimental request, a high temperature furnace (HTF) fitting the FRM II 7,5 T cryogen free magnet has been constructed and tested (figure 1.18). Operation takes place via our standard HTF control rack. The maximum temperature is about 2000 K. The maximum available sample dimensions are 15 mm of diameter and 30 mm of height.

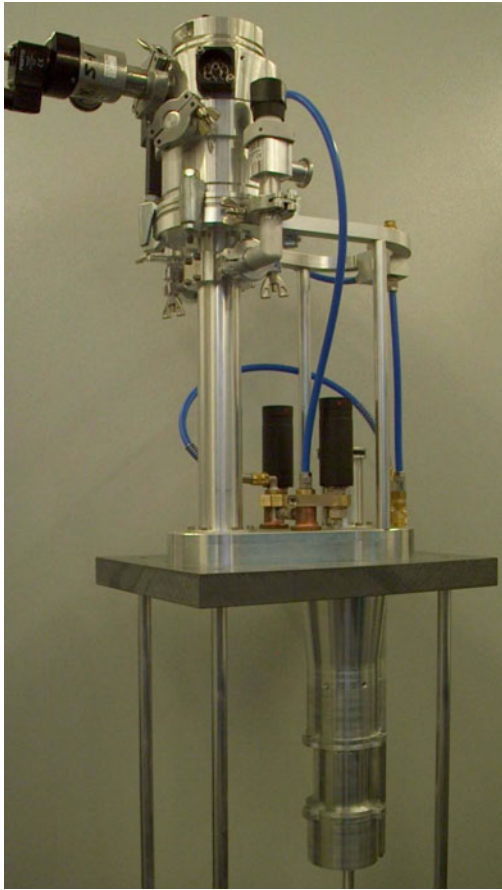


Figure 1.18.: High temperature furnace for the 7,5 T magnet.

1.6. HELIOS – polarized ^3He gas for neutron instrumentation

S. Masalovich¹, O. Lykhvar¹, H. Schölderle¹, G. Borchert¹, W. Petry^{1,2}

¹ZWE FRM II, TU München

²Physik-Department E13, TU München

Polarized ^3He Neutron Spin Filters (NSF) have a great impact on the instrumentation for neutron polarization and polarization analysis since polarized nuclei of ^3He possess very high spin-dependent neutron absorption efficiency over a wide range of neutron energies. The straight-line passage of a neutron beam through a NSF with no change of a neutron trajectory enables one to measure a neutron polarization for nearly any divergent scattered beam. Furthermore, the NSFs offer homogeneous analyzing efficiency with a predictable value, predictable transmission, a negligible small angle scattering from a ^3He cell and a low gamma-ray background produced. Taken together, these features make NSF technique extremely useful in applications such as neutron imaging with polarization analysis, small-angle neutron scattering, off-specular reflectometry and large solid angle polarization analysis. When necessary, NSF allows for a very precise measurement of a neutron beam polarization either with an opaque spin filter or with a recently proposed 2x1 NSF. Obviously, the ^3He NSFs have great potential in neutron instrumentation.

One hundred NSF cells have been polarized in 2008. They were used in part for internal tests, but basically in neutron experiments at FRM II. The total measurement time with the use of the NSFs was about 70 beam-days and we expect this time to grow in the year 2009. The demand for the ^3He NSFs is illustrated in Fig. 1.19.

Experimental results

In 2008, ^3He NSFs were used in the measurements performed at HEIDI, MEPHISTO, MIRA, TREFF, N-REX+ and ANTARES. Some examples are presented below.

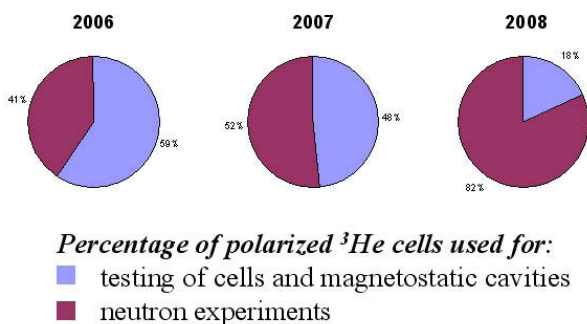


Figure 1.19.: The proportion of the ^3He NSFs used in neutron experiments in 2006-2008.

N-REX+

The grazing incidence small angle neutron scattering (GISANS) at the N-REX+ instrument was applied to study the sample of multilayer $[\text{Fe}/\text{Au}]_{10}$. The aim was to 'separate' the magnetic and structural roughness and to study the magnetic ordering in the layers as a function of an applied magnetic field. The ^3He NSF was used as an analyzer since it provides a uniform analyzing efficiency for an entire neutron scattering pattern with no requirement for readjustment. Hence, both specular and off-specular components of the scattered neutron beam can be analyzed in one measurement. In Fig. 1.20 the scattering pattern measured without polarization analysis (a) is compared with the pattern measured with the use of a ^3He NSF analyzer (b). In this particular example, the demagnetized sample (as received) shows Yoneda scattering (a), while when magnetically aligned, the Yoneda scattering is missing (b). This confirms the presence of the domain structure in the demagnetized sample and that this structure plays an important role in off-specular scattering.

ANTARES

A study on the spatial homogeneity of the atomic concentration in the NbFe_2 samples has been performed at the neutron radiography/tomography instrument ANTARES. The image showing the distribution of the atomic concentration was observed directly by measuring the neutron polarization distribution in the beam passed through the sample enclosed in a cryostat. The measurement is based on the fact that the Curie tem-

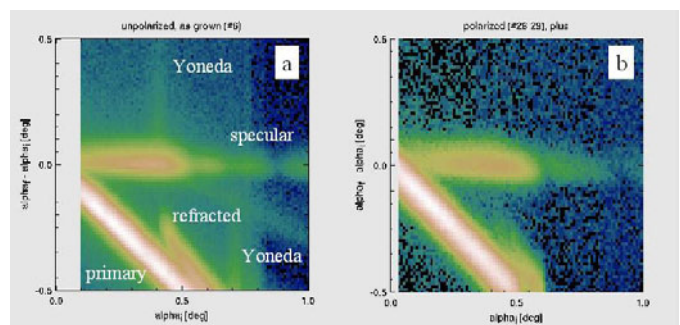


Figure 1.20.: Neutron scattering patterns measured for (a) unpolarized neutron beam incident on a demagnetized sample $[\text{Fe}/\text{Au}]_{10}$ and (b) polarized neutron beam incident on a magnetically aligned sample [M. Major, A. Rühm, J. Major, H. Dosch].

perature (T_c) of a NbFe_2 alloy depends crucially on the variation in concentration of elements. Fluctuations in concentration result in fluctuations of the local T_c in the sample volume. Hence, at a given temperature, the sample may be partially ferromagnetic and partially paramagnetic. Observation of the depolarization of the neutrons passed through the ferromagnetic regions allows one to estimate the Curie temperature distribution at a given temperature. Two ^3He NSF's were used at the same time during the measurement. The first one was located before the sample with the aim to polarize an incident neutron beam and the second one was used after the sample for the polarization analysis. The images in Fig. 1.21 show some examples of the measured polarization distribution and estimated Curie temperature distribution.

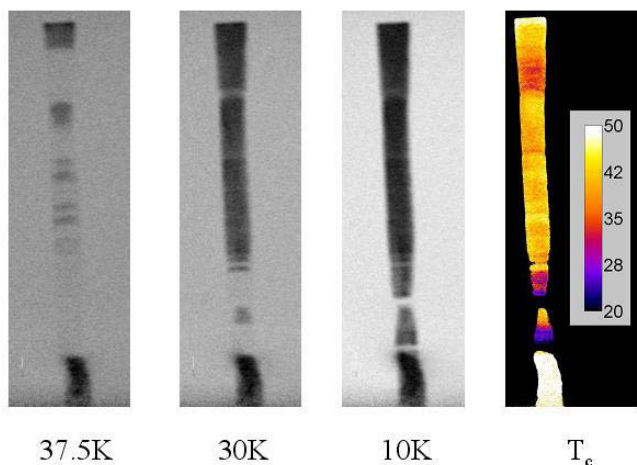


Figure 1.21.: Images of the polarization distribution in the neutron beam when passed through the NbFe_2 sample (vertical cylinder) at different temperatures. The neutron polarization is gray-color-scaled from minimum (black) to maximum (white) value. The rightmost image shows the estimated distribution of the T_c in the sample [M.Schulz, B.Schillinger, E.Calzada].

^3He NSF with ^3He spin-flip option

NSF with ^3He spin-flip option developed at the Institut Laue-Langevin (ILL) [1] has been tested at the instrument MIRA and is available now for neutron experiments at FRM II. This technique is based on the fast inversion of the ^3He spins in a NSF cell with the help of a short radio frequency pulse applied to a coil integrated into the magnetostatic cavity where the NSF is located. The gas polarization losses during this spin-flip have been estimated experimentally to be about 10^{-4} over the 10cm diameter NSF cell. Thus this device enables nearly ideal flipping of the ^3He gas polarization and hence nearly ideal flipping of the polarization of the neutron beam passed through a NSF-polarizer. In case of a NSF-analyzer this technique enables one to perform a polarization analysis without affecting the measured beam polarization and beam geometry since no other spin-flipper devices are required.

[1] E.Babcock, A. Petoukhov et al.: *Physica B* . 397 (2007), 172-175

1.7. Development of higher-m supermirrors

R. Valicu¹, R. Iannucci¹, A. Ofner¹, G. Borchert¹

¹ZWE FRM II, TU München

m=3-supermirrors

During 2008 we have managed to improve our sputtering process in order to achieve m=3 supermirrors. Our first attempt was to produce these mirrors using the conventional sputtering process and parameters, but this resulted in a large number of layers and therefore the adhesion of the layer system on the substrate was not satisfying compared to the m=2 supermirrors.

Therefore we used nitrogen as reactive gas together with argon, during sputtering of Ni[1, 2]. For this we have determined the neutron optical properties of the reactively sputtered Ni layers by simulating the neutron reflectivity curves using Simulreflec[3]. With these parameters, adapted layer systems were generated using the well known Hayter and Mook algorithm [4]. Neither in reflectivity nor in adhesion the supermirrors produced showed any advantage compared to the ones produced in conventional processes.

As it was stated in different papers [5, 6, 7, 8] it is promising to use in addition oxygen as reactive gas during sputtering of the Ni layers. To simplify matters dry air was used as reactive gas instead of nitrogen only. This further modification of the process finally resulted in a much better adhesion of the m=3 supermirrors.

As one can see from fig. 1.22 the results obtained (the reflectivity and its reproducibility) are satisfying. A reflectivity of more than 85% is very good compared to supermirrors available on the market.

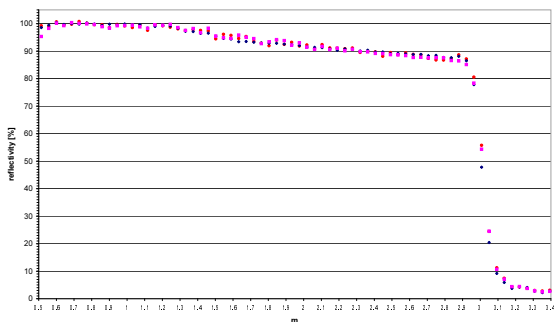


Figure 1.22.: m=3-Supermirrors, reproducibility (reactively sputtered); measured at TREFF.

m=3.5-supermirrors

Using the findings we have made for m=3 supermirrors, it was possible to produce even higher order supermirrors. This meant to increase the number of layers from around 500 to more than 700 layers. This drastic increase is expected to lead to higher intrinsic stress and lower adhesion.

First supermirrors with m=3.5 show a very good reflectivity (see fig. 1.23). In order to improve the stability and quality of these supermirrors, further experiments are currently conducted. Consequently we plan to proceed with higher m values by increasing accordingly the number of bilayers deposited on the substrate.

[1] Böni, P., Clemens, D., Kumar, M. S., Tixier, S. *Physica B*, 241-243, (1998), 1060–1067.

[2] Kumar, M. S., Tixier, S., Clemens, D., Böni, P. *Physica B*, 241-243, (1998), 95–97.

[3] <http://www-llb.cea.fr/prism/programs/simulreflec/simulreflec.html>.

[4] Hayter, J. B., Mook, H. A. *J. Appl. Crystallogr.*, 22, (1989), 35.

[5] Kumar, M. S., Böni, P., Clemens, D. *Physica B*, 276-278, (2000), 142–143.

[6] Böni, P. *Physica B*, 234-236, (1997), 1038–1043.

[7] Kumar, M. S., Böni, P., Tixier, S. *Physica B*, 248, (1998), 53–55.

[8] Kumar, M. S., Böni, P., Horisberger, M. *Physica B*, 385-386, (2006), 1265–1267.

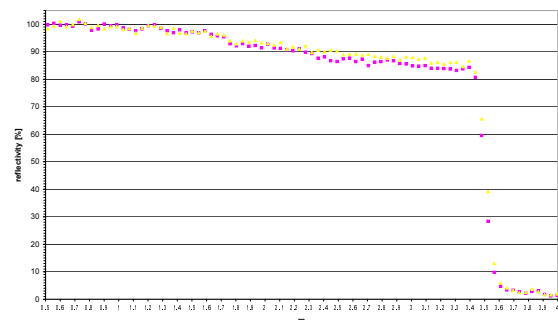


Figure 1.23.: m=3,5-Supermirrors - first samples (reactively sputtered); measured at TREFF.

2. Diffraction

2.1. Improved efficiency at the structure powder diffractometer SPODI

M. Hoelzel¹, A. Senyshyn¹, N. Jünke², H. Boysen³, W. Schmahl³, H. Fuess¹

¹Technische Universität Darmstadt, Material- und Geowissenschaften, Darmstadt

²Georg-August Universität Göttingen, Institut für Physikalische Chemie, Göttingen

³Ludwig-Maximilians-Universität, Depart. für Geo- und Umweltwissenschaften, München

Instrument development

The performance of the diffractometer SPODI has been significantly improved by the installation of a new monochromator focusing device. Both the flux and the profile of the incident beam were improved resulting in higher counting rates of about 50 %.

The efficiency of the instrument has been also significantly improved by a new algorithm in the data treatment software. As a consequence of the vertically divergent beam and the sample height, the Debye-Scherrer rings (Figure 2.1) are smeared out along the vertical direction, resulting in peak broadening and asymmetry at low and high scattering angles. Formerly, good peak profiles could only be obtained by limiting the detector height to approximately 150 mm as indicated by the straight lines in Fig. 2.1. In order to include the full height at the less affected intermediate 2θ -range, an algorithm has been developed that uses a variable height depending on 2θ as indicated by the dotted line in Fig. 2.1. This line depends on the actual sample height and on the required resolution. As a consequence, better peak profiles and higher intensities are obtained by this "variable height data".

New sample environment

A variety of tools for specific environmental conditions at SPODI have been developed in 2008 and will be set into operation at SPODI in 2009. Based on the support of Philipp Jüttner and Günther Seidl a multifunctional load frame has been developed for the instruments SPODI and STRESS-SPEC. This tool will enable diffraction studies under stress, pressure and torsion. As the load frame is attached to an eulerian cradle type wheel, the sample (i.e. load axis) can be oriented in the neutron beam. In frame of a cooperation with the Department of Chemistry of the Technische Universität München an apparatus for the investigation of catalysers has been developed. It is designed to investigate structural changes in zeolithes, metal-organic frameworks or other samples during the uptake of a solvent. An automatic sample changer has been built to run measurements for up to six samples. Finally, a device for high electric fields (up to 30 kV) has been set into operation. In 2008 also a variety of in-situ methods using special tools of sample environment have been successfully applied. Lithium-ion batteries have been studied in operando by means of a multichannel

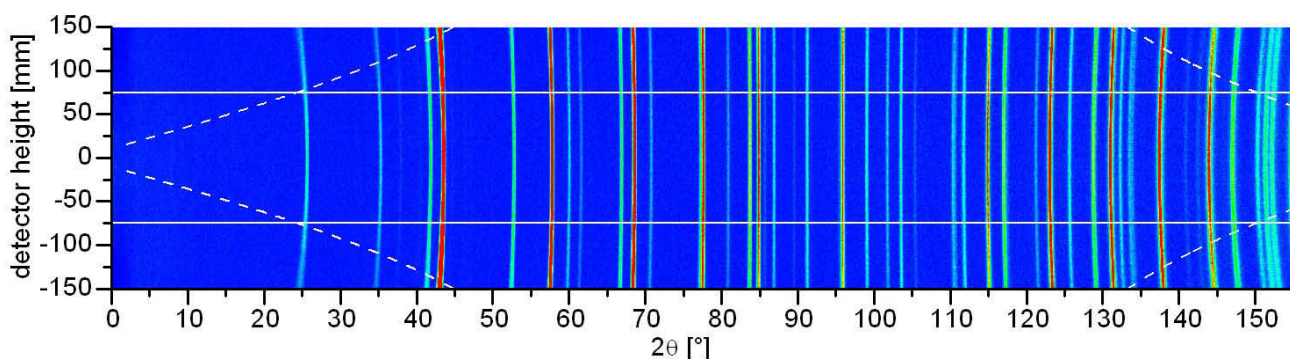


Figure 2.1.: Two-dimensional data set of a corundum reference sample. The straight white lines define a detector height of 150 mm and 0 denotes the centre of the detector. The dotted white lines encompass the data used in the "300 mm - variable height" data set.

potentiostat, revealing the structural changes due to Li-insertion and Li-extraction. Hydrogen storage materials have been studied in-situ under pressures up to 70 bar and temperatures up to 250 °C to investigate the phase transformation behavior during deuterium charging and deuterium desorbing. The developments and operation of new sample environment was supported by Jürgen Peters and his group.

User service and scientific outcome

Besides the user service, the diffractometer SPODI has also participated in the practical neutron scattering courses organised by Jülich Centre for Neutron Science and Technische Universität München. To our best knowledge 7 publications based on the results from structure powder diffractometer SPODI appeared in the literature in 2008:

- L. Nyam-Ochir, H. Ehrenberg, N. Stuesser, A. Senyshyn, H. Fuess, D. Sangaa, The magnetic structures of double tungstates, $\text{NaM}(\text{WO}_4)_2$, $M = \text{Fe}, \text{Cr}$: examples for superexchange couplings mediated by $[\text{NaO}_6]$ -octahedra, *J. Magn. Magn. Mater.*, 329, 3251-3255, (2008).
- B. Schwarz, H. Ehrenberg, H. Weitzel, A. Senyshyn, B. Thybusz, M. Knapp, G. McIntyre, H. Fuess, Crystal chemistry, structure and magnetic properties of the $\text{Cu}(\text{Mo,W})\text{O}_4$ solid solution series, *Philosophical Magazine* 88(8), 1235-1258, (2008).
- D.M. Trots, A. Senyshyn, D.A. Mikhailova, T. Vad, H. Fuess, Phase transitions in jalpaite, Ag_3CuS_2 , *J. Phys.: Condens. Matter* 20, 455204, (2008).
- R. Ranjan, R. Garg, R. Hack, A. Senyshyn, E. Schmidbauer, D. Trots, H. Boysen, Onset of spontaneous

electrostrictive strain below 520 K in Pr-doped SrTiO_3 , *Phys. Rev. B* 78, 092102, (2008).

- A.C. Komarek, S.V. Streltsov, M. Isobe, T. Möller, M. Hoelzel, A. Senyshyn, D. Trots, M.T. Fernandez-Diaz, T. Hansen, H. Gotou, T. Yagi, Y. Ueda, V.I. Anisimov, M. Grüninger, D.I. Khomskii, M. Braden, CaCrO_3 : an anomalous antiferromagnetic metallic oxide, *Phys. Rev. Lett.* 101, 167204 (2008).
- R. Garg, A. Senyshyn, H. Boysen, R. Ranjan, Structure and phase transition of $\text{Na}_{0.5}\text{La}_{0.5}\text{TiO}_3$, *J. Phys.: Condens. Matter* 20, 505215, (2008).
- J.L. Wang, S.J. Campbell, A. J. Studer, M. Avdeev, M. Hofmann, M. Hoelzel, S. X. Dou, Magnetic Structures and Phase Transitions in $\text{PrMn}_{2-x}\text{Fe}_x\text{Ge}_2$, *J. Appl. Phys.*, 104, 103911, (2008).



Figure 2.2.: At the structure powder diffractometer SPODI lithium-ion batteries and hydrogen storage materials have been studied.

2.2. HEiDi and POLI-HEiDi

M. Meven¹, V. Hutanu², G. Heger²

¹ZWE FRM II, TU München

²Institut für Kristallographie, RWTH Aachen, Aachen

HEiDi is one of the two single crystal diffractometers at the neutron source FRM II. It is located at beam line SR9B in the experimental hall of the reactor building and uses the hot source (fig. 2.3). The instrument is a collaboration between the RWTH Aachen (Institut für Kristallographie) and the Technische Universität München.

The use of the hot source increases remarkably the neutron flux below 1 Å. Diffraction experiments focussing on structural and magnetic details gain significantly from the very large reciprocal space ($Q = |\vec{Q}| = \sin \Theta_{max}/\lambda$) with $Q > 1.5$ at 0.55 Å. Additional advantages are the

- reduction of extinction effects of large and very perfect single crystals and the
- reduction of absorption effects in compounds with highly absorbing elements, e.g. samarium, gadolinium or europium.

Especially the second point is of very practical use for studies on current hot topics like multiferroics and FeAs high-temperature-superconductors, which both contain such elements.

In summary, HEiDi covers a broad range of scientific cases in the area of structural research on single crystals in the following fields of interest:

- Structure analysis (harmonic and anharmonic MSD(mean square displacements), hydrogen bonds, molecular disorder).
- Investigation of magnetic ordering (magnetic structures, spin density).
- Structural and magnetic phase transitions.

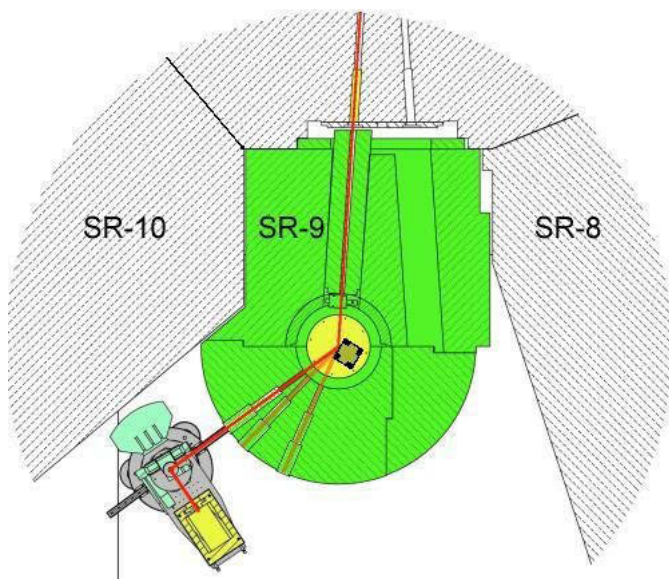


Figure 2.3.: Overview of HEiDi.

Details of the instrument and its applications were presented in 2008 on the

- XXI. IUCr Conference and General Assembly in Osaka, Japan [1],
- German Neutron Scattering Conference in Munich.

Use of beam time

Overview:

- 57% external beam time,
- 23% internal beam time,
- 5% education of students / young scientists in the
 - advanced practical course in physics at the TU München and the
 - JCNS Neutron course of the Forschungszentrum Jülich
- 9% instrument development of both HEiDi and Poli-HEiDi
- 6% maintenance.

In total 80% of beam time were given to external and internal proposals. Due to the large overbooking factor of HEiDi only eight of the sixteen external proposal were accepted and accomplished at HEiDi. In addition some beamtime was given to external users to check crystal orientations and homogenities of samples that were used for experiments on other instruments at FRM II, especially the triple axes spectrometers.

Typical scientific cases of the external proposals in this year were

- magnetic superstructures at low temperatures,
- order/disorder phase transitions at low and high temperatures,
- ionic conductors and
- local disorder or vacancies, especially of H bonds.

Scientific highlights and theses

One of the scientific highlights was the temperature dependent study of a BaFe₂As₂ single crystal. The rather small orthorhombic twinning ($\Delta a/\bar{a} = 0.25\%$) below the phase transition around 100 K was clearly confirmed by measuring accurately the FWHM of selected reflections as shown in figure 2.4 [2].

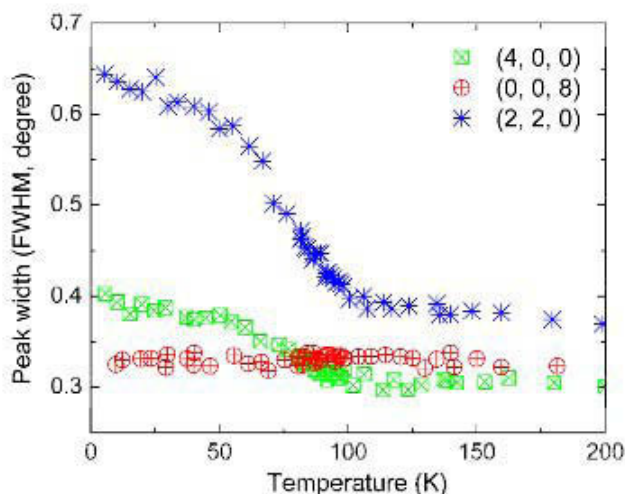


Figure 2.4.: T dependent FWHMs of BaFe_2As_2 measured on HEiDi.

In the framework of the Erasmus Mundus program "Master of Material Science exploiting European large-scale facilities" a master thesis including single crystal neutron diffraction studies on $\text{Nd}_2\text{NiO}_{4+\delta}$ revealed the very complex phase behaviour of the doped compound in dependence of this oxygen ionic conductor as shown in figure 2.5 [3].

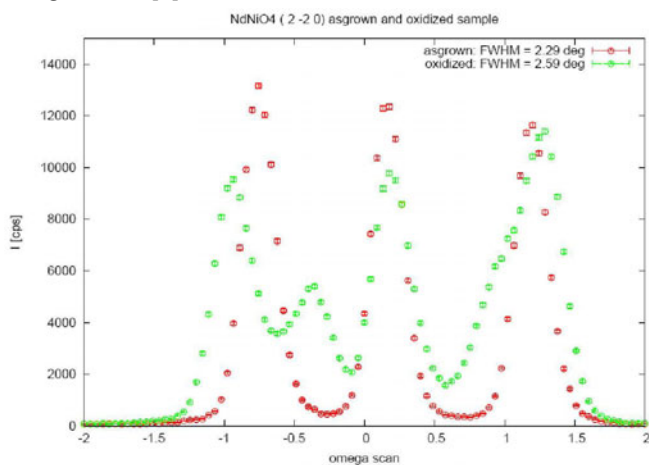


Figure 2.5.: $\text{Nd}_2\text{NiO}_{4+\delta}$ (2 2 0) reflections of two slightly different doped samples at RT.

Two bachelor theses were completed in collaboration with the *Lehrstuhl für Informatik im Maschinenwesen* at the Technische Universität München. The first one focused on automatised and optimized trajectories of movement for HEiDi to extend the available reciprocal space without the danger of collisions of parts of the instrument during those movements [4]. The second one focused on an optimized motor controller to allow continuous movements of the instrument during scans. This technique

can speed up data collections up to about 30% [5]. Currently we are waiting for suitable TACO-drivers for the new controller to use the continuous mode as default on HEiDi.

Outlook

In 2009 we intend to continue the successful work of HEiDi. Additionally we would like to establish some improvements to the instrument. These are

- Mirror furnace for temperatures above 1000°C ,
- Continuous scan mode for faster data collection,
- Analyser option for purely elastic scans,
- Area detector for detailed reflection analysis.

Development at polarised diffractometer POLI-HEiDi

The most important achievement of the POLI-Heidi project in 2008 was a successful test of the new non-magnetic goniometer together with the detector-analyser device Decpol under real experimental conditions at line SR9. In figure 2.6 the crane transport of the POLI-Heidi diffractometer to the position in front of SR9 in the experimental hall of FRM II is shown. In figure 2.7 the POLI-Heidi is shown during the experiment. Just before this experiment the motor controller for the detector and the sample movements were installed and successfully tested. Three Phytron type compact motor controller modules (each for two axes) were mounted directly on the instrument avoiding long cables in the instrumental field and are controlled remotely via Ethernet. The electronic rack with power supplies for all magnetic coils (more than 10) is situated outside the secondary radiation shielding close to the control cabin. Magnetic fields of the Decpol and nutators were also tested. Field homogeneity inside the Decpol was measured and optimised using ^3He spin filter cells in order to reach the best relaxation times in the cell. The results show that in spite of the strong magnetic field in the closest vicinity to the Decpol in the nutator, the field homogeneity inside the Decpol remains high enough to avoid supplementary magnetic relaxation of the cell. Inspired from the results of this experiment the decision to build the polariser magnetostatic cavity similar to the Decpol design was taken. The design of the new polariser was finalised in 2008, and manufacturing was started. We expect to test the new polariser early in 2009. Significant progress was achieved in the last year also concerning the construction of zero-field spherical polarimeter Cryopad. All parts were completed. Now the final assembling is under way at the Institut Laue-Langevin (ILL). Unfortunately a delay regarding to the initial planning occurred due to technical problems observed by the turning of the superconducting precession coil of the Cryopad. Therefore, it had to be redone. We expect to finalise the tests of the

new Cryopad and to install it on the POLI-Heidi in the first half of 2009. A number of SNP (Spherical Neutron Polarimetry) experiments using Cryopad on POLI-Heidi are planned for the second half of 2009.

[1] Meven, M., Hutanu, V., Heger, G. *Acta Cryst. A*, 64, (2008), C187–C188.

[2] Su, Y., Link, P., Schneidewind, A., Wolf, T., Adelman, P., Xiao, Y., Meven, M., Mittal, R., Rotter, M., Johrendt, D., Brueckel, T., Loewenhaupt, M. <http://arxiv.org/abs/0807.1743> [*cond-mat.suprcon*], *Phys. Rev. B* (accepted 12. Jan. 2009), (2009).

[3] Seinberg, L. *Master thesis in the framework of the Erasmus Mundus programme "Master of Material Science exploiting European large-scale facilities"*, (2008).

[4] Schmidt-Colinet, J. *Bachelorarbeit am Lehrstuhl für Informationstechnik im Maschinenwesen, TU München*, (2008).

[5] Schlögel, M. *Bachelorarbeit am Lehrstuhl für Informationstechnik im Maschinenwesen, TU München*, (2008).

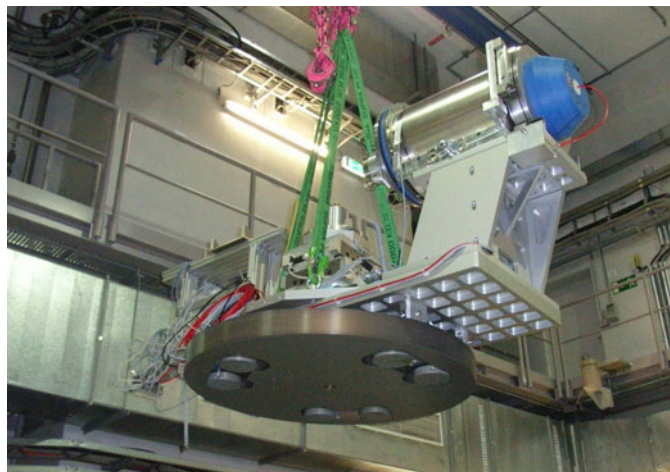


Figure 2.6.: Crane transport of the new diffractometer POLI-Heidi to the experiment site in the experimental hall of FRM II.

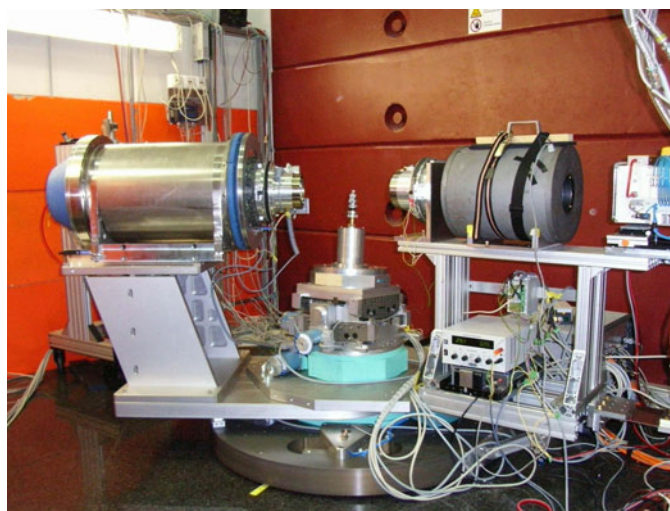


Figure 2.7.: POLI-Heidi at SR9 during the test experiment. The transportation unit from FZ Jülich was used as polariser for this experiment (dark grey cylinder on the right hand side in the picture).

2.3. The new small-angle scattering instrument SANS-1

R. Gilles¹, W. Hornauer¹, S. Semecky¹, H. Türck¹, K. Zeitelhack¹, I. Defendi¹, J. Krüger¹, C. Breunig¹, H. Barfuss², A. Beldowski², J. Buhrz², J. Burmester², O. Frank², R. Kampmann², T. Keller^{3,1}, R. Kirchhof², G. Musielak², O. Nette², K. Pranzas², S. Ruschmeyer², A. Schilf², A. Vogel², A. Schreyer², W. Petry¹

¹ZWE FRM II, TU München

²GKSS Forschungszentrum, Geesthacht, Germany

³Max-Planck-Institut für Festkörperphysik, Stuttgart

Around 50 metres long, up to 2.4 metres wide and around 150 tons of weight - these are the dimensions of the new small-angle neutron scattering instrument SANS-1 inclusive shielding. It will be located between the small angle scattering instrument KWS-1 and the prompt gamma activation analysis instrument PGAA in the neutron guide hall.

Vacuum better than 1mbar

During the year 2008 the basic components of the collimation system of SANS-1 were installed. Included in this work was the sealing of the vacuum chamber (with a volume of around $68m^3$), which allows after switching off the pumping station to keep a vacuum of better than 1mbar for one day. It has to be mentioned that more than 50 vacuum feedthrough, a neutron guide, a telescope nose, and two hatches were implemented because of the seven moveable tables and the support of the optical components. After mounting the instrument components in the vacuum chamber the final value of the vacuum changed only negligible. It is intended for the routine operation to pump the collimation system one or two hours during the night and to switch off the pumping station over the day time.



Figure 2.8.: Two polarisers (left and middle) and one neutron guide Ni^{58} (right) are mounted on a moveable table. U-shaped support of soft iron is used to mount permanent magnets.

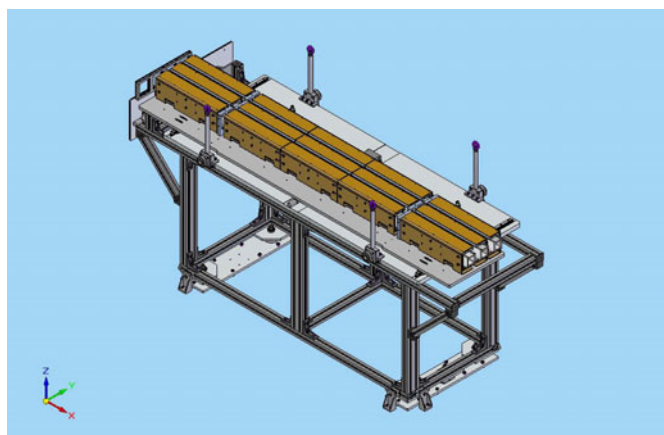


Figure 2.9.: Schematic drawing of one frame with a table and mounted optics.

The interior walls of the vacuum chamber were first backed with plates of boron epoxy. Afterwards frames were installed, which allow to position the tables with the optical components. On each table are mounted four tracks (Fig. 2.8, 2.9). One track for the neutron guide, another one for the pinhole apertures, one for a laser system and the last track is partly used for background apertures and allows to implement newly developed optical components, later. The neutron guide frames are mounted and pre-aligned. The two V-shaped polarisers are installed and the neutron guides of Ni^{58} will follow in 2009. The aperture frames are mounted and will be filled with B_4C plates soon when the cutting-out of the pinholes is ready. At the moment the laser system is tested outside the collimation system with special apertures, which will provide the possibility to align each table in the neutron beam without opening the shielded vacuum chamber.

Glass windows enable a look inside

The collimation vacuum chamber is surrounded by 70 tons of lead. If a failure happens, circled plugs of lead can be removed on special positions of the side walls, where glass windows are installed to enable a look inside. The chamber is equipped with an illumination for vacuum to perform a first check without braking the vacuum. If necessary the chamber will be vented and the lead has to be dismantled following the opening of the cover to take the optical components

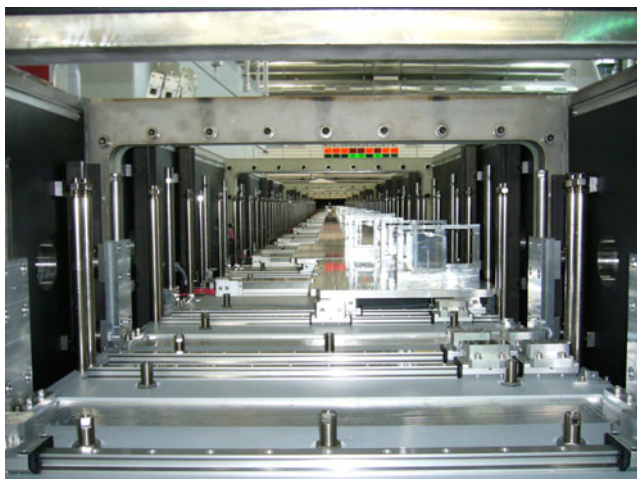


Figure 2.10.: The inner life of the collimation system with movable tables to position various components in the neutron beam.

out. This elaborated procedure should be minimized with the support of the laser system. Due to the parallel alignment of the laser to the neutron beam a further use of the laser is to assign the neutron beam centre at the sample position.

This will be very helpful because of many changes of the sample environment in the routine operation. The movements of the mounted tables were tested with the so called Beckhoff-SPS control relative to accuracy and repeatability.

Polarisers and spin flipper

The polarisation option demands a strong field of around 500 Gauss at the polariser position and a guide field in the whole collimation chamber of about 20 Gauss. The set up of the two polarisers is shown in Fig. 2.10 together with the external static magnetic field. After the polariser a spin flipper will be installed. This position has the advantage to use the gradient of the magnetic field from the polariser to the guide field. The spin flipper is shown in Fig. 2.11 with a slightly wedge-shaped iron yoke and mounted with permanent magnets which provides a DC (direct current) field of about 100 G in the centre of the spin flipper. The RF (radio frequency) coil is wound around the neutron beam on a ceramic tube (Al_2O_3) to avoid excessive eddy current losses. This set up [1] has been successfully used at the small-angle instrument V4 at the Helmholtz Zentrum Berlin. First ideas of a system to focus the neutron beam with neutron lenses are in progress. Space for such a equipment including a cooling system is reserved. Another possible option is



Figure 2.11.: Spin Flipper set up installed for a first test at the instrument MIRA.

the integration of a chopper system mounted below the neutron beam in the vacuum chamber.

More components to install

Further operations were completed as for example the connection of the neutron guide system to the selector tower with a Ni^{58} neutron guide including the shielding. The installation of the two monitors before and after the selector was performed. The support unit for electricity, water and air pressure was mounted together with various cable channels. SANS-1 will use a common pumping station with the KWS-1 and the KWS-2 from JCNS Forschungszentrum Jülich. The pipe installation from the pumping station to the foreseen detector vessel is ready. The software has to be integrated in the system to allow the possibility to work with one or both pumps in the pumping station, if there is a request. As well a coordination is necessary, if two or three detector vessels demand pumping time at the same moment.

For the detector and the detector vessel all technical drawings were performed and many components had arrived for the set up. Included in this part of the project is the integration of a platform on top of the detector vessel. This platform will be used for two hutches, a work bench, a location for sample preparation, cupboards, electronic racks etc. The delivery of the platform is scheduled for January 2009 and will be built up when the tests of the vacuum of the detector vessel is finished.

The main task in the year 2009 will be the installation of the detector vessel including the internals, especially the detector and the moveable detector system.

[1] Gilles, R., Ostermann, A., Schanzer, C., Krimmer, B., Petry, W. *Physica B*, 385-386, (2006), 1174.

2.4. Biological membranes under study at the reflectometer REFSANS

R. Kampmann¹, J.-F. Moulin¹, M. Haese-Seiller¹, M. Pomm¹, B. Nickel², J. Rädler², M. Müller¹, A. Schreyer¹

¹GKSS Forschungszentrum, Institut für Werkstofforschung, Geesthacht

²Ludwig-Maximilians-Universität München

The neutron reflectometer REFSANS (reflectometry and evanescent small-angle neutron scattering) allows to perform comprehensive analyses of vertical and lateral surface and interface structures by means of specular and off-specular neutron reflectivity as well as small-angle neutron scattering at grazing incidence (GISANS) both on solid and free liquid surfaces [1, 2]. It opens up new and unique possibilities for research into the molecular architecture and function of complex boundary layers and surfaces of materials, which are of increasing significance in technology and biotechnology. Such boundaries comprise, for example, synthetic polymer films on technical components, biocompatible films on transplants, complex biological functional materials on electro-optical components and magnetic nanostructures.

Use of REFSANS

After SC-2 had been put into operation in 2007 the quality of measurements at REFSANS could be improved due to better defined wavelength resolution over the selected λ -range and higher transmission of the chopper system. Measurements in the frame of exciting internal and external proposals have successfully been performed, some of which are introduced in the following. REFSANS could, however, not be used for user proposals to the expected extent because the operation of the instrument had been interrupted fully from May to October 2008 due to a breakdown of the chopper mechanics.

Example: Investigation on biomembrane mimics (R. Willumeit et al.)

A biomembrane mimic coating on an implant substrate (Ti-6Al-7Nb) (sputtered on a Si-wafer) was investigated with the aim to improve the biocompatibility of the implant. Three reflectivity curves were measured under ambient condition at REFSANS: i) the wafer with the metallic substrate (thickness: ≈ 100 nm), ii) after coating with POPE, and iii) after washing the coated sample in water (Fig. 2.12, [3]).

Fits to the data were performed by using a Parratt formalism (continuous lines in Fig. 2.12). These revealed that a highly disordered lipid multilayer is formed after deposition of POPE solution onto the metallic substrates. A fraction of only 20-25% of the lipids forms ordered multilayers. Further incubation of the surface in water leads to washing off of parts of the lipids and to an increase in the ordering of the remaining bilayers [3].

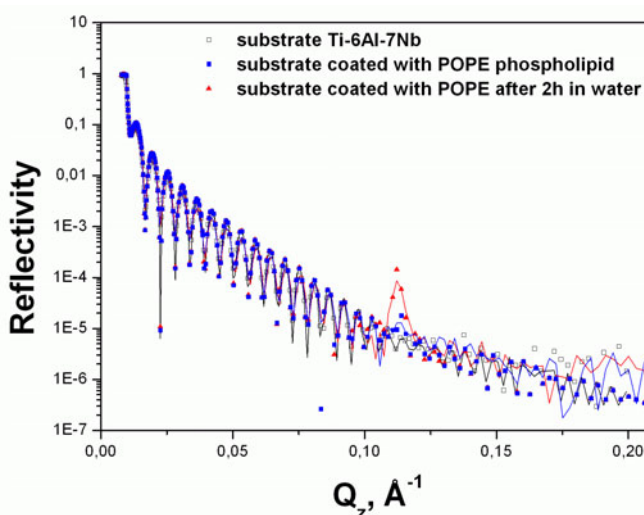


Figure 2.12.: Investigation on biomembrane mimics (R. Willumeit et al. [3])

Example: ToF-GISANS study of Al-capped Gd-nano-wires (W. Kreuzpaintner et al.)

A ToF(Time of Flight)-GISANS study of Al-capped Gd-nanowires (cross-section: $50 \text{ nm} \times 50 \text{ nm}$; spacing: 225 nm), grown on a faceted Al_2O_3 surface was performed on REFSANS for various sample rotations (ϕ) [4, 5]. The ToF-GISANS technique was a real need to find the critical wavelength of 9.2 \AA at a given incidence

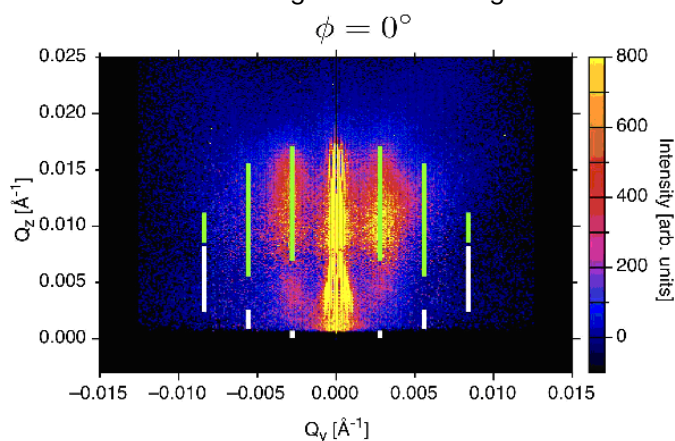


Figure 2.13.: Reconstructed GTRs in the $(Q_y - Q_z)$ -plane compared to their theoretical positions for reflected (green) and transmitted (white) neutrons (W. Kreuzpaintner et al. [4, 5])

angle of $\alpha_i = 0.67^\circ$ and to reconstruct the grating truncation rods (GTR) in the $(Q_y - Q_z)$ -plane. In contrast to fixed wavelength instruments, the angle of incidence does not have to be changed, as the radius of the Ewald sphere is varied with the wavelength. Not only the reflected, but also the transmitted intensities are explored because of the large penetration depth of neutrons. The reconstructed GTRs are compared to their expected position and length using the standard Born Approximation. Fig. 2.13 shows the reconstructed reciprocal space image for a sample rotation of $\phi = 0^\circ$ compared with the theoretical locations of the GTRs. The intensity distribution in the vicinity of the sample horizon, where refraction and multiple scattering effects must be obeyed, requires a more complex analysis [4, 5].

Example: Solid supported lipid bilayer in D_2O (B. Nickel et al.)

A solid supported lipid bilayer in D_2O has been used as a benchmark for the signal-to-noise ratio which is available for experiments at biological interfaces at REFSANS [6].

The sample structure is shown schematically in Fig. 2.14a, while the respective measurement is shown in Fig. 2.14b. First, a bare Si wafer in D_2O is measured (Fig. 2.14a i). The rapid intensity oscillations observed (Fig. 2.14b i) originate from the oxide layer. Then, a partly deuterated lipid bilayer is deposited (D31-POPC, Fig. 2.14a ii) by vesicle fusion and subsequent rinsing cycles. Homogeneity and diffusivity of the lipid layer was verified by fluorescence microscopy and then the neutron reflectivity was recorded (Fig. 2.14b ii). A huge change of the reflectivity signal due to the pres-

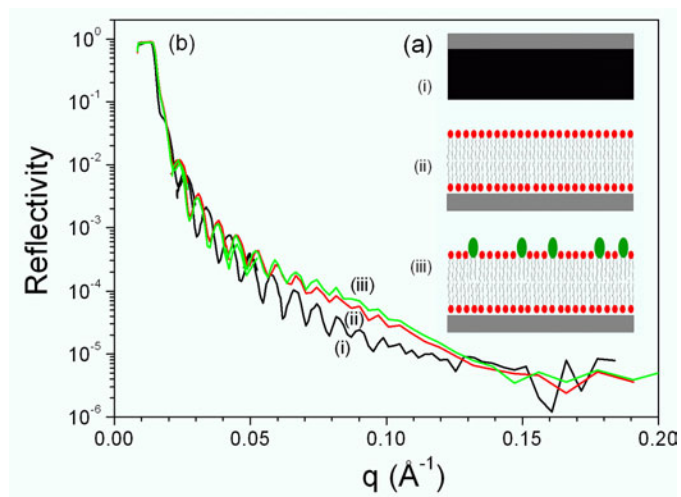


Figure 2.14.: Solid supported bilayer. (a) Schematic of the sample states. (i) Bare wafer in D_2O . (ii) Supported bilayer in D_2O . (iii) Bilayer with GM1 incorporated. (b) Corresponding neutron reflectivity curves (B. Nickel et al. [6])

ence of the 4 nm lipid layer is observed. Finally, a glycolipid (GM1) was injected into the D_2O phase. Since GM1 is fully protonated, its insertion is associated with a scattering length density change of the distal leaflet. Indeed, we observe a small increase in contrast after GM1 injection (Fig. 2.14b iii). A detailed analysis is right now in preparation to extract the amount of GM1 intercalated into the distal leaflet change in density of the scattering length.

Outlook: developments on instrument and sample environment

The soft- and hardware systems controlling the neutron systems are continuously improved and the operation of REFSANS has become more and more reliable. It is further planned to replace fully the two double disk choppers in the chopper chamber to achieve failure-free operation of the instrument. The data reconstruction software will be improved to achieve faster and on-line display of spectra and reflectivity. A sample chamber will be designed to allow background reduced measurements of the reflectivity from solid and soft samples. Polarized beam options will be available at REFSANS only in 2010.

Acknowledgements

The development of REFSANS has been supported by the German Federal Ministry of Education, Research and Technology (BMBF) under contract 03RA7LMU.

- [1] Kampmann, R., Haese-Seiller, M., Marmotti, M., Burmester, J., Deriglazov, V., Syromiatnikov, V., Okorokov, A., Frisius, F., Trisl, M., Sackmann, E. *Applied Physics A*, 74, (2002), 249–251.
- [2] Kampmann, R., Haese-Seiller, M., Kudryashov, V., Deriglazov, V., Trisl, M., Daniel, C., Toperverg, B., Schreyer, A., Sackmann, E. *Physica B*, 350, (2004), e763–e766.
- [3] Willumeit, R., Fayerabend, F., Schuster, A., Linser, S., Lott, D., Moulin, J.-F., Kampmann, R., Haese-Seiller, M., Haramus, V., Schreyer, A. *FRM II proposal 1542*, (2007).
- [4] Kreuzpaintner, W., Moulin, J.-F., Lott, D., Kampmann, R., Haese-Seiller, M., Störmer, M., , Schreyer, A. *FRM II proposal 1707*, (2008).
- [5] Kreuzpaintner, W., Moulin, J.-F., Lott, D., Kampmann, R., Haese-Seiller, M., Störmer, M., , Schreyer, A. *Eur. Phys. J. Special Topics*, 168, (2009), 73–79.
- [6] Stanglmaier, S., Hertrich, S., Haese-Seiller, M., Kampmann, R., Rädler, J., Nickel, B. *FRM II proposal 2384*, (2008).

2.5. Polarized and unpolarized neutron reflectometry with *N-REX*⁺

A. Rühm¹, M. Schmidt¹, M. Major¹, M. Nülle¹, J. Franke¹, J. Major¹, H. Dosch¹, Th. Keller², B. Keimer²

¹Max-Planck-Institut für Metallforschung, Stuttgart

²Max-Planck-Institut für Festkörperforschung, Stuttgart

Instrument status

During the year 2008 the reflectometer *N-REX*⁺ was running in regular user operation mode. The majority of the user experiments was dealing with soft matter science, the remainder with magnetism. In the last proposal round, beamtime applications of these two user communities have become almost equal in number.

Unpolarized neutron reflectometry

Two examples of unpolarized neutron reflectivity measurements are shown in Fig. 2.15. The data in panel (a) were obtained on a silicon reference sample against air and display a dynamic range of $1 : 10^{-6}$. The data in panel (b) were obtained on a solid-liquid interface consisting in a polymer film interlaced between a silicon substrate and D_2O (the beam was entering from the substrate side). Due to additional background from the sample cell and beam absorption in the substrate, the dynamic range is reduced to $1 : 10^{-5}$ in this case.

Polarized neutron reflectometry with wide-angle spin-analysis

Fig. 2.16 shows some data of a polarized neutron reflectometry and off-specular scattering experiment performed on Fe/Si multilayers [1]. The objective of the experiment was to study the interdiffusion of the adjacent Fe and Si layers, the potentially resulting alloy phase for-

mation at the interfaces, as well as the influence of the interdiffusion on the magnetic structure at the interfaces. Using a polarized ^3He gas spin-filter (supplied by the HELIOS facility of FRM II) the off-specular scattering could be conveniently spin-analyzed simultaneously with the specular reflectivity signal.

As can be seen in Fig. 2.16, at zero field (a) we obtained a clear off-specular magnetic signal, which arises from magnetic roughness or magnetic domains. This off-specular signal disappears at larger magnetic fields (b). The detailed analysis of these data sets, available for four different in-plane magnetic fields between 0 and 3100 Gauss, is in progress.

Outlook: Instrument upgrade

The instrument *N-REX*⁺ is currently being upgraded in several aspects, with a focus on the optimization of polarized neutron reflectometry experiments. One main aspect of the upgrade is the reduction of the background level by a long evacuated or gas-filled detector shielding box which can also accommodate all required components for polarization analysis. The other main aspect of the instrument upgrade is the enhancement of the primary neutron beam intensity. This will be achieved by an upgrade of the monochromator to a larger number of crystal layers as well as the insertion of a horizontally focusing neutron guide between monochromator and sample. Furthermore it is discussed to place polarizers into the neutron guide NL-1 already upstream of the monochromator of *N-REX*⁺.

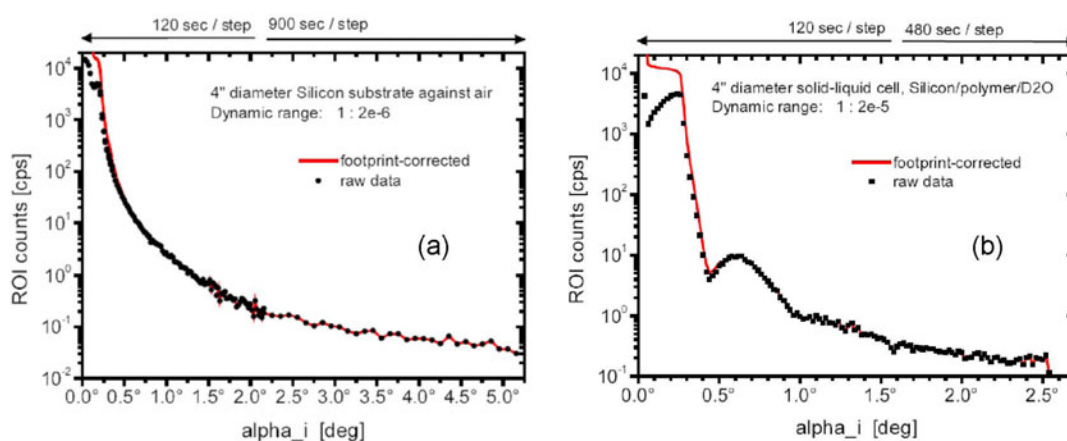


Figure 2.15.: Neutron reflectivity curves obtained on: (a) a 4-inch diameter silicon wafer, (b) a PMMA polymer brush at a 4-inch diameter Si/ D_2O solid-liquid interface. Black data points are raw data, the red lines show the same data after footprint correction.

Acknowledgements

The support of the management and staff at FRM II is gratefully acknowledged. This work has been supported by a focused neutron research funding of the Max Planck Society, Munich.

- [1] Schmidt, M. *In-situ-Untersuchungen zu Interdiffusion und Magnetismus in magnetischen Multilayern*. Diploma thesis, Max-Planck-Institut für Metallforschung, Stuttgart, und Institut für Theoretische und Angewandte Physik der Universität Stuttgart (2009).

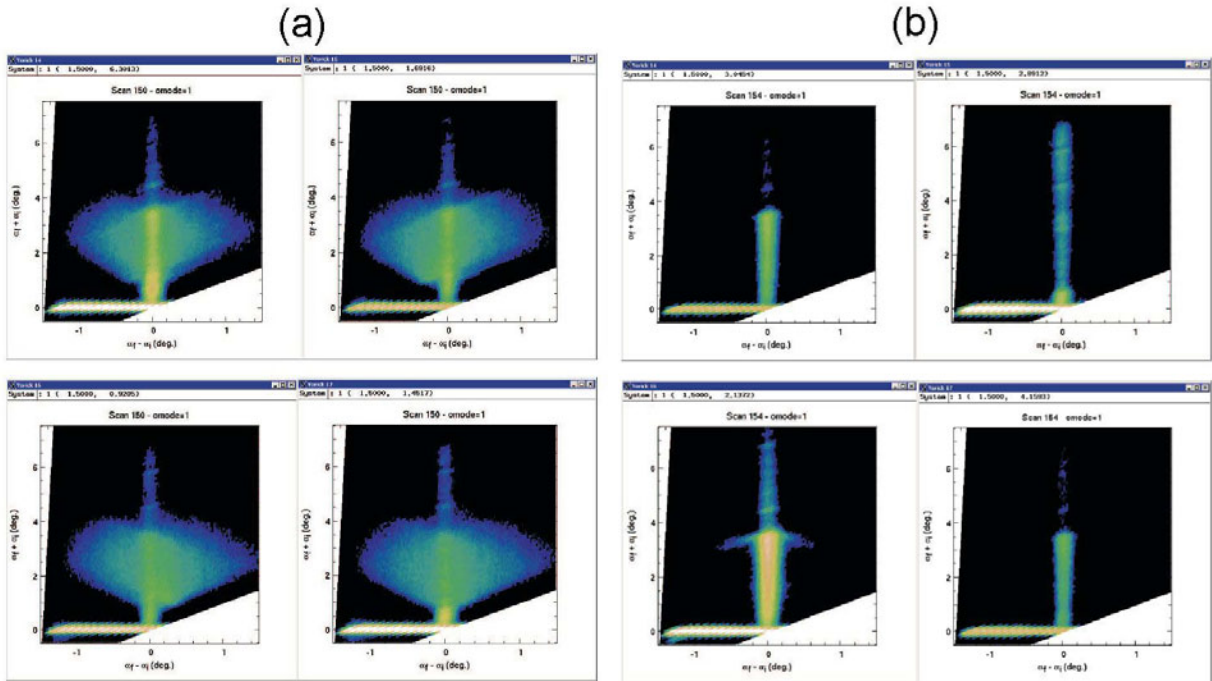


Figure 2.16.: Neutron intensity distributions obtained by polarized neutron reflectometry and off-specular scattering with wide-angle spin-analysis on an Fe/Si multilayer ($[\text{Fe}(70 \text{ \AA})/\text{Si}(70 \text{ \AA})]_5/\text{SiO}_2/\text{Si}$) exposed to different magnetic fields: (a) zero field, (b) 3100 Gauss. Each image group shows the intensity distributions obtained for the four flipper combinations (on/on, off/off, on/off, off/on). The vertical axis corresponds to the total scattering angle ($2\theta = \alpha_i + \alpha_f$), the horizontal axis to the "rocking angle" ($\alpha_f - \alpha_i$).

2.6. Proteins under study at KWS-2

A. Radulescu¹, H. Frielinghaus¹, V. Pipich¹, P. Busch¹, M.S. Appavou¹, A. Ioffe¹, D. Schwahn², T. Brückel^{1,2}, D. Richter^{1,2}

¹Jülich Centre for Neutron Science, Institut für Festkörperforschung, Forschungszentrum Jülich

²IFF-5 Neutronenstreuung, Institut für Festkörperforschung, Forschungszentrum Jülich

The KWS-2 classical pinhole small-angle neutron (SANS) diffractometer is operated by the JCNS since September 2007 at the FRM II in Garching. With a high flux supplied by the cold neutron source, the newly designed optimized neutron guide and with a new collimation system allowing a larger experimental flexibility, KWS-2 contributes both to the in-house research activity in the traditional field of soft-matter and to the user program. KWS-2 is a high intensity and wide Q-range SANS instrument dedicated to study structures and morphologies on a wide length scale and structural changes due to fast kinetic processes in soft condensed matter and biological systems. Polymer effects on microemulsions, on diesel fuels, and mineralization of inorganic compounds, thermal composition fluctuations in polymer blends and diblock copolymers, their aggregation behavior and response on shear, the rubberelasticity and the "living anionic polymerisation", denaturation of proteins by chemical agents or changes of physical parameters (temperature, pressure, etc) are usually studied. A large variety of structures and morphologies extending on a wide length scale or developing a multi-size hierarchical organization is thus targeted [1, 2]. Two examples of research topics involving the use of the KWS-2 SANS instrument are further shortly described.

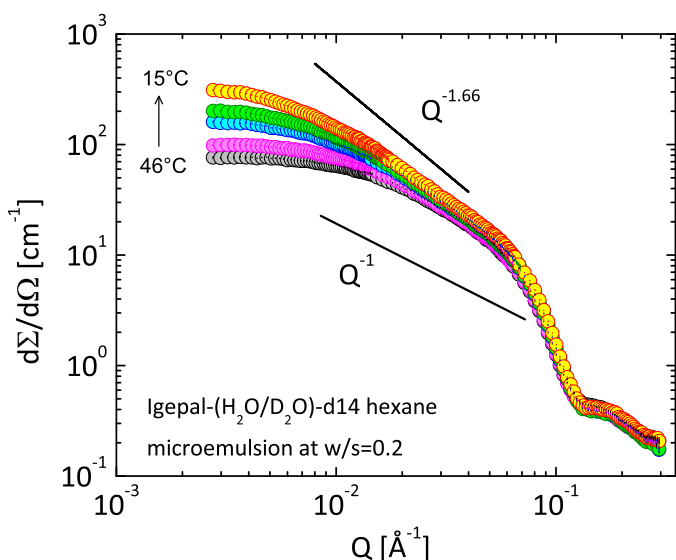


Figure 2.17.: Example of scattering patterns from oil/water microemulsion with Igepal-CO520 non-ionic surfactant.

Microemulsions for nanoparticles

Microemulsions are macroscopically homogeneous mixtures of water, oil and surfactant. On a microscopic level, the mixtures are structured into water-rich and oil-rich domains separated by an amphiphilic film. Microemulsions have many commercial and industrial applications (cosmetics, polishers and cleaners, detergents, pesticides) and show an increased interest as a method for the synthesis of nanoparticles (templates). One interesting property of microemulsion systems is the large variety of structures formed depending on the thermodynamic conditions and chemical composition. By variation of physical parameters like temperature, composition, salinity, etc., these systems can find preferred aggregation geometries such as globular or cylindrical (droplets of oil in water or water in oil) and bicontinuous, spongelike structures of entangled channels of water and oil, or long-range ordered structures (lamellar, hexagonal, cylindrical) at higher surfactant concentrations.

Transition of microemulsion observed

Fig. 2.17 presents the small angle scattering pattern from a oil/water microemulsion system with Igepal-CO520 non-ionic surfactant for a particular composition and contrast condition. A transition from a mixture of spherical and cylindrical droplets to long flexible cylindrical structures is observed in decreasing temperature. Both characteristic sizes of the elongated droplets have been accessed in this experiment. The wide Q-range covered and the contrast variation used have allowed for a complete characterization of the structures formed by this system over a wide temperature range [3].

Conformation of proteins

In the frame of biological molecules study, SANS is a suitable method to investigate denaturated states of proteins. From a fundamental point of view, the technique will make understand how a protein adopts its final conformation from its primary structure. From an industrial point of view, SANS brings answers to questions concerning the influence of physical and chemical parameters (temperature, pressure, pH, ionic strength, etc.) on biological molecules, of an essential importance in food industry (sterilization and bio-conservation). In medicine, degenerative diseases as Alzheimer or Parkinson involve

slightly unfolded proteins around brain receptors leading to the typical symptoms of lack of memory or even mal-function of muscles coordination. The use of polymer theory for data interpretation will bring quantitative information about the conformation of proteins. Recent and promising results have shown that it is possible to investigate different folding states of a model protein, the horse heart myoglobin, by using chemical denaturing agents (guanidinium hydrochloride). Fig. 2.18 shows in a Kratky representation the small angle scattering patterns

from myoglobin protein in phosphate buffer for different concentration of denaturing agent added.

[1] Pipich, V., Balz, M., Wolf, S. E., Tremel, W., Schwahn, D. *Journal of the American Chemical Society*, 130, (2008), 6879.

[2] Radulescu, A., Fetters, L. J., Richter, D. *Advances in Polymer Science*, 210, (2008), 1.

[3] Sager, W., Shanmugavadivelu, G., Radulescu, A. To be published.

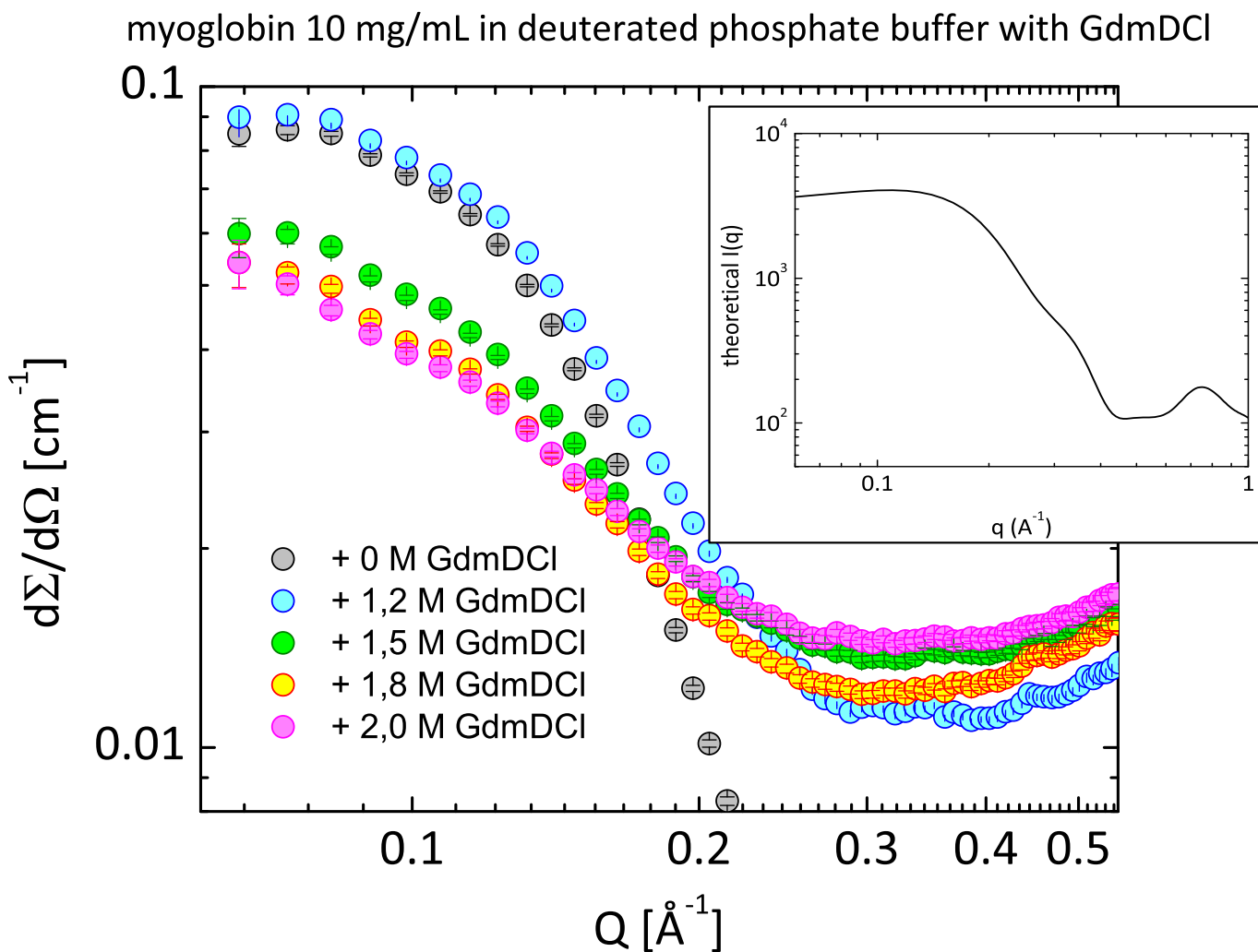


Figure 2.18.: Kratky plot of the scattering patterns from myoglobin in deuterated phosphate buffer with different concentrations of deuterated guanidinium hydrochloride.

3. Inelastic scattering

3.1. MIRA – The beam line for very cold neutrons

R. Georgii¹, P. Böni², G. Brandl², Ph. Jüttner¹, A. Mantwill¹, S. Mühlbauer¹, R. Schwikowski¹

¹ZWE FRM II, TU München

²Physik-Department E21, TU München

MIRA is a versatile instrument for very cold neutrons (VCN) using neutrons with a wavelength $\lambda > 8 \text{ \AA}$. The flux at the sample position is $5 \cdot 10^5$ neutrons/(cm² s) unpolarized. It is situated at the cold neutron guide NL6b in the neutron guide hall of the FRM II. As the instrument set-up can be changed quickly, MIRA is ideally suited as a testing platform for realizing new instrumental set-ups and ideas. In particular, MIRA is unique in its possibilities of combining different neutron scattering methods such as:

- Polarized or non-polarized small angle scattering (SANS)
- Classical NRSE (Neutron Resonance Spin Echo) setup as well as using the MIEZE (Modulation of Intensity by Zero Effort) principle
- Polarized or non-polarized reflectometry
- Spherical Polarimetry

Status

In 2008, MIRA operated successfully for 4 cycles of the FRM II, in total 240 days. A total number of 11 user-experiments, 12 internal experiments, together with extensive tests and service measurements were performed. A total of 2 weeks was devoted to the "Fortgeschrittenenpraktikum" (see 6.2) of the Physics Department for 24 students. A major part of the beam time was used for SANS measurements in helical magnets (see 5.1) and the development of MIEZE. In total 6 publications were published this year, one of them in Science. One student (Leonhard Polz) from the Fachhochschule München spent his practical semester at MIRA constructing and building the motorization of our magnet. A physics student in his fifth year from the TU Delft (Jörgen Konings) currently passes his practical training semester at MIRA performing Monte Carlo simulations of the MIEZE setup.

Upgrade for shorter wavelengths

Currently the upgrade of MIRA to shorter wavelengths is in progress. The goal is to use neutrons with wavelengths between 3 \AA and 6 \AA from the neutron guide

NL6a (beam area $120 \times 60 \text{ mm}^2$) using a PG monochromator (see Figure 3.1). The polygraphite (PG) monochromator and its mechanics have been installed and first tests at 4.3 \AA yield a sample position flux of $3 \cdot 10^6$ neutrons/(cm² s) unpolarized for a fixed focussation of the PG monochromator.

The MIEZE setup was completed and equipped with a water cooling system (see Figure 3.3). This extends the MIEZE (spin echo) times to a range from 20 ps to 10 ns. The use of the second beamport with shorter wavelengths will further extend the time range to shorter times.

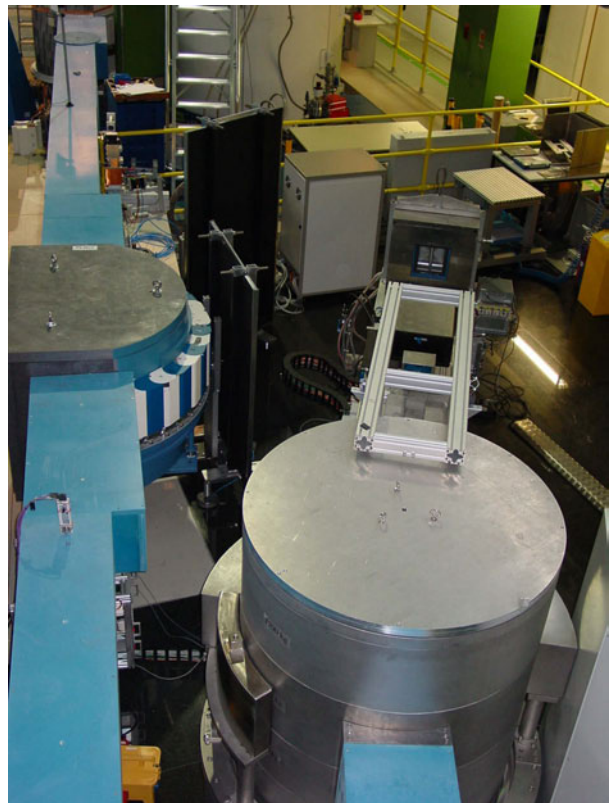


Figure 3.1.: The two beam ports for MIRA. Left the port for wavelengths between 3 \AA and 6 \AA . Right the old beam port for wavelengths above 8 \AA .



Figure 3.2.: The PG monochromator with its electronics.

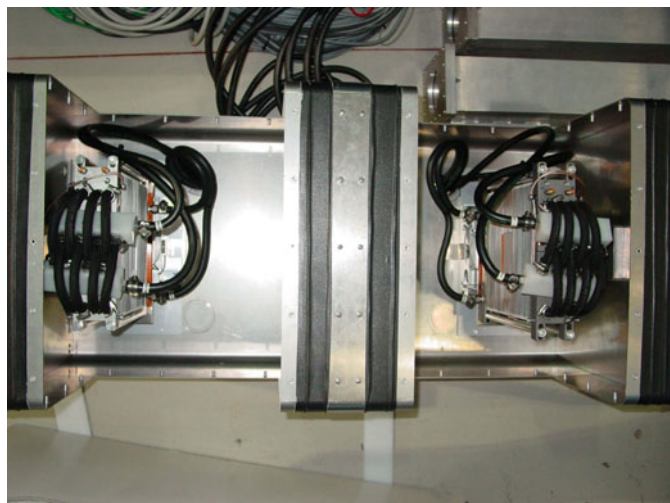


Figure 3.3.: The MIEZE NRSE coils with water cooling.

3.2. RESEDA operates with two arms

W. Häußler^{1,2}, J. Kindervater², M. Sandhofer¹, R. Schwikowski², A. Mantwill¹, P. Böni¹

¹Physik-Department E21, TU München

²ZWE FRM II, TU München

In 2008, first quasielastic experiments have been performed at the Neutron Resonance Spin Echo (NRSE) spectrometer RESEDA. Critical dynamics in a magnetic system and dynamics in a metal melt have been studied. In collaboration with a group of scientists from the university of Heidelberg, a challenging new NRSE technique detecting high frequency oscillations of the neutron polarization has been tested at RESEDA. During these first experimental studies, the neutron velocity selector had to be demounted and sent away for maintenance works. Exchanging and reinstalling the selector could be accomplished within only two days for each task - thanks to the good collaboration of several groups providing technical support at FRM II.

Commissioning phase

Before these first experiments, the commissioning phase of the instrument had taken place, during the first months of 2008, including reparation and demagnetization of the mu-metal shielding, revision of the coupling coils and the fine-tuning of the RF circuits. Having finished preliminary polarization measurements, the NRSE coils have been put into operation and we started then with spin echo test measurements, employing NRSE together with NSE, the latter by using solenoids for measurements at small spin echo times. Moreover, an improved design of the radiation shielding covering the new polarizer, shutter, attenuators and beam monitor at the primary side of the spectrometer has been constructed, and will be installed as soon as it is delivered.

After having commissioned the instrument as described above, and during ongoing NSE and NRSE experiments by scientists from Germany, England and Switzerland, the instrument is still being improved step by step. The NRSE coils suffering from corrosion due to the mixture of copper and aluminum parts are being repaired. Additional NRSE coils are going to be built, in order to make and keep RESEDA fully operational.

Doubled solid angle

RESEDA is operational with one primary and one secondary spectrometer arm. A special feature of the NRSE method will be used soon: NRSE allows in a straightforward way for installing additional secondary spectrometer arms. The secondary spectrometer of RESEDA is being doubled at the moment (Fig. 3.4): the spin echo coils used for NSE measurements at small spin echo times, the analyser and the detector have already been installed. In order to be able to simultaneously operate two secondary NRSE spectrometer arms, two of the NRSE coils being under construction at the moment, will be installed and put into operation in this supplementary spectrometer arm. During 2009, after having finished these installations, RESEDA will be going into operation with doubled solid angle for neutron detection.



Figure 3.4.: The two secondary spectrometer arms of the Neutron Resonance Spectrometer RESEDA.

3.3. First year of operation of the backscattering spectrometer SPHERES

J. Wuttke¹, G. J. Schneider¹, L. C. Pardo Soto^{1,2}, M. Prager^{†3}, A. Budwig⁴, M. Drochner⁵, U. Giesen⁴, A. Ioffe¹, H. Kämmerling⁴, H. Kleines⁵, B. Lindenau⁴, V. Ossovyi¹, U. Pabst⁴, H. Schneider¹, P. P. Stronciwilk¹, D. Richter³

¹Forschungszentrum Jülich, Institut für Festkörperphysik, Jülich Centre for Neutron Science

²Departament de Física i Enginyeria Nuclear, Universitat Politècnica de Catalunya, Barcelona

³Forschungszentrum Jülich, Institut für Festkörperphysik, Neutronenstreuung

⁴Forschungszentrum Jülich, Zentralabteilung Technologie

⁵Forschungszentrum Jülich, Zentralinstitut für Elektronik

Status

Since winter 2007/2008, our new backscattering spectrometer SPHERES is in full operation. Ten external experiments were performed in 2008.

The energy resolution is $0.65 \mu\text{eV}$, the dynamic range $\pm 30 \mu\text{eV}$. The q range of the standard (large-angle) analyzers is $0.6 \dots 1.8 \text{ \AA}^{-1}$; annular small-angle analyzers give access to $q = 0.2 \dots 0.5 \text{ \AA}^{-1}$ at reduced energy resolution. The incoming integral flux at the end of the focussing neutron guide, after the selector, is of the order 10^{10} s^{-1} ; the secondary flux at the sample position is about $8 \cdot 10^5 \text{ s}^{-1}$; it is reasonably homogeneous over an area of about $3 \times 3 \text{ cm}^2$.

Background reduction

When routine operation started in fall 2007, the signal-to-noise ratio was about 300:1. It was found that almost half of the background came from fast neutrons produced in Li absorbers in the chopper wheel. Therefore in fall 2008 the graphite deflectors were transferred

into a new wheel, where B_4C is used instead of Li (Fig. 3.5). To prepare the in-situ balancing of the new wheel, we undertook a detailed vibration analysis of the entire chopper. As a result, the signal-to-noise ratio is now at least 600:1 (Fig. 3.6); this value has been confirmed and even surpassed in real experiments with user-provided samples.

Software development

Spectrometer components are controlled by a number of independent, elementary programs (in C for tracking the monochromator motion and for accumulating neutron histograms, in Ruby for controlling the shutter, the neutron velocity selector, the Doppler drive, the sample temperature controller, and other peripherals). Instrument scientists and technicians can intervene at all levels through a command-line interface. Users can issue all commands they need through a graphical interface. At the same time, this interface gives a complete overview over the current status of the spectrometer and results from the current measurement (Fig. 3.7).



Figure 3.5.: Vu Thanh Nguyen und Björn Poschen retrieve the graphite crystals from the old chopper wheel. Michael Prager watches closely.

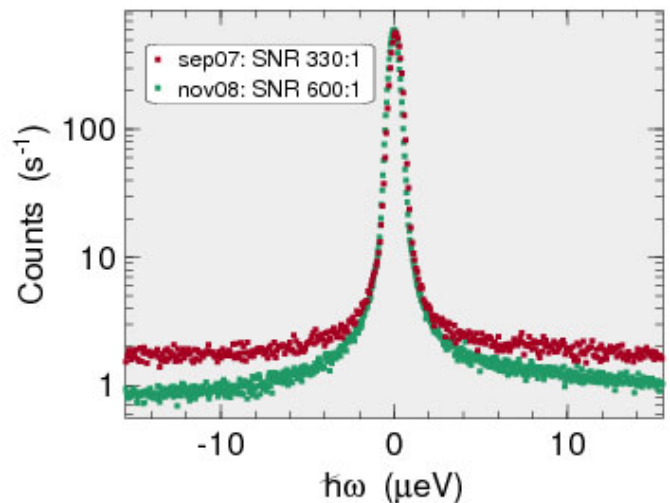


Figure 3.6.: Instrumental resolution, measured on a standard scatterer (PET plastic foil). Thanks to the refurbishment of the chopper wheel, the signal-to-noise ratio has become quite satisfactory; the resolution is now dominated by the wings characteristic of a crystal spectrometer.

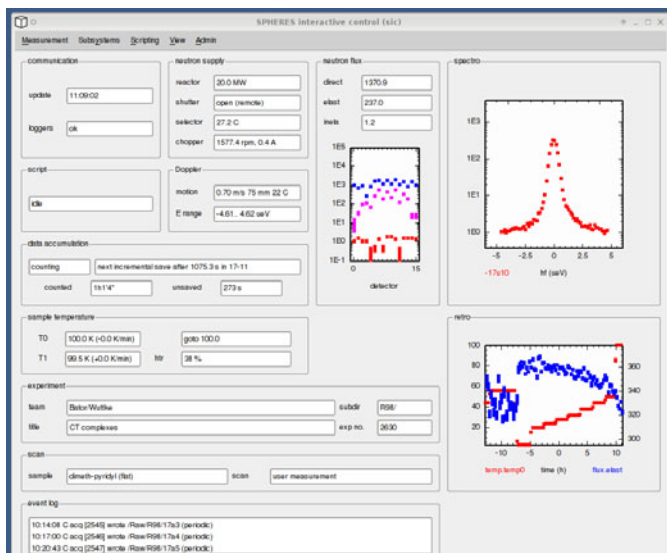


Figure 3.7.: The SPHERES interactive control (sic) gives an overview over the ongoing experiment, and allows users to enter commands via a menu bar.

We are now working on extending this dual approach (command-line based, with graphical interface on top of it) towards data reduction procedures. Conversion of inelastic raw data into normalized scattering laws is done by the new program SLAW, which will be extended to support other spectrometers, replacing legacy code like SQW. To satisfy different user needs, data can be written in a variety of formats.

Confined water

In confined geometry, water can be supercooled far below its bulk freezing point 273 K. The monolayer of water absorbed to a protein surface can be supercooled to about 150K. This hydration shell is believed to have decisive influence upon the thermal fluctuations of the protein. Recently, it has been postulated that hydration water relaxation, as measured on the backscattering spectrometer HFBS at NIST (National Institute of Standards and Technology), can be interpreted in terms of a fragile-to-strong crossover (Chen et al. 2006). Taking advantage of the better energy resolution of SPHERES, we are currently evaluating these claims (Busch, Doster et al., work in progress)

The kinetics of water in cement is particularly important for the retention of radioactive waste. SPHERES has been used to measure the diffusivity of water in different cements. Taking into account different curing conditions, contributions from pores and from cracks can be separated (Aldridge et al. [1]).

Polymer and protein dynamics

Quasielastic scattering can be used to investigate segmental dynamics of polymers and proteins. To identify and separate different types of motion, it is necessary to scan broad energy, wavenumber and temperature ranges.

In an extensive study of poly(ethyl methacrylate), methyl group rotation has been separated from backbone motion. The latter can be described by the Fourier transform of a stretched exponential (KWW function), extending observations made by dielectric spectroscopy. The q dependence, however, significantly deviates from expectations, requiring further study (Fig. 3.8, Génix et al., report 1294).

In the study of small proteins, a somewhat similar convolution approach is used to separate intramolecular motion from diffusion. Anomalies in the temperature dependence are used to detect miscellisation (Gaspar et al., report 667).

Molecular rotations

Backscattering spectroscopy is ideally suited for studying slow rotations of methyl groups or ammonium ions. With decreasing temperature, one sees a transition from classical jump rerotation to quantum-mechanical tunneling.

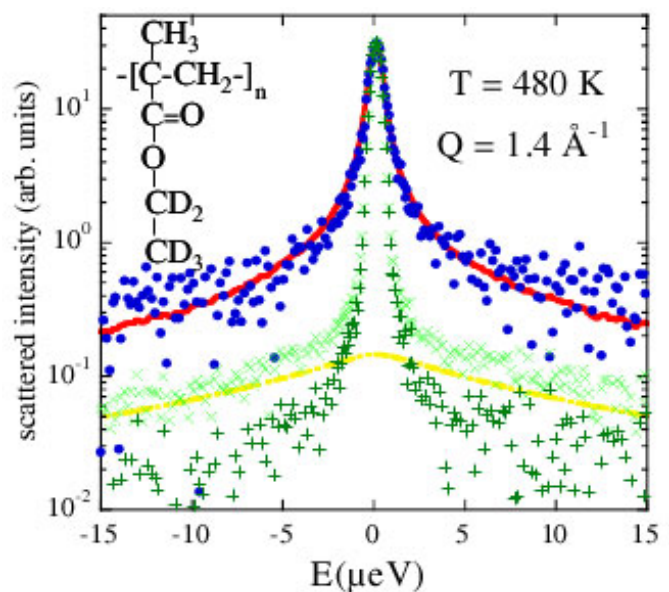


Figure 3.8.: Scattering function of poly(ethyl methacrylate) at $q = 1.4 \text{ \AA}^{-1}$, $T = 480 \text{ K}$ (blue). The fit (red) is a convolution of a KWW function (describing the overall segmental dynamics) with an effective convolution (green \times), which accounts for methyl group rotations (yellow) and the instrumental resolution (green $+$) [Génix et al.].

The ammonium ions in $(\text{NH}_4)_2\text{PdCl}_6$ are entirely located at equivalent lattice sites of cubic symmetry. Therefore, the ammonium ions are particularly simple tetrahedral rotors; the librational ground state is split into no more than three energetically different tunneling states. In the low-temperature limit, the E-T splitting is about $29 \mu\text{eV}$, which fits perfectly into the dynamic range of SPHERES ($-30.6 \dots 30.9 \mu\text{eV}$). Fig. 3.9 shows the discrete lines measured at 3.7 K. The inelastic lines at $\pm 29 \mu\text{eV}$ are significantly broader than the instrumental resolution. From the temperature dependence, we can rule out thermally activated processes. As tunneling lines are very sensitive to slight variations in the potential barriers, the broadening is probably due to a spread of tunneling splittings caused by crystal imperfections (Prager et al., continued by Wuttke).

Combining backscattering and time-of-flight spectra, the dynamics of $(\text{NH}_4)_2\text{S}_2\text{O}_8$ was studied over more than five decades in energy. Due to the absence of symmetry at the ammonium site, the librational ground state is split into four bands, with transition energies differing by orders of magnitude. In consequence, in a good first ap-

proximation, the ammonium motion can be modelled as one-dimensional rotational (Prager et al. [2]).

Nuclear spin excitations

Neutron backscattering can also be used for the study of nuclear spin excitations. On SPHERES, hyperfine splitting of antiferromagnetic NdMg_3 and of ferroelectric NdCo_2 has been measured as a function of temperature and energy (Fig. 3.10). Together with data on other Nd compounds, results allowed to establish a linear relationship between the nuclear excitation energy and the ordered magnetic moment of the Nd ion (Chatterji et al. [3]).

[1] Aldridge, L. P., Bordallo, H. N., K. Fernando, W. K. B., Wuttke, J., Pardo, L. C. *Cement Concrete Res.* Submitted.

[2] Prager, M., Grimm, H., Natkaniec, I., Nowak, D., Unruh, T. *J. Phys.: Condens. Matter*, 20, (2008), 125218.

[3] Chatterji, T., Schneider, G. J., Galera, R. M. *Phys. Rev. B*, 78, (2008), 012411.

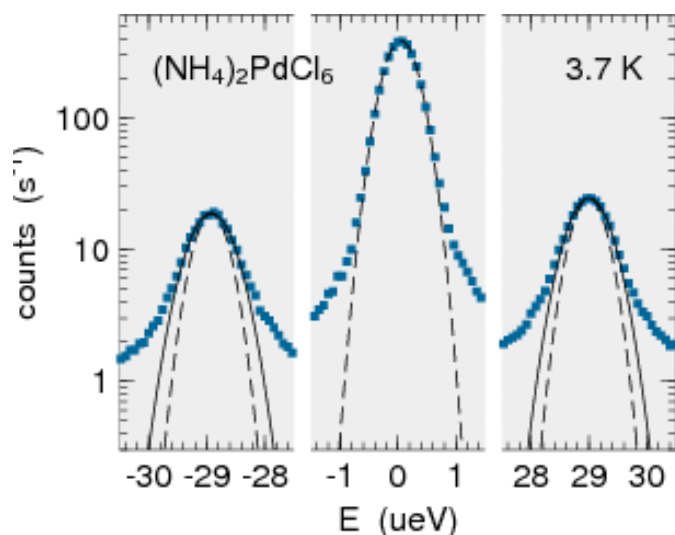


Figure 3.9.: Inelastic and elastic scattering from $(\text{NH}_4)_2\text{PdCl}_6$ in the low-temperature limit. The inelastic lines have $\text{fwhm} = 0.84 \mu\text{eV}$ (read off from Gaussian fits, solid curves). The central line has $\text{fwhm} = 0.66 \mu\text{eV}$ (dashed curve), which is compatible with the known resolution of SPHERES.

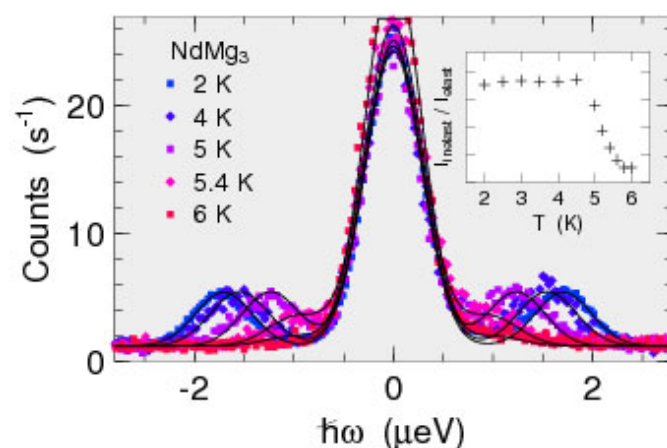


Figure 3.10.: Hyperfine spectrum of NdMg_3 . On approaching the Néel temperature 6 K, the intensity of the inelastic line decreases rapidly (inset).

3.4. Paramagnetic experiments and soft matter physics at J-NSE

O. Holderer¹, M. Monkenbusch², N. Arend¹, N.R. De Souza¹, H. Kleines³, F. Suxdorf³, M. Wagener³, M. Drochner³, W. Westerhausen⁴, C. Tiemann⁴, B. Laatsch⁴, R. Schätzler², D. Richter^{1,2}

¹JCNS, Forschungszentrum Jülich GmbH

²Institut für Neutronenstreuung, IFF, Forschungszentrum Jülich GmbH

³ZEL, Forschungszentrum Jülich GmbH

⁴ZAT, Forschungszentrum Jülich GmbH

Neutron spin echo (NSE) spectroscopy is due to its high energy resolution an indispensable tool for studying slow dynamics on mesoscopic length scales in complex fluids like polymer melts, microemulsions or protein solutions or the dynamics of glass forming systems that become slow on all length scales close to the glass transition. Slow magnetic fluctuations are another realm of the NSE method. The Jülich NSE spectrometer J-NSE has been moved from the Jülich research reactor FRJ-2 to the FRM II [1, 2]. In the context of the transfer, parts of the spectrometer have been renewed and improved, leading to a significantly larger energy resolution and larger dynamic range.

High intensity and resolution

The high energy resolution of NSE spectroscopy is obtained by encoding tiny velocity changes into changes of the spin direction of the neutrons. The normalized intermediate scattering function is measured in terms of polarization loss of the scattered neutrons. Since the high resolution, i.e. the polarization change, results from the difference of velocities of the same neutron before and after scattering, the instrument can accept a beam with a wide velocity distribution and correspondingly high intensity without compromising the resolution.



Figure 3.11.: The sample position (on the right) and second precession coil (green) of the J-NSE spectrometer.

15fold gain of intensity at FRM II

The new end position in the neutron guide hall of the FRM II provides a very intense neutron beam with a 15 fold gain of intensity at the sample position compared to the setup in Jülich at a wavelength of 8 Å. The accessible wavevector (q) range is 0.02 to 1.7 Å⁻¹, corresponding to distances of interest from 0.37 to 30 nm. Fourier times between 3 ps and 150 ns can be accessed at the moment by combining wavelength between $\lambda = 4.5 \dots 17$ Å and field integral variation from $J = 3 \times 10^{-4} \dots 0.3$ Tm. The Fourier time $\tau/\text{ns} \simeq 0.2 \times J/(\text{Tm}) \times (\lambda/\text{Å})^3$. Ongoing development will improve the correction coils, which will allow using field integrals up to the maximum of 0.5 Tm of the main solenoids, thereby increasing the dynamic range of the spectrometer by a factor of 2.

Besides its applications in studying slow processes in soft matter, neutron spin-echo spectroscopy can also serve to investigate the dynamics of paramagnetic scatterers, for example spin glasses. Additional coils ("y-coils") have therefore been installed at the sample position which allow to turn the spin in any direction at the sample position and separate paramagnetic from nuclear scattering for the normalization of the intermediate scattering function $S(q, \tau)$.

Dynamics at J-NSE

During the first year when the instrument has been open to external users, experiments have been performed addressing questions from many different parts of soft matter physics but also the first paramagnetic experiments have been carried out, some examples are given below.

The dynamics of deuterated polyethylene oxide (PEO) above the melting temperature has been studied at high q values around the structure factor peak ($q < 1.7$ Å⁻¹ and low Fourier times ($\tau > 3$ ps) (see Fig. 3.12). The collective dynamics of the PEO melt is probed in this way. The results have been compared with atomistic Monte Carlo (MC) simulations [3], showing an excellent agreement between the measured and simulated dynamic structure factor. Experimentally not accessible parameters could then be quantified by the MC simulations.

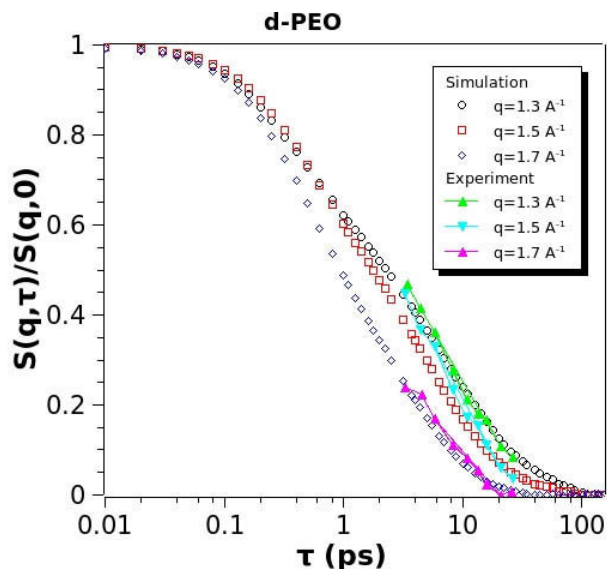


Figure 3.12.: Coherent dynamic structure factor of deuterated PEO at 391 K compared with MD simulations. At a wavelength of 5 \AA , the smallest accessible Fourier time is 3 ps, the largest q vector 1.7 \AA^{-1}

Microemulsions under pressure

Different experiments have been performed on bicontinuous (sponge like) microemulsions, consisting of oil, water and a surfactant, where the dynamics of the surfactant interface layer is measured with NSE. The influence of temperature or co-surfactants on the bending rigid-

ity can thus be studied. A new system in this context are microemulsions with supercritical CO_2 as oil at elevated pressure and temperature. First experiments on the dynamics of such "unconventional" microemulsions allowed to determine the bending rigidity of the surfactant layer therein. It has been observed that the bending rigidity is lowered by a factor of two, which can be explained by the lower average viscosity of the medium (oil, CO_2) surrounding the membrane. Additionally, the bending rigidity varies with pressure and surfactant concentration.

The dynamics of polymer chains confined in micellar systems of diblock copolymers, consisting of Polyisoprene (PI) and Polydimethylsiloxane (PDMS), has been studied in different contrasts to highlight different parts of the system [4]. Structural investigations with SANS revealed a cylindrical structure of PI domains surrounded by PDMS. In "bulk" contrast, protonated PI and deuterated PDMS has been used to measure the dynamics of the PI-PDMS interface. The dynamic structure factor over four decades of Fourier times is shown in Figure 3.13. Evaluation of results is in progress and will shed light on surface undulations of the cylindrical PI domains.

Correction coil developments

Magnetic fields of the main solenoids have been corrected by six spiral aluminum coils (Fresnel coils), which can be shaped with not only quadratic corrections, but also higher terms are taken into account. Nonetheless, the precision of different steps in the manufacturing process were the limiting factor for the quality of correction,

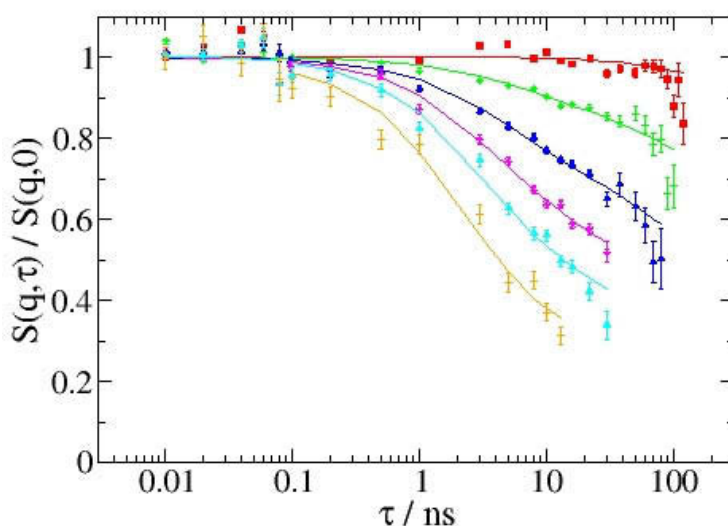


Figure 3.13.: Coherent dynamic structure factor of PI in PDMS covering more than four decades of Fourier time from 10 ps to 120 ns.

especially at high magnetic fields. Development is going on to improve the correction elements. The existing coils will, where possible, be exchanged by so called "Pythagoras" coils [5], which consist of two rectangular parts, each part applying a quadratic correction to the magnetic field in x- and y-direction. The sum of the two coils leads then to a radial quadratic correction. A first prototype has been installed at the J-NSE and showed that this concept is very promising. Other correction coils will be replaced as soon as available. The largest correction coil is located at the end of the second main precession coil where the scattered beam has the largest cross section. It is the position with the highest requirements concerning the correction and higher terms than the quadratic one play a significant role. There, a coil with the "Pythagoras" design can only do a part of the correction. Different concepts are currently studied, ei-

ther using modified spiral Fresnel coils or a combination of spiral and "Pythagoras" coils.

- [1] Holderer, O., *et al. Nucl. Instr. & Methods In Physics Research A*, 586, (2008), 90–94.
- [2] Holderer, O., *et al. Meas. Sci. Technol.*, 19, (2008), 034022.
- [3] Brodeck, M., *et al. J. Chem. Phys.*, 130, (2009), 094908.
- [4] Thanks to R. Lund, Donostia International Physics Center, San Sebastian, Spain and L. Willner (IFF, Forschungszentrum Jülich) for the permission of presenting the data.
- [5] Based on a concept developed and also used at IN15, ILL, by B. Farago and G. Kali.

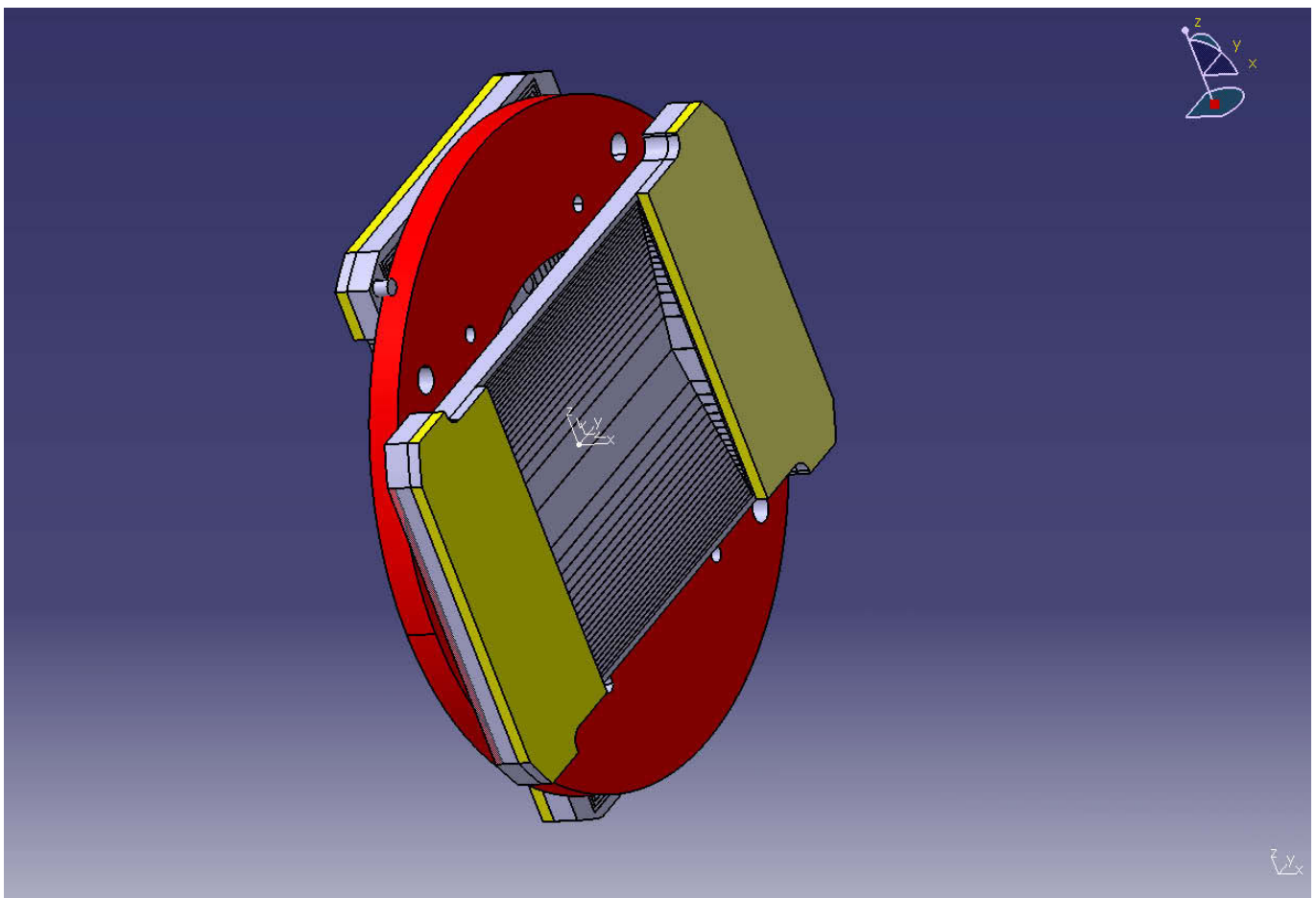


Figure 3.14.: Drawing of a "Pythagoras" correction coil. The performance of the first coil which has been installed at the J-NSE spectrometer, showed that this design corrects well the field inhomogeneities.

3.5. Molecular motions in pharmaceutical products – Research at TOFTOF

T. Unruh^{1,2}, C. Smuda^{1,2}, S. Busch^{1,2}, J. Neuhaus^{1,2}, W. Petry^{1,2}

¹ZWE FRM II, TU München

²Physik-Department E13, TU München

The TOFTOF team can look back on a very successful year 2008. Except for two weeks the spectrometer was operational for all of the 251 days of reactor operation. In this time more than 50 scientific research projects could be executed from which 29 were performed by external groups. Furthermore, 23 original contributions related to measurements performed at TOFTOF were submitted to peer reviewed journals in 2008 from which 16 are already published. Some of the inhouse research projects were initiated by the soft matter group at the spectrometer. These activities will shortly be introduced in this contribution.

Molecules in motion

In general our research is focussed on studies of molecular motions and the spatial arrangement of organic molecules in dispersions used in pharmacy as carrier systems for drug delivery but also in food or other indus-

tries. Our recent studies included experiments on the dynamics of liquid (bulk and dispersed) phases of simple molecules like oils or fats but also on the motions of stabilizer molecules or other additives as for instance drug molecules in pharmaceutical formulations. From these studies a better insight to the transport mechanism of the molecules in simple molecular liquids but also in phospholipid mono- and bilayers could be achieved. The understanding of the microscopic structure and dynamics should help to optimize macroscopic physicochemical properties of, e.g., pharmaceutical products such as drug release rate or dispersion stability [1].

Already with the first quasielastic time-of-flight neutron scattering (TOF-QENS) experiments it could be demonstrated for the pharmaceutical formulation of coenzyme Q₁₀ in the form of nanodroplets stabilized by phospholipids in an aqueous phase that QENS is best suited to study the dynamical properties of molecules inside the nanosized droplets of dispersions [2]. It was, how-

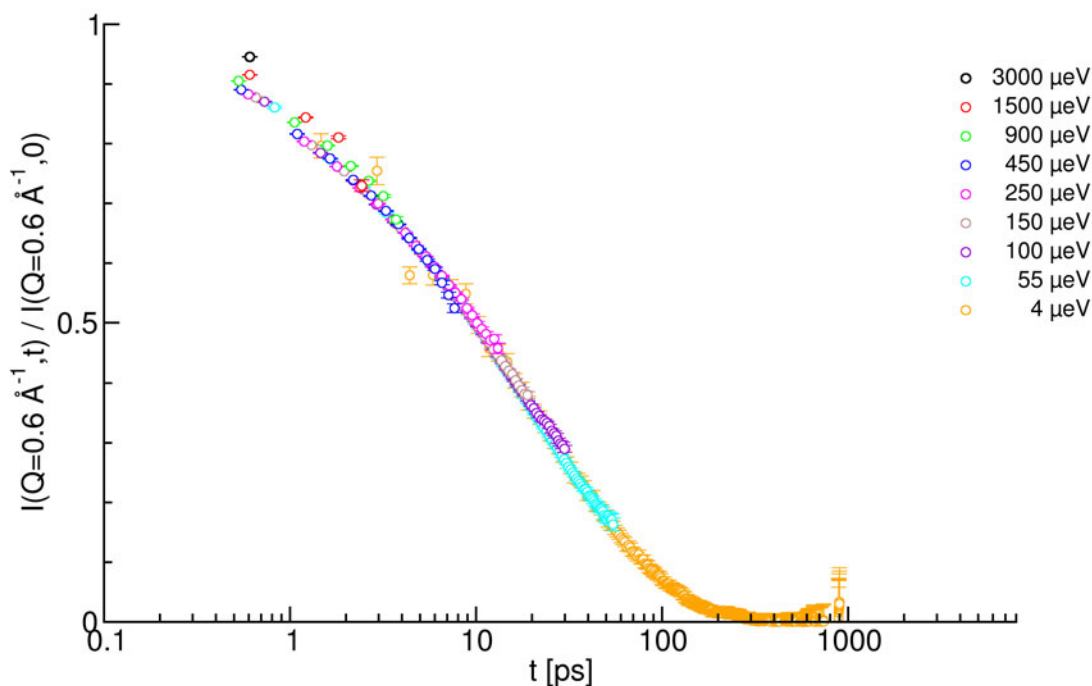


Figure 3.15.: Intermediate scattering function of the *n*-alkane C₃₂H₆₆ at 90°C measured with the TOFTOF spectrometer and using the labeled instrumental resolutions (FWHM of the elastic line). Representative trajectories of a single molecule as extracted from MD simulations of the same liquid alkane are plotted for time ranges between 0 ps and 1 ps, 20 ps, 400 ps and 8 ns, respectively. The time evolution is indicated for each picture by color intensification. For each picture 20 snapshots of the molecule equidistant in time are overlaid.

ever, found that the dynamics of medium-sized organic molecules in the liquid state is not well understood. Therefore, systematic studies on the picosecond dynamics as probed by TOF-QENS of medium-chain molecules like Q₁₀ and *n*-alkanes were performed [3]. Using the combination of QENS and molecular dynamics (MD) simulations, different diffusive motions could be disentangled ranging from fast tumbling of CH₂-groups to the long range molecular diffusion (cf. Fig. 3.15) [4]. Despite the rod like shape of the molecules the center-of-mass diffusion was found to be essentially isotropic.

Due to the fact that in many organic molecules CH₃-group rotation contributes significantly to the QENS signal, this special local motion has been studied in detail [5, 6, 7]. It could be demonstrated that CH₃-group rotation can be extrapolated from low temperatures of the glassy state to the liquid state by the Arrhenius behavior of the rotational diffusion coefficient. In the liquid state the CH₃-groups rotate free of barrier.

From TOF-QENS studies of phospholipid (DMPC) liquid crystals, vesicles, and emulsions stabilized by DMPC an evidence was found that the long range motion on a picosecond time scale has a flow-like character. This result confirms recent MD simulations experimentally and adds another piece of knowledge to the understanding of lateral diffusion of molecules in membranes.

Structures in X-ray

The interpretation of the dynamics of phospholipid molecules in the stabilizing layer of emulsions is difficult without the knowledge of the structural arrangement of the molecules. For this purpose a special eval-

uation method of small angle X-ray scattering (SAXS) experiments (X-ray powder pattern simulation analysis, XPPSA) has been developed and first results of phospholipid layers surrounding solid triglyceride nanoparticles have been achieved [8]. The continuation of this project is now supported by the DFG for three years and a collaboration with the Department of Pharmaceutical Technology of the Technische Universität Braunschweig has been established in order to correlate our results with pharmaceutical parameters of relevant pharmaceutical systems.

- [1] Bunjes, H., Unruh, T. *Advanced Drug Delivery Reviews*, 59, (2007), 379–402.
- [2] Unruh, T., Smuda, C., Gemmecker, G., Bunjes, H. In: Sokol, P. E., Kaiser, H., Baxter, D., Pynn, R., Bossev, D., Leuschner, M., editors, *Quasi-Elastic Neutron Scattering Conference 2006*, 137–145 (Mater. Res. Soc., Warrendale, PA, 2007).
- [3] Smuda, C., Busch, S., Gemmecker, G., Unruh, T. *J. Chem. Phys.*, 129, (2008), 014513.
- [4] Unruh, T., Smuda, C., Busch, S., Neuhaus, J., Petry, W. *J. Chem. Phys.*, 129, (2008), 121106.
- [5] Smuda, C., Busch, S., Wagner, B., Unruh, T. *J. Chem. Phys.*, 129, (2008), 074507.
- [6] Smuda, C., Gemmecker, G., Unruh, T. *J. Chem. Phys.*, 128, (2008), 194502.
- [7] Smuda, C., Busch, S., Schellenberg, R., Unruh, T. *J. Phys. Chem. B*, 113, (2009), 916.
- [8] Unruh, T. *J. Appl. Cryst.*, 40, (2007), 1008–1018.

4. Nuclear physics and Applied Science

4.1. Element determination in 3D at PGAA

P. Kudejova^{1,2}, L. Canella², R. Schulze¹, J. Jolie¹, A. Türler², T. Belgya³, L. Szentmiklósi³, Z. Kis³, M. Ebert¹

¹Institut für Kernphysik, Universität zu Köln

²Institut für Radiochemie, Technische Universität München

³Institute of Isotopes, Hungarian Academy of Sciences

The beginning of 2008 was dedicated to the optimisation of the new PGAA setup. In February 2008 the instrument was opened to users. Starting from June 2008 a new configuration was added to the PGAA setup in order to achieve the goals proposed for the European Ancient Charm project. This configuration allows position sensitive PGAA measurements (Prompt Gamma-ray Activation Imaging - PGAI [1, 2]). For the selection of the active measurement regions inside the samples a neutron tomography (NT) of the samples can be performed directly at the PGAA station.

Non-destructive element analysis

Prompt Gamma-Ray Activation Analysis is a radioanalytical technique for the determination of the elemental composition of various samples. Main advantage of this method is its non-destructiveness. Therefore it is suitable for small to medium sized archaeological objects as well as for other valuable samples. This property was one of the reasons why the PGAA technique was chosen to be extended to a position sensitive measurement method in the frame of the Ancient Charm project [3, 4], a European project for the analysis of cultural heritage

objects.

Beside this project, also standard PGAA measurements were carried out. The results obtained in the first part of 2008 gave important informations concerning the direction of the further optimisation planned for 2009. An important result was the measurement of a standard reference material in order to check the reliability of our PGAA instrument.

Measurement of standard reference material

One of the most important measurements done with the standard PGAA setup, was the elemental analysis of a standard reference material (from NIST). This measurement is not particularly difficult or new, but it is a proof of the reliability of the analysis with the PGAA instrument.

The sample analysed was Estuarine sediment (SRM #1646a) [5]. In the table 4.1 the results obtained [6] are shown. With the exception of Ca the results are in good agreement with the certified values and the values measured at PSI.

Table 4.1.: Results of analysis on the standard reference material Estuarine sediment.

Element	PGAA @ FRMII	PGAA @ PSI*	Certified value
H ($\mu\text{g/g}$)	0.249 ± 0.003		
B ($\mu\text{g/g}$)	31.7 ± 0.3	41.8 ± 1.1	
Al (% _w)	2.442 ± 0.081	2.14 ± 0.05	2.297 ± 0.018
Si (% _w)	39.25 ± 0.55	40.00	40.00 ± 0.16
S (% _w)	0.26 ± 0.03	0.347 ± 0.010	0.352 ± 0.004
Cl (% _w)	0.612 ± 0.013	0.636 ± 0.008	
K (% _w)	0.860 ± 0.043	0.838 ± 0.020	0.864 ± 0.016
Ca (% _w)	0.785 ± 0.039	0.516 ± 0.010	0.519 ± 0.020
Ti (% _w)	0.421 ± 0.015	0.473 ± 0.010	0.456 ± 0.021
Fe (% _w)	1.989 ± 0.054	1.860 ± 0.048	2.008 ± 0.039
Gd ($\mu\text{g/g}$)	3.1 ± 0.2	2.640 ± 0.078	

*S. Baechler et al., J. Radioanal. Nucl. Chem., vol. 256, n°2 (2003) pp. 239-245

The PGAI/NT setup

The new PGAI/NT setup is schematically shown in figure 4.1. The intersection of the two collimators for neutrons and for gamma-rays defines the active measurement volume, the so called isovolume, inside the sample. By moving the isovolume, i.e. moving the sample on a stepping motor driven positioning table, it is possible to have position sensitive PGAA measurements. The combination of all measured points will allow a 3D map of the elements inside the sample.

The use of the neutron tomography system allows the precise positioning of the isovolume in interesting measurement positions. The final goal is to combine the elemental 3D distribution and the tomographic reconstruction to have complementary information of the structure of the object.

Two Compton-suppressed HPGe detectors were used as a detection system for PGAI measurements and simultaneous bulk PGAA measurements. For automatic PGAI scans of the samples a digital acquisition system with configurable acquisition software is in use.

Measurements of archeological objects

In June 2008, the PGAI/NT setup was installed at the PGAA station. The difficult part was the calibration and alignment of the system, especially the accurate alignment of the two collimators in order to define the isovolume. Another crucial point were the shielding materials that should reduce as effectively as possible the radiation background, because in the PGAI configuration the count rate for gamma rays is much lower than normal due to the small aperture of the Pb collimator in front of the gamma ray detector.

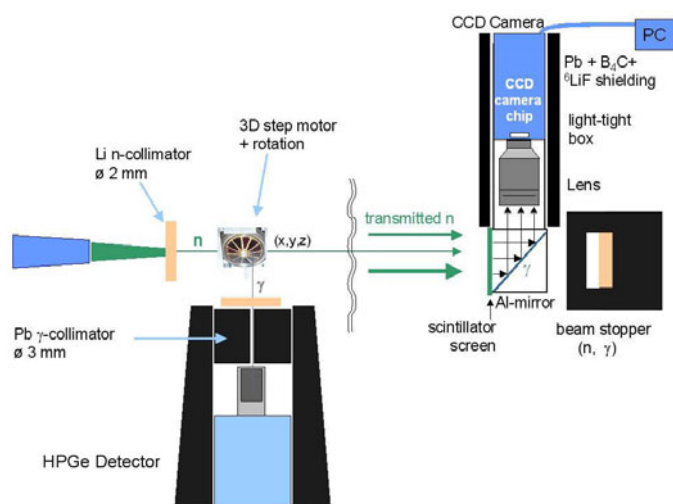


Figure 4.1.: Schematic view of the position sensitive PGAA setup and of the neutron tomography system.



Figure 4.2.: Head of the prophet of Lorenzo Ghiberti made of gilded bronze. It is part of the "Paradise Gate" of the Baptistery of Florence, Opera di Santa Maria del Fiore. The left part was cleaned with a laser technique and the right one with a wet chemistry method (Rochelle salts). The middle part is still uncleaned.

Before measurements on real cultural heritage objects were performed, the system was tested with replicas of archaeological objects which were produced in frame of the Ancient Charm project, i.e. a replica of an ancient fibula and a replica of an iron belt.

After the functionality of the PGAI/NT setup was proven, real archaeological objects were measured, e.g. two bronze heads from the *Gate of Paradise* in Florence (one of them shown in fig. 4.2).

Due to the dimensions and bulkiness of these objects in-depth 3D PGAI measurements were not possible, but instead surface measurements at different depths, with step sizes of $250 \mu\text{m}$ were performed. The positioning of the head was done with a laser beam that simulates the collimated neutron beam. Then the different depths were adjusted with the help of neutron radiographies. With this kind of measurements it was possible to determine the elements present in the first millimeter of the surface. This experiment opened a new application field for PGAI as a quasi-surface method for surface depths, where X-ray fluorescence or particle induced X-ray emission cannot be used.

One of the question to be answered with this measurements was the effectiveness of different cleaning methods (cleaning by laser and cleaning with Rochelle salts) tried at the head shown in fig. 4.2.

The analysis revealed the presence of chlorine in the dirty part of the head which is an expected component of the air pollution. The aim of the restorers is to eliminate residues of chlorine because they lead to corrosion of the bronze. In the laser cleaned part still some traces of chlorine could be found in contrast to the part cleaned with the Rochelle salts. Other elements found were: gold from the gilding, mercury, which was used in the gilding phase, so it is possible to observe traces of this element,

and copper as major element in bronze. Tin, as another compound in bronze could not be traced due to its much lower cross-section for (n,γ) -reactions and lower amount in bronze compared to copper.

Other objects investigated with PGAI/NT methods during 2008 were an ancient sealed ceramic vase with unknown content (fig. 4.3), a bronze belt point, which was assumed to contain a religious relic, and the originals of the previously mentioned replicas coming from the National Museum of Hungary in Budapest (fig. 4.4).

The investigation of the ceramic vase showed that an undefined powder is inside (see fig. 4.5), whose elemental composition is of great interest. PGAI measurements

and showed K, Ca, Ti, Si and B components. Further interpretation of the results is pending.

For the gold fibula currently the first complete PGAI grid measurement is performed which will result in a full 3D elemental map. The registration of this elemental map with the tomographic reconstruction will give the possibility to overlap the structure and elemental distribution in the fibula.

Fig. 4.6 shows the 3D image reconstruction of the fibula from the neutron tomography measurement.



Figure 4.3.: Proto corinthian ceramic vase; Museo Archeologico di Milano



Figure 4.4.: Gold fibula; Hungarian National Museum.
in different positions inside the powder were performed



Figure 4.5.: Neutron radiography of the corinthian ceramic vase.

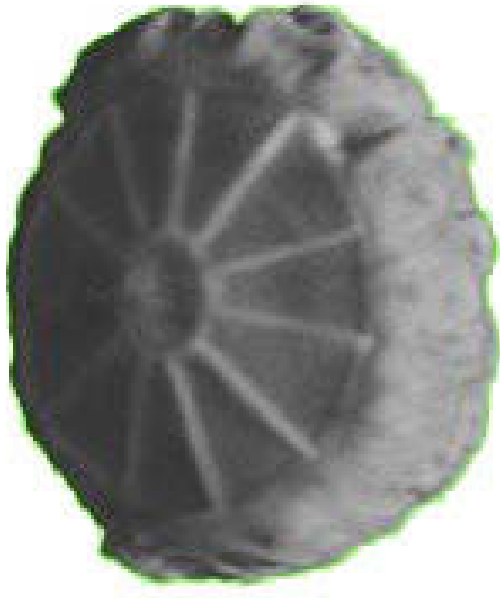


Figure 4.6.: Neutron tomography of the gold fibula.

Outlook

The PGAA station at FRM II has now a new set-up that allows the determination of the spatial distribution of elements inside samples of small and medium sizes. Currently a number of few precious objects coming from different museums were measured and are still under study.

The results obtained so far were quite important concerning the conservation and restoration of some of them and gave new information to the archaeologists and restorers.

Further analysis and interpretation of the acquired data is necessary, e.g. for obtaining modest quantitative results, the analysis of the data has to be refined by taking self-absorption effects of gammas and neutrons into account. For this task the neutron tomographies will prove to be useful, too.

Concerning the standard PGAA analysis the 2008 results allow to understand how to further optimise the instrument in the next year and also showed that the analysis is already quite reliable.

[1] Kudejova, P., Materna, T., Jolie, J., Türler, A., Wilk, P., Baechler, S., Kasztovszky, Z., Revay, Z., Belgya, T. *Journal of Radioanalytical and Nuclear Chemistry*, 265(2), (2005), 221–227.

[2] Kasztovszky, Z., Belgya, T. *Archeometriai Műhely*, 2, (2006), 16–21.

[3] Ancient Charm project. <http://ancient-charm.neutron-eu.net/ach/>.

[4] Gorini, G. *Il Nuovo Cimento*, 30(1), (2007), 47–58.

[5] NIST. NIST - National Institute of Standards and Technology
https://srmors.nist.gov/view_cert.cfm?srm=1646A.

[6] L. Canella, P. Kudejova, R. Schulze, N. Warr, J. Jolie, A. Türler, Zs. Revay, T. Belgya. In: *7th international Conference on Nuclear and Radiochemistry (24-29 August 2008)*.

4.2. Neutron periscopes used for imaging

B. Schillinger^{1,2}, E. Calzada^{1,2}, P. Böni², C. Breunig¹, C. Leroy³, M. Mühlbauer^{1,2}, A. Neubauer², M. Schulz^{1,2}

¹ZWE FRM II, TU München

²Physik-Department E21, TU München

³Ecole Centrale Paris, Chatenay-Malabry, France

A standard neutron guide is ill-suited for neutron imaging, because the reflections in the guide destroy the collimation of the neutron beam and let the cross section of the neutron guide act like a divergent area source. Most neutron imaging installations use a flight tube instead, but with the direct sight they also have a large background of gamma radiation and fast and epithermal neutrons. With the availability of high- m super mirrors [1], it has now become possible to build a neutron optical periscope that eliminates direct sight with two plain optical reflections only, without destroying the beam collimation ratio. Several prototypes have been built and tested at the ANTARES neutron imaging facility [2, 3]. Several neutron periscopes will be installed during the upgrade of the ANTARES in 2009/2010.

According to [4], a typical nickel-coated cold neutron guide delivers a collimation in the order of 70 close to its exit, a super mirror guide with $m = 2$ only half of it. The standard selectable collimation ratios of the flight tube setup at ANTARES are 400 and 800.

Only recently it has become possible to produce high- m neutron supermirrors. The critical reflection angle Θ_{max} increases linearly with m and is given by $\Theta_{max} = 0.1 m \lambda [\text{\AA}]$. Currently mirrors with m values up to $m = 4$ are commercially available [1], now also as polarizing supermirrors.

Construction of the periscope

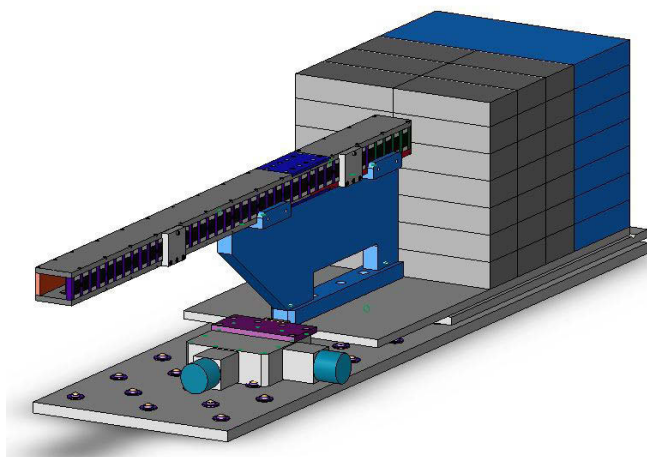


Figure 4.7.: The entire setup with the periscope in the middle and borated PE and Pb block as shielding to stop the primary beam.

For our first prototype of the periscope, we borrowed four $m = 5$ super mirrors of 0.5m length that were mounted concatenated as two 1 m-mirrors. The maximum intensity of the ANTARES spectrum is at $3.5\text{\AA} - 4\text{\AA}$, so we assumed a useful wavelength range of 3\AA to 5\AA . The maximum angle of reflection for the super mirrors is $\lambda \cdot m \cdot 0.1^\circ / \text{\AA}$, and thus for 3\AA equals 1.5° . Since the periscope must have some angle of acceptance, we defined an angle of 1.2° , so the total angle of deflection was 2.4° . For tests, the periscope was mounted within the measurement chamber of ANTARES, just before the sample position. An entrance window, made of borated polyethylene and lead, limited the incoming beam to the dimensions of the entrance window of the periscope. A beam stop also made of borated polyethylene and lead was mounted within the periscope, blocking the direct beam within. The outgoing beam had a size of $20 \times 58\text{mm}^2$ only and enabled only for the measurements of small samples. If the periscope is mounted close to the reactor, say in 12m distance to the sample, the resulting useful beam height will be 12cm. Fig. 4.8 shows a sketch of the neutron periscope.

Measurements

The open beam measurement shown in Fig. 4.9 was used to normalize the radiography measurements of a switch and potentiometer as well as a hard disk drive motor shown in Figs. 4.10 and 4.11. With these images, it was confirmed that the periscope does not alter the beam geometry on a large scale, other than shifting its axis, and introduced no visible distortion in the images.

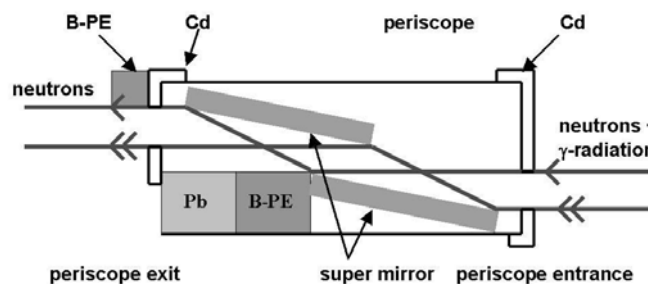


Figure 4.8.: The neutron optical periscope.

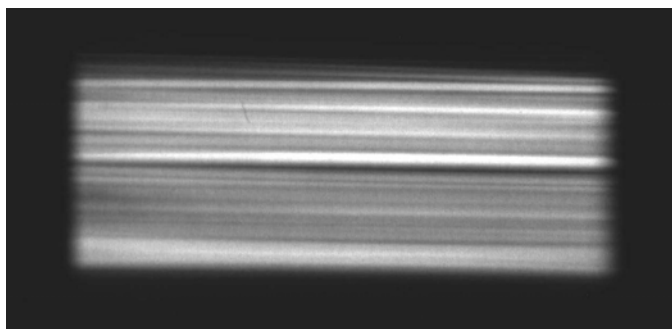


Figure 4.9.: Beam profile transmitted by the periscope.

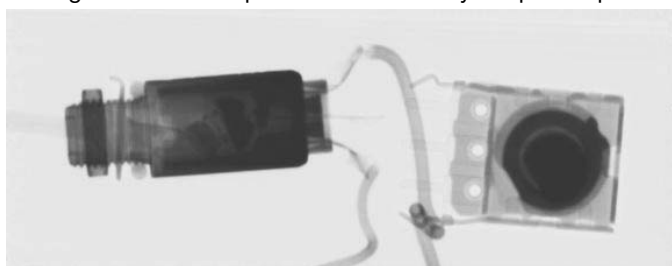


Figure 4.10.: Normalized high-resolution radiograph recorded with the periscope at $L/D=800$ at ANTARES.



Figure 4.11.: Normalized high-resolution radiograph recorded with the periscope at $L/D=800$ at ANTARES.

Specialized periscopes: Magnetic polarizer and band pass mirrors

The next obvious application was using polarizing mirrors to generate a high-resolution polarized beam.

Four polarizing supermirrors with a FeSi layer structure of $m = 3.88$ were used to build a first polarizing version of the neutron periscope. They are of $500 \text{ mm} \times 40 \text{ mm}$ size each and have a thickness of 2 mm. The periscope was optimized for a wavelength of 3.2 \AA , since at this wavelength the neutron flux of a monochromatic beam at the ANTARES facility has its maximum [5]. The mirrors are inclined by an angle of 1° with respect to the incoming beam, allowing to safely reflect a neutron beam with $\lambda = 3.2 \text{ \AA}$ and a divergence of 0.1° . The resulting beam width is approx. 17 mm. The height of the beam is approx. 36 mm and is limited by the size of the mirrors. The periscope setup has an overall length of approx. 1.8 m. An overview of the entire periscope assembly as installed at ANTARES can be seen in Fig. 4.7.

A magnetic field of 450 G necessary to saturate the coating of the supermirrors was produced by 200 Nd-FeB permanent magnets which were arranged on both sides of the polarizer housing, with their magnetization pointing in the same direction. The top and bottom parts of the periscope are made of iron which guides the return field of the permanent magnets to the space where the mirrors are mounted.

Fig. 4.12 (left) shows a striped structure, caused by imperfect mounting and surface tension of the mirrors due to the surface coating. The normalised image in Fig 4.12 (right) shows apparently lower quality than the other mirrors. This is mainly due to the large distance between the sample and the detector (more than 30 cm), caused by the bulky magnetic housing for the ^3He polarization analyzer cell for the following experiments. This leads to an inherent unsharpness of approx 0.4 mm at $L/D = 800$. Fig. 4.13 shows the polarization that was measured along the horizontal line indicated in Fig. 4.12 (left).

With an experimental setup with the periscope as a polarizer and a polarized ^3He cell as an analyzer as shown in Fig. 4.14 it was possible to do first spatially resolved neutron depolarization measurements on ANTARES. This method was used to determine the homogeneity of the concentration of Ni in various Ni_3Al samples. Since the Curie Temperature T_C of Ni_3Al depends crucially on the Ni concentration [6], even small deviations from the average concentration over the sample lead to a significant change in T_C . The samples were cylindrical rods

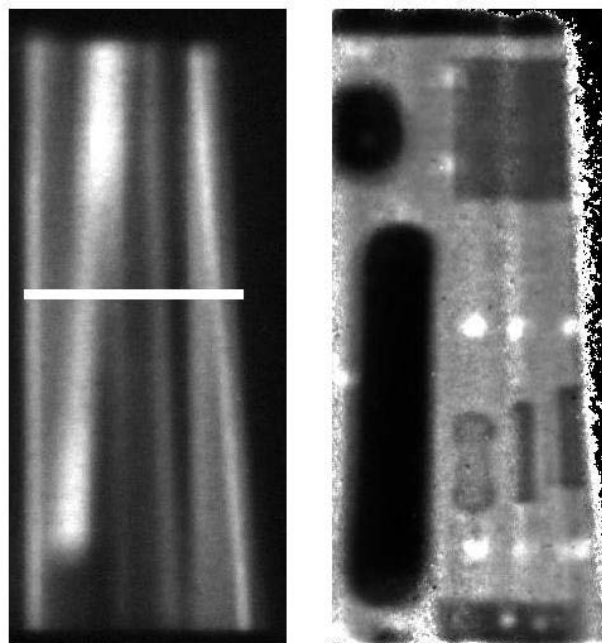


Figure 4.12.: (left): open beam image, the polarization over the white line is shown in Fig. 4.13; (right): normalized radiograph of a PCB, field of view: approx. $35 \times 15 \text{ mm}^2$.

(diameter 7 mm, length 50 – 70 mm) cast of molten mixtures of Ni and Al with different concentrations of Ni between 75% and 76% and expected Curie Temperatures of 40 K – 80 K.

By changing the sample temperature in a range between 10 K and 90 K (see Fig. 4.15) it was possible to measure the depolarization of the beam as a function of T .

In the paramagnetic state the beam polarization is not altered by the sample whereas in the ferromagnetic state the beam is depolarized due to the subsequent transmission of magnetic domains with different directions of magnetization [7]. With this method we found that T_C varies in a wide range over the sample volume. In some samples regions could be found where T_C was higher than 100 K, coexisting with regions of $T_C < 10$ K within the same sample. This lets us conclude that the distribution of Ni is inhomogeneous over the samples.

The sample was placed in a closed cycle refrigerator as short a distance away as possible from the magnetic box of a polarized ^3He cell analyzer. Thus the minimum sample to detector distance was geometrically constrained to 30 cm, which also limited the maximum resolution to 0.4 mm. Details of this method will be shown elsewhere.

The homogeneity of the beam intensity and polarization can be significantly improved by optimizing the support structures of the supermirrors thus flattening the mirrors. The future polarizing neutron periscopes will be built by the same techniques as a neutron guide. After these improvements we expect a beam polarization of $P \geq 0.99$ to be feasible.

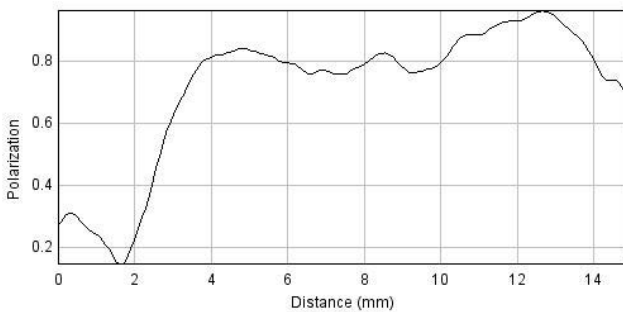


Figure 4.13.: Beam polarization over the line shown in Fig. 4.12 (left).

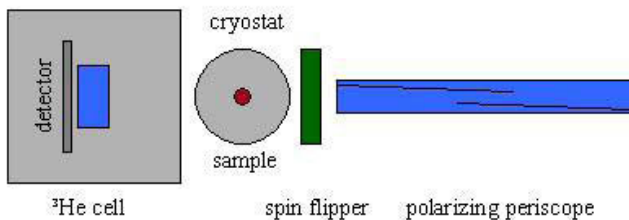


Figure 4.14.: Schematic of the experimental setup.

Coatings for super mirrors can also be adapted to a desired wavelength range, and can be built to act as band passes. We will next build a matching pair of periscopes that transmit wavelengths shorter than 3.5 Å and longer than 4.5 Å. With this set, we will be able to perform measurements above and below the Bragg cut-offs of most technical materials. By subtraction of these measurements, the separation of materials from compound work pieces will be possible. Using only the long wavelength band pass will lead to improved transmission through poly-crystalline materials such as steel.

All of these periscope types will be incorporated in the upgrade of the ANTARES-II facility in 2010.

- [1] Böni, P. *NIM A*, 1, (2008), 586.
- [2] Schillinger, B., *et al. J. Appl. Rad. Isotopes*, 61, (2004), 653–658.
- [3] Calzada, E., *et al. NIM A*, 542, (2005), 38–44.
- [4] Schillinger, B. *Nondest. Test. Eval.*, 16, (2001), 141–150.
- [5] Schulz, M., *et al. cc. pub. NIM A*, (2008).
- [6] Boer, D., *et al. J. Appl. Phys.*, 40, (1969), 1049–1055.
- [7] Halpern, O., Holstein, T. *J. Appl. Phys.*, 59, (1941), 960.

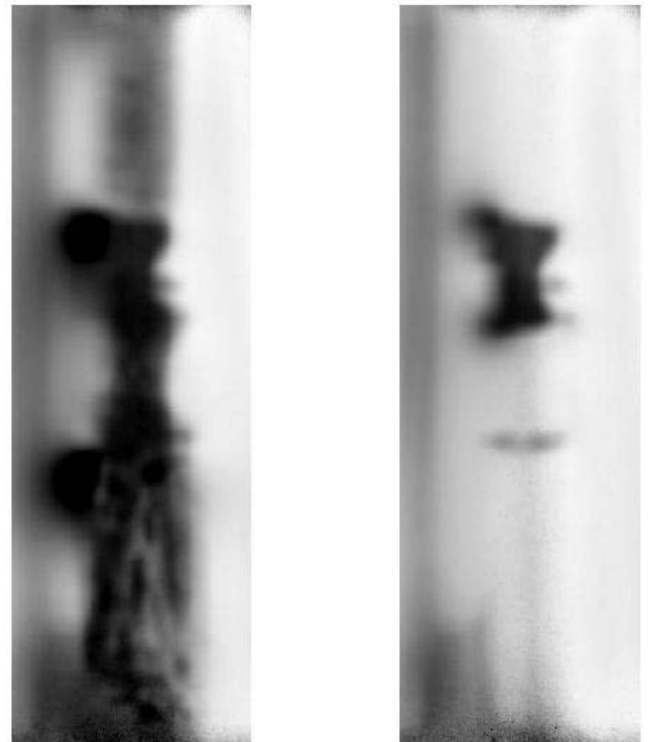


Figure 4.15.: Polarization of a neutron beam after transmission of an OFZ Ni_3Al Sample; white means $P = 1$, black means $P = 0$; (left): 45 K; (right): 70 K.

4.3. Towards a new measurement of the electric dipole moment of the neutron (nEDM)

I. Altarev¹, M. Eisele¹, W. Feldmeier¹, P. Fierlinger¹, A. Fuxman¹, E. Gutsmedl¹, F. Kuchler¹, S. Paul¹, F. Rosenau¹, R. Stoepler¹, B. Taubenheim¹

¹Physik-Department E18, TU München

An electric dipole moment (EDM) of a fundamental system is an unambiguous manifestation of time reversal symmetry (T) violation, equivalent to CP violation [1]. This phenomenon has only been observed in few systems and is not robust enough to explain a related phenomenon: the matter-antimatter asymmetry in the Universe. Already in 1967, Sakharov pointed out that a satisfying explanation of this problem requires next to baryon-number violating processes and interactions out of thermal equilibrium as well as new sources of CP violation, which are not known in the Standard Model of particle physics (SM) [2].

One of the most sensitive measurements

A famous theory beyond the SM is Supersymmetry, which will be tested at the LHC at the TeV energy scale. It turns out that due to its relatively simple composition, the neutron is a well suited system to probe such theories. This is close to the measured limit for the nEDM $d_n < 2.9 \cdot 10^{-26}$ ecm [3], making it one of the most sensitive measurements in physics. Although this limit is far away from the limits predicted by the SM ($d_n \sim 10^{-31}$ ecm), it is close to Supersymmetry ($d_n \sim 10^{-26} - 10^{-28}$ ecm).

Related to the new ultra-cold neutron (UCN) source, a novel measurement of the nEDM based on trapped polarized UCN will be performed at the FRM II by an international collaboration around Paul Scherrer Institut (PSI), the Technische Universität München and the Excellence-Cluster "Origin and Structure of the Universe". All EDM measurements are in principle based on a variation of Ramsey's technique of oscillatory fields, which deploys the Zeeman interaction of the spin with a magnetic field.

A non-zero EDM d_n interacts in a similar way with an electric field:

$$(4.1) \quad \hbar\omega = \mu_n B + d_n E$$

with the Larmor-frequency ω and the magnetic moment μ_n of the neutron.

The EDM d_n is aligned along the axis of the magnetic moment. In a constant magnetic field, an electric field E causes a change of ω .

To improve the limit on the nEDM by two orders of magnitude, the accurate control of the critical parameters of such an experiment is crucial. The "universal" formula for the accuracy of an EDM experiment is:

$$(4.2) \quad \delta d = \frac{\hbar}{\alpha T E \sqrt{N}}$$

where T is the measurement time, E the applied electric field and N the number of stored neutrons, α is a quality factor.

The new strong UCN sources will provide the required amount of neutrons for the statistical accuracy of the measurement, in the order of 1000 UCN cm^{-3} .

Another critical parameter is the accurate control of magnetic field drifts between measurements with inverted electric fields, which causes a false EDM signal $d = \mu_n B / 2E$. A stability of ~ 100 fT over typically 100 s is required to improve the experiment into the 10^{-28} em range for a year of measurements.

Next to the high temporal stability also the spacial homogeneity of the magnetic field must be controlled to an unprecedented level, with gradients of the $1 \mu\text{T}$ magnetic field below 0.3 nT/m .

The nEDM experiment is performed in phases: phase I was to test new components at the Institut Laue-Langevin (ILL) in the existing apparatus by the Rutherford Appleton Laboratory/Sussex/ILL collaboration in Grenoble (finished in 2008), in phase II (2009-2010) the modified existing apparatus is moved to PSI and operated at the strong UCN source, while the new apparatus is being built. Already in this phase, the limit on the neutron EDM should be improved by a factor of 4. In phase III, the new apparatus is operated at the UCN sources in Munich and PSI to finally achieve a new EDM limit of $d_n < 5 \cdot 10^{-28}$ ecm (2010+) based on a cooperation agreement of FRM II, E18 and PSI. A schematic layout of the new nEDM apparatus is shown in fig. 4.17.

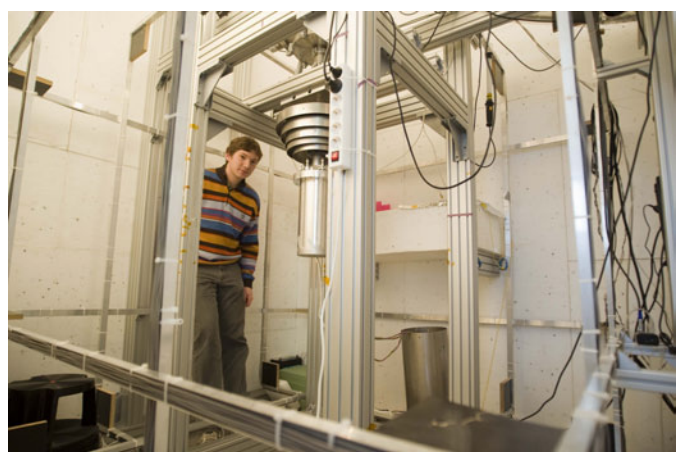


Figure 4.16.: Preparatory measurements for the dipole moment of the neutron are already performed by Prof. Peter Fierlinger in the new experimental hall east of the FRM II.

To investigate the influence of magnetic fields at such a level of precision, preparatory measurements are currently being set up in the experimental hall east in 2008. The experiments include the control of the ambient magnetic fields and disturbances at the location of the future nEDM apparatus, but also improvements of precision magnetometry. A known problem with currently used magnetometry systems (optically pumped Cs) is the lack of vector information, which is necessary to minimize gradients. Therefore, the performance of LTC-SQUID magnetometers in combination with hyperpolarized ^{129}Xe (and later ^3He) as absolute field sensors is investigated. For this purpose, a nested 5-layer Mu-metal magnetic shield was designed and placed inside a thermally stabilized 3-axis active field and gradient stabilization system. A liquid-cryogen free cryostat which houses an array of SQUID magnetometers in a constant holding field is currently being commissioned. For the same application, we developed various components for the experiment in 2008, like a stable current source for the magnetic field with a relative stability of 10^{-9} over 100 s, see fig. 4.18.

As a synergy, this test-setup is also being used to measure the EDM of the diamagnetic atom ^{129}Xe with a novel method, with the goal to improve the current limits by about 3 orders of magnitude. This is complementary to the developments for the nEDM apparatus and provides an interesting tool to investigate systematic effects.

[1] Ramsey, N. F. *Rep. Prog. Phys.*, (1982).

[2] Sakharov, A. D. *JETP Lett.*, 5, (1967), 24.

[3] Baker, C. A., Doyle, D. D., Geltenbort, P., Green, K., *et al. Phys. Rev. Lett.*, 97, (2006), 131801.

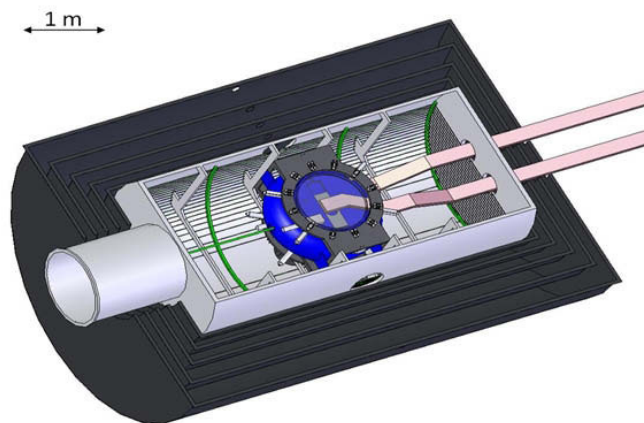


Figure 4.17.: Schematic layout of the new nEDM apparatus (horizontal cut). The actual EDM chambers (blue) are placed inside a vacuum chamber and surrounded by a multi-layer Mu-metal shield. UCN are supplied via guides from the right. The chambers are surrounded by atomic- and SQUID-magnetometers.

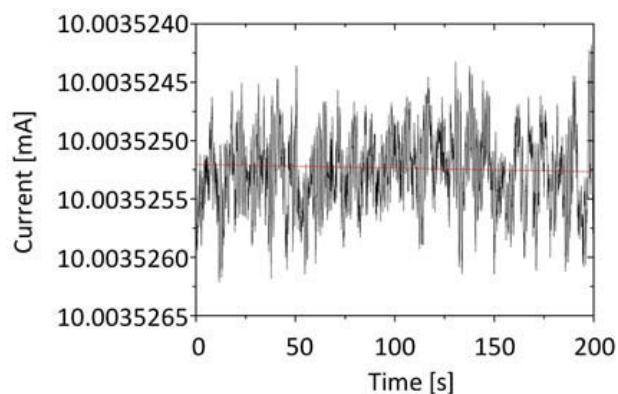


Figure 4.18.: Stability of the current source which was developed for magnetic holding field in the EDM experiment. The measurement was performed by comparing a high precision voltage standard with voltage drop across a thermally stabilized resistor.

4.4. Particle physics at the cold neutron beam facility MEPHISTO

J. Klenke¹, H. Abele²

¹ZWE FRM II, TU München

²Physik-Department E18, TU München

The white beamline MEPHISTO is a measurement facility for particle physics with cold neutrons. The experiments at this beamline fit in a greater field of precision experiments with cold and ultracold neutrons, electrons, ions, atoms and their antiparticles. These experiments are in some respect the counterpart of the high energy experiments in large accelerator labs like CERN for a search for new physics beyond the Standard Model. The Standard Model is the starting point for nearly all new theories in the field particle physics, cosmology and astronomy. During the last decades these experiments with cold neutrons have been risen to an extreme level of precision and accuracy. Tiny shifts in the predicted behaviour, base on the Standard Model, of the neutron itself or in the interaction with other material as target can now be detected. These results help to clarify basic questions and assumptions on the opposite side of the energy scale in respect to the large accelerator facilities. The consistency of the Standard Model is checked and the energy range is improved.

Angular distribution of gammas and neutrons during fission process

A basic feature of the Standard Model is the violation of symmetries. Symmetry tests have been performed in 2008 at the neutron beam position MEPHISTO for particle and nuclear physics. In particular small anisotropies of the order 10^{-5} have been searched for in the induced fission process of uranium. The most prominent

anisotropies were the TRI and the ROT effect [1]. These effects distort the angular distribution of the fission products in respect of a symmetry plane spanned by the vector of the polarisation direction of the incident cold neutrons which induce the fission process and the vector of the light fission fragment.

The beam at MEPHISTO offers a high intense white polarised beam ($P_0=98\%$), which allows to measure these small effects - in this particular experiment the angular and spectral distribution of the gamma rays of induced binary fission of a ^{235}U sample - with high precision.

The fission process is accompanied by the emission of prompt gamma rays and neutrons. The main part of the gammas are irradiated by exited fragments after the scission of the nucleus. Another part can be emitted by the fission nuclei ^{235}U before or after the neck rupture.

A study of this irradiation process needs detailed knowledge of the angular distribution and the spectrum of these gamma rays. The experiment is therefore a coincidence measurement between fission fragments and gamma rays in different angular setups.

The angular distribution of the gamma rays should give information about the origin of the gamma rays. Do they come from exited fragments after the fission or directly from the fission process of the nuclei?

The main part of the experimental setup is shown in picture 4.19. The experimental chamber is an aluminium cylinder with a diameter of 50 cm filled with isobutan gas at low pressure. The entrance window is on the end plane of the cylinder. The cold neutron beam with longitudinal polarisation passes the experimental chamber with the ^{235}U target. A beam stop is placed 2 m behind the chamber to reduce the background.

Horizontally left and right from the target multi wire counter are placed in the chamber to detect the fission fragments. The plastic scintillator detectors are arranged outside around of the sample chamber with a 25 cm distance to the sample. These detectors distinguish between prompt fission neutrons and gammas with the time of flight method. The coincidence was measured between the multiwire detectors and the plastic detectors. The difference between the angular distribution of the fission neutrons and the gammas can be monitored with this setup.

The most difficult task was the shielding of the outside detectors of this experiment against gamma rays produced by the other instruments in the neutron guide hall and to collect enough coincidence events for a suitable statistic.

The guiding magnetic field was reversed every second

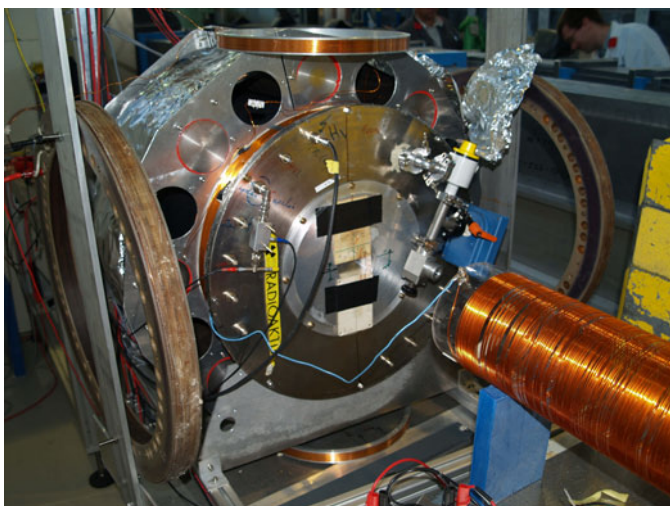


Figure 4.19.: The experimental chamber with the entrance window.

day and the polarisation of the incident neutron beam every two seconds to prevent systematic errors in the measurement. The theoretical treatment of the data taken from this experiment is up to now not finished.

The authors kindly appreciate the work of the students M. Aßmann and H. Saul

[1] Goennenwein, F., *et al.* *Physics Letters B*, vol.652, no.1, (16 Aug. 2007), 13–20.

4.5. MEDAPP: A versatile beam not only for medical applications

F.M. Wagner¹

¹ZWE FRM II, TU München

Available beam qualities

Within the moderator tank, a pair of highly enriched ^{235}U plates can be moved in front of the beam tube SR10 (Fig. 4.20). The high flux of thermal neutrons induces fission processes and generates fast neutrons (conversion). These fission neutrons with the mean energy 2 MeV can escape through the adjacent beam tube without moderation. At the exit of the beam tube, the beam quality is determined by three components: fission neutrons, gamma radiation, and thermalised neutrons. Their respective contributions to the beam can be varied. Information on the determination and quality of the neutron spectra and examples for the scientific use are given below.

Thermal neutron beam

When the converter plates are withdrawn from the moderator tank, the beam consists only of thermalized neutrons from the reactor core and the accompanying gamma radiation. As a fourfold shutter is situated in the beam tube, the radiation level at the exit of the beam tube is generally less than 1 mSv such that the cavern can be accessed during few minutes in order to mount a prepared sample. The flux at point 8 in fig. 4.20 is $3.9 \times 10^9 \text{ s}^{-1} \text{ cm}^{-2}$ with a beam area of $23 \text{ cm} \times 18 \text{ cm}$. The flux was determined by the usual differential method using gold foils bare and in tins of cadmium; the corresponding cadmium ratio is greater than 400. In this case of extreme thermalization, however, the large res-

onance integral of gold for epithermal neutrons can lead to a considerable non-thermal activation of the foils. A MCNP simulation by A. Röhrmoser which included the whole core arrangement of installations in the heavy water tank delivered the result that the flux of thermal neutrons in the beam tube is four orders of magnitude higher than the flux of fast reactor neutrons.

Fast neutron beam

When fast neutrons are needed, the converter plates are positioned in closest touch with the entrance of the beam tube (Fig. 4.20 point 3). With a thermal power of 80 kW, the fast neutron flux at the reference point at 5.9 m distance is $7.0 \times 10^8 \text{ s}^{-1} \text{ cm}^{-2}$. Thermal neutrons originating from the moderator tank are suppressed at the exit of the beam tube by a filter consisting of 1 cm B_4C (50%) in epoxy. In the irradiation room, there is a thermal flux mainly depending on the illuminated volume of the target and its hydrogen content.

The operation of the uranium converter generates also an intense flux of high energy photons which is generally unwanted. Therefore, the beam is additionally filtered by 3.5 cm lead leading to a fast neutron flux of 46% or $3.2 \times 10^8 \text{ s}^{-1} \text{ cm}^{-2}$, but reducing the gamma dose to about 18 % of the unfiltered value. This is the standard beam used for medical applications; details about the facility are given in [1].

Determination of the fast neutron spectrum

Leading scientist: S. Garny, Institut für Strahlenschutz, Helmholtz Zentrum München

The neutron spectrum of the standard beam was determined anew in a PhD-thesis [2]. A set of 16 PE-Bonner spheres ranging from 1.3 to 15 inch diameter was used (fig. 4.21). Because of the high flux, the usual electronic detector had to be replaced by gold foils in the centre of the spheres. In the thesis, the response functions of these spheres have been calculated using the GEANT code. From the measured thermal activations of the foils in the different spheres, the neutron spectrum shown in fig. 4.22 was determined by the deconvolution programme MSANDB. The result is in line with former measurements using threshold activation foils [3]. The spectrum of the converter neutrons is a Watt spectrum with a minor addition of epithermal neutrons; the mean energy is 1.9 MeV.

The fraction of gamma to neutron flux is conveniently expressed in terms of energy dose rates measured in a water phantom in 2 cm depth where equilibrium of sec-

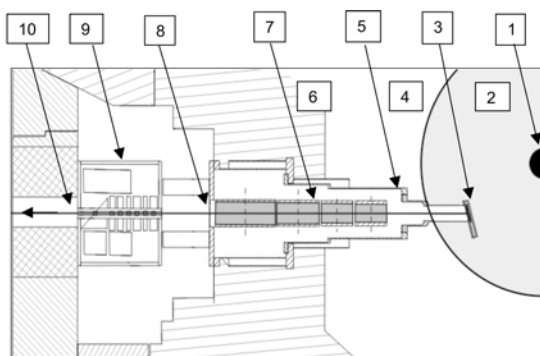


Figure 4.20.: Horizontal section of the irradiation facility: 1 Compact reactor core; 2 D_2O moderator tank; 3 Vertically movable converter plates; 4 Light water zone; 5 He-filled beam tube; 6 Biological shield; 7 Four revolving shutters; 8 Position for irradiations with thermal neutrons; 9 Filter bench; 10 Multi leaf collimator.



Figure 4.21.: View along the beam to a Bonner sphere mounted in the NECTAR room. In the background, the screen of the radiography facility is visible.

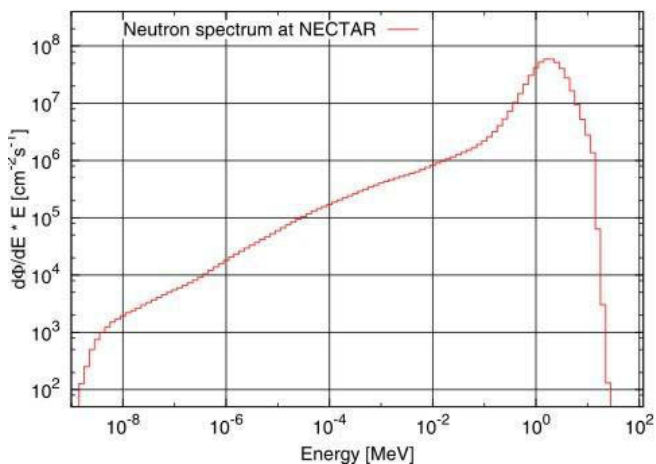


Figure 4.22.: Neutron spectrum free in air, filtered by 1 cm B-resin and 3.5 cm lead, measured in the NECTAR room.

ondary electrons is reached. With a collimator opening of $9\text{ cm} \times 9\text{ cm}$, the neutron and gamma energy dose rates on the beam axis are 0.54 and 0.20 Gy/min, respectively.

For non-medical applications, the fraction of photon flux to fast neutron flux can further be reduced. With, e.g., 6 cm lead in the beam, the remaining fast neutron flux is yet $1.9 \times 10^8\text{ s}^{-1}\text{cm}^{-2}$ at the reference point; for radiography and tomography (see NECTAR), 11 cm lead are inserted.

Trace element distribution (thermal beam)

Leading scientist: Prof. D. Gabel, Fachbereich Chemie, University of Bremen

In connection with worldwide efforts to develop suit-

able compounds for boron neutron capture therapy, boronated lipids are investigated as to their specific enrichment and sufficient retention period in a tumour. The distribution of boron in the tumour model of a mouse can be visualized and evaluated quantitatively by use of etch track films. The compound was administered intravenously. Six hours later, the mouse was euthanised and imbedded into paraffin.

Sections with a thickness of $50\text{ }\mu\text{m}$ were prepared by a cryotome. Affixed on etch track films (Kodak LR115 Type 1) and compressed in flat evacuated PE bags, the sections were irradiated with $4 \times 10^{12}\text{ n}_{\text{th}}\text{cm}^{-2}$ at position 8 in Fig. 4.20. The radioactivity of the irradiated samples (Na-24 and Sb-122) was small and decayed within a few days so that they could be handed out inactive. After removal of the section and etching with 10%-NaOH, a picture like in Fig. 4.23 is obtained. The darker the area the higher is the concentration of boron; the tumour contains about 5 ppm ^{10}B . Due to the low contamination by fast neutrons, the background due to recoil protons is very low; a minimum detectable fraction of boron (element) of 0.1 ppm can be reached when counting single tracks.

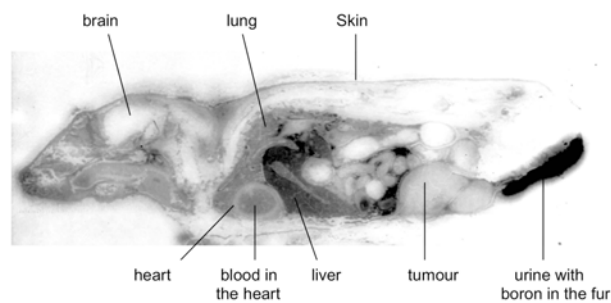


Figure 4.23.: Scan of an etch track film which was irradiated together with a whole-body section of a mouse.

Medical and biological applications (fast neutron beam with standard filters)

Human Cancer Therapy

Leading Scientists: Dr. med. B. Loeper (FRM II), Prof. P. Kneschaurek (MRI/TUM)

Biological and clinical applications are principally motivated by the high lineal energy transfer (LET) up to $100\text{ keV}/\mu\text{m}$ of fission neutrons. The high LET leads to biological radiation effects different from photons of the same energy, e.g., a much weaker dependence of the cell deactivation on the oxygenation. The quick energy loss, however, is also a cause for the poor penetration depth so that fission neutron therapy can be applied only to tumours situated near to the body surface.

The types of tumours with the best prospects for

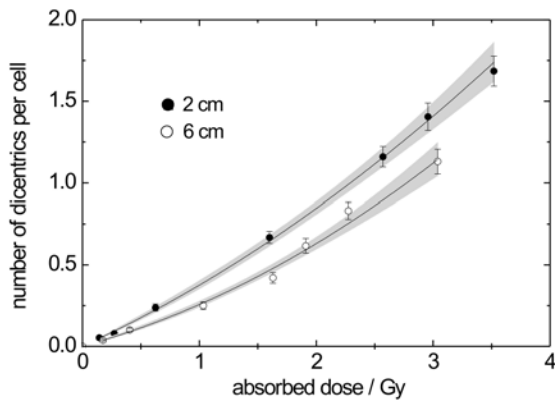


Figure 4.24.: Yield of dicentric chromosomes as a function of dose obtained for the MEDAPP beam at PE phantom depths of 2 and 6 cm. The solid lines show the weighted least-squares best fit to the data with the shadowed areas representing the standard error bands.

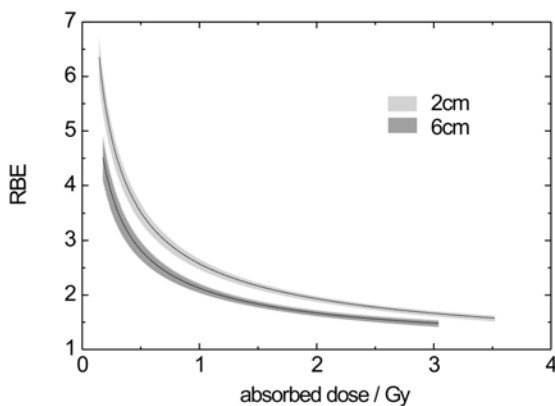


Figure 4.25.: RBE of the MEDAPP beam vs. dose at depths of 2 and 6 cm, resp., in a PE-phantom.

longterm cure are adenoid cystic carcinoma of the salivary glands, because these are often rather resistant to conventional therapy with accelerator-Bremsstrahlung, further lymph node metastases or skin metastases from various cancer diseases, and chest wall metastases of breast cancer. In the latter case, the poor penetration is an advantage because the radiation dose to the lungs and the heart is generally not prohibitive even with vertical incidence. At FRM II, in 2008, 20 patients have received 129 irradiations. 40 % of the patients have been treated with curative intent, the others for palliation.

Biological dosimetry

Leading scientist: Prof. E. Schmid, Strahlenbiologisches Institut der Universität München

The dose-response relationship of dicentric chromosomes in human lymphocytes for fission neutrons has been investigated at different depths in a polyethylene phantom [4]. Whole blood samples were exposed to total doses of 0.14 - 3.52 Gy at 2 cm depth, and 0.18 - 3.04 Gy at 6 cm depth of the phantom. The neutron and γ -ray absorbed dose rates were measured to be $D_n = 0.55 \text{ Gy min}^{-1}$ and $D_\gamma = 0.27 \text{ Gy min}^{-1}$ at 2 cm depth, while they were 0.28 and 0.25 Gy min^{-1} at 6 cm depth, respectively. Different response curves for dicentric chromosomes were obtained for the MEDAPP therapy beam at 2 and 6 cm depth suggesting a significantly lower biological relative effectiveness RBE (compared to ^{60}Co γ -rays) with increasing depth (Figs. 4.24 and 4.25).

Using the best possible conditions of consistency, i. e., using blood samples from the same donor and the same measurement techniques for about two decades, avoiding the inter-individual variations in sensitivity or the differences in methodology usually associated with interlaboratory comparisons, a linear-quadratic dose-response relationship was obtained not only for the mixed neutron- γ -field, but also for the neutron part alone. Equation 4.3 describes the biological effect y under additive prediction (i. e. no interaction of the components) whereas equation 4.4 is valid under the assumption of a synergistic interaction between the different primary lesions.

$$(4.3) \quad y = \alpha_n D_n + \alpha_\gamma D_\gamma + k(D_n^2 + D_\gamma^2)$$

$$(4.4) \quad y = \alpha_n D_n + \alpha_\gamma D_\gamma + k(D_n + D_\gamma)^2$$

As all known dicentric data on fission spectra could be best fitted by a linear dependence on dose, the surprising existence of a significant quadratic coefficient k of D_n was established at the therapy beams of both FRM and FRM II. However, no obvious differences in the dose-response curves for dicentric chromosomes estimated for an additive assumption as well as for the synergistic prediction for neutrons and γ -rays, and the experimentally obtained dose-response curves could be determined so that the debate on whether or not the fission-neutron induced yield of dicentric chromosomes increases linearly with dose remains open.

Radiation hardness of electronic components (fast neutron beam with additional filters)

Leading Scientist: M. Deveaux, Institut für Kernphysik, Goethe-Universität Frankfurt

CMOS sensors, also being referred to as Monolithic Active Pixel Sensors (MAPS), demonstrated their ability to serve as sensors for minimum ionising particles (MIPs). They represent a novel technology for charged particle tracking in high-energy particle and nuclear physics. In this technology, the epitaxial layer is used as sensor material and read out by active pixel cells imbedded in the p+ bulk material of the chip. Pixel sizes as small as $10\ \mu\text{m} \times 10\ \mu\text{m}$ allow unprecedented spatial resolutions and a low material budget at the same time. Consequently R&D is pursued to apply this technology in various future micro vertex detector systems. Among such possible applications are the future Heavy Flavour Tagger of the STAR experiment (RHIC, USA), the vertex detector of the Compressed Baryonic Matter (CBM) experiment (FAIR, Germany) and the vertex detector of the International Linear Collider (ILC). The Technology Laboratory of the University Frankfurt, Institute of Nuclear Physics, participates in the R&D, design and construction of the vertex detector of the CBM experiment.

An essential performance criterion in such applications is the radiation tolerance of the pixel chip. The detectors are foreseen to operate in close vicinity to the primary interaction vertex and exposed to the maximum track density. Moreover, the experiments are optimized to measure rare probes such as open charm and, hence, cope with very high integral particle fluences. First exploratory studies showed that non-optimized detector chips may tolerate non-ionising doses of $1 \times 10^{12}\ \text{neq}/\text{cm}^2$ what does not satisfy the requirements of all applications. An intense R&D programme has therefore been started in a common activity of the Institut Pluridisciplinaire Hubert Curien (IPHC) - Strasbourg, the Helmholtz Zentrum für Schwerionenforschung (GSI) - Darmstadt and the Institut für Kernphysik (IKF) of Goethe University Frankfurt. First results have been published in [5].

Within this R&D activity, different strategies for improving the radiation hardness of the detectors will be tested by implementing them into dedicated new sensing elements. The modified sensors are first evaluated to gain reference parameters, then exposed to radiation and hereafter characterized again. Comparing the performances of the irradiated sensors with those of non-irradiated ones as well as of elder designs allows judging the design progress and gives important input for further optimization. At FRM II, irradiations

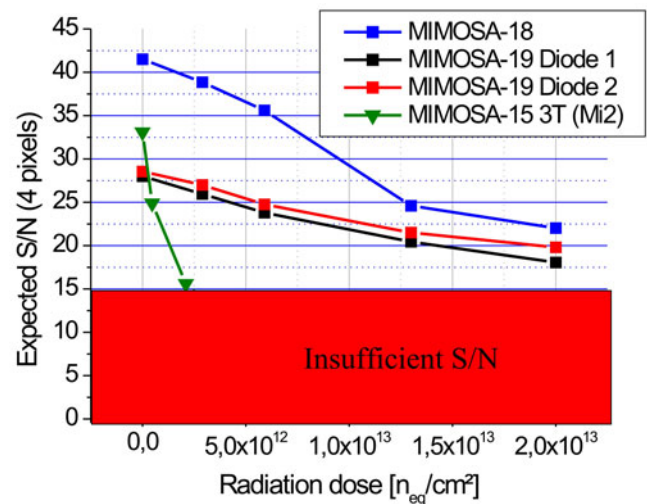


Figure 4.26.: The signal-to-noise ratio S/N as expected for clusters of four pixels being generated by minimum ionising particles in CMOS sensors. One observes the substantially improved radiation hardness of the novel sensors MIMOSA-18 and MIMOSA-19 with respect to the elder design MIMOSA-15.

were performed using fission neutrons with fluences up to $1 \times 10^{13}\ \text{neq}/\text{cm}^2$. They proved that the latest MAPS generation (MIMOSA-18) may stand more than $1 \times 10^{13}\ \text{neq}/\text{cm}^2$. This represents a progress of one order of magnitude with respect to previous designs.

- [1] Wagner, F. M., Kneschaurek, P., Kampfer, S., Kastenmüller, A., Loeper-Kabasakal, B., Waschkowski, W., Bretkreutz, H., Molls, M., Petry, W. *Strahlenther. Onkol.*, 184, (2008), 643–646.
- [2] Garny, S. *Development of a Biophysical Treatment Planning System for the FRM II Neutron Therapy Beamline*. Dissertation, Technische Universität München, Fakultät für Physik / Helmholtz Zentrum München. (2008).
- [3] Bretkreutz, H., Wagner, F. M., Röhrmoser, A., Petry, W. *Nucl. Instr. and Meth. Phys. Res. A*, 593, (2008), 466–471.
- [4] Schmid, E., Wagner, F. M., Romm, H., Walsh, L., Roos, H. *Radiat. Environ. Biophys.*, 48, (2009), 67–75.
- [5] Amar-Youcef, S., Deveaux, M., Doering, D., Müntz, C., Wagner, F. M., Schrader, C., Stroth, J. In: *IEEE - 16th International Workshop on Room-Temperature Semiconductor X- and Gamma-Ray Detectors* (Dresden, 2008).

4.6. Radiology and partial tomography of large wooden samples using fission neutrons at NECTAR

K. Osterloh¹, M. Jechow¹, U. Zscherpel¹, U. Ewert¹, T. Bücherl², A. Hasenstab³

¹Federal Institute for Materials Research and Testing (BAM)

²Lehrstuhl für Radiochemie, TU München

³LGA Bautechnik GmbH, TÜV Rheinland

Wood constitutes a uniquely structured material consisting predominantly of low Z materials and being rich in hydrogen. So an interrogation with neutrons would be expected to result in images high in contrast. Neutron radiology promises to provide a powerful tool to investigate non-destructively material related internal features such as inclusions, distribution of glue or moisture, or may even provide indication for putative pathological states. However, the penetration of thicker layers requires a minimum energy level, i.e. thermal neutrons are not applicable for this purpose.

Annual ring structures visible

Voluminous wooden objects have been successfully penetrated with fission neutrons available at the NECTAR facility achieving a radiologic image. As an example, figure 4.27 shows a sample of 23.5 cm x 49.2 cm x 100.0 cm consisting of 5 conglutinated timbers. At a layer thickness of nearly 50 cm, some blurred features indicate areas of higher densities such as knots. In the range of some 20 to 35 cm, certain features could be identified such as annual ring structures, knots, voids and some cracks. The achieved radiographic density distributions differed from those obtained with X-ray or gamma radiography [1]. In difference to those photon based technologies, shielding with heavy metals only had a minor impact on showing all the details of the wooden structures [2].

The next step was to gain a spatial image from the inside though the size of the specimen exceeded the dimensions of the image detector screen (30 cm x 30 cm). This problem was resolved by partial tomography



Figure 4.27.: Penetration of 49.2 cm wood with an additional Lucite block as a contrast giving body (positioned between wood specimen and the detector screen, photo left). Centre: Sum of filtered raw images. Right: Image after median filtering and correction for the open beam intensity distribution (structural details of the wood becoming visible).

similar to the laminographic technologies with a restricted number of angular projections (91 projections with 1° angular distance). The results are summarized in figure 4.28. In particular, the density distribution in the glued contact area was checked for homogeneity. The practical background of this kind of research was the collapse of a wooden roof construction of a sports hall recently in Bad Reichenhall (Germany) [3].

Different types of glue

The reconstruction of the partial tomography reveals different density distributions in the three selected glued areas: While the central one (figure 4.28 d) shows large rather homogenous areas with a few irregularities (the central line is due to a reconstruction artefact, it was the pivotal axis), the left and the right one have some obviously repetitive crude patterns (figure 4.28 c and e). The interpretation of these features requires further investigations. Interestingly, the glue of the central contact area was based on resorcin resin and the glue of the others based on urea. In context of damage analysis, it is crucial to know, which kind of glue has been used. Particularly, if the intrusion of moisture may have played a role. Urea based glues are biodegradable while the resin based one is not [3]. In the centre of the interrogated area, a feature has been found resembling an inclusion of resin which may have a contact to the glued area. The selected sections (figures 4.28 f to h) clearly show that the included body is in the vicinity of the glued layer, but separated. It appears that there might be a contact at the rear upper edge (to the left in figure 4.28 f). The whole shape of this body becomes more evident when presented in a semi-transparent visualisation of the volume data.

This study has principally shown that radiology and (partial) tomography with fast neutrons can be an appropriate tool to investigate large wooden specimens non-destructively. This approach has the advantage of being more sensitive to contrast differences due to density variations of low Z materials such as hydrogen than X-ray and gamma-ray based technologies.

[1] Osterloh, K., Raedel, C., Zscherpel, U., Meinel, D., Ewert, U., Buecherl, T., Hasenstab, A. *Insight*, 50, (2008), 307–311.

J., Ewert, U. In: *DIR 2007 – International Symposium on Digital Industrial Radiology and Computed Tomography* (Lyon, France, 2007).

[2] Osterloh, K., Bücherl, T., Hasenstab, A., Rädcl, C., Zscherpel, U., Meinel, D., Weidemann, G., Goebbels,

[3] Sennewald, R. In: *Fachtagung Bauwerksdiagnose 2008, DGZfP-Berichtsband BB 112*, 62–71 (2008).

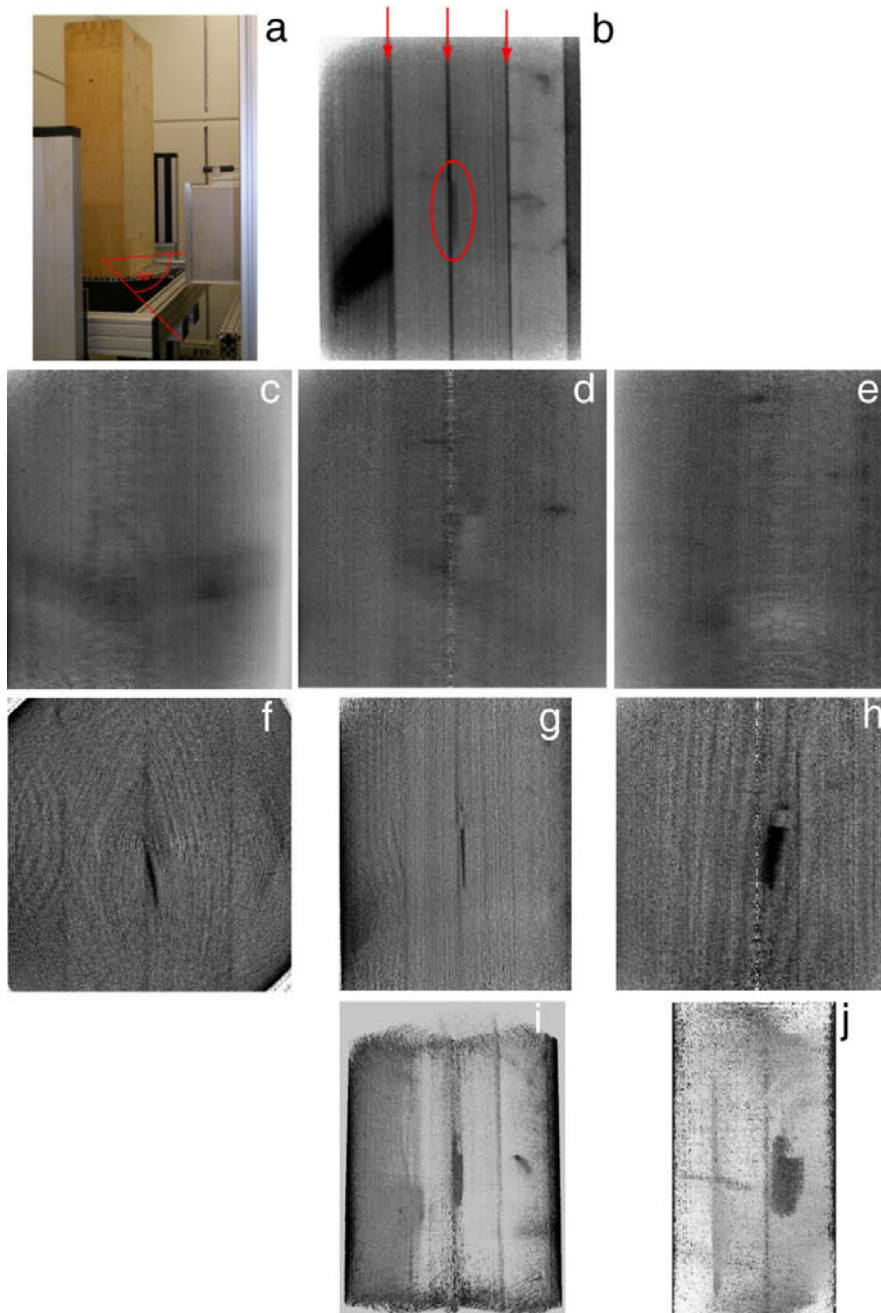


Figure 4.28.: Partial tomography of a selected area within a large wooden sample. a) Specimen in beam position with rotation angle indicated in red, b) radiologic image in exact perpendicular position, c) sum of 10 reconstructed layers aligned with glued contact area to the left (left red arrow in b), d) same in central position (middle red arrow), e) same to the right (right red arrow), f) single axial layer through the inclusion in the centre (red circle in b), g) single layer parallel to the radiological plane (as in panel b), h) single layer perpendicular to the previous image plane (parallel and adjacent to the central glued contact area), i) semitransparent spatial visualisation of g and j) same of h.

4.7. Unprecedented intensity of low-energy positrons at NEPOMUC

Ch. Hugenschmidt^{1,2}, G. Dollinger³, W. Egger³, G. Kögel³, B. Löwe^{2,3}, J. Mayer¹, Ph. Pikart^{1,2}, Ch. Pi-ochacz^{1,2,3}, R. Repper^{1,2}, P. Sperr³, M. Stadlbauer^{1,2}, K. Schreckenbach^{1,2}

¹Physik-Department E21, TU München

²ZWE FRM II, TU München

³Institut für Angewandte Physik und Messtechnik (LRT 2), Universität der Bundeswehr München

In 2008, a new in-pile γ -converter and Pt-moderator was installed at the neutron induced positron source NEPOMUC. The intensity of the moderated positron beam is unprecedented and amounts to $(9.0 \pm 0.8) \cdot 10^8$ moderated positrons per second at an energy of 1 keV. Hence, the beam facility NEPOMUC provides the world highest intensity of a monoenergetic positron beam reported so far. Up to now, no degradation of the positron yield has been observed for several months of operation. Thus, the long-term stability of the positron beam enables experiments with high reliability.

New in-pile source

The design of the new positron source was only little changed in order to eliminate the observed deteriorations of the positron beam. The outer geometry – in particular the Cd-cap for the production of high-energy γ 's and the magnetic field coils – remained the same. For the new in-pile component, the last Pt-ring was replaced by a Ti-ring which acts as electrical lens as well. Consequently, the lower amount of Pt may lead to an intensity reduction, but the beam brightness should increase, since positrons that were emitted from this last Pt-section obtain large transversal momentum that hence mainly contributed to the halo of the beam. In addition, the use of the lighter Ti instead of Pt reduces the γ -heating of the ring-electrodes by about 50%. In order to optimize the heat dissipation to the outer beamtube additional spiral springs at the inner Al-tube guarantee a much better thermal contact.

As previously reported, a small amount of oxygen during reactor operation leads to an increase of the beam intensity which was attributed to the cleaned Pt-surface [1]. The same cleaning procedure with oxygen was first applied for the new source right after the start-up of the reactor in order to clean both, the insulators and the Pt-foils.

During the first months of operation, no degradation of the positron source was observed. The short-term stability of the beam is determined by the variation of the reactor power which is less than 1 %. Due to the long-term stability of the beam, experiments can be performed routinely with an intensity close to 10^9 moderated positrons per second. The beam diameter is the same as at the former in-pile source and amounts to less than 18 mm (full width) in a magnetic guiding field of 6 mT.

Positron intensity

The positron beam intensity was determined by the detection of the 511 keV γ -radiation of positrons that annihilate at an aluminium target which was moved into the beamline. The background-subtracted γ -spectra obtained for the 1 keV positron beam and of a ^{22}Na reference source, respectively, are depicted in Figure 4.29. From the analysis of the 511 keV photopeak a beam intensity of $(9.0 \pm 0.8) \cdot 10^8$ moderated positrons per second was deduced. Details of the data analysis taking into account Compton-scattered 1275 keV γ 's from the reference source, pile-up events, back-scattered positrons and o-Ps-formation with subsequent 3γ -decay are reported elsewhere [2].

Positron instrumentation at NEPOMUC

A remoderation device for brightness enhancement delivers a 20 eV positron beam (efficiency of about 5%), which is used for all connected experiments, where the beam is additionally accelerated to the desired energy. Presently, four spectrometers are connected to the NEPOMUC positron beamline: A coincident Doppler broadening spectrometer (CDBS), a positron annihilation

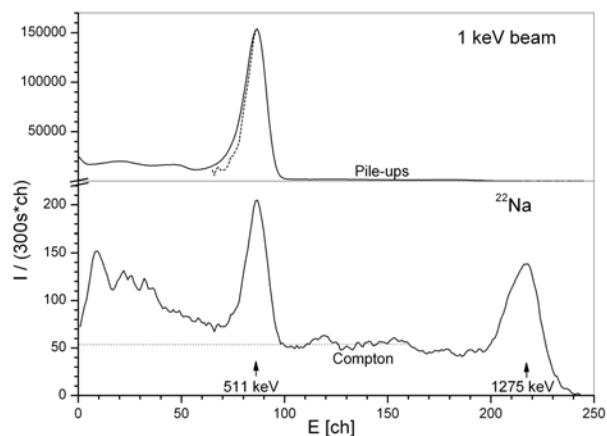


Figure 4.29.: Spectra of the annihilation radiation released from 1 keV positrons annihilating at the target in the beamline. Dashed line in 511 keV photopeak: shape of the ^{22}Na -measurement. Below: Spectrum of ^{22}Na -calibration source for comparison.

induced Auger electron spectrometer (PAES), a pulsed low-energy positron system for positron lifetime measurements (PLEPS), and a set-up for the production of the negatively charged positronium ion Ps^- . The latter experiment is mounted at the multi-purpose beamport, where various experimental set-ups can be connected to the positron beamline. An overview of NEPOMUC and

the positron instruments connected to the positron beam facility is given e.g. in [1] and references therein.

- [1] Hugenschmidt, C., Brunner, T., Legl, S., Mayer, J., Piochacz, C., Stadlbauer, M., Schreckenbach. *Phys. Status Solidi C*, 4, (2007), 3947.
- [2] Hugenschmidt, C., Lowe, B., Mayer, J., Piochacz, C., Pikart, P., Repper, R., Stadlbauer, M., Schreckenbach, K. *Nucl. Instr. Meth. A*, 593, (2008), 616.

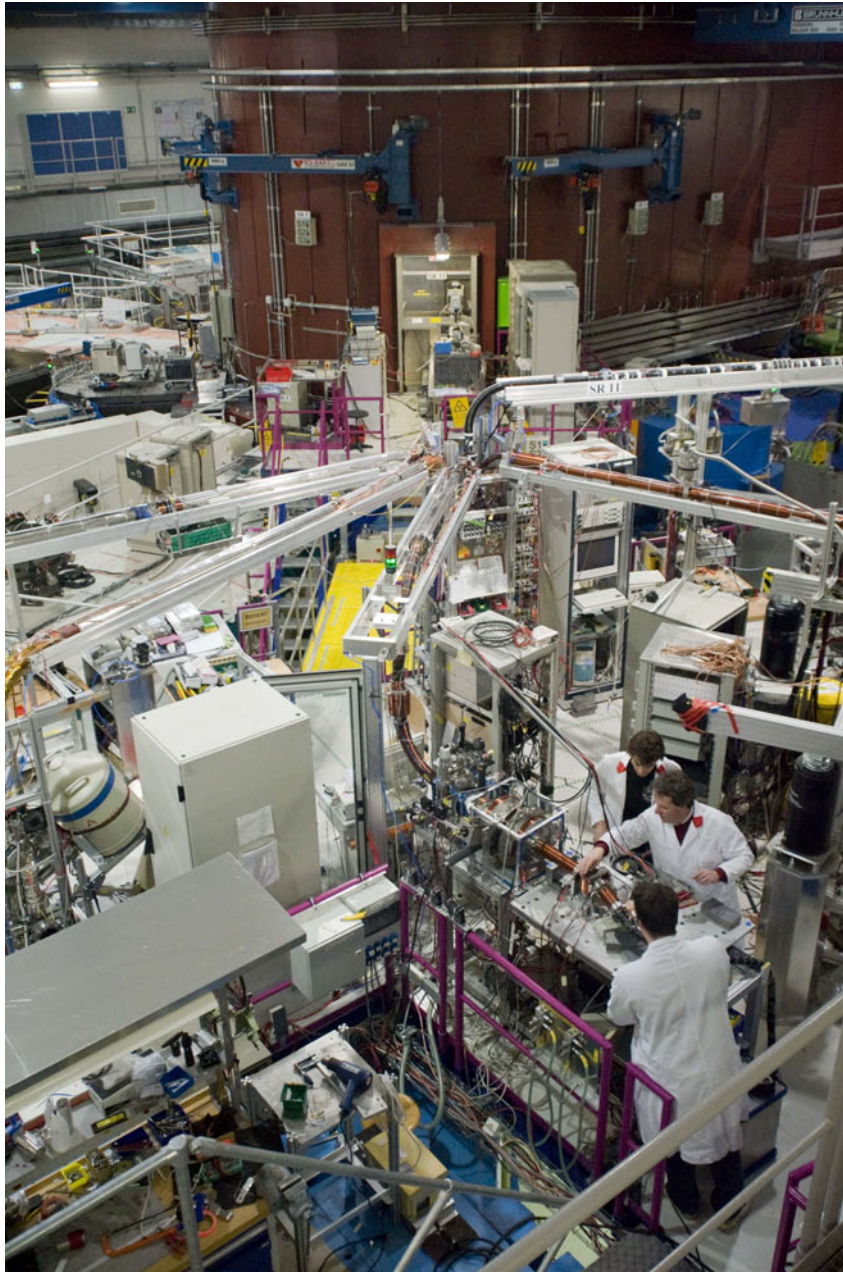


Figure 4.30.: The neutron induced positron source NEPOMUC at the experimental hall of FRM II.

4.8. Microscopy with positrons

C. Piochacz^{1,2}, G. Kögel³

¹Physik-Department E21, TU München

²ZWE FRM II, TU München

³Institut für Angewandte Physik und Messtechnik (LRT 2), Universität der Bundeswehr München

Positron annihilation is a highly sensitive method to study defects of atomic size. Both, the types and the concentrations of defects can be determined by positron lifetime measurements. To perform such measurements with micrometer spatial resolution, a pulsed positron beam is focused down to micrometer spot size in the Munich Scanning Positron Microscope (SPM). For a much higher event rate it is intended to operate this SPM at the high intense positron source NEPOMUC at FRM II. Since the beam of NEPOMUC has a lower phase space density than the beam used in the lab, an interface is under construction, which prepares the beam according to the demands of the last optical column of the SPM. In this interface the DC beam of NEPOMUC is pulsed with a repetition rate of 50 MHz and the energy is raised by newly developed high frequency devices. Moreover, this interface will enhance the beam brilliance [1].

Modulating energy

To achieve both, sharp pulses and a high efficiency, the pulsing is done by two different devices. Both perform a linear energy modulation in order to accelerate positrons, which are behind the reference particle and slow down those, which pass too early. After a certain distance the faster positrons will catch up the slower positrons and therefore the positrons drift together to short bunches. The devices differ in the

manner the energy modulation is done. The first device is a pre-bunching unit, whose primary aim is not to form very sharp pulses, but to compress as many positrons as possible into a time window of some nanoseconds while the beam is disturbed as less as possible. This buncher utilizes a sawtooth function with a long linear part and therefore it can compress a large amount of the incoming positrons. The following buncher uses a sine function and therefore high amplitudes could be reached by resonant amplification. A further advantage of the sine wave is that the leading and the trailing edge can be used to achieve a small time focus. The disadvantage, that only these positrons could be compressed, which pass the buncher during the small linear parts of the sine wave, is overcome by means of the pre-buncher.

Enhanced intensity

After the successful implementing of this first pulsing components [2] the performance of the pre-bunching unit could be enhanced by a redesign of the HF-excitation of the pre-bunching electrodes. By this improvement, the background could be reduced and the intensity of the pulse was enhanced, while the pulse width is kept as small as before (see Fig 4.31).

In order to enhance the brilliance of the beam, the interface includes a re-moderator. The setup which is used (see Fig 4.32), is very similar to that one used for the re-moderator at the NEPOMUC beam facility [3]. After extracting the beam from the magnetic transport field, it is guided electrostatically to a magnetic lens which focuses the beam onto a W(100) single crystal. The positrons, which enter the solid, are scattered inelastically until they reach thermal equilibrium. Now they can diffuse over a distance on the order of 100 nm and some of the thermalized positrons can reach the surface, where they have been implanted. Because tungsten has a negative work function for positrons, those positrons which have reached the surface can leave the solid perpendicular to the surface with a sharp energy. These positrons are formed to a beam by a set of electrodes and guided again electrostatically. Due to the fact that the primary beam and the remoderated beam are on the same axis but propagating in opposite direction they have to be separated by a magnetic dipole. With this setup it was possible to focus the remoderated beam with a long distance electronic lens down to 700 μm .

Due to the installation of the first bunching units and the remoderator, a big step toward the completion of

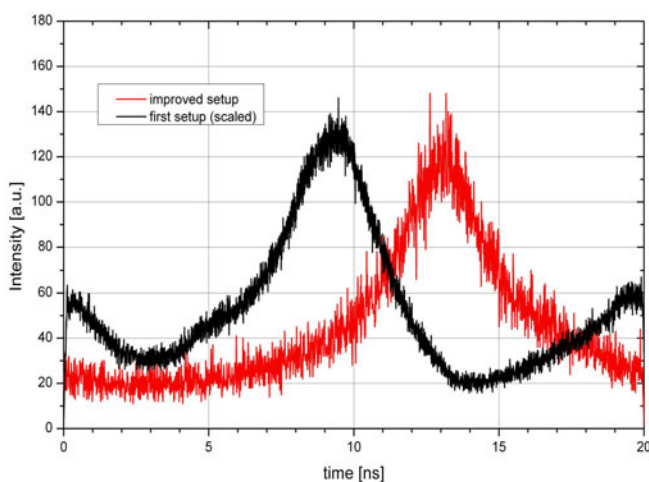


Figure 4.31.: Comparison between the time spectra achieved with the pre-buncher before and after the redesigned HF-excitation.

the interface and therefore for the implementation of the SPM was done.

[1] Piochacz, C., *et al. physica status solidi (c)*, 4(10), (2007), 4028–4031.

[2] Piochacz, C., Kögel, G., Egger, W., Sperr, P., Dollinger, G. *Annual report of E21*, (2007).

[3] Piochacz, C., *et al. Applied Surface Science*, 255(1), (2008), 98–100.

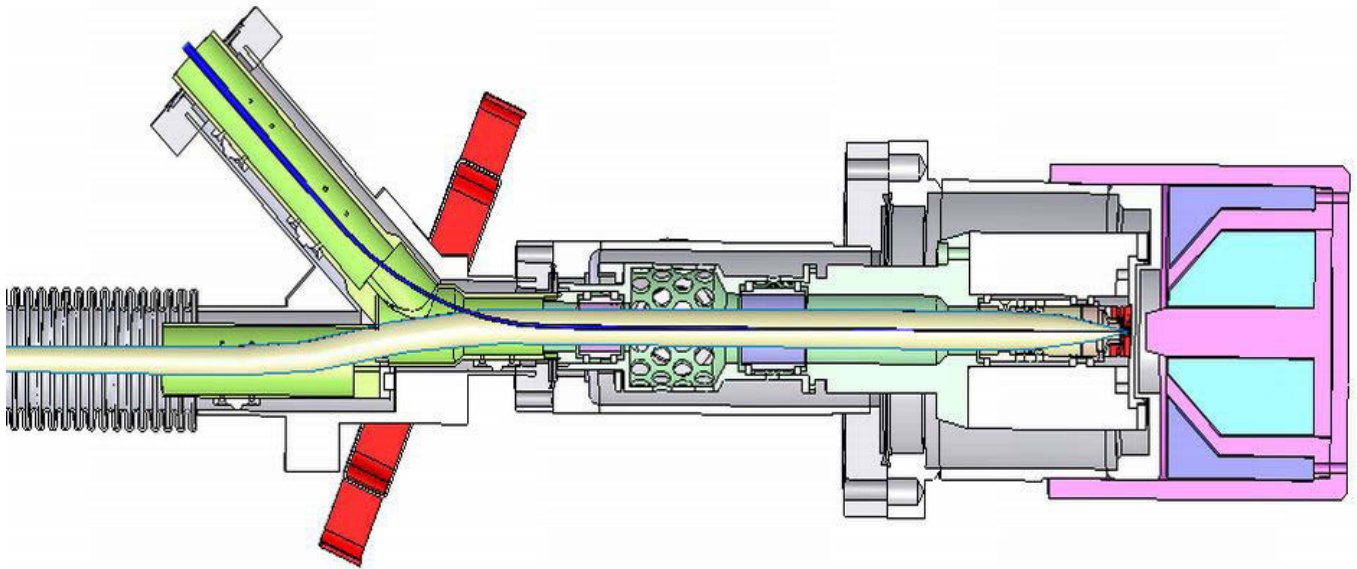


Figure 4.32.: Setup of the remoderator. The primary beam comes from the left side and is indicated by the light yellow tube. The main magnetic dipole field, which is perpendicular to the plane of projection, has a much stronger effect on the slow remoderated beam (blue tube) than on the fast primary beam.

4.9. High resolution analysis of the Auger-transition in copper

J. Mayer¹, K. Schreckenbach¹, Ch. Hugenschmidt^{1,2}

¹Physik-Department E21, TU München

²ZWE FRM II, TU München

PAES and EAES

Electron induced Auger Electron Spectroscopy (EAES) is a conventional method for characterizing sample surfaces in solid state physics. This widely used surface sensitive method probes the first two up to five atomic layers of a sample. But the Positron annihilation induced Auger Electron Spectroscopy (PAES) is even more sensitive, since more than 90% of the emitted Auger electrons stem from the topmost atomic layer [1]. Moreover, the secondary electron background in the energy range of the Auger electrons with PAES is considerably reduced compared to EAES. This is caused by the different ionization process which is matter-antimatter annihilation in PAES whereas in EAES the atoms are ionized via impact. Thus, the beam energy of the positrons is at its maximum 20 – 30 eV compared to a few keV with electrons. In summary, PAES is a non destructive, surface sensitive, background free method for surface measurements.

PAES setup at NEPOMUC

The PAES-facility at the FRM-II [2] has been rebuilt in several aspects, most of it due to the newly installed state of the art hemispherical electron energy analyzer. The mean radius of 150mm and the position sensitive MCP-CCD readout of the electrons enable a higher energy resolution and simultaneously reduce the total measurement time considerably. The elaborate lens design in

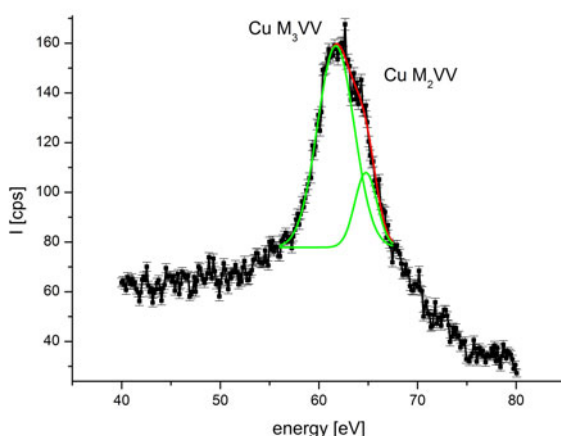


Figure 4.33.: The double peak of the Cu M_{2,3}VV-transition measured with high resolution PAES.

front of the entrance of the hemispheres and the pass energy of up to 600 eV enhance the transmission and thus make PAES with positron currents of 2×10^7 e⁺/s at the sample site feasible.

Measurements

Besides the surface selectivity and the reduction of the secondary electron background the incoming low energy positron does not perturb the electron shell of the atom, which is to be ionized. This is a further advantage of PAES over EAES. Hence, it is possible to get new information about the exact line shape of the Auger transition.

Figure 4.33 shows the Auger-spectrum of a (100)-copper single crystal (cleaned with Ar⁺-ions) released after impact by a 17 eV-positron beam. Firstly the high signal to noise ratio (SNR) is striking. Compared to conventional EAES (SNR \approx 1 : 2), here the SNR can be estimated conservatively to be at least SNR \approx 4 : 1. PAES-spectra at higher energies than 80 eV showed, that the background drops even below 30 cps, so that the SNR is even an order of magnitude better than with EAES. The higher background (see Fig. 4.33) results from the backscattered Auger electrons of the Cu₁VV-peak at 105 eV that was not yet studied in detail.

High resolution and short measurement time

It is the first time that the positron annihilation induced Auger transition of copper with the initial hole in the 3p_{3/2} and in the 3p_{1/2} shell respectively, is shown with PAES with such a good energy resolution (< 1 eV) and a first analysis of the lineshape reveals an energy gap of these transitions of (2.80 ± 0.08) eV. Furthermore the measurement time for the spectrum shown in figure 4.33 was only three hours whereas with other PAES-facilities a spectrum with low energy resolution takes several days. A detailed discussion of the Auger-line shape of copper will be published soon. In addition, we succeeded to reduce measurement time for a rough spectrum from 20 – 140 eV to typically less than 15 minutes.

Improvements on the way

Presently a MCP-phosphor screen assembly at the sample site is installed to improve the focus of the beam. Additionally a grid in front of the MCP will be installed in order to measure (in the absence of magnetic fields) the energy spread of the positron beam at the sample

position. Since the new electron energy analyzer is now working properly, measurements of ultrathin metal films or organic molecules on metallic surfaces are planned.

[1] Jensen, K. O., Weiss, A. *Phys. Rev. B*, 41, (1990),

3928–3936.

[2] Hugenschmidt, C., Mayer, J., Schreckenbach, K. *Surf. Sci.*, 601, (2007), 2459–2466.

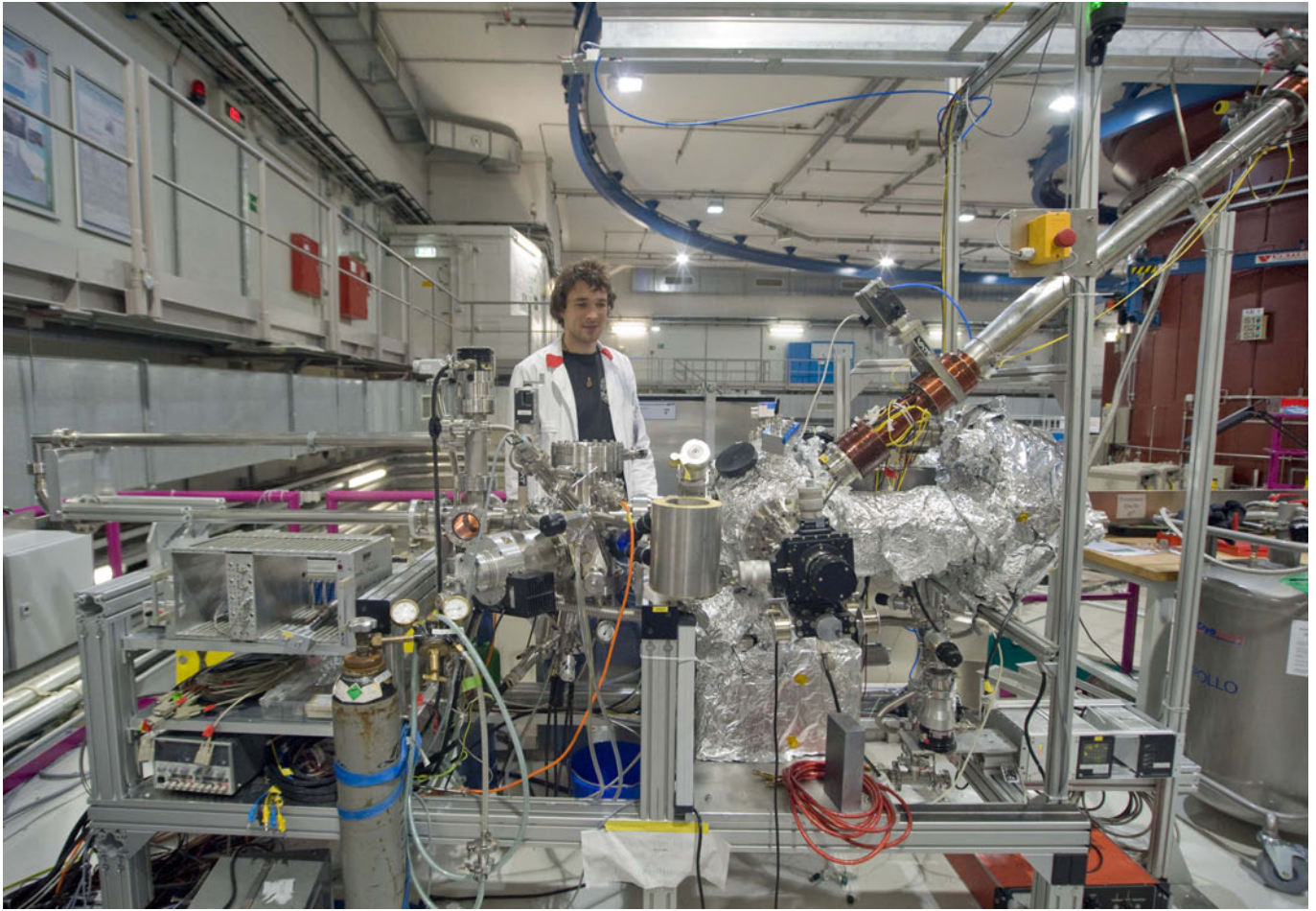


Figure 4.34.: Jakob Mayer and the setup of Positron annihilation induced Auger Electron Spectroscopy (PAES) at the positron source.

Part II.

Scientific highlights

5. Condensed Matter

5.1. Skyrmion lattice in a chiral magnet

S. Mühlbauer^{1,2}, B. Binz³, F. Jonietz¹, C. Pfleiderer¹, A. Rosch³, A. Neubauer¹, R. Georgii², P. Böni¹

¹Physik-Department E21, TU München

²ZWE FRM II, TU München

³ITP, Universität zu Köln

At ambient pressure and zero applied magnetic field the chiral itinerant-electron magnet MnSi develops helical magnetic order below a critical temperature, $T_c = 29.5\text{K}$, that is the result of three hierarchical energy scales. The strongest scale is ferromagnetic exchange favoring a uniform spin alignment. The lack of inversion symmetry of the cubic B20 crystal structure results in chiral spin-orbit interactions, which may be described by the Dzyaloshinsky Moriya (DM) interaction. The ferromagnetic exchange together with the chiral spin-orbit coupling lead to a rotation of the spins with a periodicity $\lambda_h = 190\text{\AA}$ that is large compared with the lattice constant, $a = 4.56\text{\AA}$. This large separation of length scales implies an efficient decoupling of the magnetic and atomic structures. Therefore, the alignment of the helical spin spiral along the cubic space diagonal $\langle 111 \rangle$ is weak and is only fourth power in the small spin-orbit coupling. These crystalline field interactions, which break the rotational symmetry, are by far the weakest scale in the system.

Structure like a vortex lattice

We have performed small angle neutron measurements on MIRA, FRM II to examine the detailed structure of the so-called A-phase, a phase pocket close to T_c at $1/2B_{c2}$, where the propagation vector \mathbf{Q} of the helical order aligns perpendicular to the applied magnetic field. By applying the magnetic field parallel to the incoming neutron beam, we unveiled the complete structure of the A-phase: As shown in Fig. 5.1, panels B and D, the A-phase is characterized by a regular, sixfold scattering pattern reminiscent of a vortex lattice. This peculiar structure aligns strictly perpendicular to the applied magnetic field, regardless of the underlying crystal symmetry direction. If the scattering plane contains a crystalline $\langle 110 \rangle$ direction, weak pinning was observed.

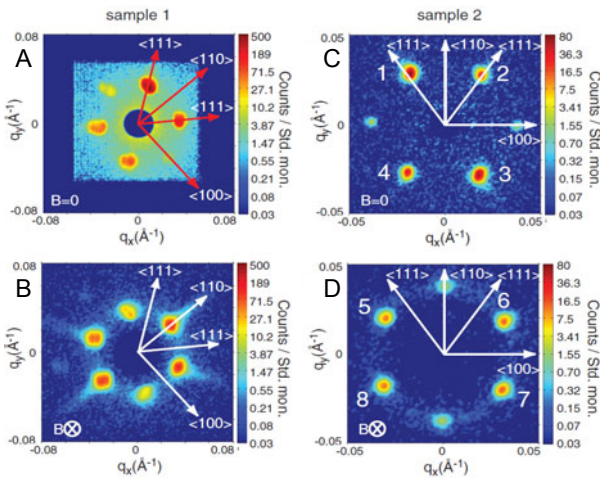


Figure 5.1.: Typical neutron scattering patterns of MnSi: Panel A and C show the known helical state at zero ambient field, where the propagation vector is aligned along the crystalline $\langle 111 \rangle$ direction. Panel B and D show the scattering pattern obtained in the A-Phase. For details see text.

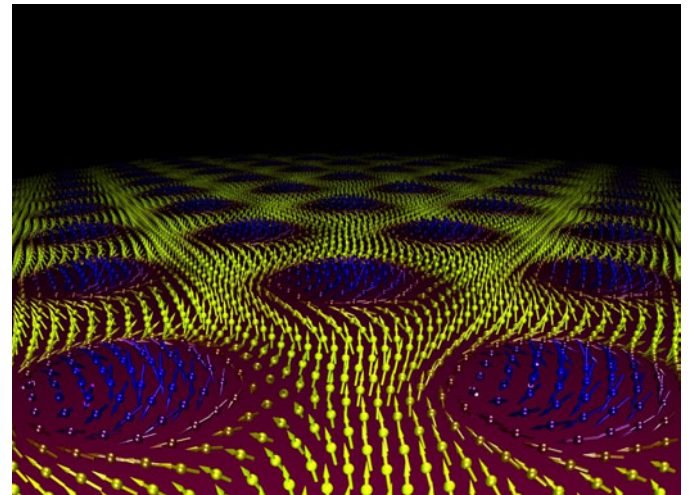


Figure 5.2.: Real space depiction of the spin structure of the skyrmion line lattice. Note that the depiction shows a cut through the skyrmion line lattice in a plane perpendicular to the applied magnetic field.

New stable magnetic topology

This structure was identified as triple-**Q** state, which is a spin-crystal composed of the superposition of three helices under 120° but perpendicular to the magnetic field. The free energy of the triple-**Q** state was calculated by means of a Ginzburg-Landau ansatz and found to be metastable. By including Gaussian fluctuations of the form $G \sim F[\mathbf{M}_0] + 1/2 \log \det \left(\frac{\delta^2 F}{\delta \mathbf{M} \delta \mathbf{M}} \right) \Big|_{\mathbf{M}}$ as leading correction to the mean field theory, the free energy of the triple-**Q** state was found to have a global minimum. To consider the topology, we compute the winding density of this doubly-twisted magnetic spin crystal $\phi = \frac{1}{4\pi} \mathbf{n} \cdot \frac{\partial \mathbf{n}}{\partial x} \times \frac{\partial \mathbf{n}}{\partial y}$. Integration over one unit cell of the spin crystal yields a skyrmion number $\phi = -1$ per unit cell. Thus a new stable magnetic topology is identified. Topologically stable knots of the magnetisation with particle-

like properties arrange themselves in a lattice, which is translation invariant in magnetic field direction. The spin crystal, found in the A-phase of MnSi can be regarded as skyrmion line lattice [1], as shown in Fig. 5.2.

The skyrmion lattice in the chiral magnet MnSi reported here represents an example, where an electronic liquid forms a spin crystal made of topologically non-trivial entities. Our study experimentally establishes magnetic materials lacking inversion symmetry as an arena for new forms of crystalline order composed of topologically stable spin states. This provides a glimpse of the large variety of magnetic states that may be expected from the particle-like magnetic objects currently discussed in the literature.

[1] Mühlbauer, S., Binz, B., Jonietz, F., Pfleiderer, C., Rosch, A., Neubauer, A., Georgii, R., Böni, P. *Science*, 323(5916), (2009), 915 – 919.

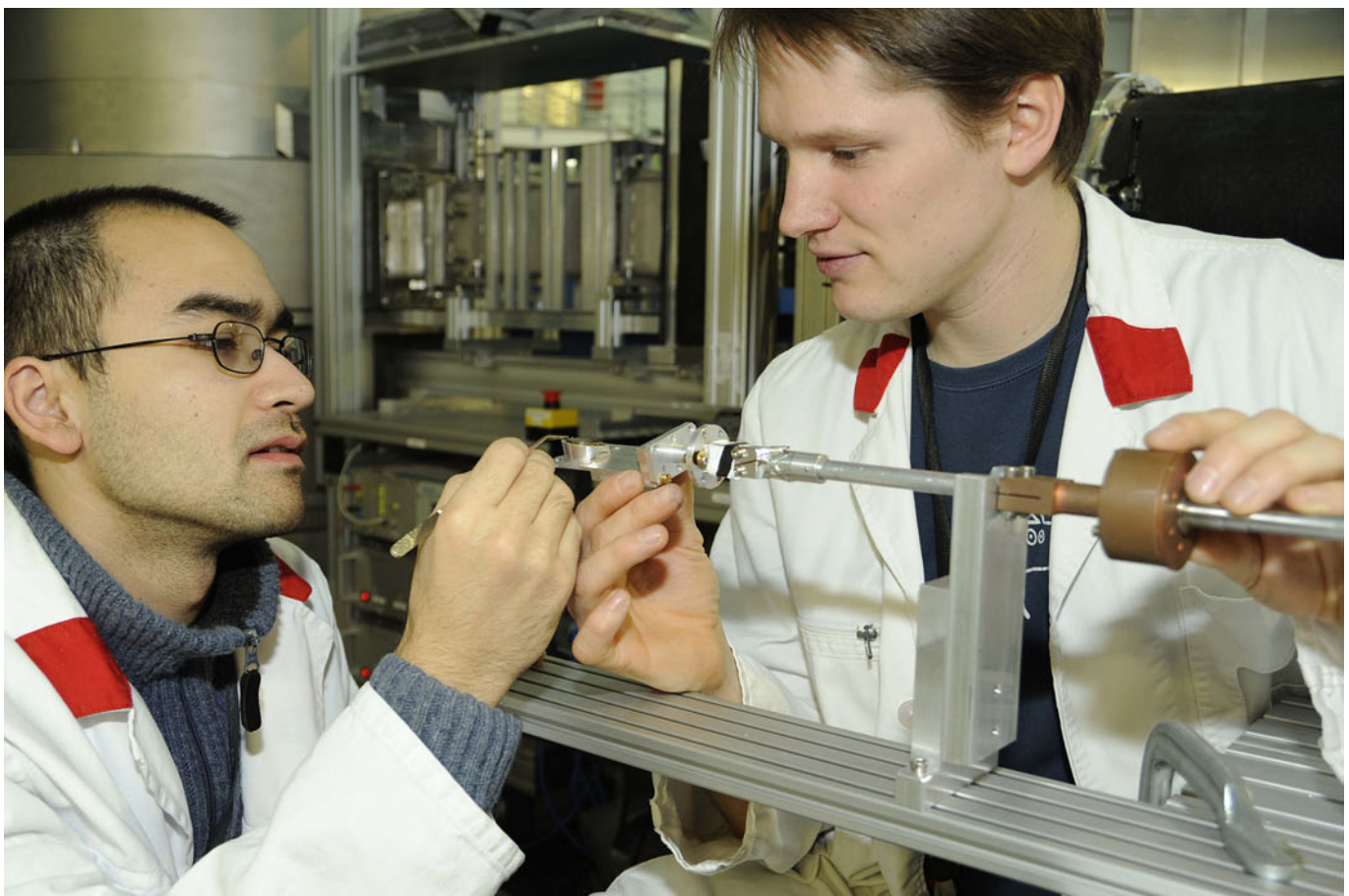


Figure 5.3.: The two young scientists, who discovered the skyrmion lattice, Sebastian Mühlbauer (right) and Florian Jonietz, working on the instrument MIRA.

5.2. Phonon Anomalies and the Energy Gap in Superconductors

P. Aynajian¹, T. Keller^{2,1}, L. Boeri², S. Shapiro³, K. Habicht⁴, B. Keimer²

¹Max-Planck-Institute for Solid State Research, Stuttgart

²ZWE FRM II, TU München

³Brookhaven National Laboratory, Upton, NY, USA

⁴Hahn-Meitner Institute, Berlin

The momentum and temperature dependence of the lifetimes of acoustic phonons in the elemental superconductors lead and niobium were determined at the high resolution neutron spin-echo spectrometer TRISP at the FRM II [1]. In both elements, the width of the superconducting energy gap $2\Delta(T = 0K)$ (i.e. the binding energy of the Cooper pairs at zero temperature) extracted from these measurements was found to converge with sharp anomalies in the phonon spectrum originating from Fermi-surface nesting (Kohn anomalies). As Nb and Pb have different structure and Fermi-surfaces, the observed effect cannot be an accidental coincidence. A locking between $2\Delta(0)$ and the Kohn anomaly was recently demonstrated by doping Pb with Bi, which increases the width of the gap and shifts the Kohn anomaly to higher energies [2]. The results indicate electron many-body correlations beyond the standard theoretical framework for conventional superconductivity. A possible mechanism is the interplay between superconductivity and spin- or charge-density-wave fluctuations, which may induce dynamical nesting of the Fermi surface.

Over the past half-century, a comprehensive framework based on the Bardeen-Cooper-Schrieffer formulation [3] has been developed for the interpretation of experimental data on superconductors. Although this framework has been challenged by the discovery of high-temperature superconductivity, it provides a remarkably successful description of the physical properties of conventional low-temperature superconductors. Even today, however, the prediction of two of the most important quantities characterizing a superconductor, the transition temperature and the energy gap at the Fermi level, from first principles presents a formidable challenge to theory because they depend exponentially on material-specific parameters such as the phononic and electronic densities of states and the electron-phonon coupling.

The energy gap $2\Delta(T)$ can be directly determined in phonon lifetime measurements, because electron-phonon scattering is suppressed (and the phonon lifetimes are thus enhanced) for phonon energies below the gap. In Fig. 1 the energy of the gap is varies with temperature. As expected, the linewidth (inverse

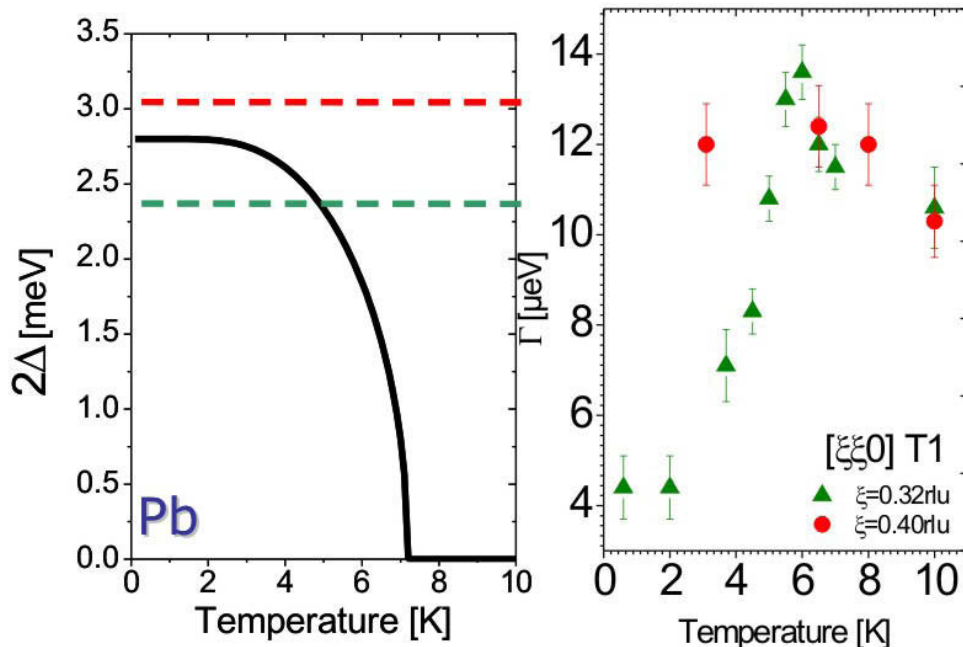


Figure 5.4.: Width of the superconducting gap in Pb ($T_c = 7.2K$, left) and the linewidth of two transverse acoustic phonons (right) with energies indicated by dotted horizontal lines. Phonons with an energy below $2\Delta(T)$ can't break the Cooper pairs and thus have an increased lifetime (smaller linewidth).

lifetime) increases if $2\Delta(T)$ becomes smaller than the phonon energy (green line) [4]. Phonons with an energy above $2\Delta(T)$ are not affected (red line). In Fig. 2, the phonon energy is varied at constant temperature (3.5K and 10K, below and above T_c). The linewidths at low temperatures (3.5K) show again the expected behavior: for phonon energies above $2\Delta(0)$ (blue arrow), the linewidth increases.

A surprising feature is observed above T_c in the normal conducting state, where the linewidths peak at a phonon energy corresponding to $2\Delta(0)$. This peak originates from a hitherto unknown Kohn anomaly [5]. The phonon wave vector at this anomaly connects two nearly parallel segments of the Fermi surface, leading to enhanced electron phonon scattering and thus to a reduced lifetime (enhanced linewidth).

We have recorded several hitherto unknown Kohn anomalies in both Pb and Nb and found that the low-temperature energy gap coincides with such an anomaly in both materials. This phenomenon has not been antici-

pated by the standard theoretical framework for conventional superconductors and is not reproduced by state-of-the-art *ab initio* calculations. Although the origin of the observed coincidence is presently unclear, a specific scenario to explore in future theoretical work is the interplay between density-wave and superconducting correlations.

We thank Kathrin Buchner and the FRM II sample environment group for technical assistance.

[1] Aynajian, P., Keller, T., Boeri, L., Shapiro, S. M., Habicht, K., Keimer, B. *Science*, 319, (2008), 1509.

[2] Munnikes, N., Aynajian, P., Keller, T., Keimer, B. To be published.

[3] Bardeen, J., Cooper, L. N., Schrieffer, J. R. *Phys. Rev.*, 108, (1957), 1175.

[4] Keller, T., Aynajian, P., Habicht, K., Boeri, L., Bose, S. K., Keimer, B. *Phys. Rev. Lett.*, 96, (2006), 225501.

[5] Kohn, W. *Phys. Rev. Lett.*, 2, (1959), 393.

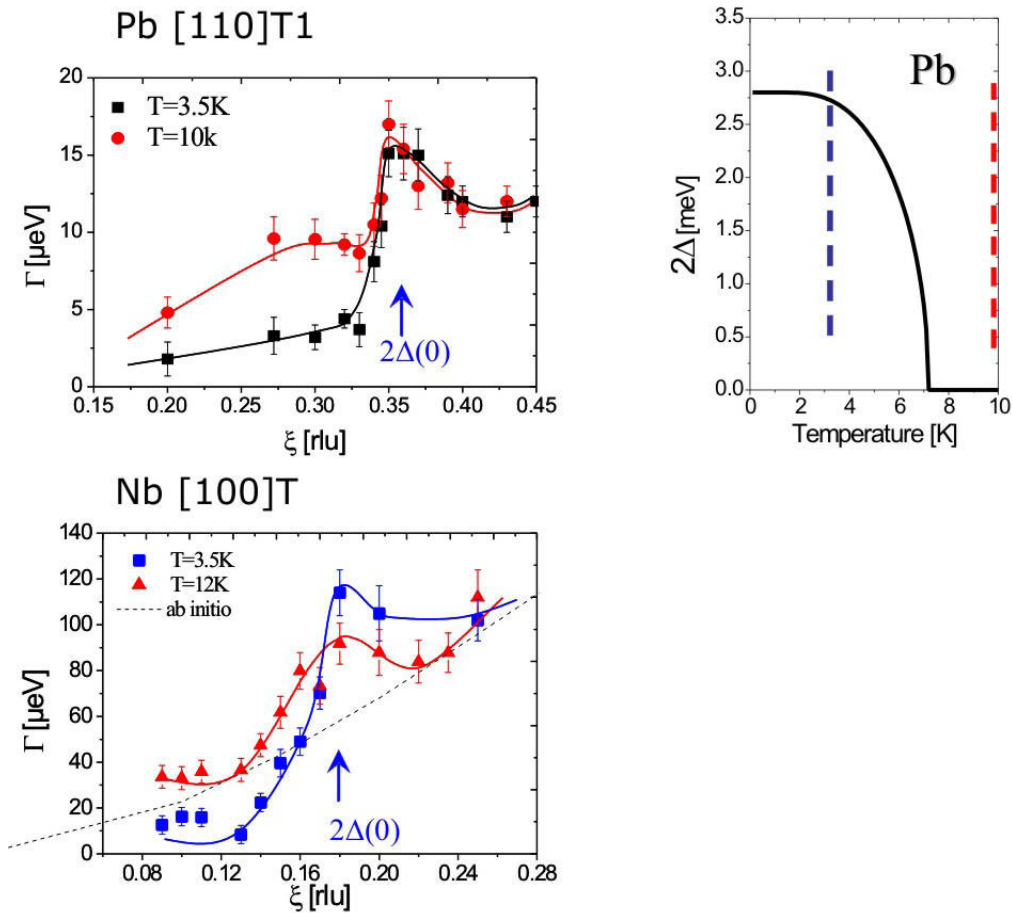


Figure 5.5.: Linewidth vs. phonon momentum (proportional to the phonon energy) in Pb and Nb, below and above T_c as indicated by the dotted vertical lines (right). The width of the gap $2\Delta(0)$ at $T = 0$ is indicated by blue arrows. Ab-initio LDA calculations (dotted line in the lower left panel) do not reproduce the low energy Kohn anomaly.

5.3. Absolute d -spacing value determination by Larmor diffraction

J. Repper¹, T. Keller^{1,2}, M. Hofmann¹, C. Krempaszky³, W. Petry¹, E. Werner⁴

¹ZWE FRM II, TU München

²Max-Planck-Institut für Festkörperphysik, Stuttgart

³Christian-Doppler-Labor, Technische Universität München

⁴Lehrstuhl für Werkstoffkunde und Werkstoffmechanik, Technische Universität München

Residual stress analysis using neutron diffraction relies on the comparison of the lattice spacing d of a stressed component with the lattice spacing d_0 of a macroscopic stress free reference sample. These d -spacings are determined on dedicated diffractometers like the STRESS-SPEC at the FRM II via the accurate determination of the Bragg angle θ . For the determination of the reference values d_0 thin stress free samples are used. For these thin samples the exact positioning in the beam center is crucial, as small displacements result in significant shifts in the measured Bragg angles.

High accuracy

We performed an independent test of the d_0 determination using the new neutron *Larmor diffraction* (LD) technique available at the TRISP spectrometer at the FRM II. In LD, the lattice spacing d is encoded in the spin precession of a polarized neutron beam rather than in an accurate measurement of diffraction angles like on conventional diffractometers (for an introduction see refs. [1, 2]). The resolution is independent of the divergence and monochromaticity of the incident beam and insensitive to alignment errors of the sample [1]. Hence, the method enables the measurement of reference values d_0 with a very high accuracy (in the order of $\Delta d/d = 10^{-6}$) hitherto not possible using classical diffractometers [3]. A further new option available with LD is the determination of the spread of d -values with high resolution. The major disadvantage of LD are the intensity losses resulting from polarization analysis and the more complicated spin-echo technique, leading to much longer counting times than in conventional diffraction. Thus LD will never replace conventional diffraction, where ultra-high resolution generally is not needed. But it has the potential to extend the range of neutron stress analysis to important fields of current materials research where other techniques fail, i.e. to the analysis of microstrains or lattice mismatches between different phases.

Here we report on a study of single-phase Inconel 718 samples, a nickel alloy which is widely used for high temperature applications, such as blades in gas turbines. Both conventional diffraction on STRESS-SPEC [4] and LD on TRISP [5] (figure 5.6) were used to determine *absolute* values of lattice spacing d . In addition, the results of investigations on the spread of d -values are presented.

Two sample sets of cylindrical Inconel 718 samples were studied. Each set consisted of three samples

with different radii (1 mm, 5 mm and 10 mm). The samples were cut from two differently treated pancakes (diameter = 240 mm, thickness = 20 mm) at a radius of $r = 80$ mm. Both pancakes were forged at a temperature of 990°C and cooled down to room temperature in different ways: The first disk was water quenched (WQ), whereas the second disk was cooled down in air (AC). The reference sample to calibrate the instrument was a perfect germanium single crystal (fcc) with a lattice parameter of $a = 5.65726(7)$ Å [6]. The correct and stable operation of TRISP was verified with a powder sample of SRM640c silicon with well defined d -spacing [7]. All measurements were taken at incident wave vectors k_i around 3.5 Å⁻¹ ($\lambda = 1.8$ Å). All samples were fully illuminated by the neutron beam (max 40×40 mm²).

Agreement with literature

The lattice spacing of the Si{422} lattice planes determined by LD calibrated with the Ge reference specimen is $d_{\text{Si,Larmor}} = 1.108620(14)$ Å. This shows a reasonable agreement with the values given in literature [7] ($a = 5.431195(9)$ Å resulting in $d_{\text{Si}(422)} = 1.108638(2)$ Å). The error of $1.4 \cdot 10^{-5}$ Å is to a large fraction due to the error of the literature value of the Germanium lattice constant ($\Delta a/a = 1.3 \cdot 10^{-5}$). Thus for further experiments the more accurate silicon standard powder should be used as reference sample.

The d -spacing of the IN718 samples determined by Larmor diffraction was compared to the results achieved by a conventional neutron diffraction experiment (figure 5.7). A very good agreement of the two methods can be found for the samples with radii of 5 and 10 mm (differences in the order of $10^{-5}/10^{-6}$ Å). In case of the 1 mm samples a discrepancy in the d -spacing values (in the order of $8 \cdot 10^{-4}$ Å) is observed. This is most likely due to the difficulties to align the sample in the center of gravity of the conventional diffractometer. Small shifts in the sample position can cause large shifts in the 2θ values and as a consequence in the lattice spacing d . For the larger samples small misalignment effects are negligible compared to the sample size.

The spread of lattice spacing is found in the order of 10^{-6} in both sample materials (WQ and AC). Whereas, the values are approximately equal within one sample state, the water quenched (WQ) samples have slightly higher values ($\sim 1.55 \cdot 10^{-6}$) than the air cooled (AC) sam-

ples ($\sim 1.10 \cdot 10^{-6}$). This effect clearly depends on the sample process history.

During the slow air cooling process the matrix material reduces the defect density which increases during the forging process. The higher defect density in the water quenched sample material results in a broader spread of the lattice spacing.

This first experiments on single-phase materials demonstrated the potential to determine accurate reference d_0 -values for neutron residual stress analysis. In addition, the ability of the method to investigate defect densities and thus microstrains and stresses are shown. A combination of both methods can provide new insight in materials (e.g. defect densities, d_0 determination for stress analysis, microscopic stress and strain analysis). Whereas, all results show reasonable values for single-phase materials, the analysis of the data for multi-phase materials is more complex and needs more sophisticated studies. The next steps of a comparative study include a systematic investigation of the reliability of LD method and its applications for multi-phase materials.

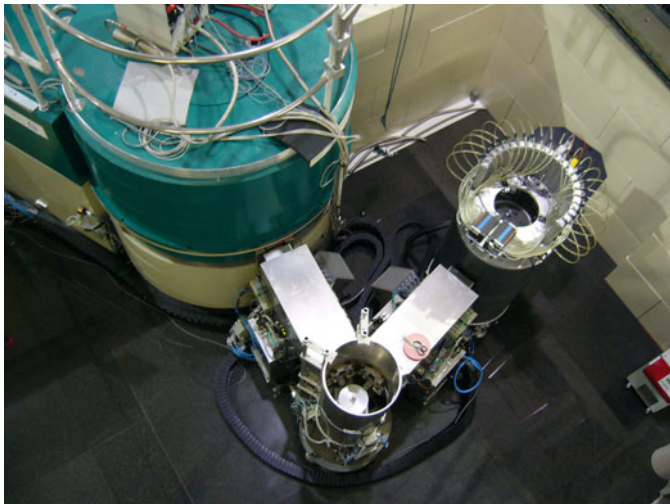


Figure 5.6.: The TRISP spectrometer at the FRM II. The components from left: Monochromator, spin-echo units, sample table, detector.

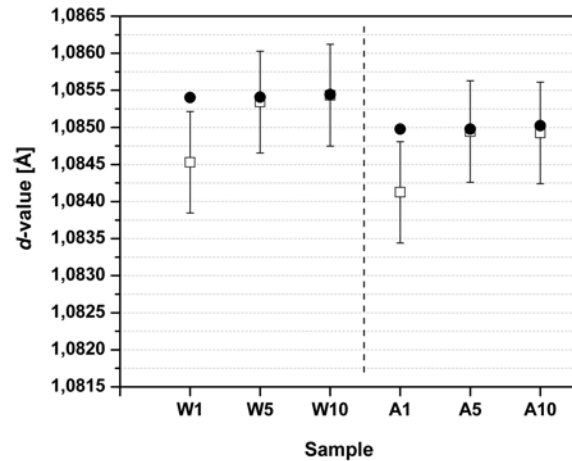


Figure 5.7.: Comparison of d -values determined by LD (solid circles) and CND (open cubes). The errors of the LD results are in the same size as the symbols.

- [1] Rekveldt, M. T., Keller, T., Kraan, W. H. *Europhys. Lett.*, 54, (2001), 342–346.
- [2] Rekveldt, M. T. *Mater. Sci. Forum*, 321-324, (2000), 258–263.
- [3] Pfeleiderer, C., Böni, P., Keller, T., Rößler, U. K., Rosch, A. *Science*, 316, (2007), 1871–1874.
- [4] Hofmann, M., *et al.* *Neutron News*, 18(4), (2007), 27–30.
- [5] Keller, T., *et al.* *Neutron News*, 18(2), (2007), 16–18.
- [6] Brümmer, O., Alex, V., Schulze, G. *Ann. Phys.*, 483(2), (1972), 118–134.
- [7] Freiman, S. W., Trahey, N. M. National Institute of Standards & Technology Certificate, Standard Reference Material® 640c (2000). Gaithersburg, MD 20899.

5.4. Inelastic neutron scattering on solid deuterium

E. Gutmiedl¹, A. Frei¹, A.R. Müller¹, S. Paul¹, C. Morkel², H. Schober³, T. Unruh⁴

¹Physik-Department E18, TU München

²Physik-Department E21, TU München

³Institut Laue Langevin (ILL), Grenoble, France

⁴ZWE FRM II, TU München

Introduction

Solid deuterium (sD_2) and solid hydrogen are typical quantum molecular solids. Each D_2/H_2 molecule exhibits large zero-point vibrations due to the small molecule mass. These quantum solids have been investigated theoretically [1] and by experimental techniques like inelastic neutron scattering [2] and Raman scattering [3]. Solid deuterium has an almost perfect hcp crystal structure, when it is prepared under suitable conditions [4] (low pressure and $T > 5$ K).

The D_2 molecule has internal rotational modes, which are described by the rotational quantum number J . In the solid phase, J is still a good quantum number. D_2 in states with even J ($J=0,2,4,\dots$) is called ortho-deuterium ($o-D_2$), whereas D_2 in states with odd J ($J=1,3,5,\dots$) is called para-deuterium ($p-D_2$).

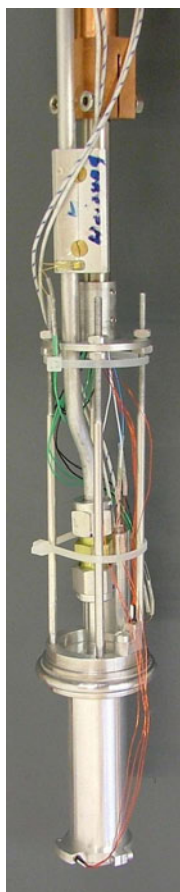


Figure 5.8.: Cryogenic sample holder for freezing deuterium

Solid and liquid deuterium are good converters for production of cold and ultra-cold-neutrons (UCN). They have a significant cross section for neutron scattering (several barns). In the case of UCN almost the complete energy of the incoming neutron (thermal or cold neutrons) is transferred to the converter material via excitation of phonons or other energy loss channels like rotational transitions [4]. The understanding of the dynamics of solid deuterium is important to optimize this converter as a strong source for production of UCN.

UCN are slow enough to be confined in traps, which can be formed by material with a high Fermi potential or by a magnetic field (60 neV/T). UCN can be observed for more than 1000 s in these traps, and are excellent tools for high precision measurements, concerning the life time of the neutrons itself, and also for determining a possible small electric dipole moment of the neutron [5].

Therefore a measurement of inelastic neutron scattering with the TOFTOF instrument at the FRM II was performed to study solid deuterium with respect to different methods of freezing this cryogenic crystals and the influence of these methods on the dynamic and structure of sD_2 .

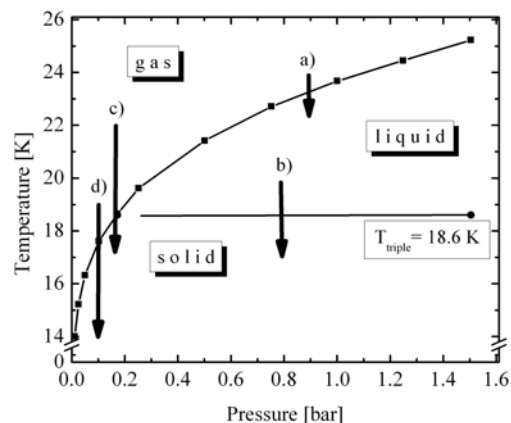


Figure 5.9.: D_2 phase diagram with different process paths studied: a) liquefaction from the gas, b) solidification from liquid, c) sublimation at high temperature, d) direct condensation.

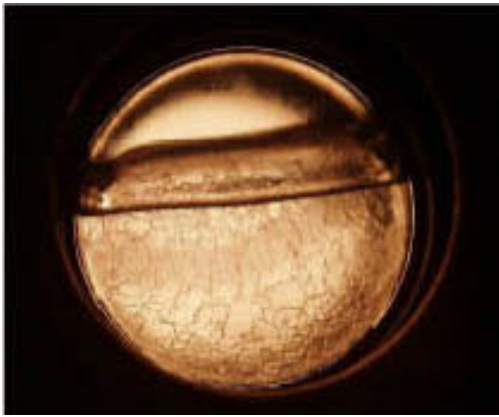


Figure 5.10.: Crystal prepared by direct condensation at lowest temperature $T_{cell} = 8$ K from the gas phase with high over saturation.



Figure 5.11.: Melting of the gas crystal as a function of time ~ 10 min at $T_{cell} = 22$ K. The crystal melts in vertical layers and from the top.

Experimental setup

A special cryogenic sample holder was designed and built for this experiment (see fig. 5.8). The deuterium is

frozen out inside the sample cell in a double-wall cylinder. The thickness of the solid deuterium was adjusted to $\delta \sim 3$ mm. The measurements at TOFTOF were carried out at two different wavelengths of the incoming neutrons ($\lambda \simeq 2.0$ Å and $\lambda \simeq 6.0$ Å). The sample cell is connected to the D_2 gas handling system via a $12 \text{ mm} \times 1 \text{ mm}$ stainless steel pipe.

The gas handling system is especially designed to keep the pressure of the D_2 gas flowing into the sample cell quasi-independent of the temperature within the cell. This is done by using needle valves for the gas flow. With this technique it is possible to follow a special path in the phase diagram (see fig. 5.9) of D_2 . This can be either the path from the gas via the liquid to the solid phase, or the path directly from the gas to the solid phase (sublimation). The triple point of D_2 is at [$T_c = 18.7$ K, $P_c \sim 180$ mbar]. At pressures below P_c direct sublimation of D_2 is possible, while at pressures above P_c the D_2 is liquefied before it becomes a solid.

In fig. 5.10 a typical example of a solid deuterium crystal, which was frozen via the path d is shown.

Results and discussion

Structure

Fig. 5.12 shows the structure of different prepared solid deuterium samples.

The structure of different frozen sD_2 is in all cases a hcp structure. The different freezing methods have only an impact on the intensity of the individual Bragg peaks. It is clearly seen, that the structure of sD_2 contains large textures for most of the investigated sD_2 samples. Only the fast cooled down (from liquid) samples (see fig. 5.12 d)) show an almost powder like hcp structure. Annealing at $T \sim 12$ -13K does not change the hcp structure, but

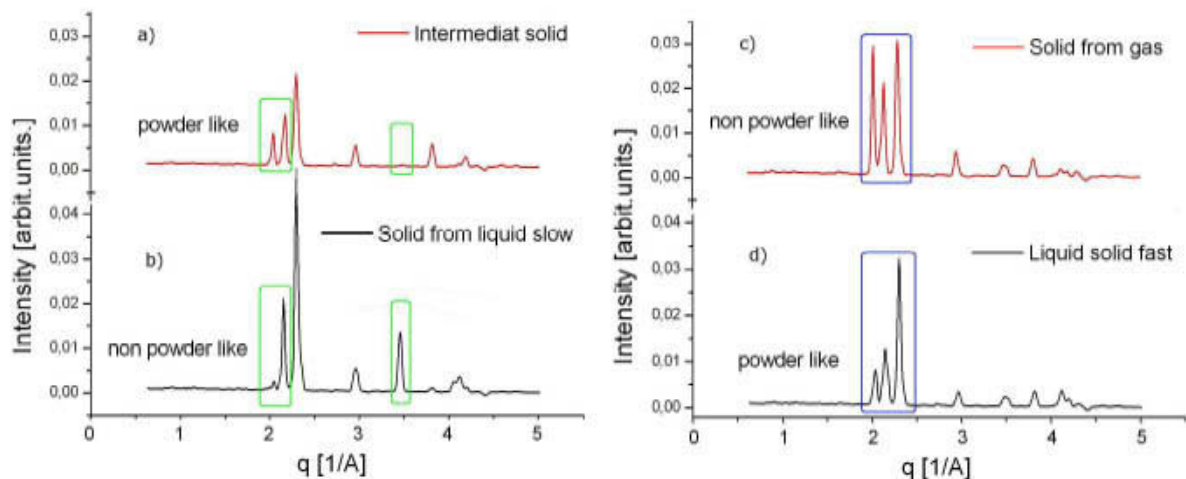


Figure 5.12.: Solid deuterium structure $S(q, \omega = 0)$ as function of the momentum transfer q and different freezing procedures. The square shows the region of interest.

modifies the intensities of the different Bragg peaks.

It seems, that annealing leads to a reorientation of small crystals in the sample and therefore to a changed texture in the solid deuterium structure. The analysis of these data is still ongoing and will be presented in a future publication.

Dynamic

Fig. 5.14 shows the inelastic neutron scattering on sD_2 for two ortho concentrations (ortho- D_2 66% and 98%). On the neutron energy gain side there is a clear signal of the $J = 1 \mapsto 0$ transition ($E \sim -7.5$ meV). At the neutron

energy loss side there is also the transition $J = 0 \mapsto 1$ ($E \sim 7.5$ meV) visible.

The main scattering in sD_2 is determined by emission and destruction of phonons in the crystal. These data are necessary for determination of the production cross section for creating UCN (neutron energy loss side) and also for the loss channels (upscattering) for UCN (energy gain side). With the aid of these data it's possible to optimize the new planned UCN source at the FRM II.

Summary and outlook

Inelastic neutron scattering on advanced converter materials like solid deuterium with high resolution neutron time-of-flight instruments are very helpful for optimizing new powerful UCN sources. The results, reported here, demonstrate the fruitful liaison between the advanced neutron techniques in solid state physics and the requirements of strong UCN sources in particle physics.

[1] Saito, H., *et al. J. Chem. Phys.*, 11, (2000), 953.

[2] Nielsen, H., *et al. Phys. Rev. B*, 7, (1973), 1626.

[3] Dries. Private communication.

[4] Silvera, I. *F. Rev. Mod. Phys.*, 52, (1980), 393.

[5] Silvera, I. *F. Adam Hilger, New York*, (1991).

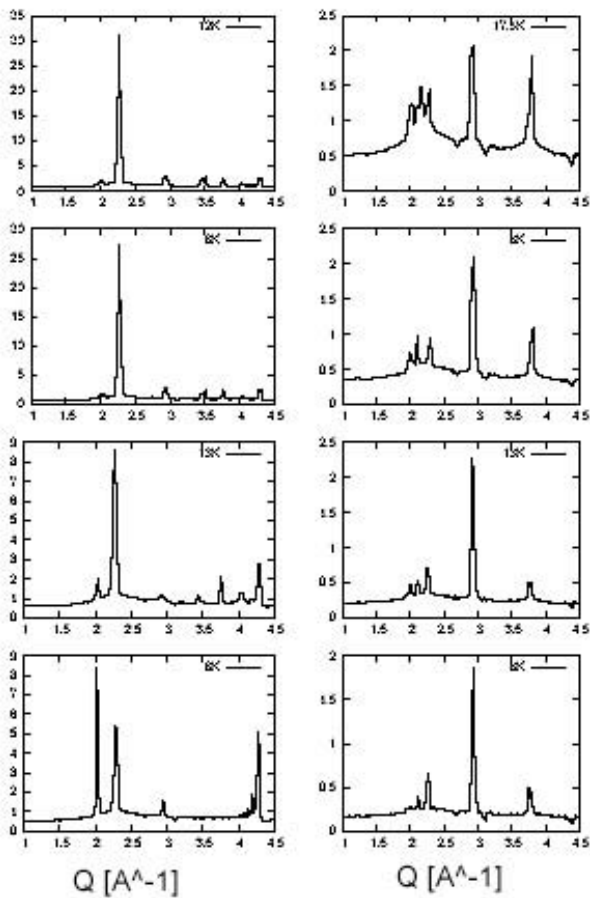


Figure 5.13.: Influence of Annealing of sD_2 on the structure. Left side: natural deuterium (66% ortho- D_2). Right side: ortho- D_2 .

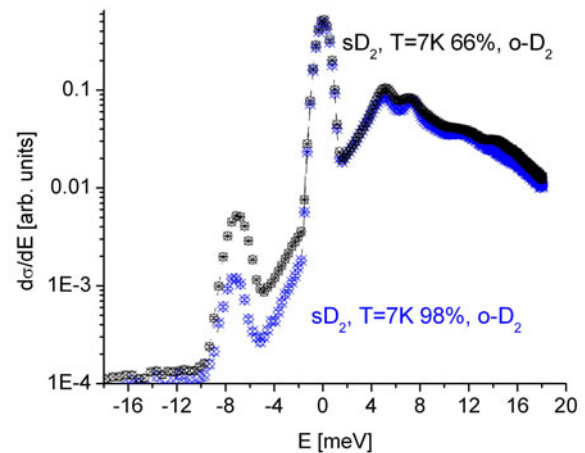


Figure 5.14.: Dynamical neutron scattering cross section of solid D_2 for $c_o = 66\%$ (black) and $c_o = 98\%$ (blue) at $T = 7$ K. Data from the TOFTOF measurements.

5.5. Development of residual strains in composite castings

U. Wasmuth², M. Hofmann¹

¹ZWE FRM II, TU München

²Lehrstuhl für Umformtechnik und Gießereiwesen, UTG, Technische Universität München

The composite casting process is mainly used in the automotive sector to produce for example composite engine blocks with in-cast liners or pistons with steel ring carriers. Due to different thermal expansion of the casting material and the material of the insert residual stresses occur during solidification. These residual stresses can reduce fatigue strength and lead to distortions of the part. They can be minimised by constructive measures. Here finite element simulations (FEM) are valuable tools to predict residual stresses and distortions and thus to optimise the design of parts.

Simulated stress three times higher than the experimental reference

In order to improve the accuracy of stress simulations simple composite test castings (consisting of a fer-

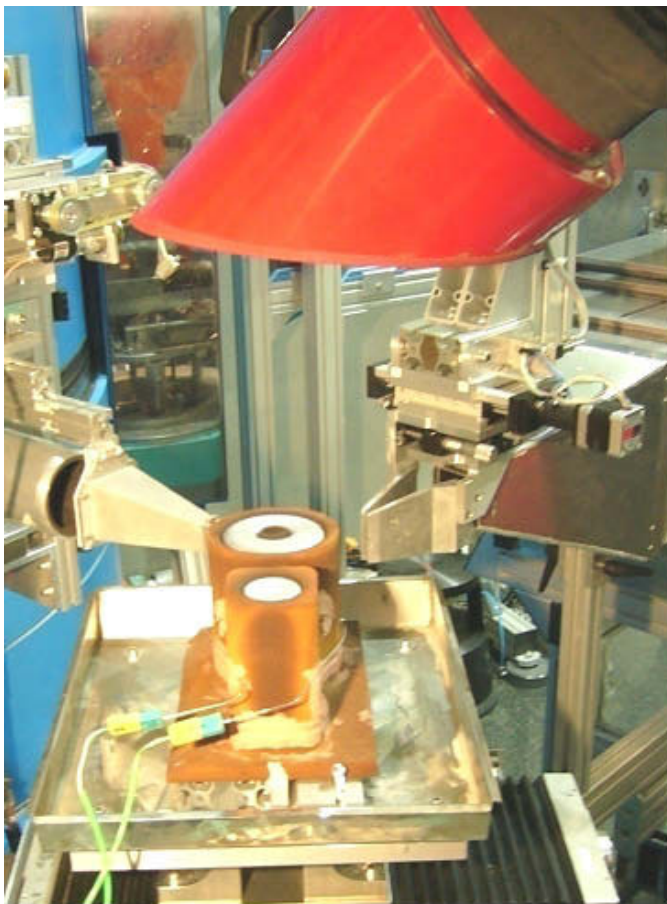


Figure 5.15.: Sand mould after casting the aluminium on the STRESS-SPEC sample table.

ritic steel insert and diffraction experiments on STRESS-SPEC, as reported earlier [1, 2]. The simulated aluminium cast) were designed and characterised by neutron stresses showed to be three times higher compared to the experimental reference, as the material model in the mechanical simulation does not include stress relaxation processes during solidification (for details see [2]).

In general stress relaxation depends strongly on temperature, stress level and time [3]. Especially composite casting processes are influenced by stress relaxation, as stresses are formed even at high temperatures due to different thermal expansion coefficients of materials. As stress relaxation data is difficult to determine experimentally at high temperatures, we conducted in-situ strain measurements using neutron diffraction during the solidification process of the aluminium cast of the test specimen. Using these data the simulation model can now be extended to include a temperature and a time dependent stress relaxation model to predict residual stresses in our test specimens accurately.

The time-resolved, in-situ experiments were carried out at the diffractometer STRESS-SPEC during the cool down of the composite cast test specimen after casting aluminium in a single sand mould installed on the sample table (figure 5.15). All diffraction data were taken in the hoop strain direction of the steel insert. The measurement was started approximately two minutes after the cast at a temperature of $T = 550\text{ °C}$ in the aluminium melt ("semi-liquid" region). The time resolution was 66 seconds. Thermal expansion of the steel was measured separately in the same experimental configuration and subtracted from the diffraction data to obtain the mechanical strain.

Figure 5.16 shows the onset of the build up of compressive, mechanical strain at about 350 °C . At higher temperatures the aluminium is in the plastic regime due to low high temperature strength and relaxation effects. At temperatures below $T \approx 150\text{ °C}$ no further increase of mechanical strains is found, as the yield point of aluminium is exceeded locally within the aluminium cast.

Standard simulation overestimates elastic strain

As mentioned above, the experimentally determined residual strains and the results from a time independent numerical simulation (elastic-plastic simulation as implemented in standard FEM casting routines) differ considerably (figure 5.17). The value of the time independent numerical simulation is about $-2200\ \mu\text{m/m}$ (in fact exceed-

ing the yield point of steel), whereas the in situ experiment yields a compressive strain of about $-730 \mu\text{m/m}$ at 25°C in good agreement with the residual hoop strain value of $-792(38) \mu\text{m/m}$ derived from earlier ambient measurements [2]. These discrepancies in the simulation and experiments are attributed solely to incomplete material modelling of the casting alloy as the stress-strain behaviour of the steel insert is purely elastic in reality as well as the simulation during the cast. The standard time independent simulation overestimates the elastic strain in the aluminium cast. Using the assumption that stress relaxation processes, like creep, occur during the solidification of the aluminium cast, a time dependent creep model based on a routine in [4] was developed and included in the standard simulation. Figure 5.17 shows the excellent agreement of the extended, now time and temperature dependent numerical simulation with the experimental data and the results of the earlier ambient temperature experiments [2]. It is believed that these experi-

mental results could be used to verify universal relaxation models in casting simulations.

Acknowledgement

The investigations presented in this paper have been performed with support of the German Research Foundation (DFG) within the research project "Steigerung der Berechnungsgenauigkeit im Aluminiumformguss mittels Neutronendiffraktometrie".

- [1] Hofmann, M., Seidl, G. A., Schneider, R. *Ann. Report FRM-II*, (2007).
- [2] Wasmuth, U., Meier, L., Hofmann, M., Stege, V., Hoffmann, H. *CIRP Annals*, 57, (2008), 579.
- [3] Funkenbusch, P. D. *Practical Guide to Designed Experiments* (Marcel Dekker, 2005).
- [4] Boyle, J. T., Spence, J. *Stress Analysis for Creep* (London Butterworths, 1983).

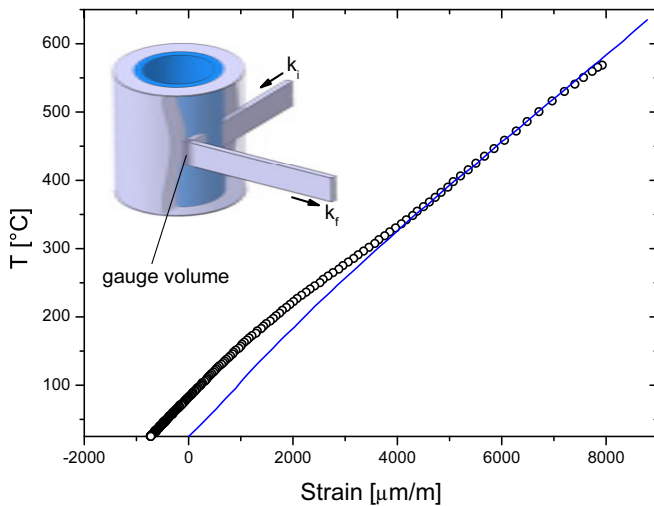


Figure 5.16.: Measured values of the total hoop strain together with the measured thermal expansion curve (blue line). The insert shows the experimental setup with the incoming and diffracted beam arranged as to measure the hoop strain direction of the steel insert (blue).

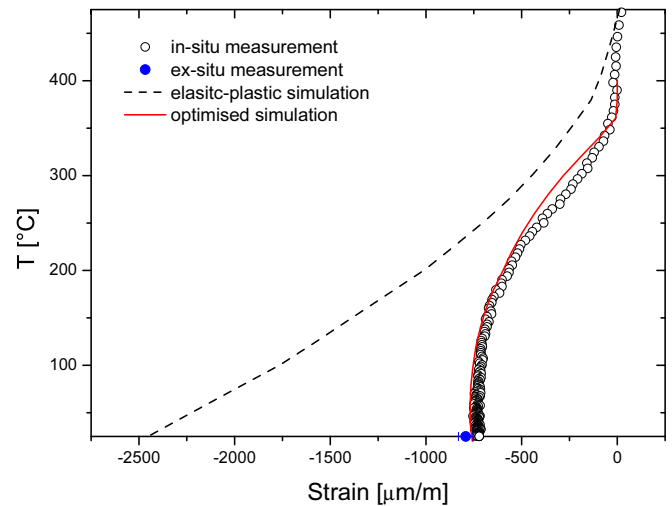


Figure 5.17.: Values of the extracted mechanical hoop strain (after subtraction of thermal strains) together with results for the time independent simulation (dotted line) as well as the optimised, time dependent simulation (red line). The blue data point marks the result of the ex-situ experiment in good agreement with the in-situ measurement and the optimised simulation.

5.6. Insight into the symmetry of a mineral

A. Senyshyn¹, R. Ranjan⁴, M. Hoelzel¹, H. Boysen³

¹Technische Universität Darmstadt, Material- und Geowissenschaften, Darmstadt

²Georg-August Universität Göttingen, Institut für Physikalische Chemie, Göttingen

³Ludwig-Maximilians-Universität, Depart. für Geo- und Umweltwissenschaften, München

⁴Indian Institute of Science, Department of Materials Engineering, Bangalore, India

The perovskite $\text{Na}_{0.5}\text{La}_{0.5}\text{TiO}_3$ (NLT) belongs to the Loparite family of minerals found in foidolites and aegirine-albite metasomatic rocks [1]. Apart from its mineralogical importance, NLT exhibits an interesting dielectric property, known as quantum paraelectricity, at low temperatures (<50 K) [2], i.e. its dielectric permittivity increases on cooling but saturates below a certain temperature T_a . It is believed that the zero point quantum fluctuations prevent freezing of a ferroelectric soft mode and stabilize the paraelectric phase below T_a [3]. The structure of $\text{Na}_{0.5}\text{La}_{0.5}\text{TiO}_3$ has been under controversy for a long time. Different structures namely cubic [4, 5, 6], rhombohedral (space group $R\bar{3}c$) [2], orthorhombic (space group $Pbnm$) [7, 8], and tetragonal (space group $I4/mcm$) [9], have been proposed. All these studies were based on laboratory x-ray powder diffraction data. The ambiguity with regard to the structure of this compound persisted due to the fact that the distortion of the structure with respect to the ideal cubic structure (space group $Pm\bar{3}m$), brought about by tilting of the oxygen octahedra, is very weak. For small octahedral tilts, x-ray diffraction becomes ineffective in deter-

mining the nature of distortion and hence the symmetry of the distorted phase. It was this problem that led different authors to propose different structures of NLT. The inadequacy associated with the x-ray diffraction can be overcome by high-resolution neutron diffraction experiment.

Rhombohedral structure most plausible

Neutron powder diffraction data as a function of temperature was collected on the powder diffractometer SPODI at a wavelength of 1.548 Å. Systematic analysis of the tilts present in structure ruled out the possibility of orthorhombic (space group $Pbnm$) modification. Thus the rhombohedral (space group $R\bar{3}c$) and tetragonal (space group $I4/mcm$) structures consist of only out-of-phase tilts. The significantly lower χ^2 value for the rhombohedral structure (χ^2 for the tetragonal and the rhombohedral structures were found to be 7.0 and 3.6, respectively) suggests that this is the most plausible structure among the two, which is indirectly confirmed by the misfit between the observed and the calculated patterns for

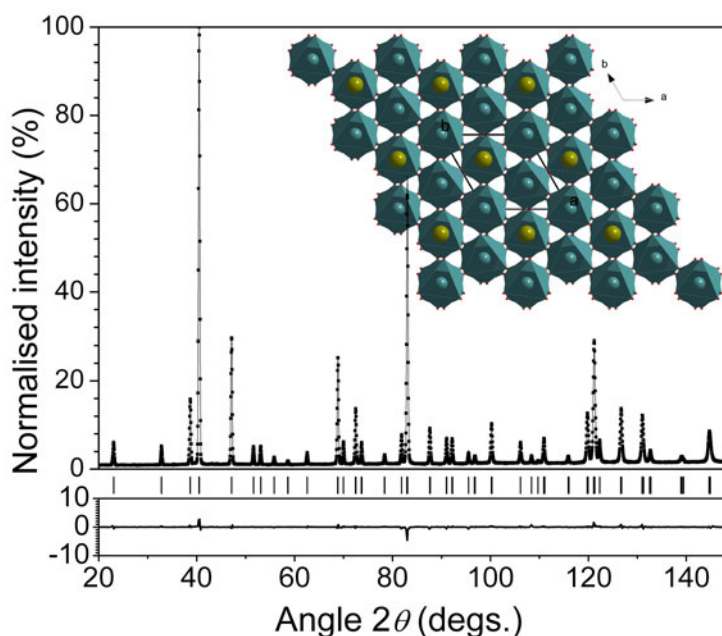


Figure 5.18.: Observed (dots), calculated (continuous line) and difference profiles obtained after Rietveld refinement of the rhombohedral ($R\bar{3}c$) structure using neutron powder diffraction data of NLT at 300 K. The vertical bars represent calculated positions of the Bragg peaks. Inset represents a fragment of the NLT crystal structure as a framework of the corner-sharing TiO_6 octahedra.

the tetragonal model as well as the tetragonal distortion of the pseudocubic subcell.

On heating the specimen, the intensity of the superlattice reflections decreased and finally vanished above 873 K, suggesting a cubic structure. Figure 3 shows the variation of the octahedral tilt angle (φ), which is also the primary order parameter of the system. The refined exponent 0.47(2), within the uncertainty, has been found very close to the mean field or Landau theory prediction of 0.5 for a second order phase transition. Furthermore, well below the phase transition temperature, the spontaneous lattice strain, η , associated with the rhombohedral phase, is proportional to φ^2 and becomes zero at a finite value of tilt angle. The details of this work have been published in references [10, 11].

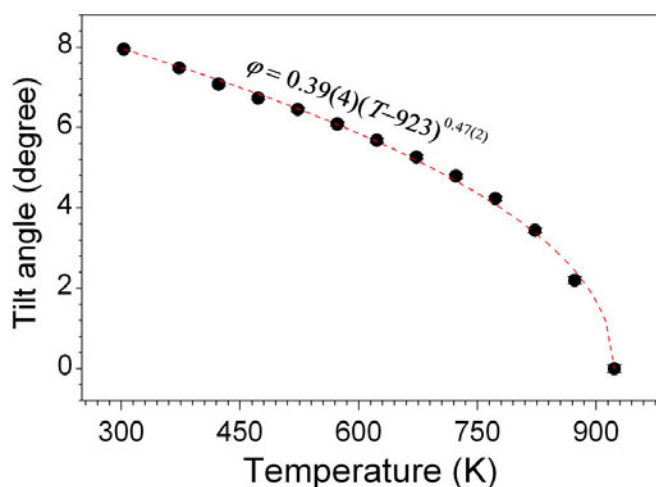


Figure 5.19.: Temperature dependence of the octahedral tilt angle of NLT. The continuous curve represents the fit to the data points as per the equation mentioned in the graph.

- [1] Mitchell, R. H., Chakhmouradian, A. R., Woodward, P. M. *Chem. Minerals*, 583.
- [2] Sun, P., Hsuan, T., Nakamura, Y., Shan, J., Inaguma, Y., Itoh, M. *Ferroelectrics*, (1997).
- [3] Müller, K. A., Burkard, H. *Phys. Rev.*, B19, (1979), 3593.
- [4] Brous, J., Fankuchen, I., Banks, E. *Acta Crystallogr.*, 6, (1953), 67.
- [5] Agranovskaya, A. I. *Izv. Akad. Nauk. SSSR Ser. Fiz.*, 24, (1960), 1275.
- [6] Miao, J. P., Li, L. P., Liu, H. J., Xu, D. P., Lu, Z., Song, Y. B., Su, W. H., Zheng, Y. G. *Mater. Lett.*, 42, (2000), 1.
- [7] Mitchell, R. H., Chakhmouradian, R. *J. Sol. State Chem.*, 138, (1998), 307.
- [8] Knapp, M. C., Woodward, P. M. *J. Sol. State Chem.*, 179, (2006), 1076.
- [9] Li, Y., Qin, S., Seifert, F. *J. Sol. State Chem.*, 180, (2007), 824.
- [10] Ranjan, R., Senyshyn, A., Boysen, H., Baehtz, C., Frey, F. *J. Sol. State Chem.*, 180, (2007), 995.
- [11] Garg, R., Senyshyn, A., Boysen, H., Ranjan, R. *J. Phys.: Condens. Matter*, 20, (2008), 505215.

5.7. Coincident Doppler broadening measurement on thin tin layers

Ph. Pikart¹, Ch. Hugenschmidt^{1,2}, K. Schreckenbach^{1,2}

¹Physik-Department E21, TU München

²ZWE FRM II, TU München

Positron annihilation spectroscopy has proved its very high sensitivity to thin tin layers embedded in an aluminium specimen [1]. This high sensitivity is explained by the various trapping effects which cause thermally diffusing positrons to be trapped near the tin-layer (see Fig. 5.20). The Sn-clusters are expected to be the main attractive trap for positrons due to the high positron affinity of tin (-7.6 eV) compared to aluminium (-4.4 eV). In this project the trapping process is further studied by measuring different material combinations and implantation energies. To date, the existing results could be confirmed with differently grown samples and measurements at various positron energies, corresponding to different mean implantation depths (see Fig. 5.22).

Sample preparation

The new layered samples consist of a 5.5 μm thick aluminium substrate, a single 0.1 nm tin layer and a top covering layer of 200 nm aluminium. Aluminium and tin are thermally evaporated out of high-purity materials on a glass carrier. The thickness of the substrate is chosen such that even positrons of highest energy (30 keV) do not penetrate into the glass carrier, and the thickness of the covering layer is chosen such that medium energy (6

keV) positrons are mainly implanted at its lower border. Since the intermediate tin layer is less than one atomic monolayer, single tin atoms are dispersed or form “nanoclusters” (see Fig. 5.20).

Depth profiles

The Doppler Broadening (DB) technique allows quick measurements of the S-parameter, which characterises the Doppler-broadened shape of the annihilation line. It depends on the following features: First the material, second the amount of positrons diffusing back to the surface and third the type and amount of defects in the region of the positron implantation profile. The slope of the S-parameter (see Fig. 5.21) at low energies is explained by positrons diffusing back to the surface and the much higher S-parameter of the layered system compared to the reference materials is explained by defects caused by the thermal evaporation process.

CDB measurements

The S-parameter in Fig. 5.21 is steadily increasing in the layered sample, although the implanted tin-atoms should attribute to high-momentum Doppler shifts, which would decrease this value. Hence no tin is visible at simple S-parameter measurements. The Coincident Doppler Broadening technique allows to analyze not only the width of the Doppler broadening, but also the shape of the broadened photo-peak. By this way each element has its characteristic line shape, and if normalized to a reference spectrum of the substrate (see Fig. 5.22), the elemental signatures can be clearly seen. The tin signature decreases with higher positron energy because the mean positron implantation depth is shifted below the tin-layer.

Positron trapping in nanoclusters

The aluminium-tin layered system has proven its high suitability for fundamental studies of the positron trapping at nanoclusters. Within this project, we plan to perform measurements to analyze different material combinations, to distinguish between effects caused by positron affinity and defect trapping.

[1] C. Hugenschmidt, P. Pikart, M. Stadlbauer, and K. Schreckenbach, *Phys. Rev. B*, **77**, 092105 (2008).

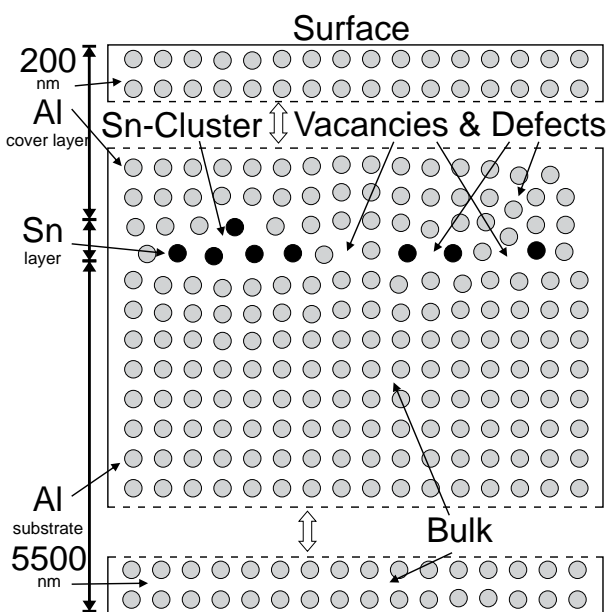


Figure 5.20.: Structure of the layered sample: After implantation, positrons diffuse thermally until annihilation with an electron in the bulk area, or until trapping at a defect site (vacancy, lattice defect or Sn-cluster).

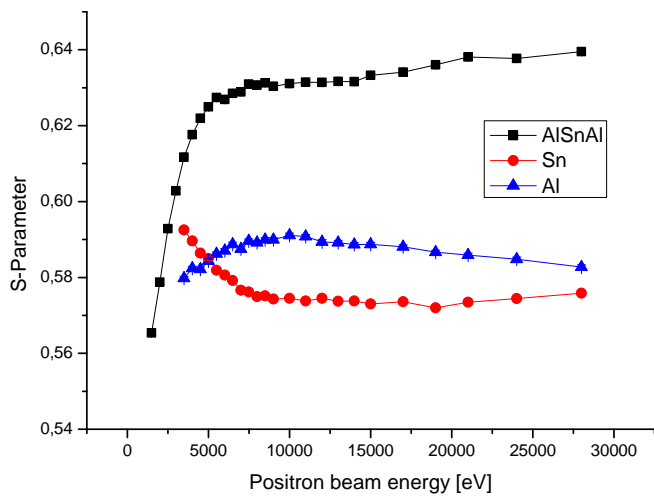


Figure 5.21.: Depth profile of the layered sample and reference materials.

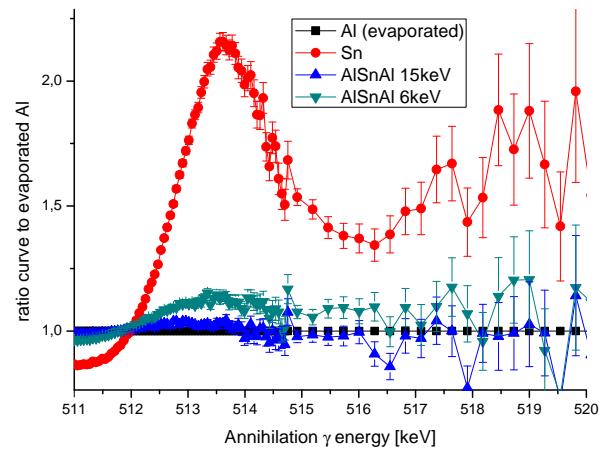


Figure 5.22.: Coincident Doppler Measurement (CDB) of the layered sample and reference materials.

Part III.

Facts and figures

6. Events

6.1. 2nd VDI expert meeting - Modern failure analysis with neutron radiation

R. Gilles¹

¹ZWE FRM II, TU München

On the invitation of the Verein Deutscher Ingenieure (VDI)-Gesellschaft Werkstofftechnik a meeting was held in Garching on April, 10th, 2008. This event was organized by the Forschungs-Neutronenquelle Heinz Maier-Leibnitz (FRM II) and Thomas Ullmann from Deutsches Zentrum für Luft- und Raumfahrt (DLR). The idea of this meeting was to present the advantages and possibilities of non-destructive test procedures as 3D-computer tomography, radiography, ultrasound or lockin thermography on examples of industrial and scientific relevance. The main focus was on how neutrons can support such activities.

After a general introduction of Prof. Winfried Petry which showed the various number of applications where neutrons as a probe solve industrial requests, industrial partners presented their recent results. For example Armin Hofmann (Volkswagen AG) gave an overview of the application of neutrons in the automotive engineering to certify components after the development and made an outlook about the visions of Volkswagen to automate the non-destructive controlling. Dr. Rodolfo S. Aoki (DLR Stuttgart) focused his talk on carbon fibers for aeroplanes using the tomography method to study defects whereas the presentation of Dr. Stephan Schmidt (EADS-Astrium Space Transportation) included results of ceramic fiber composites measured with neutron and x-ray radiation. Dr. John Bouchard (British Energy) built a bridge to the combination of FE-simulation and neutron/x-ray measurements which is an important issue for stress measurements.

In the afternoon a panel discussion under the direction of the VDI advisory committee speaker Prof. Heinz Voggenreiter (DLR) was performed to get on one side a

feedback from the audience and on the other side allowing the speakers to comment the presentations with regard to new ideas for common projects. This motivation led to excited discussions of many people from the audience during and after the poster session. At the end of the meeting for many participants the guided tour through the FRM II facility was the highlight. It enabled them to visit the instruments and to catch a glimpse into the heart of the facility, the reactor pool.

A continuation of the VDI expert meeting with a new specific topic is planned in 2010. Further information on the talks are available under <http://www.frm2.tum.de/veranstaltungen/vdi-expertenforum-08/index.html>



Figure 6.1.: Lively discussions in the coffee break about how to start new common projects.

6.2. Neutron scattering at the FRM II as a part of the "Fortgeschrittenenpraktikum"

R. Georgii¹, S. Busch¹, H. Frielinghaus², O. Holderer², M. Hölzel¹, P. Link¹, M. Hoffman¹, M. Meven¹, R. Mole¹, B. Pedersen¹, C. Smuda¹, G. J. Schneider², A. Schneidewind³, K. Schreckenbach⁴, T. Unruh¹

¹ZWE FRM II, TU München

²Institut für Festkörperforschung, Forschungszentrum Jülich, Jülich Centre f. Neutron Science at FRM II, Garching

³Institut für Festkörperphysik, Technische Universität Dresden, c/o FRM II

⁴Physik-Department E21, TU München

In summer and winter 2008 the practical training in neutron scattering for undergraduate students of the Technische Universität München was continued at the FRM II. The practical forms part of the "Fortgeschrittenenpraktikum" offered by the Physik Department. A total of 60 students in the fifth and sixth semester of physics were participating in it. After half a day of introduction to the neutron source FRM II and the theory of neutron scattering, each student performed two different experiments out of 11 participating instruments (HEIDI, JNSE, KWS-2, MIRA, PANDA, PUMA, RESI, SPHERES, SPODI, Stress-Spec and TOFTOF). The experiments were adopted from standard user experiments typical for the physics investigated at these instruments. The experiments lasted a day each including overnight measurements. During their stay the students had the possibility of a guided tour through the reactor. To complete the practical the students had to write a short report detailing the experimental results and present this in a short colloquium.

The response of the students to a short questionnaire was very enthusiastic. The main highlight for them was the possibility to work on "real" user experiments in normal operation contrary to standard demonstration experiments.



Figure 6.2.: Robert Georgii during the introductory talk.



Figure 6.3.: Students at PANDA with Peter Link.

6.3. NEUWAVE: International workshop on energy selective neutron imaging

B. Schillinger¹

¹ZWE FRM II, TU München

For the first time, from April 20 to 24 a meeting was held outside the “normal” sequence of conferences in neutron imaging for a dedicated topic gaining such high interest and participation. During 3 ½ days, about 40 leading experts from 9 countries all over the world exchanged at NEUWAVE (NEUtron WAVElength-dependent Imaging) their knowledge about two promising topics: Energy-dependent Imaging with cold neutrons and the progress in fast neutron imaging. A new format was successfully applied for the first time, with the number of talks very limited but with plenty of time for vivid discussion.

The FRM II was chosen as conference site due to its expertise in both fields with its facilities ANTARES (cold neutron imaging) and NECTAR (fast neutron imaging). This activity was supported by the European network NMI3 (Integrated Infrastructure Initiative for Neutron Scattering and Muon Spectroscopy).

First studies of local textures in high resolution

During this meeting it became obvious that the new approach to do transmission imaging measurements with narrow energy bands of the applied neutron spectrum will enable a new field of material research and material characterization with cold neutrons. The number of facilities presently available for such kind of studies is very limited (about five worldwide). Consequently the presented results just give a first glance on future perspectives of the method.

It was demonstrated that the scattering behavior of most metallic materials for cold neutrons is characterized by the Bragg edges in the cross-section data due to diffractions at the lattices of the micro-crystallites. Depending on the neutron wavelength and the material properties, either the structural parameter of the material can be derived from transmission data, or local textures can be visualized in high spatial resolution. First impressive results of such imaging studies were presented.

These findings have direct impact on the decisions to go ahead to install also beam lines for neutron imaging at the upcoming new spallation neutron sources (ISIS-



Figure 6.4.: About 40 experts in neutron imaging gathered in April 2008 at FRM II for a first meeting.

TS2, SNS, J-PARC, ESS-S). The pulse structure at these strong neutron sources is extremely promising for energy selective imaging, using the Time Of Flight (TOF) technique with high performance in respect to energy resolution and pulse intensity. The intense pulses can also be used for stroboscopic imaging of fast processes.

New setup for fuel cell research

Beside these very important considerations about the future imaging capabilities at pulsed spallation sources, interesting new results in neutron imaging were presented. This was in particular about imaging with polarized neutrons for magnetic field and structure determination, phase contrast imaging, new set-up for fuel cell research and options for high resolution neutron imaging detectors. It became also clear that imaging and scattering methods will be more and more integrated and combined in future experiments.

The meeting was concluded with the explicit aim of the participants to continue the approaches and discussion in a follow-up event (NEUWAVE 2) to be held at one of the four sites of the pulsed spallation sources.

6.4. 12th JCNS laboratory course neutron scattering

T. Gutberlet¹

¹Forschungszentrum Jülich, Institut für Festkörperphysik, Jülich Centre for Neutron Science

The 12th Laboratory Course on Neutron Scattering was held by the Jülich Centre for Neutron Science September 1-12. The lectures took place at Forschungszentrum Jülich and the experiments were carried out at the FRM II. 50 young students and scientists from a variety of disciplines such as physics, chemistry etc. from all around the world took the chance to learn theory and hands-on neutron scattering on selected instruments at FRM II. The course was supported by the Integrated Infrastructure Initiative for Neutron Scattering and Muon Spectroscopy (NMI3) and SoftComp, the European Network of Excellence for Soft Matter Composites.

The lectures gave a comprehensive introduction to neutron sources, into scattering theory and instrumentation. Furthermore, selected topics of condensed matter research were presented. At FRM II the students performed experiments at the backscattering instrument SPHERES, the neutron reflectometer TREFF, the Jülich neutron spin-echo spectrometer J-NSE, small angle scattering at KWS-2, single crystal and powder diffraction at HEIDI and SPODI, polarisation analysis at DNS, zero field spin echo spectroscopy at RESEDA, three-axis spectroscopy at PUMA and time-of-flight spectroscopy at TOFTOF.

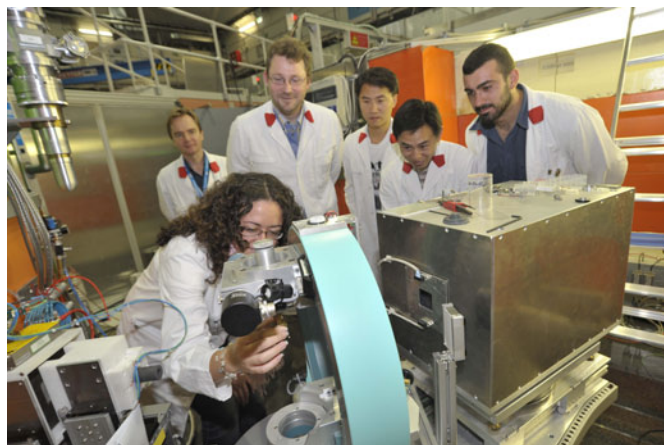


Figure 6.5.: At the experimental part of the laboratory, students can work on the instruments of FRM II, like on the single crystal diffractometer HeiDi of Martin Meven (third from left).

The response was overwhelmingly positive. The splitting of the locations was surprisingly not seen as a burden although it implied a daylong bus trip from Jülich to Munich. Rather the students appreciated the possibility to get to know two major research centres in Germany. The next Laboratory Course will be held again at Jülich and Garching on September 7-18, 2009.

6.5. 8th German neutron scattering conference

J. Neuhaus¹

¹ZWE FRM II, TU München

The 8th German Neutron Scattering Conference was held on 15-17 September 2008, organised by FRM II. It was a joint event of the German and Austrian Committees for Research with Neutrons, gathering 261 participants. Plenary talks and two parallel sessions dealing with the broad range of topics inherent to neutron scattering made up the programme, including 2 poster sessions on Monday and Tuesday, presenting 251 contributions. Special mini-symposia had been organised to highlight current topics in solid-state physics: “Function from Frustration in Modern Multiferroics”, “Dynamics, Kinetics, Complex Materials in the Light of SANS and Reflectometry” and “Materials Science” with the focus on applied science.

Obviously, the event’s interest focused strongly on

the development of new methods and instruments using neutrons. A special session was dedicated to the new spallation sources SNS, ISIS’s second target station and the developments related to the eagerly anticipated European Spallation Source. Topical sessions covered magnetism, soft matter, materials and dynamics.

All participants enjoyed the dinner in the Hofbräukeller, and Richard Wagner, director of the ILL, provided a memorable speech about the world of soccer quoting sentences from prominent players. At the conference dinner, Götz Eckold, Universität Göttingen, the new head of the Committee for Research with Neutrons, thanked Helmut Schober, ILL, for his excellent work and engagement during the past three years.



Figure 6.6.: Lively discussion during the conference dinner at Hofbräukeller München.

6.6. Neutrons for crystallographers

M. Meven¹

¹ZWE FRM II, TU München

The working group Neutron Scattering (AK7) of the German Society for Crystallography (Deutsche Gesellschaft für Kristallographie, DGK) held the workshop Neutrons for Crystallographers following the 8th German Neutron Scattering Conference at Garching at Technische Universität München from 17th to 18th September 2008. The workshop was aimed at students and scientists of the different disciplines in natural and materials sciences.



Figure 6.7.: The lectures in the physics department were well attended.

A general introduction to the use of neutrons was given, followed by the application of neutrons for the research in different scientific topics. On the first day, the analysis of atomic and magnetic structures using neutron diffraction was explained. During four lectures, two on powder methods and two on single crystal diffraction, subdivided into structure determination and magnetism (R. Gilles, A. Schneidewind, M. Meven, M. Braden). On the second day four lectures were held on phonons and magnons, diffuse scattering, material science and soft matter (M. Braden, F. Frey, W. Brokmeier, V. Haramus). Details were given about the instruments for the different applications during a guided tour through the neutron source Heinz Maier-Leibnitz after the lectures.

The workshop was very well attended. Beside the numerous participants from all over Germany attendees of the neutron scattering conference joined the workshop. Thus, more than 50 participants filled the lecture hall. With the support of FRM II and DGK this workshop could be realised without any participation fee.

6.7. Workshop on biomolecular dynamics and protein-water interactions

T. Gutberlet¹

¹Forschungszentrum Jülich, Institut für Festkörperphysik, Jülich Centre for Neutron Science

More than 60 scientists from Europe, USA, Australia and Japan attended the international workshop on Biomolecular Dynamics and Protein-Water Interactions on September 24-26, 2008 in the beautiful surrounding of the InWent Education Center close to Lake Starnberg south of Munich. The workshop was jointly organized by Wolfgang Doster of Physics Department of Technische Universität München and Thomas Gutberlet of Jülich Centre for Neutron Science. Forschungs-Neutronenquelle Heinz Maier-Leibnitz (FRM II) and Forschungszentrum Jülich GmbH gave generous financial support.

The focus of the workshop was the discussion of the mechanism of the protein dynamical transition, protein hydration and protein dynamics studied by neutron scattering and other methods. The highlights of the workshop were the intense discussion between the participants and an evening poster session. Most participants

appreciated the open and informal way to discuss current competing dynamic models and experimental approaches to study protein dynamics.

Demand for more sophisticated neutron experiments

A clear demand for more sophisticated neutron experiments to study dynamical phenomena in proteins and biological systems was expressed. Regarding the use of neutron spectroscopy in the field of water dynamics the participants were very delighted with recent developments to use of new instruments such as the time-of-flight spectrometer TOFTOF or the backscattering instrument SPHERES. Combining these techniques with dedicated simulation efforts and complementary NMR studies to gain more insight into protein and water dynamics is clearly going to be a strong topic for the future.

7. Facts

7.1. The FRM II goes public

A. Voit¹, U. Kurz¹, B. Tonin-Schebesta¹

¹ZWE FRM II, TU München

The year 2008 at FRM II reflected in the media offered some news on research at the neutron source. Besides, a few politicians of different parties visited the site.

The year started with good news: The FRM II scientific director, Prof. Dr. Winfried Petry, was awarded with the “Bundesverdienstkreuz” for his extraordinary efforts in science and teaching. The former Bavarian Minister for Science, Dr. Thomas Goppel (CSU), granted Winfried Petry the Federal Cross of Merit and praised him as internationally important scientist (see p. 4).

Visit of the Bavarian Minister for Environment

One month later, on March 18th, the Bavarian Minister for Environment, Dr. Otmar Bernhard (CSU), visited FRM II. The Chancellor of Technische Universität München, Albert Berger, as well as the three directors of FRM II, Dr. Klaus Seebach, Dr. Ingo Neuhaus and Prof. Dr. Winfried Petry, showed him around the experimental and neutron hall as well as the reactor pool. Otmar Bernhard is the head of the Bavarian authority concerned with radiation protection of FRM II and was interested in the nuclear operation of the research reactor. In his function as Minister for Health and Environment Dr. Bernhard showed interest in the actual environmental and medical research projects.

Industrial cooperation

That both industrial development as well as politics play an important role at FRM II, proved the next event. The Bavarian Ministerpräsident Günther Beckstein (CSU) was present on May 8th, when the itm AG signed a contract with Draximage, a Canadian manufacturer of radiopharmaceuticals. The company itm “Isotopen Technologien München” is located on the area of FRM II, producing radioactive isotopes in the reactor, which are used for medical treatment. With the collaboration, which was signed in the presence of the Premier of the Canadian Province Québec Jean Charest, itm AG and Draximage agreed on the supply of isotopes to Canada and North America and the distribution of products in Europe (see p. 5).



Figure 7.1.: The Bavarian Minister for Health and Environment, Dr. Otmar Bernhard (CSU, right), throws a glance into the reactor pool listening to the explanations of Dr. Ingo Neuhaus.

City council and Members of the Bundestag

Not only international business and politicians are often-received guests. On July 14th, the community council of Garching visited the neutron source. Members of the directory of FRM II showed the local politicians around: Obligatory was the visit in the neutron and experimental halls and a glance into the reactor pool. Mayor Hannelore Gabor (SPD) and her colleagues were very interested (see p. 5).

Another important group of politicians visited the Neutron source Heinz Maier-Leibnitz on September 5th. The CDU/CSU Members of Parliament belonging of the committee on education were welcomed. It was a great pleasure for the Scientific Director Prof. Dr. Winfried Petry and the entire directorate to present to them the development of the neutron source since its commissioning in 2004, to point out the strong interest of the international user community, and to show the further potential for scientific and industrial use. The visitors were very impressed with the broad range of the scientific application of neutrons and promised to further support the facility (see p. 5). Among the members of the commit-

tee was the actual German Minister for Agriculture, Ilse Aigner (CSU).

Discussion about medium enriched uranium

One of the more surprising visits took place on September 9th. Despite his full calendar the German Minister for Environment, Sigmar Gabriel (SPD) took the time for a tour through FRM II and a discussion about the progress in the development of medium enriched uranium fuel for the reactor. In the end, Sigmar Gabriel even discussed with students, who work at different projects at FRM II. The Minister assured, that he highly appreciates the neutron source and that the prolongation of the operating licence for the reactor is beyond all question. Initiator of the visit was the university pastor Dr. Hermann Probst. The press echo was unsurprisingly high.

Almost 500 visitors at the open day

Since the beginning of October, FRM II has its own press officer. Andrea Voit will enhance the media relations and communicate scientific results to the press — in close collaboration with the TUM Corporate Communications Center.

The biggest event every year at FRM II is the open day. In 2008, it took place on October 19th from 11 to 19h. With totally 488 visitors the FRM II staff members had a long day, as the tours lasted from 10h to 20h. The visitors had a look inside the reactor, the experimental hall and the neutron guide hall. In 32 groups of 15 people and in 15 minutes cycles they got to know more about the research at the neutron source. During their 45 minutes visit, visitors could also take a look into the reactor pool. The interest in visiting the reactor was so huge, that three hours after the start of registration the groups were



Figure 7.2.: The German Minister for Environment Sigmar Gabriel (SPD, left) on his tour through the experimental hall with the FRM II Scientific Director Prof. Dr. Winfried Petry.

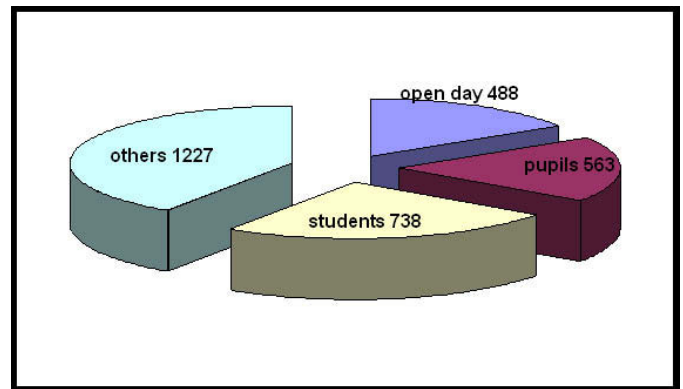


Figure 7.3.: In total, 3016 visitors were guided through the FRM II in 2008.

fully booked. Many spectators visited the presentations on research and industrial development of Prof. Dr. Klaus Schreckenbach, the former operational director, the scientific director Prof. Dr. Winfried Petry and the deputy director, Dr. Jürgen Neuhaus.

Focus on the young visitors

Many people still take the opportunity to have a look inside the FRM II throughout the year. In total 2528 visitors were guided through the neutron source (see fig. 7.3). Including the open doors' day, there were 3016 visitors in 2008. Focus of the guided tours are and will be the young generation: 708 of the total visitors throughout the year were students and 563 were pupils. This equals 50 percent of the total visitors. More than 30 visiting groups out of totally 196 groups came from abroad, for example from the USA, China or Singapore. The most frequented month for the visitors service and the tour guides from FRM II was September with 308 visitors.

To attract even more young visitors, a poster has been designed to inform students about the possibility of a guided tour through the FRM II (7.4).

TUM

**Einladung
an Studenten zur
Exkursion an die
Forschungsneutronenquelle
Heinz Maier-Leibnitz (FRM II)**

Technische Universität München,
Lichtenbergstraße 1, 85747 Garching

Terminabsprache bitte über
Besucherdienst@fm2.tum.de
oder unter Tel. 089 289 12147






Figure 7.4.: A poster invites students to go on a guided tour through the FRM II.

**Schwerelose
Metallschmelze**
Experimente am FRM II
ersetzen Weltraumversuche

Strahlende Hilfe aus Garching
NUKLEARMEDIZIN Der Forschungsreaktor FRM II soll dem Notstand bei der Radioaktivitätsmessung helfen

FORSCHUNGS-REAKTOR



Radioaktive Nuklide zur Krebsdiagnose 30.10.08
Technische Universität lässt prüfen, ob im Garching-Reaktor das seltene „Molybdän 99“ hergestellt werden darf

Verdienstkreuz für Winfried Petry

GÄRCHING
Geld für Neutronen

Gabriel attackiert TU
Minister sieht „Vertragsbruch“ bei Garching-Reaktor

**Goppel verteidigt
Forschungsreaktor**

Figure 7.5.: Headlines in the media reporting about FRM II in the year 2008.

7.2. User office: Organizing the increasing number of scientists

T. Gutberlet¹, I. Lommatzsch², U. Kurz², B. Tonin-Schebesta²

¹JCNS, Forschungszentrum Jülich GmbH

²ZWE FRM II, TU München

In 2008 the FRM II faced an increasing number of user visits and requests for beam time. For the two proposal rounds in January and July the User Office received a total of 393 proposals asking for 3164 beam days at the instruments of the FRM II. For that, the 18 operating instruments delivered 3818 beam days to external and internal scientific users. On average, the total overload factor of the instruments was 1.8. During the year 733 experiments were performed. The visitors' service took care of 619 registered user visits not taking in account all the permanent users located at TUM, LMU and other participating institutions and universities.

Mounting number of proposals

These figures illustrate the mounting interest of the community of neutron scatterers in the FRM II. Not only German scientists accept it as one of the most powerful neutron sources, but also those from Europe and abroad. Since the start of user operation the number of proposals have grown continuously (cf. Fig. 7.6). There are also included the proposals submitted to the instruments of the Jülich Centre of Neutron Science (JCNS) operating for users at FRM II since 2007.

The distribution of proposals and requested beam days according to scientific areas is given in Fig. 7.7 and Fig. 7.8 for the second proposal round in 2008. The number of proposals as well as the distributed beam time show a quite equal scientific interest between classical areas in condensed matter physics, soft matter

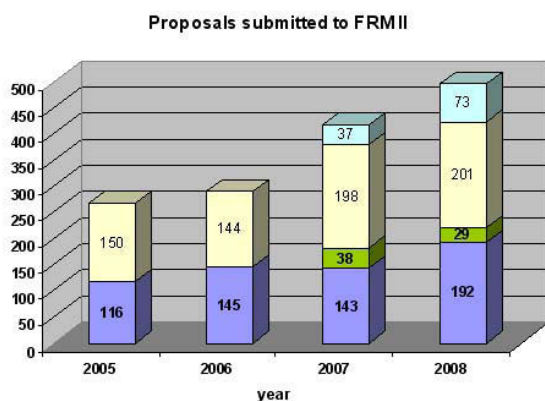


Figure 7.6.: Submitted proposals to FRM II including proposals submitted to JCNS. Blue and yellow represent the proposals submitted in the two FRM II proposal rounds, the two proposal rounds of JCNS are coloured green and light blue.

Requested beam days (round 8)

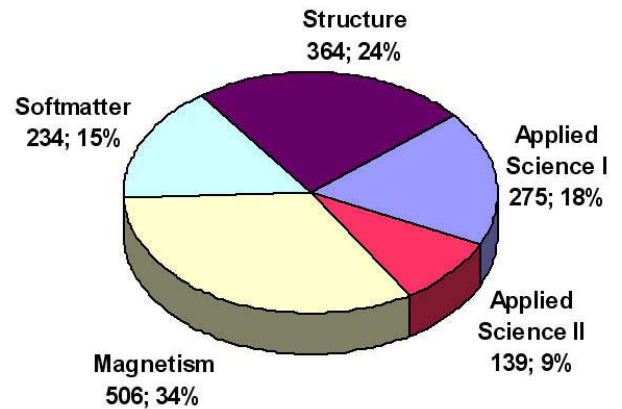


Figure 7.7.: Distribution of beam time requested in the second proposal round.

Received proposals (round 8)

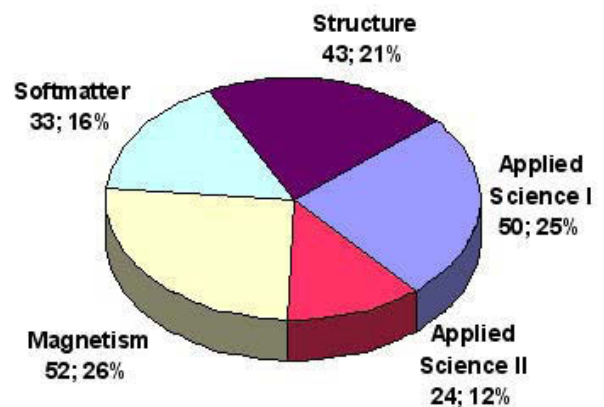


Figure 7.8.: Proposals submitted in the second proposal round 2008 according to scientific areas.

including biology and applied sciences. Fundamental physics and imaging are located in the areas Applied Science I and II.

Nearly half of the external proposals submitted to FRM II are from Germany (cf. Fig. 7.9). This number has decreased slightly in the latest proposal rounds reflecting the increasing interest of external users in the instruments at FRM II. About 40 % of the external pro-

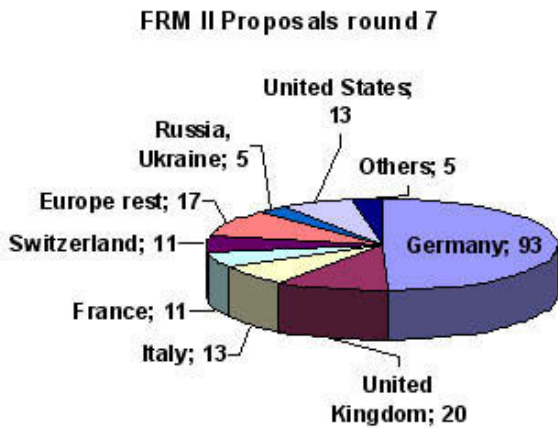


Figure 7.9.: Geographical distribution of the proposals in the first proposal round 2008.

posals come from Europe and the rest from the US and other countries abroad.

Combined user office

To enable the FRM II User Office to handle the increasing number of beam time requests and user visits the user offices of FRM II and JCNS have unified their administrative activities in a common group led by Dr. Thomas Gutberlet of JCNS and assisted by Dr. Ina Lommatzsch of FRM II. The combined activities of both user offices

have improved the administrative procedures for users at FRM II. This alteration now simplifies for example the organization of user visits and the travel reimbursement.

After four successful years of action the Integrated Infrastructure Initiative for Neutron Scattering and Muon Spectroscopy NMI3 of the EU Sixth Framework Programme (FP 6) ended in June 2008. Hundreds of European users had benefited in this period from financial support for their travel and stay for experiments at FRM II. This very successful program will be continued by the next NMI3 Access Program within FP7 starting February 1st, 2009.

Good news: FRM II News

In the end of 2008 the User Office in close collaboration with the FRM II Public Relation Office launched the first FRM II Newsletter. It communicates not only latest information on new developments at the facility and the instruments at FRM II to all users but contains also general topics of interest. The newsletter is accessible via internet at <http://www.frm2.tum.de/informationen/einzelnews/article/frm-ii-newsletter-erschienen>

Most updated information for users like calls for proposal or other events are found at <https://user.frm2.tum.de>

The User Office not only is a central access point for the users at FRM II but it also actively supports their mobility and health by offering bicycles for rent. This service has become very popular in no time and will be enlarged soon due to the increasing demand.

7.3. Publications

- [1] **Abul Kashem M. M. A., Perlich J., Diethert A., Wang W., Memesa M., Gutmann J. S., Majkova E., Capek I., Roth S. V., Petry W., Müller-Buschbaum P.**
Array of magnetic nanoparticles via particle co-operated self-assembly in block copolmer thin films.
Macromolecules, submitted.
- [2] **Arruebarrena G., Hurtado I., Garbe U., Bamberger M.**
Texture development in magnesium HPDC alloys.
Scripta Materialia, to be submitted.
- [3] **Auriemma F., de Rosa C., Ricciardi R., Lo Celso F., Triolo R., Pipich V.**
Time-resolving analysis of cryotropic gelation of water/poly(vinyl alcohol) solutions via small angle neutron scattering.
J. Phys. Chem. B, **112**, (2008), 816.
- [4] **Aynajian P., Keller T., Boeri L., Shapiro S. M., Habicht K., Keimer B.**
Energy gaps and Kohn anomalies in elemental superconductors.
Science, **319**, (2008), 1509–1512.
- [5] **Baessler S., Ayala Guardia F., Borg M., Glück F., Heil W., Konrad G., Konorov I., Munoz Horta R., Petzoldt G., Rich D., Simson M., Sobolov Y., Wirth H.-F., Zimmer O.**
First measurements with the neutron decay spectrometer aSPECT.
European Physical Journal A, **38**, (2008), 17.
- [6] **Balaskó M., Horváth L., Horváth A., Tóth P., Kammel L., Schillinger B.**
Study of the special properties of supercritical water by dynamic cooled neutron radiography.
6th International Topical Meeting on Neutron Radiography, Sept. 2008, Kobe, Japan. Nuclear Instruments and Methods, in press.
- [7] **Bauer B., Pedersen B., Gille P.**
Al₄(CR, FR): single crystal growth by the Czochralski method and structural investigation with neutrons at FRM II.
Z. Kristallogr., **224**, (2009), 109–111.
- [8] **Bouwman W. G., Plomp J., de Haan V. O., Kraan W. H., van Well A. A., Habicht K., Keller T., Rekveldt M. T.**
Real-space scattering methods.
Nuclear Instruments and Methods A, **586**, (2008), 9–14.
- [9] **Breitkreutz H., Wagner F. M., Röhrmoser A., Petry W.**
Spectral fluence rate of the fast reactor neutron beam MEDAPP at FRM II.
Nuclear Instruments and Methods in Physics Research A, **593**, (2008), 466 – 471.
- [10] **Brodeck M., Alvarez F., Arbe A., Juranyi F., Unruh T., Holderer O., Colmenero J., Richter D.**
Study of the dynamics of poly(ethylene oxide) by combining molecular dynamic simulations and neutron scattering experiments.
J. Chem. Phys., **130**, (2009), 094908.
- [11] **Böni P.**
New concepts for neutron instrumentation.
Nuclear Instruments and Methods A, **586**, (2008), 1–8.
- [12] **Böning K., Petry W.**
Test irradiations of full sized U₃Si₂ – Al fuel plates up to very high fission densities.
Journal of Nuclear Materials, **383**, (2009), 254–263.
- [13] **Bücherl T., Wagner F. M., Lierse von Gostomski C.**
First steps towards real-time radiography at the NECTAR facility.
Nuclear Instruments and Methods in Physics Research, in press, **A**.

- [14] **Canella L., Kudejova P., Schulze R., Warr N., Türler A., Jolie J., Revay Z., Belgya.**
First experiments at the new PGAA facility at the research reactor FRM II.
Proceedings of the 7th International Conference on Nuclear and Radiochemistry, 25 - 29 August 2008, Budapest, -, (2008), -.
- [15] **Chang J., Christensen N. B., Niedermayer C., Lefmann K., Ronnow H. M., McMorrow D. F., Schneidewind A., Link P., Hiess A., Boehm M., Mottl R., Pailh s S., Momono N., Oda M., Ido M., Mesot J.**
Inelastic neutron-scattering measurement of a magnetic excitation gap in the high-temperature $La_{1.855}Sr_{0.145}CuO_4$ superconductor: evidence for a field-induced quantum phase transition.
Phys. Rev. Lett., accepted.
- [16] **Chatterji T., Schneider G. J., van Eijck L., Frick B., Bhattacharya D.**
Direct evidence for the Nd magnetic ordering in $NdMnO_3$ from the hyperfine field splitting of Nd nuclear levels.
J. Phys. Condens. Matter, **21**, (2009), 126003.
- [17] **Chatterji T., Schneider G. J., Galera R. M.**
Low-energy nuclear spin excitations in $NdMg_3$ and $NdCo_2$.
Phys. Rev. B, **78**, (2008), 012411.
- [18] **Chi S., Schneidewind A., Zhao J., Harriger L. W., Li L., Luo Y., Cao G., Xu Z., Loewenhaupt M., Dai P.**
Inelastic neutron scattering measurements of a three-dimensional spin resonance in the FeAs-based $BaFe_{1.9}Ni_{0.1}As_2$ superconductor.
Phys. Rev. Lett., **102**, (2009), 107006.
- [19] **Davies C. M., Wimpory R. C., Dye D., Nikbin K. M.**
The effects of plate dimensions on residual stresses in welded thin steel plates.
Proceedings of the 2008 ASME Pressure Vessels and Piping Conference, PVP2008, July 27-31, 2008, Chicago, Illinois, USA, -, (2008), 11.
- [20] **Deveaux M., Amar-Youcef S., B denbender A. , D ring D., M ntz C., Wagner F. M., Stroth J.**
Random telegraph signal in monolithic active pixel sensors for charged particle tracking.
Proceeding of "IEEE 2008 Nuclear Science Symposium, Medical Imaging Conference and 16th Room Temperature Semiconductor Detector Workshop", October 19 - 25, 2008, Dresden, Germany, -, (2008), -.
- [21] **Druker A., Sobero C., Brokmeier H. G., Malarr a J., Bomaro R.**
Texture evolution during thermomechanical treatments in Fe-Mn-Si shape memory alloys.
Materials Science and Engineering A, **481-482**, (2008), 578-581.
- [22] **Eichh fer A., Wood P. T., Viswanath R. V., Mole R. A.**
Synthesis, structure and physical properties of the manganese (II) selenide/selenolate cluster complexes $[Mn_{32}Se_{14}(SePh)_{36}(PnPr_3)_4]$ and $[Na(benzene - 15 - crown - 5)(C_4H_8O)_2]_2[Mn_8Se(SePh)_{16}]$.
Chemical Communications, -, (2008), 1596 - 1598.
- [23] **Foster L. J. R., Schwahn D., Pipich V., Holden P. J., Richter D.**
SANS characterisation of polyhydroxyalkanoates and their bioPEGylated hybrids in solution.
Biomacromolecules, **9**, (2008), 315.
- [24] **Francis J. A., Turski M., Hurrell P. R., Watson C. T., Bate S. K., Warren A. P., Rebelo-Kornmeier J., Withers P. J.**
Residual stress measurements in autogenous steel welds.
Proceedings of the 2008 ASME Pressure Vessels and Piping Conference, PVP2008, July 27-31, 2008, Chicago, Illinois, USA, -, (2008), 7.
- [25] **Frei A., Gutmiedl E., Morkel C., M ller A. R., Paul S., Urban M., Schober H., Rols S., Unruh T.**
Inelastic neutron scattering on solid deuterium Part I: density of states.
Phys. Rev. B, submitted.
- [26] **Garg R., Senyshyn A., Boysen H., Ranjan R.**
Structure and phase transition of $Na_{0.5}La_{0.5}TiO_3$.
J. Phys. Condens. Matter, **20**, (2008), 505215.

- [27] **Garny S., Mares V., Roos H., M. W. F., Rühm W.**
Measurement of neutron spectra and neutron doses at the munich therapy beam with Bonner spheres.
to be submitted.
- [28] **Garny S., Rühm W., Wagner F. M., Paretzke H. G.**
Neutron therapy at the FRM II - calculation of dose inside a Voxel phantom.
Transactions: World congress of medical physics and biological engineering: September 7 -12, 2009, submitted.
- [29] **Gaspar A. M., Appavou M.-S., Busch S., Unruh T., Doster W.**
Dynamics of well-folded and natively disordered proteins in solution: A time of flight neutron scattering study.
Eur. Biophys. J.
<http://dx.doi.org/10.1007/s00249-008-0266-3>.
- [30] **Gebhard R., Haas-Gebhard B., Thomas C., Calzada E., Mühlbauer M., Schillinger B.**
Untersuchung einer frühmittelalterlichen Spathascheide mit Neutronentomographie.
Restaurierung und Archäologie, **1**, (2008), 89–98.
- [31] **Giblin S. R., Freeman P. G., Hradil K., Prabhakaran D., Boothroyd A. T.**
Spin orientation and glassy dynamics in $\text{La}_{1.55}\text{Sr}_{0.45}\text{NiO}_4$.
Phys. Rev., **B78**, (2008), 184423–1–9.
- [32] **Gibmeier J., Rebelo-Kornmeier J., Hofmann M.**
Neutron diffraction stress analysis of near surface stress gradients of surface treated steel samples.
Proceedings of the ICRS8: The Eighth International Conference on Residual Stresses August 6- 8, 2008, Marriott Tech Center, Denver, Colorado, USA, –, (2008), –.
- [33] **Gilles R., Hofmann M., Gao Y., Johnson F., Iorio L., Larsen M., Liang F., Hoelzel M., Barbier B.**
Probing the relationship of ordering in nanodomain FeCo alloys with ternary additions using neutron diffraction.
Metallurgical and Materials Transactions A, submitted.
- [34] **González Sánchez F., Jurányi F., Gimmi T., Loon L. V., Seydel T., Unruh T.**
Dynamics of supercooled water in highly compacted clays studied by neutron scattering.
J. Phys. Condens. Matter, submitted, –, (2008), –.
- [35] **González Sánchez F., Jurányi F., Gimmi T., Loon L. V., Unruh T., Diamond L. W.**
Translational diffusion of water and its dependence on temperature in charged and uncharged clays: a neutron scattering study.
J. Chem. Phys., submitted.
- [36] **Hameed F., Schillinger B., Rohatsch A., Zawishky M., Rauch H.**
Investigations of stone consolidants by neutron imaging.
6th International Topical Meeting on Neutron Radiography, Sept. 2008, Kobe, Japan. Nuclear Instruments and Methods, in press.
- [37] **Hervias J. R., Hofmann M., Rebelo Kornmeier J., Luzin V., Elices M.**
Residual Stresses in cold-drawn rods: effect of an alternative treatment.
Proceedings of the ICRS8: The Eighth International Conference on Residual Stresses August 6- 8, 2008, Marriott Tech Center, Denver, Colorado, USA.
- [38] **Hofmann M., Wimpory R. C.**
NET TG1: Residual stress analysis on a single bead weld on a steel plate using neutron diffraction at the new engineering instrument STRESS-SPEC.
International Journal of Pressure Vessels and Piping, **86**, (2009), 122–125.
- [39] **Holderer O., Monkenbusch M., Borchert G., Breunig C., Zeitelhack K.**
Layout and performance of the polarizing guide system for the J-NSE spectro at the FRM II.
Nuclear Instruments and Methods in Physics Research A, **568**, (2008), 90–94.
- [40] **Holderer O., Monkenbusch M., Schätzler R., Kleines H., Westerhausen W., Richter D.**
The JCNS neutron spin-echo spectro J-NSE at the FRM II.
Measurement Science and Technology, **19**, (2008), 034022 (6pp).

- [41] **Holland-Moritz D., Stüber S., Hartmann H., Unruh T., Hansen T., Meyer A.**
Structure and dynamics of liquid Ni₃₆Zr₆₄ studied by neutron scattering.
Phys. Rev. B, **79**, (2009), 064204.
- [42] **Huang E.-W.**
Study the high-cycle-fatigue behavior of a nano-precipitate strengthened alloy by in-situ neutron-diffraction experiments.
Proceedings: MRS Fall Meeting 2008 (Symposium EE: Nano- and Microscale Materials–Mechanical Properties and Behavior under Extreme Environments), –, (2008), –.
- [43] **Hugenschmidt C., Pikart P., Stadlbauer M., Schreckenbach K.**
High elemental selectivity to Sn submonolayers embedded in Al using positron annihilation spectroscopy.
Phys. Rev. B, **77**, (2008), 092105–1–4.
- [44] **Hutanu V., Meven M., Janoschek M., Böni P., Heger G.**
MuPAD test at the hot single-crystal diffractometer HEiDi at FRM II.
Nuclear Instruments and Methods A, submitted.
- [45] **Hutanu V., Meven M., Lelièvre-Berna E., Heger G.**
POLI-HeiDi: the new polarised neutron diffractometer at the hot source (SR9) at the FRM II - Project status.
Physica B, submitted.
- [46] **Hutanu V., Meven M., Sazonov A., Heger G.**
Development of compact magnetostatic cavities for ³He spin filter cells.
Measurement Science and Technology, **19**, (2008), 034010–15.
- [47] **Häußler W.**
Neutron spin echo studies on ferritin: free-particle diffusion and interacting solutions.
Eur Biophys. J., **37**, (2008), 563 – 571.
- [48] **Häußler W., Streibl D., Böni P.**
RESEDA: double and multi detector arms for neutron resonance spin echo spectrometers.
Measurement Science and Technology - Proceedings ECNS 2007, **19**, (2008), 034015.
- [49] **Ioffe A.**
A new neutron spin-echo technique with time gradient magnetic fields.
Nuclear Instruments and Methods A, **586**, (2008), 31–35.
- [50] **Ioffe A., Bodnarchuk V., Bussmann K., Müller R., Georgii R.**
A new neutron spin-echo spectrometer with time-gradient magnetic fields: First experimental test.
Nuclear Instruments and Methods in Physics Research A, **586**, (2008), 36–40.
- [51] **Jungwirth R., Petry W., Schmid W., Beck L., Bergmaier A.**
Progress in heavy-ion bombardment of U-Mo/Al dispersion fuel.
Transactions of the RRFM 2008, Hamburg, Germany, March 2008, –, (2008), 5.
- [52] **Komarek A. C., Streltsov S. V., Isobe M., Möller T., Hoelzel M., Senyshyn A., Trots D., Fernandez-Diaz M. T., Hansen T., Gotou H., Yagi T., Ueda Y., Anisimov V. I., Grüninger M., Khomskii D. I., Braden M.**
CaCrO₃: an anomalous antiferromagnetic metallic oxide.
Phys. Rev. Lett., **101**, (2008), 167203.
- [53] **Kreuzpaintner W., Moulin J.-F., Lott D., Kampmann R., Haese-Seiller M., Störmer M., Schreyer A.**
Time of flight grazing incidence small angle neutron scattering on Gd nanowires.
European Physical Journal, Special Topics, **167**, (2009), 73–79.
- [54] **Kudejova P., Canella L., Schulze R., Jolie J., Warr N., Türler A.**
The new PGAA installation at the FRM II.
Proceedings of the 13th International Symposium on Capture Gamma-Ray Spectroscopy and Related Topics (CGS 13), AIP Conference Proceedings 1090, p. 89, **1090**, (2008), 89.

- [55] **Kudejova P., Canella L., Schulze R., Warr N., Türler A., Jolie J.**
Characterization of the new PGAA and PGAI facility at the research reactor FRM II.
Proceedings: 7th International Conference on Nuclear Materials and Radiochemistry (NRC 7), Budapest 25 - 29 August 2008, -, (2008), -.
- [56] **Kudejova R., Meierhofer G., Zeitelhack K., Jolie J., Schulze R., Türler A., Materna T.**
The new PGAA and PGAI facility at the research reactor FRM II in Garching near Munich.
Journal of Radioanalytical and Nuclear Chemistry, submitted.
- [57] **Köper I., Comet S., Petry W., Bellissent-Funel M.-C.**
Dynamics of C-Phycocyanin in various deuterated Threhalose/Water environments by quasielastic and elastic neutron scattering.
European Biophysical Journal, **37**, (2008), 739–748.
- [58] **Leenaers A., VanDenBerghe S., Anselmet M., Noiret J., Lemoine P., Röhrmoser A., Petry W.**
Irradiation behavior of atomized and ground U(Mo) dispersion fuel.
Transactions of RERTR 2008 - 30th International Meeting on Reduced Enrichment for Research and Test Reactors, 5 - 9 October, 2008, -, (2008), -.
- [59] **Leist J., Gibhard H., Hradil K., Eckold G.**
Electric field induced anomalies in ferroelectric K_2SeO_4 .
J. Phys. Condens. Matter, **20**, (2008), 415209.
- [60] **Lewis S. J., Hossain S., Truman C. E., Smith D. J.**
Measurement and modelling of residual stresses in fracture toughness specimens extracted from large components.
Proceedings of the 2008 ASME Pressure Vessels and Piping Conference, PVP2008, July 27-31, 2008, Chicago, Illinois, USA, -, (2008), 6.
- [61] **Li Y.-L., Maurel M.-C., Ebe C., Vergne J., V. P., Zaccai G.**
Self-association of adenine dependent hairpin ribozymes.
Eur. Biophys. J., **37**, (2008), 173.
- [62] **Liljedahl D. M., Fitzpatrick M. E., Edward L.**
Residual stresses in structures reinforced with adhesively bonded straps designed to retard fatigue crack growth.
Composite Structures, **86**, (2008), 344–355.
- [63] **McGrady G. S., Sirsch P., Chatterton N. P., Ostermann A., Gatti C., Altmannshofer S., Herz V., Eickering G., Scherer W.**
Nature of the bonding in metal-silane sigma-complexes.
Inorganic Chemistry, **48(4)**, (2009), 1588–1598.
- [64] **Mehaddene T., Neuhaus J., Petry W., Hradil K., Bourges P., Hiess A.**
Interplay of structural instability and lattice dynamics in Ni_2MnAl .
Phys. Rev. B, **78**, (2008), 104110–1–9.
- [65] **Meierhofer G., Canella L., Grabmayr P., Jochum J., Jolie J., Kudejova P., Warr N.**
Prompt gamma rays in ^{77}Ge after neutron capture on ^{76}Ge .
Proceedings of the 13th International Symposium on Capture Gamma-Ray Spectroscopy and Related Topics (CGS 13), AIP Conference Proceedings, **1090**, (2008), 559.
- [66] **Mergia K., Grattarola C., Gualco S., Messoloras S., Hofmann M.**
Residual stress measurements on Mo/Cu and Mo/CuCrZr tiles using neutron diffraction.
Advanced Materials Research, **59**, (2008), 299–303.
- [67] **Meyer A., Horbach J., Heinen O., Holland-Moritz D., Unruh T.**
Self-diffusion in liquid titanium: quasi-elastic neutron scattering and molecular dynamics simulation.
Defect and Diffusion Forum, submitted.

- [68] **Meyer A., Stüber S., Holland-Moritz D., Heinen O., Unruh T.**
Determination of self-diffusion coefficients by quasielastic neutron scattering measurements on levitated Ni droplets.
Phys. Rev. B., **77**, (2008), 092201–1–4.
- [69] **Mole R. A., Cottrell S. R., Stride J. A., Wood P. T.**
Muon spin relaxation study of manganese hydroxy squarate.
Inorganica Chimica Acta, **361**, (2008), 3718 – 3722.
- [70] **Mole R. A., Stride J. A., Unruh T., Wood P. T.**
Non-classical behaviour in an $S = 5/2$ chain with next nearest neighbour interactions observed from the inelastic neutron scattering of $Mn_2(OD)_2(C_4O_4)$.
J. Phys. Condens. Matter, **21**, (2009), 076003.
- [71] **Mukherji D., Del Genovese D., Strunz P., Gilles R., Wiedenmann A., Rösler J.**
Microstructural characterisation of a Ni-Fe-based superalloy by in-situ SANS measurements.
J. Phys. Condens. Matter, **20**, (2008), 104220–104228.
- [72] **Mühlbauer S., Binz B., Jonietz F., Pfleiderer C., Rosch A., Neubauer A., Georgii R., Böni P.**
Skyrmion lattice in a chiral magnet.
Science, **323**, Issue **5916**, (2009), 915–919.
- [73] **Mühlbauer S., Böni P., Georgii R., Schmehl A., Schlohm D. G., Mannhart J.**
Field and temperature dependence of the magnetisation in the ferromagnetic EuO thin films.
J. Phys. Condens. Matter, **20**, (2008), 104230.
- [74] **Mühlbauer S., Niklowitz P. G., Stadlbauer M., Georgii R., Link P., Stahn J., Böni P.**
Elliptic neutron guides - focusing on tiny samples; Proceedings "European Workshop on Neutron Optics", March 5 - 7, 2007, Paul-Scherer-Institute, Villingen, Switzerland.
Nuclear Instruments and Methods in Physics Research A, **586**, (2008), 77 – 80.
- [75] **Müller-Buschbaum P., Metwalli E., Moulin J. F., Kudryashov V., Haese-Seiller M., Kampmann R.**
Time-of flight grazing incidence small angle neutron scattering - a novel scattering technique for the investigation of nanostructured polymer films.
European Physical Journal E ST, 107–112.
- [76] **Müller-Buschbaum P., Moulin J. F., Kudryashov V., Haese-Seiller M., Kampmann R.**
Time of flight grazing incidence small angle neutron - a novel scattering technique for the investigation of nanostructured polymer films.
Anal. Bioanal. Chem.
- [77] **Nyam-Ochir L., Ehrenberg H., Stuesser N., Senyshyn A., Fuess H., Sangaa D.**
The magnetic structures of double tungstates, $NaM(WO_4)_2$, $M = Fe, Cr$: examples for superexchange couplings mediated by $[NaO_6]$ -octahedra.
Journal of Magnetic Materials, **329**, (2008), 3251–3255.
- [78] **O'Dowd N. P., Nikbin K. M., Wimpory R. C., Biglari F. R., O'Donnell M. P.**
Computational and experimental studies of high temperature crack initiation in the presence of residual stress.
Journal of Pressure Vessel Technology, **130**, (2008), p041403/1–7.
- [79] **Ocenasek J., Krempasky C., Repper J., Werner E.**
Numerical analysis of micro-stress evolution in dual phase polycrystals.
Proceedings: 6th International Congress on Industrial and Applied Mathematics, ICIAM 2007, Zürich, Switzerland, 16 - 20 July; Proc. Appl. Math. Mech. 7 (PAMM2007), in press.
- [80] **Ohms C., Martins R. V., Uca O., Youtsos A. G., Bouchard P. J., Smith M., Keavey M., Bate S. K., Gilles R., Wimpory R. C., Edward L.**
The European network on neutron techniques standardization for structural integrity – NET.
Proceedings of ASME PVP 2008 ASME Pressure Vessels and Piping Conference July 27-31, 2008, Chicago, Illinois, USA, –, (2008), –.

- [81] **Ohms C., Wimpory R. C., Katsareas D. E., Youtsos A. G.**
Residual stress assessment by neutron diffraction and finite element modelling on a single bead weld on a steel plate.
International Journal of Pressure Vessels and Piping, **86**, (2009), 63–72.
- [82] **Orsingher L., Fontana A., JR. C., Tripodo G., Unruh T., Buchenau U.**
Vibrational dynamics of densified vitreous GeO₂.
submitted.
- [83] **Ortner B., Antretter T., Hofmann M., Werner E.**
Measurement of all six components of X-ray elastic factors.
Mat. Sci. Forum, **571-572**, (2008), 225–229.
- [84] **Palancher H., Wieschalla N., Martin P., Tucoulou R., Sabathier C., Petry W., Berar J.-F., Valot C., Dubois S.**
Uranium-molybden nuclear fuel plates behaviour under heavy ion irradiation: An x-ray diffraction analysis.
Journal of Nuclear Materials, **385**, (2009), 449–455.
- [85] **Papagiannopoulos A., Fernyhough C. M., Waigh T. A., Radulescu A.**
Scattering study of the structure of polystyrene sulfonate comb polyelectrolytes in solution.
Macromolecular Chemistry and Physics 209, **209**, (2008), 2475.
- [86] **Parnell S. R., Babcock E., Nünighoff K., Skoda M. W. A., Boag S., Masalovich S., Chen W. C., Georgii R., Wild J. M., Frost C. D.**
Study of spin-exchange optically pumped ³He cells with high polarisation and long lifetimes.
Nuclear Instruments and Methods in Physics Research A, **598**, (2009), 774 – 778.
- [87] **Pawlukojc A., Prager M., Dobrowolska W. S., Bator G., Sobczyk L., Ivanov A., Rols S., Grech E., Nowicka-Scheibe J., Unruh T.**
The structure, methyl rotation reflected in inelastic and quasielastic neutron scattering and vibrational spectra of 1,2,3,5-tetramethoxybenzene (TMOB) and its 2:1 complex with 1,2,4,5-tetracyanobenzene (TCNB).
J. Chem. Phys., submitted, –, (2008), –.
- [88] **Perlich J., Koertgens V., Metwalli E., Schulz L., Georgii R., Müller-Buschbaum P.**
Solvent content in thin spin-coated polystyrene homopolymer films.
Macromolecules, **42 (1)**, (2009), 337–344.
- [89] **Petry W.**
Nicht zu schaffen - Die für 2010 vereinbarte Umrüstung des Forschungsreaktors FRM II auf Brennelemente mit geringerer Urananreicherung muss bis mindesten 2016 verschoben werden.
Physik Journal, **2**, (2009), 7.
- [90] **Peyker L., Gold C., Scheidt E.-W., Eyert V., Scherer W., May F., Unruh T., Link P., Kehrein S., Michor H., Bauer E.**
Crystal field induced non-Fermi-liquid behavior in CeNi_{9-x}Cu_xGe₄.
Phys. Rev. Lett., submitted.
- [91] **Pintschovius L., Weber F., Reichardt W., Kreyssig A., Heid R., Reznik D., Stockert O., Hradil K.**
Phonon linewidths in YNi₂B₂C.
Pramana Journal (2008) International Symposium on Neutron Scattering, Mumbai, India, 15-18 January 2008., **71 (4)**, (2008), 687–693.
- [92] **Pipich V., Balz M., Wolf S. E., Tremel W., Schwahn D.**
Nucleation and growth of CaCO₃ mediated by the egg-white protein ovalbumin: a time-resolved in situ study using small-angle neutron scattering.
J. Am. Chem. Soc., **130**, (2008), 6879.
- [93] **Pipich V., Willner L., Schwahn D.**
The A-B diblock copolymer as a nonordering external field in a three-component A/B/A-B polymer blends.
J. Phys. Chem. B, **112**, (2008), 16170.

- [94] **Pommrich A. I., Meyer A., Holland-Moritz D., Unruh T.**
Nickel self-diffusion in Silicon-rich Si-Ni melts.
Appl. Phys. Lett., **92**, (2008), 241922–1–3.
- [95] **Prager M., Desmedt A., Unruh T., Allgaier J.**
Dynamics and adsorption sites for guest molecules in methyl chloride hydrate.
J. Phys. Condens. Matter, **20**, (2008), 125219 – 6 pp.
- [96] **Prager M., Grimm H., Natkaniec I., Nowak D., Unruh T.**
The dimensionality of ammonium reorientation in $(\text{NH}_4)_2\text{S}_2\text{O}_8$: the view from neutron spectroscopy.
J. Phys. Condens. Matter, **20**, (2008), 125218–11–18.
- [97] **Radulescu A., Fetters L. J., Richter D.**
Polymer driven wax crystal control using partially crystalline polymeric materials.
Advances in Polymer Science, **210**, (2008), 1.
- [98] **Radulescu A., Ioffe A.**
Neutron guide system for small-angle neutron scattering instruments of the Jülich Centre for Neutron Science at the FRM II.
Nuclear Instruments and Methods in Physics Research A, **586**, (2008), 55.
- [99] **Ranjan R., Garg R., Hack R., Senyshyn A., Schmidbauer E., Trots D., Boysen H.**
Onset of spontaneous electrostrictive strain below 520 K in Pr-doped SrTiO_3 .
Phys. Rev. B, **78**, (2008), 092102.
- [100] **Rebelo-Kornmeier J., Hofmann M., Garbe U., Randau C., Repper J., Ostermann A., Tekouo W., Seidl G. A., Wimpory R. C., Schneider R., Brokmeier H. G.**
New developments at materials science diffractometer STRESS-SPEC at FRM II.
Proceedings of the ICRS8: The Eighth International Conference on Residual Stresses August 6- 8, 2008, Marriott Tech Center, Denver, Colorado, USA, –, (2008), –.
- [101] **Repper J., Hofmann M., Krempasky C., Wimpory R. C., Petry W., Werner E.**
Micro strain accumulation in multiphase superalloys.
Proceedings of the ICRS8: The Eighth International Conference on Residual Stresses, August 6-8, 2008, Marriott Tech Center, Denver, Colorado, USA, –, (2008), 7.
- [102] **Repper J., Hofmann M., Krempaszky C., Petry W., Werner E.**
Influence of microstructural parameters in macroscopic residual stress analysis of complex materials by neutron diffraction method.
Proceedings of Meca-SENS, Vienna, 24 - 26 September 2007; Materials Science Forum, **571-572**, (2008), 39–44.
- [103] **Repper J., Hofmann M., Krempaszky C., Regener B., Petry W., Werner E.**
Microscopic influence of macroscopic relaxation of complex materials.
Acta Materialia, submitted.
- [104] **Repper J., Keller T., Hofmann M., Krempasky C., Petry W., Werner E.**
Investigations of lattice spacing on IN718 via neutron Larmor diffraction.
Proceedings of the ICRS8: The Eighth International Conference on Residual Stresses, August 6-8, 2008, Marriott Tech Center, Denver, Colorado, USA, –, (2008), –.
- [105] **Repper J., Keller T., Hofmann M., Krempaszky C., Petry W., Werner E.**
Neutron larmor diffraction for the determination of absolute lattice spacing.
Proceedings Internationale Eigenspannungskonferenz, –, (2008), 8.
- [106] **Ripoll M. R., Ocenasek J.**
Microstructure and texture evolution during the drawing of tungsten wires.
Engineering Fracture Mechanics, in press.
- [107] **Russina O., Triolo A., Beiner M., Pappas C., Arrighi V., Russina M., Unruh T., Mullan C., Hardacre C.**
Temperature dependence of the primary relaxation in 1-hexyl,3-methylimidazolium bis(trifluoromethyl)sulfonylimide.
J. Phys. Chem. B, accepted.

- [108] **Röhrmoser A., Petry W.**
Fuel plate temperatures during operation of FRM II.
Transaction of RRFM 2009, March, 23 - 25, Vienna, Austria, -, (2009), 7.
- [109] **Röhrmoser A., Petry W., Boulcourt P., Chabre A., Dubois S., Lemoine P., Jarousse C., Falgoux J. L., van den Berghe S., Leenaers A.**
UMo full plate size irradiation experiment IRIS - TUM - a progress report.
Transactions of the RRFM 2008, Hamburg, Germany, March 2008, -, (2008), 11.
- [110] **Sazonov A., Meven M., Hutanu V., Heger G., Trots D., Merz M., Kaiser V.**
Structural behaviour of synthetic Co_2SiO_4 at low temperatures.
Acta Cryst. B, **64**, (2008), 661–668.
- [111] **Sazonov A. P., Hutanu V., Meven M., Heger G., Hansen T., Senyshyn A.**
Anomalous thermal expansion of cobalt olivine, Co_2SiO_4 , at low temperatures.
Phys. Rev. B.
- [112] **Schaffran T., Bergmann M., Grunwald I., Peschka-Süss R., Schubert R., Wagner F. M., Gabel D.**
Tumoral hemorrhage induced by dodecaborate cluster lipids.
ChemMedChem, to be submitted.
- [113] **Schillinger B.**
Proposed asynchronous data collection scheme for stroboscopic neutron imaging on spallation sources for the examination of running engines.
The Journal of Neutron Research, submitted.
- [114] **Schillinger B.**
Some considerations for a potential neutron imaging facility at a spallation source.
6th International Topical Meeting on Neutron Radiography, Sept. 2008, Kobe, Japan. Nuclear Instruments and Methods, in press.
- [115] **Schillinger B., Böni P., Breunig C., Calzada E., Leroy C., Mühlbauer M., Schulz M.**
A neutron optical periscope used for neutron imaging.
6th International Topical Meeting on Neutron Radiography, Sept. 2008, Kobe, Japan. Nuclear Instruments and Methods, submitted.
- [116] **Schillinger B., Calzada E., Mühlbauer M., Schulz M.**
Neutronen zeigen, was Röntgenstrahlen nicht sehen können.
Proceedings: CT-Tagung 27.-28. Feb. 2008 an der FH-Wels, Oberösterreich, -, (2008), -.
- [117] **Schmid E., Wagner F. M., Romm H., Walsh L., Roos H.**
Dose-response relationship of dicentric chromosomes in human lymphocytes obtained for the fission neutron therapy facility MEDAPP at the research reactor FRM II.
Radiat. Environ Biochemistry, **48**, (2009), 67–75.
- [118] **Schmid E., Wagner F. M., Romm H., Walsh L., Roos H.**
RBE of the fission neutron therapy facility MEDAPP at the new research reactor FRM II determined by dicentrics in human lymphocytes.
Radiation and Environmental Biophysics, 21 pp.
- [119] **Schmid W., Jungwirth R., Petry W., Böni P., Beck L.**
Manufacturing of thick monolithic layers by DC-magnetron sputtering.
Transactions of the RRFM 2008, Hamburg, Germany, March 2008, -, (2008), 4.
- [120] **Schulte A., Guo Y., Schirmacher W., Unruh T., Cardinal T.**
Low-frequency vibrational excitations in a niobium-phosphate glass for Raman gain applications.
Vibrat. Spectrosc., in press, -, (2008), -.
- [121] **Schulz M., Böni P., Calzada E., Mühlbauer M., Schillinger B.**
A polarizing option for the neutron periscope.
6th International Topical Meeting on Neutron Radiography, Sept. 2008, Kobe, Japan. Nuclear Instruments and Methods, in press.

- [122] **Schulz M., Böni P., Calzada E., Mühlbauer M., Schillinger B.**
New design for the Antares-II facility for neutron imaging at FRM II.
6th International Topical Meeting on Neutron Radiography, Sept. 2008, Kobe, Japan. Nuclear Instruments and Methods, submitted.
- [123] **Schulz M., Calzada E., Mühlbauer M., Schillinger B.**
Various neutron imaging methods at the FRM II reactor source and potential features at a spallation source installation.
Nuclear Instruments and Methods in Physics Research, accepted, A.
- [124] **Schulz M., Calzada E., Mühlbauer M., Schillinger B.**
Energy-dependent neutron imaging with a double crystal monochromator at the ANTARES facility at FRM I.
6th International Topical Meeting on Neutron Radiography, Sept. 2008, Kobe, Japan. Nuclear Instruments and Methods, submitted.
- [125] **Schwarz B., Ehrenberg H., Weitzel H., Senshyn A., Thybusz B., Kanpp M., McIntyre G., Fuess H.**
Crystal chemistry, structure and magnetic properties of the $\text{Cu}(\text{Mo}, \text{W})\text{O}_4$ solid solution series.
Philosophical Magazine, **88** (8), (2008), 1235–1258.
- [126] **Senff D., Aliouane D. N., Hiess A., Regnault L. P., Link P., Hradil K., Sidis Y., Braden M.**
Magnetic excitations in a cycloidal magnet: the magnon spectrum of multiferroic TbMnO_3 .
J. Phys. Condens. Matter, **20**, (2008), 434212.
- [127] **Senff D., Link P., Aliouane N., Argyriou D. N., Braden M.**
Field dependence of magnetic correlations through the polarization flop transition in multiferroic TbMnO_3 : Evidence for a magnetic memory effect.
Phys. Rev. B, **77**, (2008), 174419–1–6.
- [128] **Senff D., Schumann O., Benomar M., Kriener M., Lorenz T., Sidis Y., Habicht K., Link P., Braden M.**
Melting of magnetic correlations in charge-orbital ordered $\text{La}_{1/2}\text{Sr}_{2/3}\text{MnO}_4$: competition of ferromagnetic and antiferromagnetic states.
Phys. Rev. B., **77**, (2008), 184413–1–14.
- [129] **Smuda C., Busch S., Gemmecker G., Unruh T.**
Self-diffusion in molecular liquids: medium-chain n -alkanes and coenzyme Q_{10} studied by QENS.
J. Chem. Phys., **129**, (2008), 014513–1–10.
- [130] **Smuda C., Busch S., Schellenberg R., Unruh T.**
Methyl group dynamics in polycrystalline and liquid ubiquinone Q_0 studied by neutron scattering.
J. Phys. Chem. B, **113**, (2009), 916–922.
- [131] **Smuda C., Busch S., Wagner B., Unruh T.**
Methyl group dynamics in glassy, polycrystalline and liquid coenzyme Q_{10} studied by quasielastic neutron scattering.
J. Chem. Phys., **129**, (2008), 074507–1–9.
- [132] **Smuda C., Gemmecker G., Unruh T.**
Quasi-elastic and inelastic neutron scattering study of methyl group rotation in solid and liquid pentafluorobenzene and pentafluorotoluene.
J. Chem. Phys., **128**, (2008), 194502–1–11.
- [133] **Sobczyk L., Prager M., Sawka-Dobrowolska W., Bator G., Pawlukojć A., Grech E., van Eijck L., Ivanov A., Rols S., Wuttke J., Unruh T.**
The structure of diaminodurene and the dynamics of the methyl groups.
J. Chem. Phys., **130**, (2009), 164519.
- [134] **Stadler A. M., Digel I., Embs J. P., Unruh T., Tehei M., Zaccai G., Büldt G., Artmann G. M.**
From powder to solution: hydration dependence of human hemoglobin dynamics correlated to body temperature.
Biophysical Journal, submitted.

- [135] **Stockert O., Arndt J., Schneidewind A., Schneider H., Jeevan H. S., Geibel C., Steglich F., Loewenhaupt M.**
Magnetism and superconductivity in the heavy-fermion compound CeCu₂Si₂ studied by neutron scattering.
Physica B Condensed Matter, **403**, 5-9, (2008), 973–976.
- [136] **Strunz P., Gilles R., Mukherji D., Hofmann M., Genovese D., Roesler J., Hoelzel M., Davydov V.**
SANS contrast dependence on difference in thermal expansions of phases in two-phase alloys.
Journal of Applied Crystallography, accepted.
- [137] **Strunz P., Mukherji D., Rösler J., Gilles R., Näth O., Haug J., Wiedenmann A.**
In-situ SANS investigation of solution treatment of single crystal Ni-base superalloys containing rhenium.
tbc, submitted.
- [138] **Su Y., Link P., Schneidewind A., Wolf T., Adelman P., Xiao Y., Meven M., Mittal R., Rotter M., Johrendt D., Brückel T., Löwenhaupt M.**
Antiferromagnetic ordering and structural phase transition in Ba₂Fe₂As₂ with Sn incorporated from the growth flux.
Phys. Rev. B, **79**, (2009), 064504.
- [139] **Teixeira S. C. M., Ankner J., Bellissent-Funel M. C., Bewley R., Blakeley M. P., Coates L., Dahint R., Dalgliesh R., Dencher N., Dhont J., Fischer P., Forsyth V. T., Fragneto G., Frick B., Geue T., Gilles R., Gutberlet T., Haertlein M., Hauß T., Häußler W., Heller W. T., Herwig K., Holderer O., Juranyi F., Kampmann R., Knott R., Kohlbrecher J., Kreuger S., Langan P., Lechner R., Lynn G., Majkrzak C., May R., Meilleur F., Mo Y., Mortensen K., Myles D. A. A., Natali F., Neylon C., Niimura N., Ollivier J., Ostermann A., Peters J., Pieper J., Rühm A., Schwahn D., Shibata K., Soper A. K., Straessle T., Suzuki U.-I., Tanakai I., Tehei M., Timmins P., Torikai N., Unruh T., Urban V., Varvrin R., Weiss K., Zaccai G.**
New sources and instrumentation for neutrons biology.
Chemical Physics, **345**, (2008), 133–151.
- [140] **Trots D. M., Senyshyn A., Mikhailova D. A., Vad T., Fuess H.**
Phase transitions in jalpaite, Ag₃CuS₂.
J. Phys. Condens. Matter, **20**, (2008), 455204.
- [141] **Tsyulin N., Pardini T., Singh R. R. P., Xiao F., Link P., Schneidewind A., Hiess A., Landee C. P., Turnbull M. M., Kenzelmann M.**
Quantum effects in a weakly-frustrated S=1/2 two-dimensional Heisenberg antiferromagnet in an applied magnetic field.
Phys. Rev. Lett., accepted.
- [142] **Unruh T., Smuda C., Busch S., Neuhaus J., Petry W.**
Diffusive motions in liquid medium-chain n-alkanes as seen by quasielastic time-of-flight neutron spectroscopy.
J. Chem. Phys., **129**, (2008), 121106–1–4.
- [143] **Voigtmann T., Meyer A., Holland-Moritz D., Stüber S., Hansen T., Unruh T.**
Atomic diffusion mechanisms in Zr-Ni melts.
Europhysics Letters, **82**, (2008), 66001–p1–p6.
- [144] **Wagner F., Kneschaurek P., Kastenmüller A., Loeper-Kabasakal B., Kampfer S., Breitzkreutz H., Waschkowski W., Molls M., Petry W.**
The Munich fission neutron therapy facility MEDAPP at FRM II.
Strahlentherapie und Onkologie (Urban & Vogel), **12**, (2008), 643 – 646.
- [145] **Wagner F. M., Loeper B., Bücherl T., Breitzkreutz H., Petry W.**
Use of fission radiation in life sciences and materials characterisation.
Transaction of RRFM 2009, March, 23 - 25, Vienna, Austria, –, (2009), –.
- [146] **Wang J. L., Campell S. J., Studer A. J., Avdeev M., Hofmann M., Hoelzel M., Dou S. X.**
Magnetic structures and phase transitions in PrMn_{2-x}FexGe₂.
Journal of Applied Physics, **104**, (2008), 103911.

- [147] **Wasmuth U., Meier L., Hofmann M., Mühlbauer M., Stege V., Hoffmann H.**
Optimisation of composite castings by means of neutron-measurements.
CIRP Annals- Manufacturing Technology, **57/1**, (2008), 579–582.
- [148] **Weber F., Kreyssig A., Pintschovius L., Heid R., Reichardt W., Reznik D., Stockert O., Hradil K.**
Direct observation of the superconducting gap in phonon spectra.
Phys. Rev. Lett., **101**, (2008), 237002.
- [149] **Weber T., Pedersen B., Gille P., Frey F., Steurer P.**
The Co – Ni distribution in decagonal $Al_{69.7(4)}Co_{10.0(4)}Ni_{20.3(4)}$.
Z. Kristallogr., 863–867.
- [150] **Welcomme E., Palancher H., Sabathier C., Martin P., Allenou J., Valot C., Charollais F., Anselmet M., Jungwirth R., Petry W., Beck L., Jarousse C., Tucoulou R., Lemoine P.**
Heavy ion irradiation of UMo7Al fuel: methodological approach.
Transactions of RRFM 09, Vienna/Austria, March 22 - 25, 2009, accepted, –, (2009), –.
- [151] **Wimpory R. C., Mikula P., Saroun J., Poeste T., Li J., Hofmann M., Schneider R.**
Efficiency boost of the materials science diffractometer E3 at BENSC: one order of magnitude due to a horizontally and vertically focusing monochromator.
Neutron News, **19 /1**, (2008), 16 – 19.
- [152] **Wimpory R. C., Ohms C., Hofmann M., Schneider R., Youtsos A. G.**
Statistical analysis of residual stress determination using neutron diffraction.
International Journal of Pressure Vessels and Piping, **86**, (2009), 48–62.
- [153] **Wimpory R. C., Ohms C., Hofmann M., Schneider R., Youtsos A. G.**
Problems in the averaging of neutron diffraction stress data from round- robin campaigns.
Mat. Sci. Forum, **571-572**, (2008), 283–288.
- [154] **Wood K., Haeussler W., et al.**
A benchmark for protein dynamics: Ribonuclease A measured by neutron scattering in a large wavevector-energy transfer range.
Chemical Physics, **345/2-3**, (2008), 305– 314.
- [155] **Yu G., Ki Y., Motoyama E. M., Zhao X., Barisic N., Cho Y., Bourges P., Hradil K., Mole R. A., Greven M.**
Magnetic resonance in the model high-temperature superconductor $HgBa_2CuO_{4+\delta}$.
Phys. Rev. Lett., submitted.
- [156] **Yu G., Li Y., Motoyama E., Hradil K., Mole R., Greven M.**
Spectral weight redistribution and two low-energy scales of the magnetic excitations in the electron-doped superconductor $Nd_{2-x}Ce_xCuO_{4+\delta}$ ($x = 0.155$, $T_c = 25k$).
Phys. Rev. Lett., submitted, –, (2008), –.
- [157] **Zaeh M. F., Hornfeck T.**
Development of a robust laser beam bending process for aluminum fuselage structures.
Production Engineering, **2**, (2008), 149–155.

7.4. Committees

Strategierat FRM II

Chairman

Prof. Dr. Gernot Heger
Institut für Kristallographie
RWTH Aachen

Members

MRin Dr. Ulrike Kirste
Bayerisches Staatsministerium für Wissenschaft,
Forschung und Kunst

Dr. Rainer Koepke
Bundesministerium für Bildung und Forschung

Prof. Dr. Georg Büldt
Institut für Biologische Informationsverarbeitung
Forschungszentrum Jülich

Prof. Dr. Dosch
Max-Planck-Institut für Metallforschung
Stuttgart

Prof. Dr. Dieter Richter
Institut für Festkörperphysik
Forschungszentrum Jülich

Prof. Dr. Dirk Schwalm
Max-Planck-Institut für Kernphysik
Heidelberg

Prof. Dr. Helmut Schwarz
Institute of Chemistry
Technische Universität Berlin

Prof. Dr. Dr. Michael Wannemacher
Radiologische Klinik und Poliklinik
Abteilung Strahlentherapie
Universität Heidelberg

Prof. Dr. Ewald Werner
Lehrstuhl für Werkstoffkunde und -mechanik
Technische Universität München

Prof. Dr.-Ing. Heinz Voggenreiter
Director of the Institute of Structure and Design
German Aerospace Center (DLR) Köln

Prof. Dr. Markus Braden
Physikalisches Institut
Universität zu Köln

Honorary Members

MDgt i.R. Jürgen Großkreutz

Prof. Dr. Tasso Springer

Guests

Prof. Dr. Dr. h.c. mult. Wolfgang A. Herrmann
Präsident
Technische Universität München

Prof. Dr. Winfried Petry
ZWE FRM II
Technische Universität München

Dr.-Ing. Rainer Kuch
Beauftragter der Hochschulleitung
Technische Universität München

Dr. Ingo Neuhaus
ZWE FRM II
Technische Universität München

Dr. Michael Klimke
Referent der Hochschulleitung
Technische Universität München

Dr. Klaus Seebach
ZWE FRM II
Technische Universität München

Secretary

Dr. Jürgen Neuhaus
ZWE FRM II

**Instrumentation advisory board
(Subcommittee of the Strategierat)****Chairman**

Prof. Dr. Markus Braden
Physikalisches Institut
Universität zu Köln

Members

Prof. Dr. Dirk Dubbers
Physikalisches Institut
Universität Heidelberg

Prof. Dr. Michael Gradzielski
Institut für Chemie
Technische Universität Berlin

Prof. Dr. Rainer Hock
Lehrstuhl für Kristallographie und Strukturphysik
Universität Erlangen

Prof. Dr. Werner Kuhs
GZG Abteilung Kristallographie
Universität Göttingen

Prof. Dr. Stephan Paul
Physik Department E18
Technische Universität München

Prof. Dr. Wolfgang Scherer
Lehrstuhl für Chemische Physik
Universität Augsburg

Prof. Dr. Wolfgang Schmahl
Dept. für Geo- und Umweltwissenschaften
Ludwig-Maximilians-Universität München
Deputy of the Chairman

Dr. habil. Dieter Schwahn
Institut für Festkörperforschung
Forschungszentrum Jülich

Prof. Dr. Andreas Türler
Institut für Radiochemie
Technische Universität München

Prof. Dr. Albrecht Wiedenmann
Abteilung SF3
Hahn-Meitner-Institut Berlin

Dr. habil. Regine Willumeit
GKSS Forschungszentrum Geesthacht

Guests

Dr. Michael Klimke
Referent der Hochschulleitung
Technische Universität München

Dr. Jürgen Neuhaus
ZWE FRM II
Technische Universität München

Dr. Klaus Feldmann
BEO-PFR
Forschungszentrum Jülich

Prof. Dr. Winfried Petry
ZWE FRM II
Technische Universität München

MRin Dr. Ulrike KIRSTE
Bayerisches Staatsministerium für Wissenschaft,
Forschung und Kunst

Dr. Klaus Seebach
ZWE FRM II
Technische Universität München

Prof. Dr. Gernot Heger
Institut für Kristallographie
RWTH Aachen

Dr. Ingo Neuhaus
ZWE FRM II
Technische Universität München

Secretary

Dr. Peter Link
ZWE FRM II

**Committee for industrial and medical use
(Subcommittee of the Strategierat)****Chairman**

Prof. Dr.-Ing. Heinz Voggenreiter
German Aerospace Center (DLR) Köln

Members

Automobile industry
Dr.-Ing. Rainer Simon
BMW AG München

Dr.-Ing. Maik Broda
Ford Forschungszentrum Aachen

Aerospace industry
Dr.-Ing. Rainer Rauh
Airbus Deutschland Bremen

Chemistry and environment
Dr. Jens Rieger
BASF AG Ludwigshafen

Secretary

Dr. Ralph Gilles
ZWE FRM II

Scientific committee - Evaluation of beamtime proposals (Subcommittee of the Strategierat)

Chairman

Prof. Dr. Wolfgang Schmahl
Dep. für Geo- und Umweltwissenschaften
Ludwig-Maximilians-Universität München

Members

Dr. Dimitri Argyriou
Helmholtz Zentrum Berlin für Materialien und Energie

Prof. Dr. John Banhart
Abteilung Werkstoffe (SF3)
Helmholtz Zentrum Berlin für Materialien und Energie

Dr. Philippe Bourges
Laboratoire Léon Brillouin
CEA Saclay

Prof. Dr. Markus Braden
Physikalisches Institut
Universität zu Köln

Prof. Dr. Heinz-Günther Brokmeier
Institut für Werkstofforschung
GKSS - Forschungszentrum Geesthacht

Dr. Olwyn Byron
Infection and Immunity
University of Glasgow

PD Dr. Reiner Dahint
Fakultät für Chemie und Geowissenschaften
Ruprecht-Karls-Universität Heidelberg

Prof. Dr. Antonio Deriu
Dipartimento di Fisica
Università degli studi di Parma

PD Dr. Mechthild Enderle
Institut Laue Langevin
Grenoble

Dr. Björn Fak
Institut Laue Langevin
Grenoble

Prof. Dr. Ch. Genzel
Helmholtz Zentrum Berlin für Materialien und Energie

Dr. Matz Haaks
Helmholtz-Institut für Strahlen- und Kernphysik Bonn

Dr. Rudi Hackl
Walther-Meissner-Institut
Technische Universität München

Dr. Thomas Hansen
Institut Laue Langevin
Grenoble

Prof. Dr. Jan Jolie
Institute of Nuclear Physics
Universität zu Köln

Prof. Dr. Andreas Magerl
LS für Kristallographie und Strukturphysik
Universität Erlangen

Prof. Dr. Karl Maier
Helmholtz-Institut für Strahlen- und Kernphysik
Universität Bonn

Dr. Elena Mashkina
Forschungszentrum Karlsruhe

Prof. Reinhard Dr. Krause-Rehberg
Department of Physics
Universität Halle

Dr. Bernd Leiss
Geowissenschaftliches Zentrum
Universität Göttingen

Dr. Stéphane Longeville
Laboratoire Léon Brillouin
Laboratoire de la Diffusion Neutronique
CEA Saclay

Dr. Michael Monkenbusch
Institut für Festkörperforschung
Forschungszentrum Jülich

Prof. Dr. Werner Paulus
Structures et Propriétés de la Matière
Université de Rennes 1

Prof. Dr. Joachim Rädler
Fakultät für Physik
Ludwig-Maximilians-Universität München

PD. Dr. Klaus Raetzke
Materialverbunde
Christian-Albrechts-Universität zu Kiel

Prof. Dr. Henrik Ronnow
Laboratory for Quantum Magnetism
Ecole Polytechnique Fédérale de Lausanne

Prof. Dr. Günther Roth
Institut für Kristallographie
RWTH Aachen

Prof. Dr. Michael Ruck
Institut für Anorganische Chemie
Technische Universität Dresden

Dr. Jürg Schefer
Laboratory for Neutron Scattering
ETH Zürich und Paul Scherrer Institut

Dr. Henk Schut
Technische Natuurwetenschappen
Technische Universität Delft

Dr. Werner Schweika
Institut für Festkörperforschung
FZ-Jülich

Prof. Dr. Jean-Michel Sprauel
IUT/Dept. Génie Mécanique et Productique
Université de la Méditerranée

Dr. Peter Staron
Forschungszentrum Geesthacht(GKSS)

Prof. Dr. Bernd Stühn
Institut für Festkörperphysik
Technische Universität Darmstadt

Prof. Dr. Helena van Swygenhoven-Moens
Paul-Scherrer-Institut Villigen, Schweiz

PD Dr. Katharina Theis-Bröhl
Process Engineering and Energy Technology
Hochschule Bremerhaven

Prof. Dr. Monika Willert-Porada
Lehrstuhl für Werkstoffverarbeitung
Universität Bayreuth

Prof. Dr. Oliver Zimmer
Institut Laue Langevin Grenoble

Scientific secretaries

Dr. Jürgen Neuhaus
ZWE FRM II

Dr. Klaudia Hradil
Universität Göttingen

Dr. Christoph Hugenschmidt
ZWE FRM II

Dr. Peter Link
ZWE FRM II

Dr. Martin Meven
ZWE FRM II

Dr. Tobias Unruh
ZWE FRM II

TUM Advisory board

Chairman

Prof. Dr. Ewald Werner
Lehrstuhl für Werkstoffkunde und -mechanik
Technische Universität München

Members

Prof. Dr. Peter Böni
Physik Department E21

Technische Universität München

Prof. Dr. Andreas Türler
Institut für Radiochemie
Technische Universität München

Prof. Dr. Bernhard Wolf
Heinz Nixdorf-Lehrstuhl für medizinische Elektronik
Technische Universität München

Prof. Dr. Markus Schwaiger
represented by Prof. Dr. Senekowitsch-Schmidtke
Nuklearmedizinische Klinik und Poliklinik
Klinikum Rechts der Isar
Technische Universität München

Prof. Dr. Arne Skerra
Lehrstuhl für Biologische Chemie
Technische Universität München

Guests

Dr. Klaus Seebach
ZWE FRM II
Technische Universität München

Prof. Dr. Winfried Petry
ZWE FRM II
Technische Universität München

Dr. Ingo Neuhaus
ZWE FRM II
Technische Universität München

Scientific steering committee

Chairman

Prof. Dr. Winfried Petry
ZWE FRM II
Technische Universität München

Members

Dr. Hans Boysen
Sektion Kristallographie
Ludwig-Maximilians-Universität München

Prof. Dr. Dieter Richter
Jülich Centre for Neutron Science
Forschungszentrum Jülich

Prof. Dr. Bernhard Keimer
Max-Planck-Institut für Festkörperforschung Stuttgart

7.5. Partner institutions



Georg-August-Universität Göttingen
 Institut für Physikalische Chemie
 Tammannstr. 6
 37077 Göttingen
<http://www.uni-pc.gwdg.de/eckold/>



GKSS-Forschungszentrum Geesthacht GmbH
 Max-Planck-Str. 1
 21502 Geesthacht
<http://www.gkss.de>



Helmholtz Zentrum Berlin für Materialien und Energie
 GmbH (HZB)
 Glienickerstr. 100
 14109 Berlin
<http://www.helmholtz-berlin.de>



Jülich Centre for Neutron Science JCNS
 Forschungszentrum Jülich GmbH
 52425 Jülich
 Außenstation am FRM II: 85747 Garching
<http://www.jcns.info>



Ludwig-Maximilians-Universität München
 Sektion Kristallographie (Prof. Schmahl)
 Theresienstr. 41
 80333 München
<http://www.krist.geo.uni-muenchen.de>
 und Sektion Physik (Prof. Rädler)
 Schellingstr. 4
 80799 München
<http://www.physik.uni-muenchen.de>



MAX-PLANCK-GESELLSCHAFT

Max-Planck-Institut für Festkörperphysik
 Heisenbergstr. 1
 70569 Stuttgart
<http://www.fkf.mpg.de>



RWTH Aachen
 Institut für Kristallographie
 Jägerstr. 17 - 19
 52066 Aachen
<http://www.xtal.rwth-aachen.de>



Technische Universität Clausthal
 Institut für Werkstoffkunde und Werkstofftechnik
 Agricolastr. 6
 38678 Clausthal-Zellerfeld
<http://www.iww.tu-clausthal.de>



Technische Universität Darmstadt
 Fachbereich Material- und Geowissenschaften
 Petersenstr. 23
 64287 Darmstadt
<http://www.tu-darmstadt.de/fb/matgeo/>



Technische Universität Dresden
 Institut für Festkörperphysik
 01062 Dresden
<http://www.physik.tu-dresden.de/ifp>



Universität Augsburg
Institut für Physik
Lehrstuhl für Chemische Physik und Materialwissenschaften
86135 Augsburg
<http://www.physik.uni-augsburg.de/cpm/>



Universität der Bundeswehr München
Institut für Angewandte Physik und Messtechnik
Werner-Heisenberg-Weg 39
85577 Neubiberg
<http://www.unibw.de/lrt2/>

Universität zu Köln



Universität zu Köln
Institut für Kernphysik
und II. Physikalisches Institut
Zùlpicher Str. 77
50937 Köln
<http://www.ph2.uni-koeln.de>
<http://www.ikp.uni-koeln.de>

7.6. Staff

Board of directors

Scientific director

Prof. Dr. W. Petry

Technical director

Dr. Ingo Neuhaus

Administrative director

Dr. K. Seebach

Experiments

Head

Prof. Dr. W. Petry

Secretaries

W. Wittowetz

E. Jörg-Müller

S. Valentin-Hantschel



Instruments

Prof. Dr. H. Abele (E18)

P. Aynajian (MPI-Stuttgart)

Prof. Dr. P. Böni (E21)

K. Buchner (MPI-Stuttgart)

Dr. T. Bücherl

S. Busch

H. Breitzkreutz

Dr. H.-G. Brokmeier (GKSS)

E. Calzada

L. Canella (Radiochemie, TUM)

D. Etdorf

J. Franke (MPI-Stuttgart)

Dr. W. Gan (GKSS)

Dr. R. Georgii

Dr. R. Gilles

R. Hähnel

Dr. M. Haese-Seiller (GKSS)

Dr. W. Häußler

Dr. M. Hofmann

Dr. M. Hölzel (TU Darmstadt)

W. Hornauer

Dr. K. Hradil (Univ. Göttingen)

Dr. C. Hugenschmidt

Dr. V. Hutanu (RWTH Aachen)

N. Jünke

S. Kampfner

R. Kampmann (GKSS)

Dr. T. Keller (MPI-Stuttgart)

Dr. W. Klein

Dr. J. Klenke

Dr. P. Kudejova (Universität zu Köln)

Dr. P. Link

Dr. B. Loeper-Kabasakal

K. Lorenz

A. Mantwill (E21)

Dr. J. Major (MPI-Stuttgart)

Dr. M. Major (MPI-Stuttgart)

Dr. T. Mehaddene

Dr. M. Meven

Dr. R. Mole

Dr. P. Moulin (GKSS)

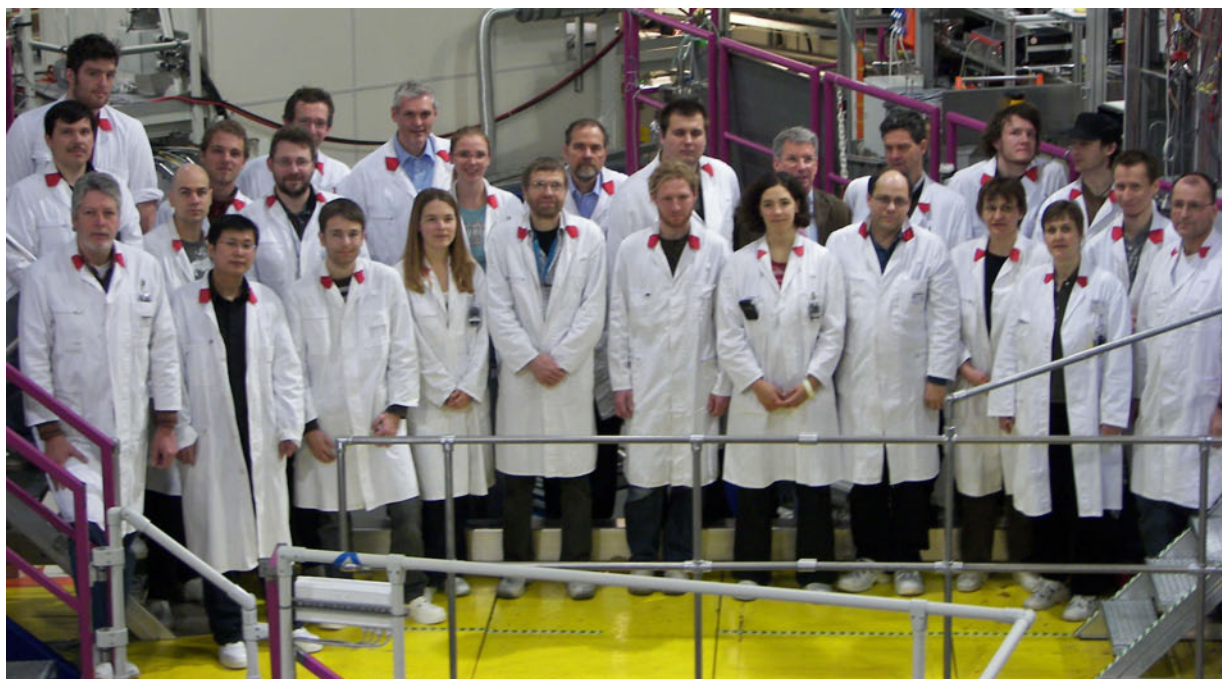
S. Mühlbauer

Dr. A. Ostermann

Coordination

Dr. J. Neuhaus

H. Türck



Scientific staff in the experimental hall



Scientific staff in the neutron guide hall

Dr. B. Pedersen
 Ph. Pikart
 C. Piochacz
 M. Pomm (GKSS)
 Dr. J. Rebelo-Kornmeier
 (HMI Berlin)
 F. Repper
 J. Repper
 R. Repper
 J. Ringe
 Dr. A. Rühm (MPI Stuttgart)
 Ch. Sauer
 A. Sazonov
 Dr. B. Schillinger
 Dr. A. Schneidewind (TU Dresden)
 Prof. Dr. K. Schreckenbach (E21)
 M. Schulz
 R. Schulze (Universität zu Köln)
 R. Schwikowski
 Dr. A. Senyshyn (TU Darmstadt)
 G. Seidl
 C. Smuda
 M. Stadlbauer
 Dr. R. Stöpler (E18)
 B. Straßer
 Dr. T. Unruh
 F. M. Wagner
 Dr. R. Wimpory (HMI Berlin)
 Dr. H.-F. Wirth
 A. Wolf
 Prof. Dr. O. Zimmer (E18)

Instruments - JCNS

Prof. Dr. D. Richter (Director JCNS)
 Prof. Dr. T. Brückel (Director JCNS)
 Dr. A. Ioffe (Head of outstation at
 FRM II)

Secretary

F. Michel

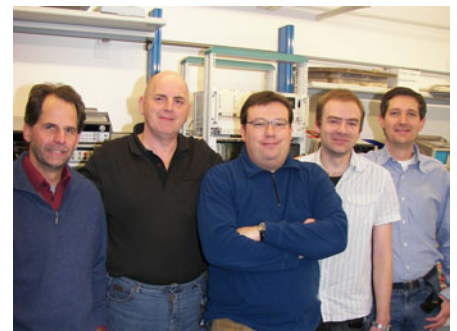
 Dr. M.-S. Appavou
 Dr. E. Babcock
 Dr. P. Busch
 Dr. N. de Souza
 A. Erven
 Dr. H. Frielinghaus
 Dr. X. Frielinghaus
 C. Gerstl
 Th. Glomann
 M. Gödel
 Dr. G. Goerigk
 D. Gurzi
 Dr. Th. Gutberlet
 Dr. O. Holderer
 M. Kerscher
 Th. Kohnke
 E. Kentzinger
 Th. Kohnke
 Dr. D. Korolkov
 H. Kusche
 Dr. St. Mattauch

Dr. R. Mittal

A. Nebel
 S. Neueder
 K. Nusser
 V. Ossovyi
 Dr. M. Prager
 Dr. V. Pipich
 Dr. A. Radulescu
 H. Schneider
 Dr. G. J. Schneider
 P. Stronciwilk
 Dr. Y. Su
 Dr. J. Voigt
 Dr. J. Wuttke

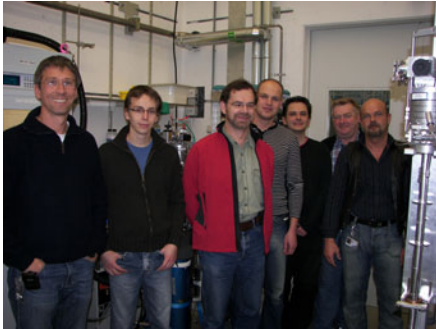
Detectors and electronics

Dr. K. Zeitelhack
 I. Defendi
 Chr. Hesse
 M. Panradl
 Dr. M. Petertill
 Th. Schöffel



Sample environment

Dr. J. Peters
P. Biber
H. Kolb
A. Pscheidt
A. Schmidt
M. Wiesheu
J. Wenzlaff



E. Kahle
O. Lykhar
Dr. S. Masalovich
A. Ofner
H. Schölderle
R. Valicu



G. Kaspar
B. Oberholz
A. Steinberger
M. Stowasser

**Auszubildende**

A. Erb
F. Hänsel
J.-P. Innocente
C. Kick
A. Lenz
A. Preller
C. Rajczak
A. Schwertner

Neutron optics

Prof. Dr. G. Borchert
C. Breunig
H. Hofmann
R. Iannucci

IT services

J. Krüger
J. Pulz
H. Wenninger
J. Ertl
S. Galinski
N. Ivanova

Administration**Head**

Dr. K. Seebach

Secretary

C. Zeller

Members

R. Obermeier
B. Bendak
B. Gallenberger

I. Heinath

K. Lüttig

Public relations

Dr. Ulrich Marsch(ZV TUM)

Dr. A. Battenberg(ZV TUM)

A. Voit (FRM II)

Visitors service

U. Kurz

Dr. B. Tonin-Schebesta

User office

Dr. Th. Gutberlet (JCNS)

Dr. I. Lommatzsch (FRM II)



Administration (left) and User office (right).

Reactor operation

Head

Dr. Ingo Neuhaus

Secretaries

M. Neuberger
S. Rubsch

Management

Dr. H. Gerstenberg
(Irradiation and fuel cycles)
Dr. J. Meier
(Reactor operation)
R. Schätzlein
(Electric and control technology)
Dr. A. Kastenmüller
(Reactor enhancement)

Shift members

F. Gründer
A. Bancsov
A. Benke
M. Danner
Chr. Feil
M. Flieher
H. Groß
L. Herdam
F. Hofstetter
K. Höglauer
T. Kalk
G. Kaltenegger
U. Kappenberg
F. Kewitz
M. G. Krümpelmann
J. Kund
A. Lochinger
G. Mauermann
A. Meilinger
M. Moser
L. Rottenkolber
G. Schlittenbauer

Technical services

K. Pfaff
R. Binsch
O. Breu
A. Cziasto
H. Gampfer
W. Glashauser
G. Guld
S. Manz
B. Heck

G. Wagner
A. Weber
M. Wöhner
C. Ziller
J. Zöybek

Sources

C. Müller
D. Päthe
A. Wirtz

Electric and control technology

R. Schätzlein
G. Aigner
W. Buchner
A. Düring
R. Krammer
K.-H. Mayr
Ü. Sarikaya
H. Schwaighofer
J. Wildgruber

Job safety

H. Bamberger

Irradiation

Dr. H. Gerstenberg
J.-M. Favoli
W. Fries
Dr. X. Li
M. Oberndorfer
W. Lange
V. Loder
J. Molch
A. Richter
T. Scheit
H. Schulz
F.-M. Wagner
N. Wiegner

Reactor enhancement

W. Bünten
F. Henkel
R. Lorenz
B. Pollom
M. Schmitt
V. Zill

Technical design

F.-L. Tralmer
J. Fink

H. Fußstetter
J. Jüttner
S. Küçük
K. Lichtenstein



Workshops

C. Herzog
U. Stiegel
A. Begic
M. Fuß
A. Huber
A. Scharl
R. Schlecht
J. Waronitz

Radiation protection

Dr. B. Wierczinski
W. Dollrieß
H. Hottmann
D. Lewin
B. Neugebauer
D. Schrulle
H.-J. Werth
S. Wolff
D. Bahmet
W. Kluge
A. Schindler
M. Schmidt
D. Strobl

Chemical laboratory

C. Auer
R. Bertsch
P. Müller
S. Uhlmann

Technical safety service

J. Wetzl
R. Maier
J. Aigner
K. Otto
N. Hodzic
J. Schreiner

Reactor physics

Dr. A. Röhrmoser
C. Bogenberger

R. Hengstler
R. Jungwirth

W. Schmid

Security department

L. Stienen

J. Stephani

Imprint

.....

Publisher:
Technische Universität München
Forschungs-Neutronenquelle Heinz Maier-Leibnitz
(FRM II)
Lichtenbergstr. 1
85747 Garching
Germany
Phone: +49 89-289-14966
Fax: +49 89-289-14995
Internet: <http://www.frm2.tum.de>
email: <mailto://userinfo@frm2.tum.de>

.....

Editors:
A. Voit, TUM
B. Pedersen, TUM
E. Jörg-Müller, TUM

.....

Photographic credits:
All images: TUM, except otherwise noted

.....

Design:
A. Voit, TUM
B. Pedersen, TUM
E. Jörg-Müller, TUM

.....

Typesetting(L^AT_EX 2_ε):
B. Pedersen, TUM
A. Voit, TUM
E. Jörg-Müller, TUM

.....